FREE VIBRATION CHARACTERISTICS AND IMPACT RESPONSE OF FUNCTIONALLY GRADED CONICAL SHELL

A Thesis
Submitted By

APURBA DAS

Doctor of Philosophy (Engineering)

DEPARTMENT OF MECHANICAL ENGINEERING
FACULTY COUNCIL OF ENGINEERING & TECHNOLOGY
JADAVPUR UNIVERSITY
KOLKATA, INDIA-700 032
2018

JADAVPUR UNIVERSITY

KOLKATA – 700 032

INDEX NO. 114/15/E

1. **Title of Thesis:**

   Free Vibration Characteristics and Impact Response of Functionally Graded Conical Shell

2. **Name, Designation & Institution of the Supervisor:**

   Dr. Amit Karmakar,

   Associate Professor,

   Mechanical Engineering Department,

   Jadavpur University, Kolkata-700032.

3. **List of Publications**

   a. Das. A and Karmakar A "Vibration Characteristics of functionally graded Pre-Twisted turbo machinery blade with rotational effect" **Advanced Science Letters. American Scientific Publishers**, pp 111-117 (2016). doi.org/10.1166/asl.2016.6769

   b. Das. A and Karmakar A "Free vibration Characteristics of functionally graded pre-twisted conical shells under rotation" **J. Inst. Eng. India Ser. C (2017). Springer Publication**, doi.org/10.1007/s40032-017-0378-6

   c. Das. A, Banerjee R and Karmakar A "Transient dynamic analysis of pretwisted functionally graded conical shells subject to low velocity impact: A finite element approach" **ASME Gas Turbine India, (2017).** doi:10.1115/GTINDIA2017-4611

   d. Das. A, Rout. M and Karmakar A "Time dependent response of impact induced functionally graded conical shell considering porosity" **Sadhana-Springer Publication**. Manuscript ID SADH-S-18-00650 [Communicated].

4. **List of Patents: Nil**

5. **List of Presentations in National/International/Conferences/Workshops:**

   a. Das. A, Sarkar. S and Karmakar A "Vibration characteristics of functionally graded pre-twisted turbo machinery blade with rotational effect" Sixth International

Conference on Theoretical, Applied, Computational and Experimental Mechanics, **(ICTACEM-2014)** December 29 – 31, 2014 IIT Kharagpur, India, pp-77-79.

b. Das. A, Banerjee R and Karmakar A "Temperature Dependent Natural Modes for Sigmoidal Functionally Graded Conical Shell" International Conference on emerging materials: characterization and application, **(EMCA-2017)**, March 15-17, NIT Durgapur, India.

c. Das. A, Debsinha T and Karmakar **A "**Low Velocity Normal Impact Analysis of Functionally Graded Conical Shell with Simple Power Law" International Conference on emerging materials: characterization and application, **(EMCA-2017)**, March 15-17, NIT Durgapur, India.

d. Das. A, Rout. M and Karmakar A "Finite-element multi-point impact performance of functionally graded turbo-machinery blades" Seventh International Conference on Theoretical, Applied, Computational and Experimental Mechanics, **(ICTACEM-2017)**, December 28 – 30, 2017 IIT Kharagpur**.**

e. Das. A, Rout. M and Karmakar A "Time dependent response of low velocity impact induced Ni/Cu functionally graded conical shell" **(INCOM 2018)**, 1st International Conference on Mechanical Engineering 4th - 6th January, 2018, Jadavpur University, Kolkata.

f. Das. A and Karmakar A "Free vibration analysis of rotating porous functionally graded conical shell considering even and uneven porosity" National Conference on Advanced Materials, Manufacturing and Metrology **(NCAMMM–2018)**, February 16-17, 2018, CSIR-CMERI, Durgapur, India.

JADAVPUR UNIVERSITY

KOLKATA–700032, INDIA

CERTIFICATE FROM THE SUPERVISOR

This is to certify that the thesis entitled "**Free Vibration Characteristics and Impact Response of Functionally Graded Conical Shell***"*, submitted by Shri Apurba Das**,** who got his name registered on 23/06/2015 for the award of **Ph.D. (Engineering) degree** of **Jadavpur University** is absolutely based upon his own work under my guidance and supervision. Neither the results obtained from this work nor any part of this thesis has been submitted for any degree / diploma or any other academic award anywhere before.

_____

(Dr. Amit Karmakar)
Associate Professor
Mechanical Engineering Department
Jadavpur University, Kolkata-700032, India

ACKNOWLEDGEMENT

The author expresses his deep sense of gratitude to his supervisor, Dr. Amit Karmakar for his keen interest, cherished guidance and constant inspiration during the course of the research work. The author is grateful to him for his guidance to enter into new field of advanced class of composites namely functionally graded material. Above all, without his moral support and constant guidance the author would not have completed the work.

The author is thankful to Dr. D. K. Maiti (IIT Kgp), Dr. D. K. Mandal, Dr. A. Nandi, Dr. K Inaba (TIT, Japan), Dr. T. Bandopadhyay for their encouragement and advice. The author acknowledges to the reviewers of journals and conference papers and from the audience, while presenting papers in conferences. The author extends specials thanks to the Applied Mechanics Laboratory of Jadavpur University, Kolkata and Kishimoto-Inaba Laboratory of Tokyo Institute of Technology, Japan, for providing the facility and support during this research work. The author acknowledges Titagarh Wagons Ltd, Kolkata and Titagarh Wagons-AFR, France, Douai office for providing the permission and facility to carry out the research work.

The author takes great pleasure to thank the fellow researchers Mrutyunjay Rout, Tripuresh Deb Singha, Zachary Stephen Moore (Washington University) and Su Ziyi (TIT, Japan) from whom he received immense support and assistance. The author expresses extreme gratefulness to his wife (Leena) for her constant support and motivation, without that he would not have come to this stage.

Above all, it is the wish of The Almighty that the author has been able to complete this work.

Date: Apurba Das

LIST OF PUBLICATIONS

The below technical papers are prepared based on the present research work which have been published/accepted or submitted in the International Journals and International/National conferences:

INTERNATIONAL JOURNAL:

1. Das. A and Karmakar A "Vibration Characteristics of functionally graded Pre-Twisted turbo machinery blade with rotational effect" **Advanced Science Letters. American Scientific Publishers**, pp 111-117 (2016). doi.org/10.1166/asl.2016.6769
2. Das. A and Karmakar A "Free vibration Characteristics of functionally graded pre-twisted conical shells under rotation" **J. Inst. Eng. India Ser. C (2017). Springer Publication**, doi.org/10.1007/s40032-017-0378-6
3. Das. A, Banerjee R and Karmakar A "Transient dynamic analysis of pretwisted functionally graded conical shells subject to low velocity impact: A finite element approach" **ASME Gas Turbine India, (2017).** doi:10.1115/GTINDIA2017-4611
4. Das. A, Rout. M and Karmakar A "Time dependent response of impact induced functionally graded conical shell considering porosity" **Sadhana-Springer Publication**. Manuscript ID SADH-S-18-00650 [Communicated].

INTERNATIONAL/ NATIONAL CONFERENCE:

1. Das. A, Sarkar. S and Karmakar A "Vibration characteristics of functionally graded pre-twisted turbo machinery blade with rotational effect" Sixth International Conference on Theoretical, Applied, Computational and Experimental Mechanics, **(ICTACEM-2014)** December 29 – 31, 2014 IIT Kharagpur, India, pp-77-79.
2. Das. A, Banerjee R and Karmakar A "Temperature Dependent Natural Modes for Sigmoidal Functionally Graded Conical Shell" International Conference on emerging materials: characterization and application, **(EMCA-2017)**, March 15-17, NIT Durgapur, India.
3. Das. A, Debsinha T and Karmakar **A "**Low Velocity Normal Impact Analysis of Functionally Graded Conical Shell with Simple Power Law" International Conference on emerging materials: characterization and application, **(EMCA-2017)**, March 15-17, NIT Durgapur, India.

4. Das. A, Rout. M and Karmakar A "Finite-element multi-point impact performance of functionally graded turbo-machinery blades" Seventh International Conference on Theoretical, Applied, Computational and Experimental Mechanics, **(ICTACEM-2017)**, December 28 – 30, 2017 IIT Kharagpur**.**
5. Das. A, Rout. M and Karmakar A "Time dependent response of low velocity impact induced Ni/Cu functionally graded conical shell" **(INCOM 2018)**, 1st International Conference on Mechanical Engineering 4th - 6th January, 2018, Jadavpur University, Kolkata.
6. Das. A and Karmakar A "Free vibration analysis of rotating porous functionally graded conical shell considering even and uneven porosity" National Conference on Advanced Materials, Manufacturing and Metrology **(NCAMMM–2018)**, February 16-17, 2018, CSIR-CMERI, Durgapur, India.

ABSTRACT

Functionally graded materials (FGMs) categorized as an advanced class of composite materials, consist of novel inhomogeneous mixture of materials like ceramic and metals with smooth changes of its constituents' volume fraction along the thickness direction. These materials do not contain well distinguished boundaries or interfaces between their different regions as in the case of conventional composite materials but have numerous advantages that make them appropriate in potential applications due to reduction of in-plane and through-the thickness transverse stresses, improved thermal properties, high toughness, etc. FGMs possess good chances of reducing mechanical and thermal stress concentration in many structural elements because of smooth transition between the properties of the components and thereby cracking or delamination, which are often observed in conventional multi-layer systems are avoided. FGMs consisting of metallic and ceramic components are well-known to enhance the properties of high temperature thermal-barrier application where the ceramic part has good thermal resistance and metallic part has superior fracture toughness. Thus FGMs have great potential in applications where the operating conditions are severe, including spacecraft heat shields, nuclear reactors, biomedical implants, etc. A functionally graded shallow conical shell is a structural element of considerable technical significance and can be idealized as turbo machinery blades under rotation that can be extensively used in the aviation, energy, nuclear and mechanical industries. In a weight-sensitive and high thermal gradient application, FGM materials are advantageous because of their light weight, high strength, stiffness and thermal barrier ceramics components. In addition, FGM materials can be tailored to cater the design requirements of strength, stiffness thermal barrier application. The prior knowledge of free vibration characteristics of such turbomachinery blades is utmost important to avoid resonance effect ensuring longer life of such components, preventing unscheduled shutdown of the machineries. The composition of FGM constituents' such as ceramics and metals can be used with help of prior knowledge of natural frequencies. Moreover, the initial stress system in a rotating shell due to centrifugal body forces has the cascading effect on the natural frequency appreciably. Thus, the free vibration characteristics have crucial influence on safe performance of such FGM shell structures.

On the other hand outside/inside debris or small torn out objects from the turbo machines can have impact of such conical shell blade with low velocity. Therefore, the

susceptibility to damage due to low velocity impact caused by foreign objects can accelerate the degradation of strength and can promote the structural instability. Hence the low velocity impact performances are crucial for designing of an impact mitigating system In realistic situations, pretwisted conical shell structures have geometrical complexities arising due to their specific applications in various service environments. A typical dynamic parameters need to be used considering the rotation effect of these structural elements. Therefore a good understanding of the dynamic behaviour of FGM pretwisted conical shells requires close attention in order to confirm the operational safety. Accordingly, the present study is intended to investigate two key aspects of the dynamic behaviour of pretwisted FGM rotating conical shells, namely, free vibration characteristics and dynamic low velocity impact response. Being a proficient analysis tool to the design engineer the finite element method is employed to address the present problems.

An eight-noded isoparametric shell element is used for the finite element formulation considering rotary inertia effect and transverse shear deformation based on Mindlin's theory. The dynamic equilibrium equation is derived from Lagrange's equation neglecting the Coriolis effect for moderate rotational speeds. A modified Hertzian contact law considering permanent indentation is used to calculate the contact force along with other impact response parameters. Using the Newmark's time integration scheme the time dependent equations of the shell and the impactor are solved. The static equilibrium equations and the standard eigen value problem are solved by Gauss elimination technique and QR iteration algorithm, respectively. Finite element codes are developed and validated with those published results in the open literature after performing a suitable convergence study and verification of the results.

The results are primarily obtained for FGM pretwisted and untwisted conical shells for the triggering parameters like different FGM power law index, rotational speeds, twist angles and porosity factors on the natural frequencies. The mode shapes for the FGM conical shells are also presented. Numerical solutions are also obtained for time dependent impact response of FGM conical shells subjected to low velocity impact. Parametric studies are conducted to investigate the effects of prime parameters like different FGM power law index, angle of twist, velocity of impactor, location of the impactor, shell thickness, mass of the impactor and porosity factors on impact performance. The results are discussed in detail with graphs and tables and the conclusions are laid down concentrating on the significant findings. The future scopes of the present work are also projected to carry out the further investigations.

NOMENCLATURE

E	Young's modulus
G	Shear modulus
N	Material property graded index (or Power law exponent)
U	Potential strain energy = $U_1 + U_2$
VOI	Initial velocity of impactor
T, W	Kinetic energy and work done by conservative and nonconservative forces, respectively
N_{xy}	In-plane shear force resultant
M_{xy}	Torsional moment resultant
M_x, M_y	Bending moment resultants
N_x, N_y	In-plane normal force resultants
Q_x, Q_y	Transverse shear resultants
$A_{ij}, B_{ij}, D_{ij}, S_{ij}$	Extension, bending-extension coupling, bending and transverse shear terms of laminate stiffness matrix respectively
$C_o - C_7$	Constant terms of displacement polynomial
F_c	Contact force at the impact point
L_f	Lagrangian function
L_o	Length
L_o/s	Aspect ratio
P_i	Material property
S_j	Shape functions
U_1	Linear elastic strain energy
U_2	Strain energy by initial stresses generated due to rotation
V_f	Volume fraction
$[\bar{K}], [\bar{k}_{imp}]$	Effective stiffness matrix of shell and impactor, respectively
$[D']$	Elasticity matrix
$[B']$	Strain-displacement matrix
$[\bar{Q}]$	Transformed reduced stiffness matrix
$[C_e], [C]$	Element Coriolis matrix and Global Coriolis matrix
$[J]$	Jacobian Matrix.

$[K_e]$, $[K]$	Element elastic stiffness matrix and Global elastic stiffness matrix
$[K_{Re}]$, $[K_R]$	Element rotational stiffness matrix and Global rotational stiffness matrix
$[K_{\sigma e}]$, $[K_\sigma]$	Element geometric stiffness matrix, Global geometric stiffness matrix
$[M_e]$, $[M]$	Element mass matrix and Global mass matrix
$[S]$	Shape function matrix
$\{F(\Omega^2)\}$	Global vector of nodal equivalent centrifugal forces
$\{F_{ce}\}$, $\{F_e\}$, $\{F\}$	Element load vector due to centrifugal force, Element load vector due to externally applied load and Global vector of externally applied load
$\{M\}$	Moment resultant
$\{N\}$	In-plane stress resultant
$\{Q\}$	Transverse shear resultant
u, v, w	Displacement components in x, y and z directions, respectively.
$\vec{r}$	Position vector
$\hat{i}, \hat{j}, \hat{k}$	Unit vector along x-, y- and z-directions, respectively
$\vec{V}$	Velocity vector
u^o, v^o, w^o	Displacement along mid-surface of x-,y- and z-directions, respectively.
h_x, h_y, h_z	Fixed translational offset with reference to local coordinate system
x', y', z'	Global coordinate axes
b_o	Reference width
h	Thickness of conical shell
r_x	Radius of curvature in x-direction
r_{xy}	Radius of twist
r_y	Radius of curvature in y-direction
x, y, z	Local coordinate axes
$m_{imp}, \ddot{w}_{imp}$	Mass and acceleration of the impactor
β_c	A constant
$\vec{\Omega}$	Angular velocity vector
ϕ_o	Base subtended angle of cone
$\{\varepsilon^*\}$	Generalized strain vectors
$\{\varepsilon\}$	In-plane strain vectors

$\{\varepsilon^o\}$	In-plane strain vectors at the mid-surface
α	Local indentation
ρ	Mass density
α_m	Maximum indentation
$\xi, \eta,$	Natural co-ordinates
α_o	Reference minor radius
β_o	Reference major radius
χ, β	Rotational degrees of freedom
Ω	Rotational speed about z'-axis of inertial coordinate system
θ_x, θ_y	Rotations of cross-sections along the x- and y-axes, respectively
γ	Shear strain
γ^0	Shear strain at the mid-surface
$\{\varepsilon\}$	Strain vector
$\{\sigma\}$	Stress vector
Δt	Time step
$\hat{u}, \hat{v}, \hat{w}$	Translational degrees of freedom
$\{\gamma\}$	Transverse shear strain vectors
ϕ_{ve}	Vertex angle
$\Omega_x, \Omega_y, \Omega_z$	Angular velocity component along x-, y- and z-directions, respectively
K^*	Shear correction factor (=5/6)
α_{ep}	Even porosity factor
α_{up}	Uneven porosity factor
$[\varepsilon']$	Non-linear strain matrix
$\{\delta\}$	Global displacement vector=$\{\delta_s\}+\{\delta_p\}$
$\{\delta_e\}$	Element displacement vector
$\{\delta_p\}$	Small linear time dependent perturbation about the static displaced position $\{\delta_s\}$
$\{\delta_s\}$	Static equilibrium solution as a result of centrifugal force
$\{\sigma_o\}$	Initial stress vector
$\{\phi\}$	Eigen vectors

Δt	Time step
λ	Non-dimensional frequency
ς, χ	Local natural coordinates of the element
υ	Poisson's ratio
Ψ	Twist angle
ω	Non-dimensional frequency parameter
Ω	Non-dimensional speed of rotation (Ω'/ω_o)
Ω'	Actual angular speed of rotation
ω_n	Natural frequency of rotating shell $\varpi = \omega_n L^2 \sqrt{(\rho / E_1 h^2)}$

Numbering of Figures, Tables and Equations

Figures, tables and equations have been numbered in accordance with the chapters in which they appear in the thesis. Each table, figure and equation has two distinct numbers. The first number specifies the number of the chapter and the second number denotes to the actual number of the figure, table and equation in that chapter.

Representation of References

The list of references has been furnished at the end of the thesis. These references have been represented by the respective name of the author(s) along with the year of publication.

CONTENTS

LIST OF TABLES

LIST OF FIGURES

Dedicated to

My Family

CHAPTER 1

INTRODUCTION

1.1 GENERAL INTRODUCTION

1.1.1 PREAMBLE

Advanced materials are playing a pivotal role in the development of our modern society and culture. The scientific use of available base materials into various inorganic and organic compounds has made the path for developing the advanced polymers, engineering alloys, structural ceramics, etc. The structural development considering modern material is illustrated in Figure 1.1. Functionally graded materials (FGMs) are the advanced materials in the family of engineering composites made of two or more constituent phases with continuous and smoothly varying composition along the thickness. These advanced materials with engineered gradients of composition, structure and/or specific properties in the preferred direction/orientation are superior to homogeneous material composed of similar constituents. The mechanical properties such as Young's modulus of elasticity, Poisson's ratio, shear modulus of elasticity and material density, vary smoothly and continuously in preferred directions in FGMs. FGMs have been developed by combining the advanced engineering materials in the form of particulates, fibers, whiskers, or platelets. In the continuous drive to improve structural performance, FGMs are being developed to tailor the material architecture at microscopic scales to optimize certain functional properties of structures. These materials are gaining wide applications in various branches of engineering and technology with a view to make suitable use of potential properties of the available materials in the best possible way. This has been possible through research and development in the area of mechanics of FGMs for application in special nuclear components, spacecraft structural members, and high temperature thermal barrier coatings, etc. These materials possess numerous advantages that make them appropriate in potential applications. It includes a potential reduction of in-plane and through-the thickness transverse stresses, improved thermal properties, high toughness, etc. A typical FGMs consisting of metallic and ceramic components are well-known to enhance the properties of thermal-barrier systems, because cracking or delamination, which are often observed in conventional multi-layer systems are eliminated due to the smooth

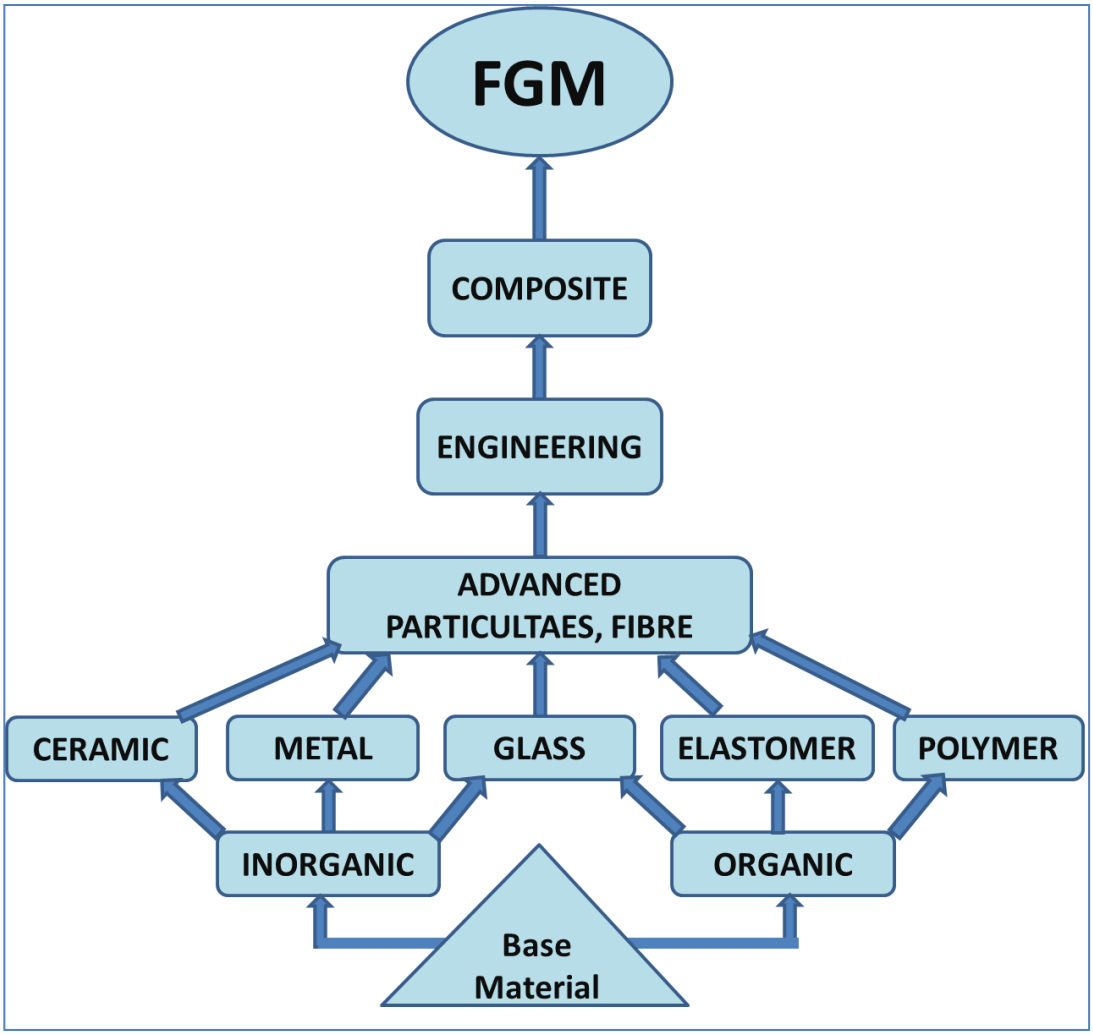

Figure.1.1 Representation of modern material hierarchy showing FGM

transition between the properties of the components. By varying percentage contents of volume fractions of two or more materials spatially, FGMs can be formed which will have desired property gradation in spatial directions. Delamination has been a problem of main concern in the reliable design of advanced fiber reinforced composite laminates. In laminated composites, the separation of layers caused by high local inter-laminar stresses result in destruction of load transfer mechanism, reduction of stiffness and loss of structural integrity, leading to final structural and functional failure (Reddy, 2004). FGM eliminates these problems of delamination or debonding and are gaining huge importance as an advanced materials used for innovative engineering applications. The constituents of FGMs can be metal-ceramic, ceramic-ceramic and metal-metal. Among those metal-ceramic is the most common FGM constituents, where the ceramic constituent acts as a good thermal resistance and metallic constituent bears the mechanical load. A continuously graded microstructure with metal-ceramic constituents is represented in Figure 1.2 schematically for illustration. FGMs have gained an important position as structural elements in comparison to traditional

metals and ceramics thereby opening a new horizon for the designers in the fields of aerospace, civil, marine and automobile industries since its introduction in the last two decades. A shell structure by virtue of its geometry in curved shape can carry functional loads mainly by its direct stresses lying in their plane considering bending action. This curve shape

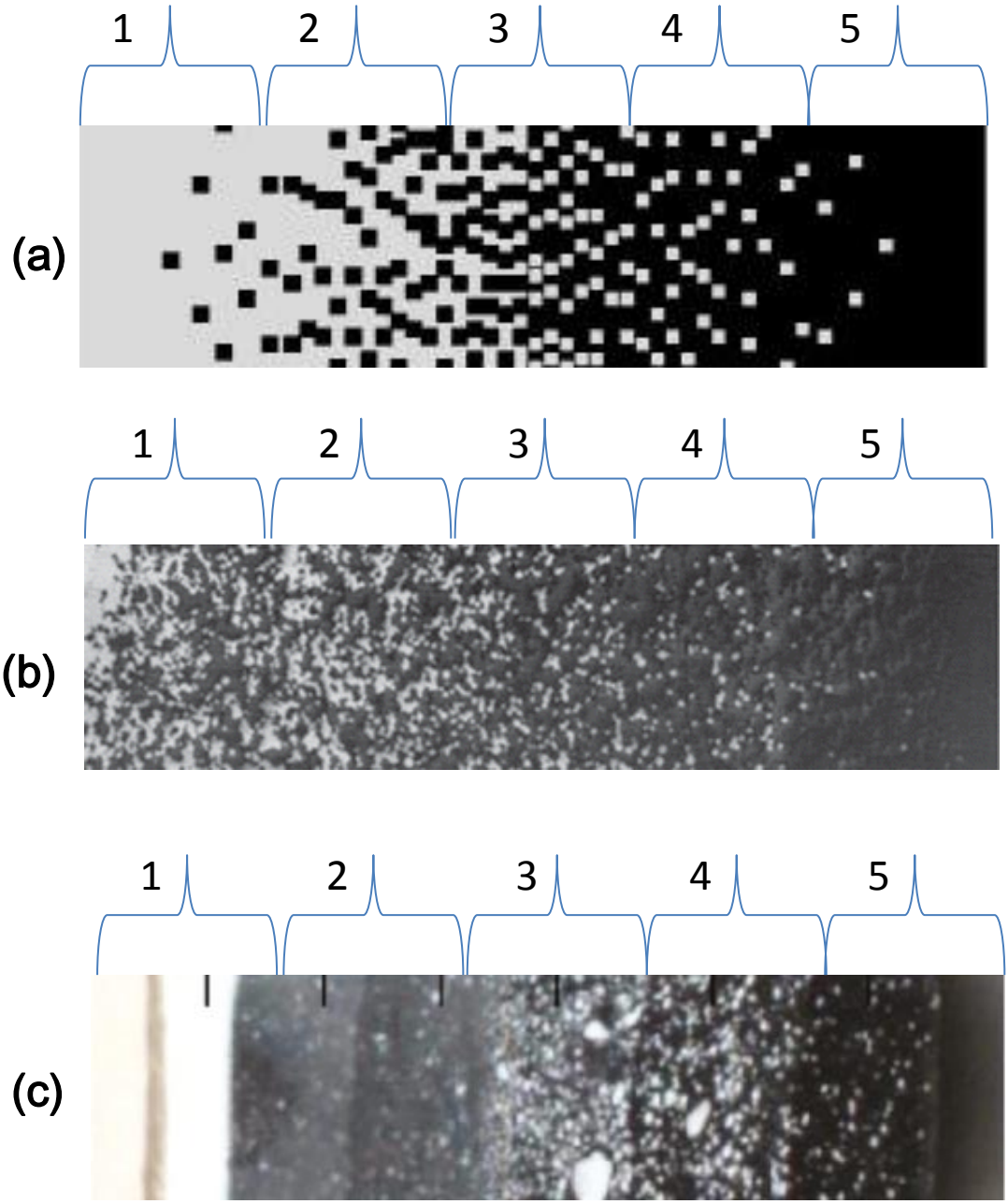

Figure. 1.2 Schematic of continuously graded microstructure with metal-ceramic constituents (a) Smoothly graded microstructure (b) Enlarged view and (c) Ceramic–Metal FGM where the zone 1 represnts ceramic phase, zone 2 represnts ceramic matrix with metal inclusions, zone 3 represnts the transition phase, zone 4 represnts metalic matrix with with inclusions, zone 5 represnts metalic phase.

of shells results in a non-coplanar surface which introduces both axial and flexural (bending and shear) forces thereby resulting in higher structural stiffness of the shell structures. The high strength of the shell structures combined with their ability to resist deformation have made them suitable for many engineering applications such as roofs, bridges, water and oil tanks, aeroplane and spacecraft fuselages, ship hulls, automobile bodies, turbomachinery and fan blades, defense structures etc. The shell action is a combination of membrane action due to in-plane direct stresses and bending action due to flexural stresses, which attribute to high strength of shell structures. A pretwisted conical shell is a special case wherein the curvature of mid-surface in one orthogonal direction is absent ($r_x = \infty$) and the curvature of the mid-surface in other orthogonal direction and the curvature due to twist are of non-zero magnitude ($r_y \neq 0$ and $r_{xy} \neq 0$). Thus the resulting surface of such pretwisted shell is conical helicoids. The pretwisted FGMs shells are structural elements of potential engineering importance. Most of the turbomachinery blade configurations used in practice like blades of fan, compressor, gas turbine, steam turbine, water turbine, marine propeller, windmill, helicopter and flow guide vane are typically very complicated because of its geometry. Neither cross-sectional area nor the planforms of such structures are perfectly rectangular. Hence, the geometric parameters may vary along the length. The design requirement necessitates that a blade must possess certain amount of pretwist and the functional requirement demands the rotational speeds as well. Among all shell geometries, conical shell profile is the most pragmatic form which is popularly employed in turbomachinery blades. Hence, the pretwisted FGMs shallow conical shell with low aspect ratio could be idealized as a turbomachinery blade.

In general, a turbomachinery blade is mounted on a rotating disc or hub wherein the rotation of blade root chord occurs about the blade axis. The pretwist angle of the blade causes coupling in bending planes. The disc and its attached blades rotate about an axis perpendicular to the plane of the disc. The failure of blade in turbomachines occurs frequently as a consequence of blade vibration problems. Therefore knowledge of these frequencies is of fundamental importance. The blades are also subjected to centrifugal body forces arising out of rotation. Due to centrifugal force, the initial stress system affects natural frequencies appreciably. Moreover, the effect of low velocity impact by a foreign object on the transient dynamic behaviour of the FGMs turbomachinery blade is of great concern due to relatively low through the thickness strength. Hence, all these complicated issues need to be analyzed for accurate prediction of dynamic characteristics of the turbomachinery blades. An effort is made in the present study to cover two broad areas namely, free vibration analysis and transient response due to low velocity normal impact.

1.1.2 INNOVATION AND HISTORY OF FGMs

The concept of gradation in material composition was first proposed for composites and polymeric materials by Shen and Bever (1972). Most of these materials were used as coating materials, in order to improve the bonding strength and to reduce thermal stresses. The first practical application of FGMs was carried out at National Aerospace Laboratories of Japan in 1984 to create square shells for the base of fuselage and hemispherical bowls for nosecones of a space plane. Present available industrial materials are not capable to withstand at very high-temperature gradients without losing their structural integrity. Hence, the unique idea of gradation of material composition was conceived by using a heat-resistant ceramic material on high-temperature side and tough metals with high-thermal conductivity on the other side, and thereby gradually varying the composition from ceramic to metal. These functionally graded materials have the advantage of the physical and chemical properties of the materials, thereby increasing the bond strength and reducing the interfacial stress and thermal stress.

The concept of FGMs to the modern materials science appears to be an advanced engineering invention and our capability to fabricate them for tailor made engineering application have built a new foundation in the high temperature structural application but the concept of FGM is not new. These classes of resources have been occurring in natures. Some examples of natural resources of FGMs are depicted in Fig. 1.3 showing the layer wise smooth transition of phases. Human and animal bones are having functionally grading in the depth direction. Even human and animal skin is also graded to provide certain toughness, tactile and elastic qualities as a function of skin depth and location on the body. The FGM constituents engineered by humans commonly involve two isotropic material phases although any number of chemically and spatially compatible configurations is possible. These components often include the engineering alloys of magnesium, aluminum, copper, titanium, steel, etc. and the advanced structural ceramics such as zirconia, alumina and silicon nitrite.

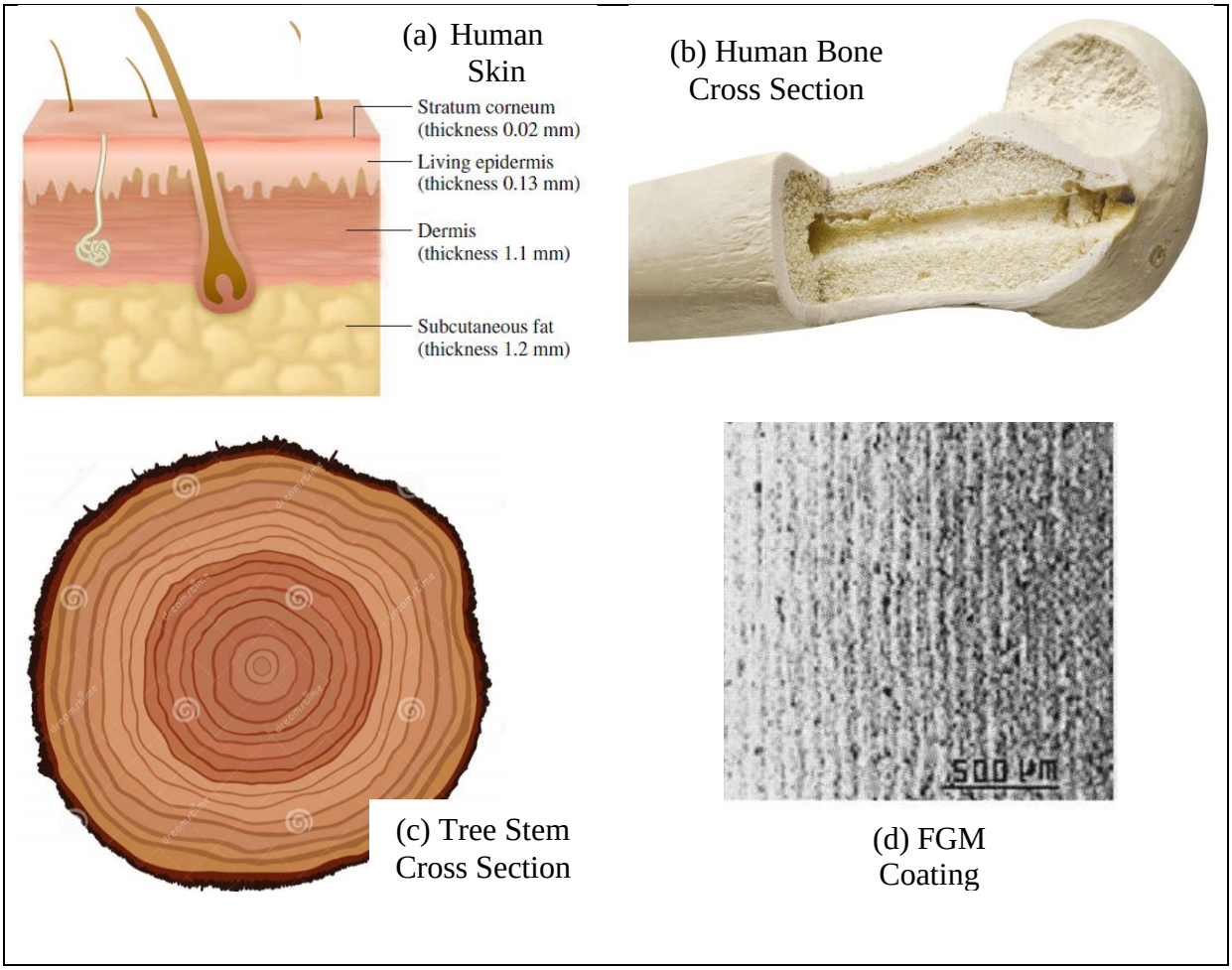

Figure 1.3 Some Example of naturally occurring FGM and Engineered FGM (a) human skin (b) human bone (c) tree stem (d) FGM coating

1.1.3 APPLCATION OF FGMs TO MODERN ENGINEERING

FGMs were essentially conceptualized for the need of high thermal gradient applications in aerospace and energy field. Due to its several advantages, recently FGMs are gaining potential applications in various sectors as shown in figure 1.4.

In the first application of space-plane project, FGMs like SiC/C, Ni-based alloy/ZrO_2, TiC/Ni were capable of withstanding high temperature fluctuations, thermal shocks and stress concentrations at the interfaces (Reddy, 2004). FGMs can also act as a thermal barrier system and are found in insulation of combustion chambers, rocket engine components and exhaust wash structures of space vehicles. FGMs with TiAl/SiC fibers are used in heat exchange panels, rocket nozzles, spacecraft truss structure, nose caps and leading edge of missiles and space shuttle. FGMs in space craft truss structure which can withstand huge mass of 200 metric tons with high temperature resistant and high gravity gradient features. Carbon nanotube (CNT) FGMs are thermally stable and exhibit excellent mechanical properties with high toughness, hardness, abrasion resistance, flexural strength which can be used in both

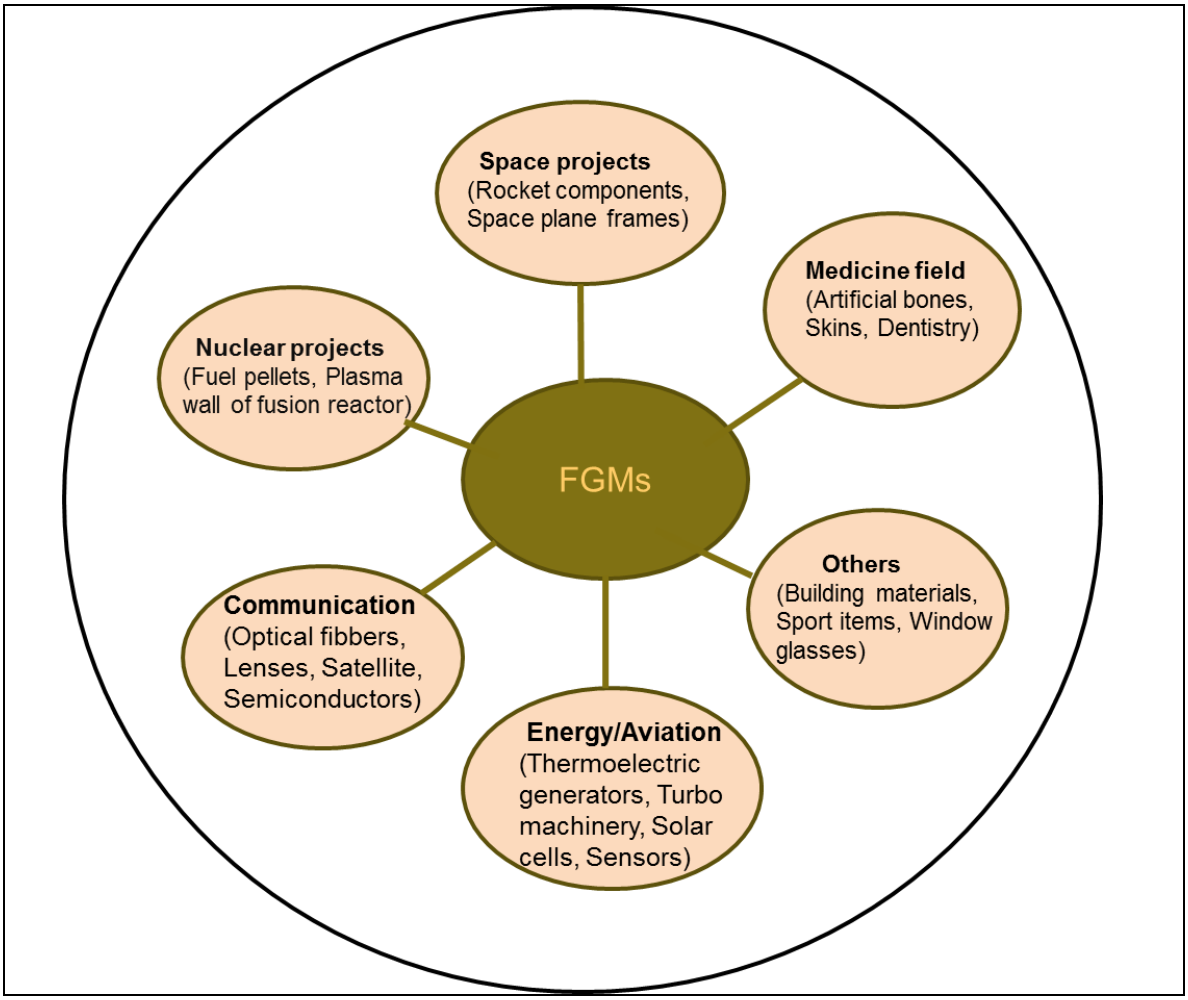

Figure. 1.4 Application areas of the FGMs in various fields.

high and low temperature zones. Most of the helicopters, fighter jets, defence tanks, weapons and armor suits are made of FGMs. These possess good damping properties with thermal and chemical inertness and hence used in Fuselage tanks, stabilizers, rotor blades, aircraft wings, cryogenic propellant tanks, gas turbine engines, nozzles and compressor components of fighter planes and helicopters. Ultra-light weights FGMs are used in defence sector to develop weapon platform, armor plates, barrier materials, bullet proof jackets, etc. Military submarine components like sonar domes composite piping systems are made with Glass/ Epoxy FGM, propulsion shafts with Carbon/Glass fiber FGM, Cylindrical pressure hulls with Graphite / Epoxy FGM and diving cylinders with Al/SiC FGM. Medical applications include the replacement of living tissues in human body with biopolymer FGMs. Orthopaedic and dental implants are usually composed of Collagen Hydroxyapatite (HAP) and titanium alloys. High density Polyethylene with a graded biopolymer coating is used in orthopaedic implants like total hip, shoulders and knee joint replacements (Watari et al., 1997 and Pompe et al., 2003). Nanohydroxyapatite reinforced polyvinyl alcohol (nanoHA/PVA) gels are used as an artificial articular cartilage repair material (Bharti et al., 2013). Ti-29Nb-13Ta-4.6Zr (TNTZ)

with graded microstructure is used as dental implants to reconstruct the masticatory function when tooth root is completely lost or extracted (Li et al., 2014). In photo electronic devices the refractive index modulation, diffusion length, energetic band gap and other properties can be adjusted using material gradation technique thereby enhancing the absorption capabilities and generation efficiencies. Hence, these are widely used in antireflective layers, optical fibers, optical lenses, photo-detectors, solar cells, optical sensors, semiconductor devices, computer circuit boards, cellular phones. FGMs embedded with piezoelectric layers are used in shape memory alloys. Automotive parts require high strength with resistance to crack, fracture and thermal shocks. FGM with Al/SiC are used as engine cylinder liners, flywheels, drive shafts and racing car breaks. Diesel engine pistons are made of SiCw/Al-alloy and leaf springs with Al/C FGMs. Few others include motor cycle drive sprockets, pulleys, shock absorbers, radiator end caps, etc. Most of the forming tools, cutting tools, forging and machine tools are manufactured using FGM. Few examples include lathe, drill press, broaching machine, gear shaper, hone etc. FGM is also used as a coating material which in turn reduces heat loss from engine exhaust system components like turbocharger casings, exhaust headers, exhaust manifolds, tail pipes and down pipes, thereby reducing consumption of coolant (Bohidar et al., 2014 and Kohli and Singh , 2015). Turbine wheel blades of gas turbine engine operating at 40,000 rpm are coated with TiAl/SiC FGM to provide thermal barrier. Also, anti-abrasion sports equipment's like tennis rackets, baseball cleats, sports shoes, racing bicycle frames, etc are developed based on the property of relaxation of stresses. Some of the comonly used FGMs include razor blades, cutting tools, eye glass frames, helmets, X-ray tables, automobile fuel tanks and pressure vessels, wind turbine blades, MRI scanner parts and cryogenic tubes, laptop cases, titanium watches, window glasses, camera tripods, etc.

In recent years, FGMs are found to be most advantageous over conventional structural materials and layered composites due to its continuous change in characteristic property. Though they have widespread applications in various sectors, there are few difficulties which have to be resolved by further research in this area. Mathematical modeling of the graded materials plays a vital role in predicting the accurate behaviour of FGM structure. Though experimental investigation methods are available to predict the individual thermo-physical material properties, microscopic studies have to be performed and quantitative relations have to be established for accurate evaluation of physical and thermal properties of graded materials. These relations used with various theories for analytical or numerical evaluation of various FGM structure responses.

FGMs have great potential in applications where the operating conditions are severe, including spacecraft heat shields, heat exchanger tubes, biomedical implants, flywheels, and plasma facings for fusion reactors, etc. Various combinations of the ordinarily incompatible functions can be implemented to create new materials for aerospace, chemical plants, nuclear energy reactors, etc. For example, a discrete layer of ceramic material is bonded to a metallic structure in a conventional thermal barrier coating for high temperature applications. However, the abrupt transition in material properties across the interface between distinct materials can cause large inter-laminar stresses and lead to plastic deformation or cracking (Redyy, 2004). These harmful effects can be eased by smooth spatial grading of the material constituents. In such cases, large concentrations of ceramic material are placed at corrosive, high temperature locations, while large concentrations of metal are placed at regions where mechanical properties need to be high. Later on, its applications have been expanded to also the components of chemical plants, solar energy generators, heat exchangers, nuclear reactors and high efficiency combustion systems. The concept of FGMs has been successfully applied in thermal barrier coatings where requirements are aimed to improve thermal, oxidation and corrosion resistance.

1.1.4 MANUFACTURING TECHNIQUES OF FGMs

FGMs can be classified into two types based on the distribution of constituent phases, namely continuous or discontinuous (step-wise or layered) gradation of materials. Also, based on manufacturing techniques these can be further grouped as thin and bulk FGMs (Makwana and Panchal, 2014 and Bohidar et al, 2014). Thin FGMs are manufactured by Physical Vapor Deposition (PVD), Self propagating High temperature Synthesis (SHS) method, Chemical Vapor Deposition (CVD), etc., which are generally used as surface coating material. While bulk FGMs are consolidated to form a volumetric bulk material and are manufactured using Powder Metallurgical (PM) technique, Solid Free Foam (SFF) technique, Centrifugal Casting method, etc. A comprehensive review of various processing techniques adopted to fabricate an FGM and its successful applications to numerical simulations were discussed by Kieback et al. (2003) and Gasik (2010). Recent research on improvement in the production methods has reduced the manufacturing cost and hence these FGMs are finding widespread applications in various sectors. Among all the available manufacturing techniques, sintering process is the most efficient way of manufacturing FGMs. However, it is very difficult to prepare perfect (porosity free) FGM structures by any one of the available manufacturing method. The porosities or micro-voids cannot be avoided during production of

FGM structures due to difference in the velocity and solidification of the material constituents

1.1.5 TURBOMACHINERY BLADES

The quest for advanced materials that could resist the high temperature and the associated dynamic stress generated on the turbomachinery components have grown in recent past to prolong the life of such turbomachinery blades. The structural, fatigue and resonance failure of the turbine or turbomachinery blades is still a precarious issue for researchers. The failure of the turbine blades is primarily found due to resonance of the vibrating frequencies. On the other hand the low cycle and high cycle fatigue due to high thermal gradient for conventional composite blades is key concern area in terms of blade life. Low velocity impact by external or internal mass can degrade the structural instability causing a cascading effect of such failure. Therefore the accurate prediction of the natural frequencies of the turbomachinery blades and low velocity impact performance became a topic of considerable research interest during the design phase of such components. There are numerous rotor and stator blades of different lengths and geometry are present in turbomachinery application. Therefore accurate prediction of the point of failure of such a system becomes extremely complex. Hence a detailed and careful design methodology is very essential to nullify the catastrophic failure during operation of such turbomachinery blades.

1.1.6 DYNAMIC BEHAVIOUR

Blades in the turbo machinery possess an essential role for the proper performance and maximizing efficiency. Apart from aerodynamically curvature of the turbo machinery blades the other geometrical dimensions are also important. During operation the dynamic behavior have considerable significance for safe operation and reliable component life. Turbo machinery blade commonly fails due to fatigue in the lower temperature stages of a turbine or axial flow compressor. This is due to the consequence of resonant vibrations resulting in large operating stresses, and can be costly both in terms of safety and maintenance of turbine engine. The dynamic loads on turbine blades can be generated from many sources, predominant one being the source of operation on which the turbine is designed. When the rotor blade passes past the nozzle of the stator, it experiences fluctuating lift and moments repeatedly at the nozzle passing frequency. The blades are very flexible members in the sense that a significant number of their natural frequencies may be in the region of the nozzle excitation frequencies.

Although a turbine is designed to avoid resonance at its steady operating speed, it experiences resonance several times during the starting up and shutting down of the turbine. This may give rise to shut down because of blade damage. Therefore, an in-depth knowledge of these frequencies is of prime importance to the designer of turbomachineries in order to prevent vibration and to ensure robust operation of the blades. However, an accurate prediction of these resonance conditions is usually very difficult because of their uncertainty of the excitation. Moreover, under resonance conditions what limits the blade vibration amplitude is the amount of damping available. In most cases, the damping is almost entirely aerodynamic and its assessment is just as uncertain as the excitation. Therefore the classic design practice for such blades has been mainly to rely on the knowledge of the blades' natural frequencies in order to escape from harmful resonance. The natural frequencies are found by modelling the blade as a pretwisted shallow conical shell with low aspect ratio including the geometric complexities. The natural frequencies are required to address at stationary as well as rotating condition. In addition, the transient response of FGM conical shells subjected to localized contact loading is of great concern in many advanced engineering structures and components, such as, the leading edge of an aircraft wing, fan blades in jet engine and turbine blades, because of the fact that impact situations with energies far below the penetration levels can cause severe damage to blades due to low transverse shear modulus and low inter-laminar shear properties. The deflection of to shell displacement due to impact can have adverse cascading effect on the turbomachinery blade clearance from casing. Hence, proper attention is needed for deep understanding of dynamic response of FGM pretwisted conical shells impacted at low velocity by an internal or external mass.

1.1.7 SHELL MODEL

The beam model was earlier applied to study the vibrations of turbomachinery blades based on the Euler-bernoulli‘s beam equation. However this approach yielded accurate results only when the width of the blades was negligible in comparison to its length (slender) and the blades are reasonably thick and only the first few vibration frequencies and mode shapes are required accurately. A beam model representing a turbine engine blade is highly inaccurate if the blade has a low aspect ratio, it is thin and where higher frequencies and mode shapes are needed. Chordwise bending and edgewise bending modes are completely lost by the beam representation. The beam theory is unable to predict chordwise bending modes and inaccurately estimates the torsional and spanwise bending frequencies of low aspect ratio

blades which are more likely to behave as plates or shells rather than as beams. Therefore, an accurate representation of such modes requires a two-dimensional analysis and a more correct model for turbomachinery blades may be made with pretwisted plates or shells. The plate and shells are thin structures wherein the thickness can be assumed to be negligible compared to the planar dimensions and have very small aspect ratios. This allows reducing a three-dimensional problem into an equivalent two dimensional-problem by applying the plane strain condition. The Kirchhoff–Love theory (classical plate theory) or the Mindlin–Reissner theory (first-order shear deformation theory) can be conveniently applied to model the displacement and strain fields in plate or shell structures. In general the shell theory is able to accommodate the curvature in the shell geometry and can be used to accurately model a pretwisted rotating shallow shell.

1.1.8 FINITE ELEMENT MODELLING

The solution to the engineering problems in the static and dynamic response of structures became much simplified with the introduction of computers in middle of the last century. Finite element method (FEM) is a numerical technique to evaluate approximate solutions of boundary value problems involving partial differential equations. This involves discretization of the domain into various smaller sub-domains, known as finite elements, generating element equations for each of the finite elements, assembling the element equations of all the elements at specified nodes to generate the global equations which are then solved using appropriate solution techniques. The vibration of the FGM shells involves many complex interactions between the shell structures, layer properties in thickness direction, internal strains, initial stresses and impact of foreign bodies. The solution of such problems is highly complex, computationally intensive and involves very large matrices. The availability of the modern high speed computers and finite element software code NASTRAN/PATRAN along with the commercial software packages like ANSYS, LS-DYNA, ICEM-CFD, COSMOS/M and ABACUS have been helpful in obtaining solution of problems in static and dynamic structural analysis, fluid flow, thermal analysis, electromagnetic study, seismic response along with different optimization process. The choice of a proper mathematical model, optimal and localized mesh size with proper use of solution technique and choice of solver is the prime requisite of any finite element simulation since it determines the closeness, reliability and its usability for modeling complex engineering applications. The turbomachinery blades are subjected to considerable centrifugal loading resulting in steady state deflections.

In the FGMs turbomachinery blades, the combined effects of twist angles, rotational speeds, arbitrary variation of cross-sectional areas along the length of the blade and varied material properties along the thickness are predominant which are needed to be addressed for accurate prediction of the blade dynamic characteristics by finite element method (FEM). Due to complicated nature, the blade dynamic problems can be solved exactly in some limited cases only. Under these circumstances, the finite element methods are appropriate for the dynamic analysis of stationary and rotating turbomachinery blades due to the fact that these numerical techniques are well suited to cope with the blades of general configurations. The analytical approaches are useful in obtaining physical understanding of the problem and in preliminary design, whereas finite element methods allow for refinement in the detailed design stage.

1.1.9 PRETWISTED SHALLOW CONICAL SHELL WITH FGM

In a weight sensitive and high thermal gradient application such as aircraft and turbine engine turbomachinery that demands very high fuel efficiency and longer life of the components minimizing the maintenance period, FGM materials are advantageous because of their light weight, high stiffness, strength and ability to withstand high thermal gradient. The layer wise isotropic FGM with continuous variation of ceramic to metal can be easily tailored to realize desired overall properties. In general the blades are fixed on the hub region. The blades are generally wide near the root section and there is a gradual chordwise reduction as it approaches the free end of a blade. An actual turbomachinery blade is thus in the form a cantilevered open conical shell with a trapezoidal planform and a variable curvature along the chordwise direction. There may also be a thickness variation along the length of the conical shell. In general, an initial twist is provided on the blades to vary the angle of attack for optimum blade performance, though the pretwist angle is limited by the reduction in the structural stiffness of the laminates (pretwist angle is maintained from 0^0 to 45^0). Earlier, the blades were modeled as cantilevered beams and plates which however yielded very inaccurate results in case of low aspect ratio and thin blades since they excluded the effects of the curvature effect along the chordwise camber. Later researchers have modeled them as cantilevered conical shells to account for the chordwise camber but the studies were limited owing to the difficulties in designing the complex geometry of FGM conical shells. However with the introduction of high speed computers the modeling became easier and the results generated were in better conformity with the experimental ones. The shell modeling using Kirchoff`s theory is justified only if the two dimensions (chord and shell thickness) are

negligible compared to the third dimension (length of the shell) and the change along the length direction can be neglected. The modeling of turbomachinery blades using shallow conical shell model yields accurate results only in the cases of low aspect ratios and low length to thickness ratio of the conical shells. Thus the FGM turbomachinery blades can be designed to have a predetermined static and dynamic behaviour. The FGM blades of pretwisted shallow conical shell can be manufactured in a powder manufacturing technique. Therefore, it is possible to produce complex geometries that results in efficient aircraft turbopropellers. Hence, as a pioneer to the application of FGMs in the critical parts of aero-engines or turbomachineries in general, extensive design study is required apart from the deformation and vibration characteristics. The investigation should necessarily be extended to include transient dynamic analysis due to low velocity impact. For the finite element based analysis of FGM blade structures, twisted conical shell element is capable of reproducing the blade behaviour more accurately and can also be applied to more realistic situations. The aerodynamic efficiency of engines can be maximized by introducing variable radius of curvature in the blades which is possible in case of conical shell form while the limitation of the same exists in cylindrical shell geometry.

1.1.10 TRANSIENT DYNAMIC RESPONSE

Transient dynamic response (sometimes called time-history response) is a technique used to determine the dynamic response of a structure under the action of any general time-dependent loads. The structural integrity and life of the turbomachinery blade depends on the ability of the blade to withstand the maximum stress levels at resonant and transient conditions as well as the ability to mitigate the external impact on the blade. The performances of such FGM conical shell blade in the turbomachinery are dependent on the ability to withstand in the high temperature zone as well as external/internal impact on the blade. A deep understanding of the transient dynamic performances is required for potential use of such materials in jet engine fan and compressor blades. However, an accurate estimation of the deformations is usually very difficult because of many complexities involved in such structural elements under preload being subjected to centrifugal forces which develop steady state stresses once the operating conditions are attained and may aggravate the damage due to low velocity impact leading to degradation in the stiffness and strength of the structure. The transient dynamic data provides a foundation for prediction of failure due to impact damage.

1.1.11 LIMITATIONS/DISADVANTAGES OF FEM

The finite element method is an approximate solution method and the correctness of the simulation results are primarily depends on the choice of the finite element used in the discretization process and the use of proper boundary conditions and type of solver. The solution to the differential equations may obtained at the nodal or elemental points and sometimes may not be representative of the response of an entire domain in case of complex geometries, irregularities in shape, curvature, unsymmetrical stress distribution or non-linear behavior. Thus it becomes extremely essential to ascertain that the finite element modeling conforms to each and every aspect of a complex problem. The accuracy of the FEM technique needs to be thoroughly validated against experimental results incorporating numerous cycles of mesh enhancement/refinement and error analysis until a required degree of precision is arrived at in what is known as an adaptive finite element analysis. In addition most of the finite element simulations are computationally intensive and may require large computation time and resources which must also be optimized for improved design cycle time while considering total cost incurred.

1.2 LITERATURE REVIEW

FGM structures have been recently used in turbomachinery blades for their associated behavior during service especially in the aerospace, aviation, marine and automotive industries. A good amount of research knowledge has been made available in numerous monogram, review and different scientific journals. The literature related to the analysis, design and modeling of FGM plate and shells covers a wide area of research. The shallow shell has a lesser thickness compared to its other dimensions and in which deformations are not large compared to thickness. Shell structures of twisted geometry have immense applications in the area of mechanical structural components. The literatures related to design, modeling, analyses and construction of shell structures cover a broad area of research, especially in the context of the present work. Significant development has taken place in usage of these specialized structures with the introduction of functionally graded materials. Accordingly, the main emphasis is given with reference to the dynamics of FGM structures in respect of finite element modelling, dynamic response of pretwisted rotating FGM plates and shells under low velocity impact.

Extensive applications of shell forms as turbo-machinery blade structures have a long history although plethora of investigations made on the properties of shell structures initiated

about hundred years ago. The historical review on the course of shell research and design was presented by Rotter (1998) while the principle and techniques of vibration portrayed by Meirovitch (1997). Vibration characteristics of turbomachinery blade profiles are presented by Rao (1991). Isotropic shells was initially used for research later on the focus was given to the composite laminated shell, but at high thermal gradient the delamination is major concern for the composite shell. Therefore since the introduction of FGMs from last two decades lot of attention is given on FGMs shells and structures. FGM materials are gaining wide applications in various branches of engineering and technology with a view to make suitable use of potential properties of the available materials in the best possible way. This has been possible through research and development in the area of mechanics of FGMs for the present day modern technologies of special nuclear components, spacecraft structural members, and high temperature thermal barrier coatings, etc. De-bonding or delamination are the main problem of advanced fiber reinforced composite laminates where the separation of layers caused by high local inter-laminar stresses reduces the stiffness and structural integrity no longer maintained. FGMs have the potential to eliminate these problems and due to these advantages FGMs have gained huge importance as an advanced material. The most common FGMs are metal-ceramic constituents, where the ceramic part has good thermal resistance and metallic part has superior structural support. The turbo-machinery blade materials with FGM have all these advantages compare to the composite and conventional material considering both thermal and structural aspect.

Review articles like those by Birman and Byrd (2007), Liew et al. (2011), Alijani and Amabili (2014), Jha et al. (2013), Thai and Kim (2015), Swaminathan and Naveenkumar (2015), Gupta and Talha (2015), Liew et al. (2015), Swaminathan and Sangeetha (2017) covered much of the research done within last two decades while very little attention was given to FGM conical shells prior to that except reported by Zhao and Liew (2011a) and Tornabene et al. (2014). In concurrence to above, the different shell theories, shell geometries, etiquette of dynamic analysis and the different analyses technique are discussed from Section 1.2.1 to Section 1.2.4. After that the literature review is focused on latest shell research followed by FGM porous structures which are discussed subsequently in Section 1.2.5 and Section 1.2.6, respectively. Finally in Section 1.2.7, the critical discussion of existing literatures is discussed. Each section is ramified into different sub-sections for intense presentation and ease of reading.

1.2.1 PLATE AND SHELL THEORIES

Shell structures are represented by three-dimensional structures bounded by two, relatively close curved surfaces. Most of the shell theories (thin and thick, deep and shallow) reduce the three-dimensional elasticity equations to the two-dimensional representation. This is generally done by eliminating the coordinate normal to the shell surface in the development of the shell equations. The accuracy of thin and thick shell theories can be established if these theories are compared to the three dimensional theory of elasticity. In general, the behavior of functionally graded (FG) plates/shells under mechanical and thermal loadings can be predicted using either three-dimensional (3D) elasticity theory or equivalent single-layer (ESL) theories. The ESL models are derived from the 3D elasticity theory by making suitable assumptions on the kinematics of deformation or a state of stress through the thickness of plates/shells (Reddy, 2004). These ESL theories may account for both shear and normal deformation effects depending on the level of assumptions. The simplest ESL model is the classical plate theory (CPT), also known as Kirchoff theory (1850), which ignores both shear and normal deformation effects. Thus it is only suitable for thin FG plates/shells. The next theory in the hierarchy of ESL models is the first-order shear deformation theory (FSDT) developed by Mindlin (1951). The FSDT accounts for the shear deformation effect by the way of a linear variation of in-plane displacements through the thickness. A shear correction factor is therefore required. The shear correction factor is difficult to determine since it depends not only on geometric parameters but also on the loading and boundary conditions. To avoid the use of the shear correction factor, higher-order shear deformation theories (HSDTs) were introduced. The HSDT can be developed by expanding the displacement components in power series of the thickness coordinate. In principle, the theories developed by this mean can be made as accurate as desired by including a sufficient number of terms in the series. Among the HSDTs, the third-order shear deformation theory (TSDT) of Reddy (1984) is the most widely used one due to its simplicity and accuracy. In this segment the gradual sequence related to shell research is described. This section is further ramified into distinct segments for clear understanding of the systematic and chronological progress of the different aspects of shell research.

1.2.1.1 Classical Plate Theory (CPT)

The classical plate theory (CPT) Model is primarily based on the Kirchhoff–Love hypothesis which tells the straight lines remain straight and perpendicular to the mid-plane after deformation. These forms suggest the disappearance of the shear and normal strains, and

thus the shear and normal deformation effects are not considered. The CPT is the simplest ESL model and it is only suitable for thin FG plates/shells where the shear and normal deformation effects are not required to consider. The CPT is preferably used for FG shell model due to its simplicity. Loy et al. (1999) studied the vibration of FG cylindrical shells with simply supported boundary conditions using the CPT and Rayleigh–Ritz method. A similar approach was adopted by Arshad et al. (2007) to investigate the vibration characteristics of FG cylindrical shells under three different types of volume fraction laws. The vibration characteristics of FG cylindrical shells under various boundary conditions were examined by Pradhan et al. (2000) using the CPT and Rayleigh method. This problem was re-examined by Naeem et al. (2010) using Ritz method. Nonlinear forced vibrations of FG doubly curved shallow shells were investigated by Alijani et al. (2011) using the CPT with von Karman assumptions and the multi-modal Galerkin discretization. Du et al. (2014) studied the nonlinear vibration of FG cylindrical shells under excitation based on the CPT with von Karman assumptions in combination with a multiple scale method. Du and Li (2013) studied the nonlinear vibration response of FG cylindrical shells in thermal environments following a similar approach. Ebrahimi and Najafizadeh (2014) studied the free vibration of FG cylindrical shells using the CPT in conjunction with the generalized differential quadrature and generalized integral quadrature methods. The nonlinear behavior of imperfect eccentrically stiffened FG panels resting on an elastic foundation was studied by Nguyen and Tran (2013) using the CPT and Lekhnitsky smeared stiffener technique. Duc and Quan (2012, 2015) performed the nonlinear dynamic analysis of imperfect FG doubly curved shallow shells resting on an elastic foundation subjected to mechanical and thermal loadings using the CPT with von Karman assumptions. It is worth noting that the stretching–bending coupling exists in FG plates due to the variation of material properties through the thickness. Therefore, the neutral surface of the FG plate does not coincide with its middle one. This coupling could be eliminated if the governing equations were derived based on the neutral surface. The validity of the report was established by Zhang and Zhou (2008) where the CPT for FG plates were formulated based on the neutral surface, and the governing equations of motion in the form of isotropic plates were derived. Kar et al. (2017) evaluated the effect of different temperature load on thermal post buckling behaviour of functionally graded shallow curved shell panels using CPT model.

1.2.1.2 First-Order Shear Deformation Theory (FSDT)

The FSDT established by Mindlin (1951) incorporating for the shear deformation effect in the linear variation of the in-plane displacements through the thickness. It is well-known that the theory proposed by Reissner (1945, 1947) also explanations for the shear deformation effect. However, the Reissner theory is not similar with the Mindlin theory like erroneous perception of many researchers through the use of misleading descriptions such as ‘‘Reissner– Mindlin plates’’ and ‘‘FSDT of Reissner’’. The major difference between two theories was established by Wang et al. (2001) by deriving the bending relationships between Mindlin and Reissner quantities for a general plate problem. Since the Reissner theory was based on the assumption of a linear bending stress distribution and a parabolic shear stress distribution, its formulation will inevitably lead to the displacement variation being not necessarily linear across the plate thickness (Wang et al., 2001). Thus, it is incorrect to refer to the Reissner theory as the FSDT which implies a linear variation of the displacements through the thickness. Another difference between two theories is that the normal stress which was included in the Reissner theory was omitted in the Mindlin one (Panc, 1975). The FSDT model for FG shells first used by Reddy and Chin (1998) to determine the dynamic response of FG cylinders and plates exposed to thermal loadings. Shahsiah and Eslami (2003, 2003a) proposed analytical solutions for the buckling temperature of FG cylindrical shells with simply supported boundary conditions considering to two types of thermal loadings using the FSDT and Navier solution. The geometrically nonlinear analyses of FG shells were reported by Arciniega and Reddy (2007) using the finite element method wherein the kinematic of shell was based on FSDT. More studies on geometrically nonlinear bending behavior of FSDT shells were reported by Barbosa and Ferreira (2009) using Marguerre shell element while Sheng and Wang (2011) used four-order Runge–Kutta numerical method. Behjat et al. (2009) calculated the static bending, free vibration and transient responses of FG piezoelectric cylindrical panels subjected to mechanical, thermal and electrical loadings using the FSDT and the finite element method. The static and dynamic bending behavior and free vibration characteristics of FG doubly curved panels for combined mechanical and thermal loadings were studied by Kiani et al. (2012) using the FSDT and analytical hybrid Laplace–Fourier transformation. Isvandzibaei et al. (2016) presented a study on the vibration of a supported thick-walled cylindrical FG shell subjected to pressure loading where the governing equations derived from the FSDT were analytically solved for the natural frequency of FG cylindrical shells under various boundary conditions using Ritz method. Xiang et al. (2015) implemented the meshless local collocation method and FSDT to

calculate the natural frequency of FG cylindrical shells. Pradyumna and Nanda (2013) investigated the transient response of FG plate, where the nonlinear governing equations were derived from the FSDT with von Karman assumptions and solved by using an eight-noded C^0 continuous element. The time dependent dynamic response was solved by Newmark integration scheme combined with the modified Newton–Raphson iteration method. Talebitooti (2018) presented the thermal effect on free vibration of ring-stiffened rotating functionally graded conical shell with clamped ends using FSDT.

1.2.1.3 Third-Order Shear Deformation Theory (TSDT)

The TSDT developed by Reddy (1984) for laminated composite plates incorporating the transverse shear deformation effect satisfying the zero-traction boundary conditions on the top and bottom surfaces of a plate where the shear correction factor can be ignored. Levinson (1980) presented an accurate and simple theory for statics and dynamics analysis of elastic plates based on Kirchhoff-Love hypothesis, i.e. that straight lines normal to the undeformed mid-surface of the plate remain straight and normal to the deformed mid-surface, was completely abandoned. The displacement field of Reddy (1984) theory is similar with that of Levinson (1980) theory. The equations of motion of two theories are different from each other because Levinson (1980) used the equilibrium equations of the FSDT which are variationally inconsistent while Reddy (1984) derived those equations by the variational approach. The TSDT are also commonly used for FG shells. Shen (2002) studied the postbuckling behavior of FG cylindrical panels in thermal environments subjected to axial compression while the similar work by lateral pressure was reported by Shen and Leung (2003). Shen (2003) extended his own work for the FG cylindrical shells. Oktem et al. (2012) numerally analyzed the bending pattern of simply supported FG plates and doubly-curved shells using the TSDT and boundary-discontinuous generalized double Fourier series approach. Van and Duc (2014) examined the nonlinear response of FG curved panels resting on an elastic foundation. Analytical solutions for the load–deflection curve of simply supported panels under mechanical and thermal loadings were provided using the TSDT and Galerkin method. Duc et al. (2015) extended the previous work Van and Duc (2014) to FG cylindrical shells surrounded by an elastic medium under mechanical and thermal loadings. Kapuria et al. (2015) developed a quadrilateral shallow shell element for the dynamic analysis of FG plates and shells using the TSDT. Hong et al. (2017) presented the nonlinear dynamic response of eccentrically stiffened FGM plate using Reddy's TSDT in thermal

environment. Recently Cong et al. (2018) developed a new approach to investigate nonlinear dynamic response of sandwich auxetic double curves shallow shells using TSDT.

1.2.1.4 Higher- Order Shear Deformation Theory (HSDT)

The HSDTs account for higher-order variations of the in-plane displacements or both in-plane and transverse displacements (i.e.quasi-3D theory) through the thickness, and consequently, capturing the effects of shear deformation or both shear and normal deformations. The HSDTs can be developed using polynomial shape functions or non-polynomial shape functions. Patel et al. (2005) studied the free vibration characteristics of FG elliptical cylindrical shells using a quasi-3D theory and the finite element method. Matsunaga (2008) developed a quasi-3D theory for the buckling and free vibration analyses of FG shallow shells. Pradyumna and Bandyopadhyay (2008) developed a four noded C^0 continuous shell element with nine DOFs per node for free vibration analysis of functionally graded curved panels using a higher-order finite element formulation. They extended the previous work for dynamic instability (2009) of FG curved panels. The non-polynomial function was first used by Levy (1877) with a sinusoidal function to develop a refined theory for thick isotropic plates. The sinusoidal function was later adopted by Stein (1986) to develop a five-unknown sinusoidal shear deformation theory (SSDT) for isotropic plates while Touratier (1991) presented for the laminated composite plates. The HSDT was widely used to study the dynamic behavior of FG structures. Some of the work can be found for the vibration of FG plates (Zenkour, 2005), bending of FG plates (Zenkour, 2006), thermal bending of FG plates resting on an elastic foundation (Zenkour and Sobhy, 2011).The bending relationships between the HSDT and CPT quantities were derived by Zenkour (2012) for FG Levy-type plates. Mantari et al. (2012, 2012a) combined exponential and trigonometric functions to develop a HSDT for FG plate (2012a) and FG doubly curved shells (2012). Recently Zghal et el. (2018) presented free vibration analysis of carbon nanotube-reinforced functionally graded composite shell structures using HSDT.

1.2.1.5 Simplified Theories

It is well known that the HSDTs and quasi-3D theories developed by expanding the displacements in power series of the thickness coordinate are more computationally expensive since each additional power of the thickness coordinate will induce an additional unknown to the theory. Therefore, there is a need to simplify the existing HSDTs and quasi-3D theories or to develop simple theories with fewer unknowns. Senthilnathan et al. (1987)

implimented the simplified TSDT to laminated composite plates and reported that the simplified theory accurately predicted the buckling load of laminated composite plates. Thai and Kim (2013) worked on FG plate using the simplified TSDT. Shimpi (2002) developed a refined plate theory (RPT) for isotropic plates by dividing the displacements into the bending and shear components. The RPT contains only two unknowns compared to three unknowns in the case of the FSDT and TSDT, but it has sufficient accuracy to predict the global responses of isotropic plates (Shimpi-2002, Shimpi and Patel-2006a, Thai and Kim-2013, Thai et al.-2013) and orthotropic plates (Thai and Kim-2012, 2012a, Shimpi and Patel-2006, Kim et al.-2009, Thai et al. -2013a). The RPT was also widely applied to FG plates (Mechab et al.-2010, Ahmed et al.-2011, Benachour et al.-2011, Thai and Kim-2011, Thai and Choi-2012, 2012a, Thai et al.-2013, Bouiadjra et al.-2012, Thai and Choi-2011,2014) and FG sandwich plates (Abdelaziz et al.-2011, Hadji et al.-2011, Bourada et al.-2012). Using similar assumptions of Shimpi (Shimpi-2002), several four-unknown shear deformation theories were developed using different shape functions. For example, Mechab et al. (2013) proposed a four-unknown HSDT for FG plates while and El et al. (2011) established for FG sandwich plates incorporating hyperbolic functions. By dividing the transverse displacement into the bending, shear and stretching parts, Thai and Kim (2013a) proposed a five-unknown quasi-3D theory for FG plates using the sinusoidal function. Several similar five-unknown quasi-3D theories were also proposed using different shape functions such as hyperbolic functions (Thai et al.,-2014, Hebali et al.,-2014, Bessaim et al.,-2013, Bennoun et al.,-2016), sinusoidal functions (Mantari and Soares, 2014), combined hyperbolic and exponential functions (Belabed et al.-2014, Mantari and Granados -2015) and combined hyperbolic and sinusoidal functions (Mantari et al., -2014).

1.2.1.6 3D Elasticity Theory

The development of exact solutions of 3D elasticity theory is very useful in assessing the accuracy and validity of ESL models. Mian and Spencer (1998) established exact solutions for FG and laminated composite plates. Tanigawa (1999) developed exact 3D solutions for thermal stress of FG simply supported plates under partial heating. Cheng and Batra (2000) derived exact solutions for 3D bending analysis of FG clamped elliptic plates under thermal loadings using an asymptotic expansion method. Reddy and Cheng (2001) also implemented the asymptotic expansion method to derive exact solutions for 3D bending analysis of FG simply supported plates under thermal loadings. On the other hand Vel and Batra (2002) used a power series method to derived exact solutions for the 3D bending

analysis of FG simply supported plates subjected to thermal and mechanical loadings. Alibeigloo (2010) analyzed the 3D bending behavior of FG plates under thermal and mechanical loadings where the exact solutions for the temperature, stress and displacement were derived for simply supported plates using the state-space method. Vel and Batra (2004) reported 3D exact solutions technique for free and forced vibrations of FG simply supported plates using the power series method. Natural frequencies, displacements and stresses were determined by exact solutions method and comparative studies for with ESL models were also portrayed. Vel (2010) extended the previous work Vel and Batra (2004) to FG anisotropic cylindrical shells. 3D elasticity theory and the generalized DQM method were also used for determining the free vibration characteristic of FG cylindrical shells surrounded by an elastic medium (Kamarian et al., 2014). Recently Hajlaoui et al. (2017) used the 3D elasticity theory for nonlinear dynamics analysis of FGM shell structures and Brischetto (2018) worked for the correct imposition of transverse shear/normal load conditions in FGM shells by 3D layer-wise model.

1.2.1.7 Unified Formulation

The unified formulation proposed by Carrera (1995) for multilayered composite structures was a hierarchical formulation which offers a procedure to describe and implement numerous plate/shell theories as well as finite elements in a unified manner by referring to a few fundamental nuclei. Several other theories developed in the framework of the Carrera unified formulation (CUF) by expanding the displacement variables in the thickness coordinate using Taylor's expansions of N-order with N being a free parameter. Cinefra et al. (2010) used the CUF to the thermal-mechanical analysis of FG shells. Complete details about the development and applications of the CUF reported in the books authored by Carrera et al. (2011, 2011a, 2014). Neves et al. (2013) extended the application of the CUF and the collocation method for free vibration analysis of functionally graded shells accounting for through-the-thickness deformations. Cinefra et al. (2012) combined the CUF and the mixed interpolation of tensorial components (MITC) technique to develop a nine-node shell element for the bending analysis of FG plates/ shells under transverse loadings. The MITC overcomes the locking phenomenon and all refined models contained in the CUF can be implemented in their proposed shell element. Ayoubi and Alibeigloo (2017) used the CUF technique for three-dimensional transient analysis of FGM cylindrical shell subjected to thermal and mechanical loading. Recently Beni and Dehkordi (2018) extended the Carrera

unified formulation in polar coordinate for analysis of circular sandwich plate with FGM core using GDQ method.

From literature review, it is observed that for ESL models, the CPT is extensively used to predict the nonlinear and postbuckling responses of FG thin plates/shells. All the effects of temperature, initial geometric imperfections and geometric nonlinearity can be easily included in the CPT model since it is the simplest one among the ESL models. Although the CPT ignores the shear and normal deformation effects, it can provide acceptable predictions for the thin plates/shells where the effects of the shear and normal deformations are insignificant.

Among the shear deformation theories, the FSDT and TSDT were widely used for the modeling and analysis of FG plates/shells. This might be due to the fact that both FSDT and TSDT was developed long time ago compared with other HSDTs having the same number of unknowns.

1.2.2 REVIEW OF SHELL GEOMETRY

Shells may have different geometries based mainly on their curvature characteristics. In most shell geometries, the fundamental equations have to be treated at a very basic level and are dependent upon the choice of the coordinate system (Cartesian, Polar, curvilinear or spherical), characteristics of the Lame parameters (constant or a function of the coordinates) and curvature (constant or varying curvature). A plenty of research has been carried out by researchers utilizing different shell geometries.

1.2.2.1 Shells of Revolution

The basic form for shell of revolution can be found in the book by Soedel and Qatu (2005). Free vibration analysis of functionally graded panels and shells of revolution performed by Tornabene and Viola (2009). Tornabene and Viola (2009a) extend the work by performing the free vibrations of four-parameter functionally graded parabolic panels and shells of revolution. Later Tornabene (2009) performed free vibration analysis of functionally graded conical, cylindrical shell and annular plate structures with a four-parameter power-law distribution. Qu et al. (2013) established a unified formulation for vibration analysis of functionally graded shells of revolution with arbitrary boundary conditions. Recently Li et al. (2017) used a modified Fourier-Ritz approach for the free vibration of functionally graded cylindrical, conical, spherical panels and shells of revolution with general boundary condition

while Wang et al. (2017) used a semi-analytical method to analyze the vibration of functionally graded (FG) sandwich doubly-curved panels and shells of revolution.

1.2.2.2 Cylindrical and Doubly Curved Shells

The shell geometry being addressed by most researchers is the closed cylindrical shell wherein the axis of revolution is parallel to the centre line. The widespread usage and ease of manufacturing of cylindrical shell are the main reason for such attention. For doubly curved shells, the curvatures of mid-surface in two orthogonal directions (r_x and r_y) and the curvature of twist (r_{xy}) are non-zero with a Lame's constant parameters. Pioneer work on vibration of functionally graded cylindrical shells was reported by Loy et al (1999). Pradhan et al. (2000) performed the vibration characteristics of functionally graded cylindrical shells under various boundary conditions. Dynamic stability analysis of functionally graded cylindrical shells under periodic axial loading was investigated by Ng et al. (2001) while for embedded in elastic medium was performed by Sheng and Wang (2008). Sofiyev and Schnack (2004) worked on the stability of functionally graded cylindrical shells under linearly increasing dynamic torsional loading. Haddadpour et al. (2007) examined the free vibration analysis of functionally graded cylindrical shells including thermal effects. Non-linear analysis of dynamic stability for functionally graded cylindrical shells under periodic axial loading performed by Darabi et al. (2008). Chorfi and Houmat (2010) worked on non-linear free vibration of a functionally graded doubly-curved shallow shell of elliptical plan-form. Nonlinear vibrations of functionally graded doubly curved shallow shells with a rectangular base are investigated by Alijani et al. (2011) using Donnell's nonlinear shallow-shell theory. Oktem et al. (2012) performed the static response of functionally graded plates and doubly-curved shells based on a higher order shear deformation theory. Tornabene and Viola (2013) examined the static analysis of functionally graded doubly-curved shells and panels of revolution. Bich et al. (2013) performed the nonlinear dynamic analysis of eccentrically stiffened imperfect functionally graded doubly curved thin shallow shells. Tornabene and Ceruti (2013) used GDQ method to study the mixed static and dynamic optimization of four-parameter functionally graded completely doubly curved and degenerate shells and panels. Later on Tornabene et al. (2014) worked on free vibrations of free-form doubly-curved shells made of functionally graded materials using higher-order equivalent single layer theories. Gong et al. (1999) studied the elastic response of functionally graded cylindrical shells subjected to low-velocity impact. Zare et al. (2017) performed the free vibration analysis of functionally graded porous doubly-curved shells based on the first-order

shear deformation theory while Punera and Kant (2017) investigated the free vibration characteristics of functionally graded open cylindrical shells based on several refined higher order displacement models. Recently Ansari et al. (2018) worked on the static analysis of doubly curved singly ruled truncated FGM cone.

1.2.2.3 Conical Shells

Conical shell is considered as a special type of shell of revolution. It is formed by revolving a straight line around an axis that is not parallel to the centre line. Parametric instability of conical shells by the generalized differential quadrature method was determined by Ng et al. (1999). Naj et al. (2008) studied the thermal and mechanical instability of functionally graded truncated conical shells. Sofiyev and Schnack (2004) studied the stability of functionally graded truncated conical shells subjected to aperiodic impulsive loading later Sofiyev (2009) worked on vibration and stability behavior of freely supported FGM conical shells subjected to external pressure. Zhao and Liew (2011a) performed the free vibration analysis of functionally graded conical shell panels by a meshless method. Viola et al. (2014) studied static analysis of functionally graded conical shells and panels using the generalized unconstrained third order theory coupled with the stress recovery. Sofiyev and Kuruoglu (2016) worked on the domains of dynamic instability of FGM conical shells subjected to time dependent periodic loads.

Recently Sofiyev and Osmancelebioglu (2017) studied the free vibration of sandwich truncated conical shells containing functionally graded layers within the shear deformation theory while the thermal effect on free vibration of ring-stiffened rotating functionally graded conical shell with clamped ends was performed by Talebitooti (2018).

1.2.2.4 Spherical Shells

Spherical shells are another special case of shells of revolution. For these shells, a circular arc, rather than a straight line, revolves about an axis to generate the surface. If the circular arc is half a circle and the axis of rotation is the circle's own diameter, a closed sphere will form. If a segment of this shell is taken, an open spherical shell will be produced. If the dimensions of the segment are small when compared with the radius then it will regarded as shallow spherical shell. Shallow spherical shells can have rectangular, circular (spherical caps) or other planforms. These shallow shells can have both rectangular orthotropy as well as spherical orthotropy. Nath and Alwar (1978) first performed the non-linear static and dynamic response of spherical shells. Woo and Meguid (2001) worked on

the nonlinear analysis of functionally graded plates and shallow shells. Shahsiah et al. (2006) studied the thermal instability of functionally graded shallow spherical shell. Ganapathi (2007) determined the dynamic stability characteristics of functionally graded materials shallow spherical shell. Nonlinear static and dynamic buckling analysis of the functionally graded shallow spherical shells including temperature effects was studied by Bich and Van (2012). Recently, Brischetto (2018) applied a 3D layer-wise model for the correct imposition of transverse shear/normal load conditions that can be used for FGM spherical shells.

1.2.2.5 Shallow Shells

It should be noted that only shells on a circular planform produce a shell of revolution. The shallow shells are the open shell wherein both in-plane displacement and transverse shear forces are very small compared to the radius of curvature. In this arena, Woo and Meguid (2001) investigated nonlinear analysis of functionally graded plates and shallow shells while in another work Woo and Meguid (2005) again studied the thermo mechanical post buckling analysis of moderately thick functionally graded plates and shallow shells. Matsunaga (2008) used 2D higher-order deformation theory to study the free vibration and stability of functionally graded shallow shells while Alijani et al. (2011) used Donnell's nonlinear shallow-shell theory to study the nonlinear forced vibrations of FGM doubly curved shallow shells with a rectangular base. Bich et al. (2011) presents a semi-analytical approach to investigate the nonlinear dynamic of imperfect eccentrically stiffened functionally graded shallow shells taking into account the damping subjected to mechanical loads. In extension of their work, Bich and Van (2011) presented an analytical approach to investigate the non-linear axisymmetric response of functionally graded shallow spherical shells subjected to uniform external pressure incorporating the effects of temperature.

1.2.2.6 Parabolic and Hyperbolic Shells

Shell structures have been widespread in many fields of engineering because they give rise to optimum conditions for dynamical behaviour, strength and stability. Parabolic and hyperbolic Shell structures support applied external forces efficiently by virtue of their geometrical shape. These types of shell structures are much stronger and stiffer than other structural shapes.

The pioneer work on free vibrations of hyperboloidal shells of revolution was reported by Carter et al. (1969). Buckling stresses of stiffened hyperboloidal shells were

evaluated by Mungan (1979). Byun and Kapania (1992) performed nonlinear transient response of imperfect hyperbolic shells using a reduction method. Hyperbolic paraboloid shell model analysis using mixed finite element formulation was developed by Omurtag and Aköz (1994). Fundamental considerations for the finite element analysis of shell structures considering the parabolic and hyperbolic shell was reported by Chapelle and Bathe (1998). Pitkäranta et al. (2001) used fourier mode analysis for determining the deformations of shallow shell layers. Nasir et al. (2002) worked on dynamics of axisymmetric hyperbolic shell structures. Krivoshapko (2002) described the applications to one-sheet hyperboloidal shells of revolution and determined the static characteristics while the vibration and buckling analyses were also reported. Tornabene and Viola (2009) performed the free vibrations of four-parameter functionally graded parabolic panels and shells of revolution.

Tornabene (2011) determined the free vibrations of anisotropic doubly-curved shells and panels of revolution using 2-D GDQ solution technique. Xie et al. (2015) reported the free vibration of four-parameter functionally graded spherical and parabolic shells of revolution with arbitrary boundary conditions.

Recently, Garhwal et al. (2018) determined the static response of hyperbolic paraboloid composite shells under uniform pressure using finite element technique. Pang et al. (2018) developed a semi analytical method for the free vibration analysis of doubly-curved shells of revolution.

1.2.2.7 Conoidal Shells

Conoidal shells are distinctly used in modern shell roof structures because of their architectural aesthetics and functional advantages. They are doubly curved ruled surfaces has manufacturing advantageous during casting. Many industrial structures such as food processing and medical plants, exhibition and assembly halls, aircraft hangers and so on can be covered satisfying most of the functional requirements adopting this simple and elegant structural form. Hadid (1964) first analytically and experimentally investigated the bending characteristics of elastic conoidal shells. Choi (1984) performed a conoidal shell analysis by modified isoparametric element. Ghosh and Bandyopadhyay (1989, 1990) worked on bending analysis of conoidal shells using curved quadratic isoparametric element and Galerkin method. Finite element analysis of laminated composite conoidal shell structures was reported by Dey et al. (1992) while Das and Bandyopadhyay (1993) performed theoretical and experimental studies on conoidal shells. Chakravorty et al. (1995, 1996) used finite element approach to determine the free vibration analysis of point-supported laminated

composite doubly curved shells. Nayak and Bandyopadhyay (2002) performed free vibration analysis and design aids of stiffened conoidal shells. Pradyumna and Bandyopadhyay (2009) showed the dynamic instability of functionally graded shells using higher-order theory. Later the same authors, Pradyumna and Bandyopadhyay (2010) evaluated the free vibration and buckling of functionally graded shell panels in thermal environments. In recent past Ansari et al. (2018) worked on static analysis of doubly curved singly ruled truncated FGM cone.

1.2.3 REVIEW OF DYNAMIC ANALYSIS OF SHELLS

Both the theory and the analysis of shell structures can become more complex if one or more transverse shear deformation and rotary inertia, environmental effects are included. When the shear deformation effects are included in the FGM shell structures the order of the differential equations used for shell analysis increases from 8 to 10 or higher. In this section, complexities arising from the type of dynamic analysis, such as free vibration, impact loading, dynamic stability, rotating shells, etc. are explored.

1.2.3.1 Free Vibration

A pioneer survey on the free vibration of shells was provided by Leissa (1973) where the effects of different boundary conditions and semi-vertex angles on the frequency characteristics of conical shells were investigated. Several investigators worked on the vibration of homogeneous conical shells with different boundary conditions for the past thirty years. Lam and Hua (1999) investigated the influence of boundary conditions on the frequency characteristics of a rotating truncated circular conical shell. As far as the functionally graded shell structures are concerned, the vibration effects caused by different phenomena can be of serious consequence for their strength and safety. Loy et al. (1999) is one of the pioneers in this field, they examined the linear vibration frequency spectra of a functionally graded cylindrical shell. Later the several investigators worked on the free vibration of FGM cylindrical shells using different methods. Some notable work in this segment carried out by Pradhan et al. (2000), Ng et al. (2001), Liew et al. (2005), Batra and Jin (2005), Najafizadeh and Isvandzibaei (2007) and Matsunaga (2009). The vibration of FGM conical shells are not widely reported in literature as in the case of FGM cylindrical shells. Recently, some studies on the linear vibration and stability of FGM conical shells with different boundary conditions are published in the open literature. Naj et al. (2008) performed the thermal and mechanical instability of functionally graded truncated conical shells. Sofiyev (2009) exercised the vibration and stability behavior of freely supported FGM

conical shells subjected to external pressure. Tornabene (2009) analyzed the free vibration parameters of functionally graded conical, cylindrical shell and annular plate structures with a four-parameter power-law distribution. Zhao and Liew (2011a) used the meshless method to determine the free vibration characteristics of functionally graded conical shell panels.

Apart from the linear vibration analysis of the FGM plate and shell non-linear vibration analysis also important for different application of such structures. A profound survey on nonlinear analysis of FGM plates and shells can be found in a book by Shen (2016).

1.2.3.2 Rotational Effects

In dynamic analysis of shell structures, the rotational speed is a triggering parameter which was addressed by many researchers. Free vibration analyses of rotating FG shell of revolutions are limited to those of FG cylindrical shells. Ahmad and Naeem (2009) investigated the vibration characteristics of rotating FG cylindrical shells with different boundary conditions. The shell dynamical equations were obtained using Budiansky and Sanders thin shell theory, which were solved using wave propagation approach. Malekzadeh and Heydarpour (2012) examined the free vibration characteristics of rotating functionally graded cylindrical shells in thermal environment. Heydarpour et al. (2012) performed the thermoelastic analysis of rotating laminated functionally graded cylindrical shells using layerwise differential quadrature method. Malekzadeh and Heydarpour (2013) extended their previous work (2012) for rotating conical shells where the free vibration analysis of rotating FG conical shells were performed subjected to different boundary condition based on the FSDT of shells. The formulation included the centrifugal and Coriolis forces due to rotation of the FG shell. The differential quadrature method (DQM) was employed to solve the thermoelastic equilibrium equations and the free vibration equations of motion. Heydarpour et al. (2014) analyzed the free vibration behavior of rotating functionally graded carbon nanotube-reinforced composite truncated conical shells. Recently, Nguyen and Nguyen (2017) evaluates the dynamic response and vibration of functionally graded carbon nanotube-reinforced composite (FG-CNTRC) truncated conical shells resting on elastic foundations while Sheng and Wang (2017) determined the non-linear vibrations of rotating functionally graded cylindrical shells.

1.2.3.3 Impact Loading

The primary concept of impact problems originates from the dynamic behaviour of colliding bodies considering as rigid objects. The development of theory of elasticity enabled the multi-dimensional aspect of wave propagation in the impact problems and the stress distribution at the contact point. Impact dynamics includes the motion of both the impactor and the target and the force developed at the interface can be predicted accurately using a number of models established over the years. The characteristics of the FGM shell structures is concerned with the criticality of impacts which may induce significant internal damage undetectable by visual inspection causing degradation of the strength and stiffness of the shell structure. The first attempt to incorporate a theory of local indentation for static loading was based on a scheme suggested by Hertz. Hertz contact law between an elastic sphere and elastic half-space provides an expression for the local indentation in respect of contact force and a constant parameter depending on the radii of curvature at contact and on the elastic properties of the impactor and the target. The low velocity impact refers to a situation in which the entire structure deforms during contact duration as waves propagate to the boundary and reflect back several times. The damage modes of FGM structures under low velocity impact are significantly different from the metallic structures where-in the damage starts from the surface which can be detected by routine visual inspection. The low velocity impact may have cascading effect on the structural integrity and it can reduce the desired life of the structural component. Hence, it required a powerful analysis tool to accurately predict the internal damage of the FGM shell structures.

To overcome this limitation, finite element method was extensively employed to analyze the response of damaged FGM shell structures subjected to low velocity impact. The finite element method requires that either the force function be known or the dynamic response of both the structure and the impactor be studied simultaneously. In the latter case, it is necessary to have prior experimental knowledge of the contact behaviour between the impactor and the target. The founding investigation on low velocity impact performance of beam was performed by Goldsmith (1960). Low velocity impact performance of solid structures is a well-known area of research in structural mechanics. Various approaches can be adopted to analyze the contact phenomenon between the impactor and target surface such as spring mass models, energy balance technique and direct approach techniques. A complete work of such techniques with their relative advantages and disadvantages can be found in a book by Abrate (2005). Literature reviews of low velocity impact performance on FGM shell structures are not plentiful in the open literature. The review article on low-velocity impact

properties of composite materials (Richardson and Wisheart, 1996) and the review article on low-velocity impact on sandwich structures (chai and Zhu, 2011) gives some insight about the low velocity impact problems for composite and sandwich structures. Gong et al. (1999) first determined the elastic response of functionally graded cylindrical shells to low-velocity impact. There is a course of study available on simulation of low velocity impact performance of FGMs by the commercial available software package. Gunes and Aydin (2010) modeled the 3D response of FGM circular plate with the help of commercial finite element software package. Gunes et al. (2011) extended the earlier work and studied the elasto-plastic impact performance of circular FGM plates using Mori-Tanaka scheme. Etemadi et al. (2009) established a 3D simulation for sandwich panels with a functionally graded core subjected to low velocity impact. Later on, Larson and Palazotto (2006) established a Hertzian type of the contact force where the modified contact stiffness was used incorporate the grading profile along the thickness direction. Influences of various indicative parameters such as impactor velocity, power law index, mass of the impactor with respect to time histories of the contact force and shell deflection of the target were studied. To further extend the work on low velocity impact characteristics of FGM plates, Larson and Palazotto (2009) and Larson et al. (2009) developed a combined computational, analytical and experimental method. There are few number of studies available related to low velocity impact in FGMs structures where mathematical technique is used to solve the FGM formulation. Mao et al. (2011) studied the response of a spherical shallow shell impacted with low velocity in thermal environment also circular FGM plate was considered in their work. Yalamanchili and Sankar (2012) worked on indentation of functionally graded beams and also demonstrated its application with low-velocity impact case. Low velocity impact performance of a circular plate considering both radial and transverse graded profiles developed by Shariyat and Jafari (2013) where symmetrical motion equations were derived from the first order shear deformation theory and the results were obtained via Galerkin method. In another work, Shariyat and Farzan (2013) again explored the impact performance of a rectangular FGM plate under the eccentric impact loading where the beam model was derived based on first order shear deformation theory and the effect of in-plane loads of the beam was also taken into account. Khalili et al. (2013) investigated the low velocity impact response of a thin rectangular FGM plate neglecting the in-plane inertia effects of the plate. Dai et al. (2013) analyzed the low velocity impact performance of shear deformable FGM circular shaped plates using the contact formulation derived by Giannakopoulos and Suresh (1999). Newmark's time integration scheme was used for solving the time dependent

equations and the space domains equations were solved by orthogonal collocation point method. Due to difficulty in obtaining solutions for low velocity impact problem of FGM plate structures based on 3D elasticity theory, the alternative solution techniques are available with use of plate theories. Numerical technique based on graded finite element method (GFEM) is also used for structural analysis problem. Kim and Paulino (2002), and Zhang and Paulino (2007), established a GFEM technique for modeling nonhomogeneous structures. Dynamic characteristics of FGM cylinder considering internal impact load studied by Asemi et al. (2012) by the graded finite element method. Kubair and Lakshmana (2008) established cohesive damage model considering low-velocity impact in layered functionally graded beams. Kiani et al. (2013) reported the low velocity impact performance of thick FGM beams in thermal field considering general boundary conditions. Choi (2018) presented low-velocity impact response of convex and concave composite laminated shells using Finite element method.

1.2.3.4 Buckling Analysis

There has been extensive investigations carried out for the buckling analysis of FGM plates and shells to predict the critical buckling loads under various boundary and loading conditions. Birman (1995) was the first person who attempted to solve the buckling problem of FGM hybrid composite plates. Later on, Javaheri and Eslami (2002) first developed the buckling model of functionally graded plates under in-plane compressive loading.

Najafizadeh and Eslami (2002) presented the buckling analysis of FGM circular plates based on the Love–Kirchhoff hypothesis. Galerkin procedure was employed by Yang and Shen (2003) to investigate the postbuckling behavior of fully clamped FGM rectangular plates based on the CPT under transverse and in-plane loads. The authors have concluded that though the mechanical performance of FGM plates is quite similar to homogeneous isotropic ones, they do exhibit some unique and interesting characteristics due to the grading of material composition. Shariat et al. (2005) studied the buckling behavior of geometrically imperfect FGM plates based on the CPT. A closed form solution was presented by Najafizadeh and Heydari (2008) for the buckling of FGM circular plates based on the Reddy's TSDT subjected to uniform radial compression.

For the conical shell the vibration and stability behavior of freely supported FGM conical shells subjected to external pressure was presented by Sofiyev (2009) while in another work Sofiyev (2010) presented the buckling of FGM truncated conical shells subjected to axial compressive load and resting on Winkler–Pasternak foundations . Torabi et

al. (2013) worked on linear thermal buckling analysis of truncated hybrid FGM conical shells. Bhangale et al. (2006) performed linear thermoelastic buckling and free vibration behavior of functionally graded truncated conical shells. Several other work on buckling behavior of FGM cylindrical shell reported by Shen (2002, 2003, 2005, 2009) and Shen and Wang (2009). Zhao and Liew (2011) presented an element-free analysis method for mechanical and thermal buckling of functionally graded conical shell panels.

1.2.3.5 Dynamic Stability

The dynamic stability is an essential design criteria for the shell structures. Ng et al. (2001) applied the Bolotin's method to perform a dynamic stability analysis of functionally graded cylindrical shells under periodic axial loading. Ganapathi (2007) analyzed the dynamic stability characteristics of functionally graded materials shallow spherical shells. Sheng and Wang (2008) performed the thermal vibration, buckling and dynamic stability of functionally graded cylindrical shells embedded in an elastic medium while Darabi et al. (2008) worked on non-linear analysis of dynamic stability for functionally graded cylindrical shells under periodic axial loading. Sahmani et al. (2013) used higher-order shear deformable microshells based on the modified couple stress elasticity theory to perform the dynamic stability analysis of functionally graded microshells structure. Lei et al. (2014) used the element-free kp-Ritz method to perform the dynamic stability analysis of carbon nanotube-reinforced functionally graded cylindrical panels. Asnafi and Abedi (2017) made a comparison between the dynamic stability of three types of nonlinear orthotropic functionally graded plates under random lateral loads. Inala and Mohanty (2017) determined the flap wise bending vibration and dynamic stability of rotating functionally graded material plates in thermal environments. Torki et al. (2017) presented the dynamic stability of cantilevered functionally graded cylindrical shells under axial follower forces.

1.2.3.6 Thermal and Hygrothermal Effect

The presence of heat and moisture has significant influence on dynamic parameters of shell elements. The shell structure behaves in different pattern with high thermal gradient and in moist environment. Yang et al. (2006) studied thermo-mechanical post-buckling of FGM cylindrical panels with temperature-dependent properties. Shariyat (2009) worked on vibration and dynamic buckling control of imperfect hybrid FGM plates with temperature-dependent material properties subjected to thermo-electro-mechanical loading conditions. Zenkour (2010) reported the hygro-thermo-mechanical effects on FGM plates resting on

elastic foundations. Bouderba et al. (2013) determined the thermomechanical bending response of FGM thick plates resting on Winkler-Pasternak elastic foundations. Lee and Kim (2013) worked on hygrothermal postbuckling behavior of functionally graded plates. Lee and Kim (2014) extended the previous work by analyzing the degradation of thermal postbuckling behaviors of functionally graded material in aero-hygrothermal environments. Sobhy (2016) presented an accurate shear deformation theory for vibration and buckling of FGM sandwich plates in hygrothermal environment. Beldjelili et al. (2016) analyzed hygro-thermo-mechanical bending of S-FGM plates resting on variable elastic foundations using a four-variable trigonometric plate theory. Barati and Shahverdi (2017) considered aero-hygro-thermal stability analysis of higher-order refined supersonic FGM panels with even and uneven porosity distributions.

1.2.3.7 General Dynamic Behaviour

There are several other studies available which addressed the general dynamic behaviour of FGM shells. Wu and Lo (2006) discussed an asymptotic theory for dynamic response of laminated piezoelectric shells. Park et al. (2005) conducted a linear static and dynamic analysis of laminated composite plates and shells using finite elements. Ansari and Darvizeh (2008) worked on the prediction of dynamic behaviour of FGM shells under arbitrary boundary conditions. Ng et al. (2001) presented the dynamic stability analysis of functionally graded cylindrical shells under periodic axial loading. Dynamics of advanced rotating blades made of functionally graded materials, operating in a high-temperature field studied by Librescu, et al. (2008). Duc et al. (2015) performed nonlinear dynamic analysis and vibration of shear deformable piezoelectric FGM double curved shallow shells under damping-thermo-electro-mechanical loads. Moradi-Dastjerdi et al. (2013) investigated the dynamic behavior of functionally graded nanocomposite cylinders reinforced by carbon nanotube by a mesh-free method. Sheng and Wang (2018) performed the dynamic stability and nonlinear vibration analysis of stiffened functionally graded cylindrical shells. Tan et al. (2018) worked on static, dynamic and buckling analyses of 3D FGM plates and shells via an isogeometric-meshfree coupling approach. Frikha et al. (2018) performed the dynamic analysis of functionally graded carbon nanotubes-reinforced plate and shell structures using a double directors finite shell element.

1.2.4 REVIEW OF SOLUTION METHODS

Different analytical methods are employed to solve FGM shell problems including exact methods, different variational methods including Rayleigh and Ritz method, meshless method, Galarkin method, finite element methods and other methods. Numerous methods are available for researchers to study shell dynamics and obtain natural frequencies and mode shapes.

1.2.4.1 Exact solutions

The exact solutions are implied to obtain a solution that satisfies both the differential equations and boundary conditions exactly. For a generalized layered FGM shell and boundary conditions, the exact solution is difficult to find from the sets of shell equations and boundary conditions. The limited numbers of boundary conditions and FGM configuration with exact solutions are very limited. The pioneer work for untwisted single layered - or doubly-curved layered composite shells with two opposite edges having shear diaphragm using exact solutions method performed by Librescu et al. (1989). The complexity of the analysis and solution available for such shells with two opposite edges simply supported, while the others are arbitrary, prevented most researchers from getting results. The exact solution method is widely used for FG plate and for the FG shell very little work is found in the open literature.

The exact solutions for the 3D static bending analysis of FG plates were derived by Kashtalyan (2004), Woodward and Kashtalyan (2011a). Exact solutions for the stresses and displacements of simply supported plates under transverse pressure were obtained using Plevako displacement functions. Zenkour (2007) adopted the state-space method to derive the exact solutions for the 3D bending analysis of FG simply supported plates under transverse pressure. Zhong and Shang (2008) presented exact solutions for the 3D bending analysis of FG simply supported plates with specific variations of material properties such as exponential model, linear model and reciprocal model. Xu and Zhou (2009) developed the exact solutions for the 3D bending analysis of FG plates with continuously varying thickness. Semi-analytical solutions for the 3D bending analysis FG plate with different boundary conditions were provided by Zhang et al. (2014) using the DQM and the state-space approach. Kashtalyan and Menshykova (2009) performed 3D static bending analysis of simply supported sandwich panels with a FG core under transverse loadings. Woodward and Kashtalyan (2011) extended that to simply supported sandwich panels subjected to distributed and concentrated loadings. The 3D bending behavior of FG plates under point loading was investigated by Abali et al. (2014) using a combination of analytical and

numerical approaches. The analytical approach was based on the displacement function method, while the numerical modeling was based on Galerkin type finite element method. Yun et al. (2010) investigated the 3D axisymmetric bending of FG circular plates subjected to arbitrarily transverse loadings. Analytical solutions for the displacements, stresses, axial forces and bending moments of FG simply supported or clamped plates were obtained using the direct displacement method. Wen et al. (2011) presented exact solutions for the 3D static and dynamic bending analysis of FG plates using the RBFs. Exact solutions for the 3D free and forced vibrations of FG simply supported plates were reported by Vel and Batra (2004) using the power series method. Exact solutions for natural frequencies, displacements and stresses were compared with those predicted by ESL models. Chen et al. (2004) presented the three-dimensional vibration analysis of fluid-filled orthotropic FGM cylindrical shells. Pelletier and Vel (2006) developed an exact solution method for the steady-state thermoelastic response of functionally graded orthotropic cylindrical shells. Later on, Vel (2010) used exact elasticity solution to determine the vibration response of functionally graded anisotropic cylindrical shells.

1.2.4.2 Rayleigh and Ritz method

The Rayleigh and Ritz methods are among the most common approximate methods used in the vibration analysis of continuous systems. A displacement field is assumed in both methods. The coefficients of the displacement field are completely determined beforehand in the method of Rayleigh. In the Ritz method, undetermined coefficients are used in the displacement field. An energy functional is then obtained and minimized with respect to these coefficients, yielding equations that give the natural frequencies. The method of Rayleigh, which assumes a completely determined mode shape, generally yields a less accurate approximate frequency corresponding to it when compared with the Ritz method. The Ritz method permits to obtain as many natural frequencies as needed. If a complete set of functions is used, the Ritz method has excellent convergence characteristics and is relatively easy to formulate. This claim can be found in the Qatu (1995) and Ip et al. (1996) work. The Rayleigh-Ritz method was successfully used by Loy et al. (1999) to study the vibration of functionally graded cylindrical shells with simply supported boundary conditions. On the other hand the vibration characteristics of FG cylindrical shells under various boundary conditions were examined by Pradhan et al. (2000) using the CPT and Rayleigh method. A similar approach was adopted by Arshad et al. (2007) to investigate the vibration characteristics of FG cylindrical shells under three different types of volume fraction laws.

Shah et al. (2009) analyzed the vibrations of FGM thin cylindrical shells with exponential volume fraction law.

1.2.4.3 Meshless method

Even though FEM is being extensively used in most of the engineering problems, there are some drawbacks because of it is mesh based interpolation method. Distortion of the mesh during the large deformation of the structure and requirement of intensive remeshing in case of structures with complex geometries and discontinuities are the major drawbacks of FEM. Therefore, a new type of method called meshless method based on a set of scattered nodes rather than meshes has been developed and successfully applied in various engineering problems. Some of the drawbacks of FEM such as mesh distortion and remeshing can be circumvented by using meshless methods because of their flexibility in mesh requirements. Zhao et al. (2009, 2009a), Zhao and Liew (2009, 2011a), and Lee et al. (2009, 20010) developed the meshless model based on the FSDT and the element-free kp-Ritz method. This model is applied to FG plates for different problems e.g. geometrically nonlinear bending (Zhao and Liew, 2009), vibration (Zhao et al., 2009), thermal buckling (Zhao et al.,2009a). The meshless method was successfully applied for the mechanical and thermal buckling analysis of functionally graded conical shell panels by Zhao and Liew (2011). Mollarazi et al. (2012) worked on free vibration analysis of functionally graded cylinders by a meshless method. Recently, Xiang et al. (2015) adopted the meshless local collocation method to predict the natural frequency of FG cylindrical shells based on FSDT.

1.2.4.4 Galarkin method

The Galerkin method was employed to investigate nonlinear vibration problems. It was used to analyze doubly curved shallow shells in many research articles. Nonlinear forced vibrations of FG doubly curved shallow shells were investigated by Alijani et al. (2011) using the CPT with von Karman assumptions and the multi-modal Galerkin discretization. The buckling and postbuckling of FG sandwich plates resting on an elastic foundation under mechanical loadings was studied by Kiani and Eslami (2012) using the FSDT with von Karman assumptions. The single mode approach combined with Galerkin technique was used to calculate the critical buckling temperature and postbuckling equilibrium path of FG simply supported plates. Dai et al. (2005) extended the element-free Galerkin method to FG plates with piezoelectric layers under mechanical and thermal loadings based on the FSDT. Results show that the element free Galerkin method has many attractive

features compared to the finite element method. Zhang and Hao (2009) studied the nonlinear vibration of FG cylindrical shells under a combination of thermal loadings and external excitations using the FSDT and Galerkin method. An element-free Galerkin method were developed by Wu et al. (2011) using the differential reproducing kernel interpolation and the Reissner mixed variational theorem (RMVT). These models were applied to the 3D bending (Wu et al., 2011) and 3D free vibration (Wu and Chiu, 2011) analyses of multilayered composite and FG plates. It is found that the meshless collocation method gives slightly better performance than the element-free Galerkin method for the bending problem. However, for the free vibration problems, the element-free Galerkin method gives better performance than the meshless collocation method. Wu and Yang (2011) worked used RMVT-based meshless collocation and element-free Galerkin methods for the approximate 3D analysis of multilayered composite and FGM circular hollow cylinders. Wu and Yang (2011a) also developed a semi-analytical element-free Galerkin method for the 3D free vibration analysis of multilayered FGM circular hollow cylinders

1.2.4.5 Finite Element Method (FEM)

The finite element methods (FEM) have been rapidly augmented since last four decades, primarily based on Ritz method with minimization of the energy functional or other energy methods on an element level to obtain an element stiffness matrix. The FEM crosses the difficulties which the Ritz method has in dealing with various boundary conditions and relatively complex shapes. For simple shell structures, the Ritz method shows better convergence and less computational needs. For complex shell structures and boundary conditions, the FEM has proven to be an excellent tool. Finite element method (FEM) is the most extensively used computational techniques for solving variety of engineering problems. In FEM, the continuum is divided into a finite number of non-overlapping regions called elements. The equilibrium requirements of each element are specified in terms of a finite number of state variables. The final solution of the entire system is obtained by assembling the results of the individual elements. A considerable number of FEM commercial codes and packages exist to obtain vibration results.

Sundararajan et al. (2005) used an eight-nodded shear flexible quadrilateral plate element based on consistency approach to analyze the large amplitude free flexural vibration behavior of FGM plates based on the FSDT. It was found that the effect of skew angle is to increase the ratio of nonlinear frequency to linear frequency compared to rectangular case. Pradyumna and Bandopadhyay (2008) used an eight-nodded C^0 continuity element for the

free vibration analysis of simply-supported FGM rectangular curved panels based on the higher-order formulation proposed by Kant and Khare (1997). The authors observed that though the higherorder shear deformation theory is computationally expensive, it shows good performance for both thin as well as thick panels and hence recommended for the free vibration analysis of both thin and thick FGM plates and shell panels. A p-version of FEM in conjunction with a blending function method was adopted by Alijani et al. (2011) for the non-linear free vibration analysis of FGM doubly-curved shallow shell with an elliptical plan based on the FSDT. It was shown that FGM plates exhibit hardening behavior which depends on the volume fraction exponent and thickness ratio. Talha and Singh (2010) used a C^0 continuous element with 13 DOF at each node to present a higher-order shear deformation theory with a special modification in the transverse displacement which contributes additional freedom to the displacements through the thickness and fundamentally eradicates the over-correction for the static and free vibration analyses of FGM plates using the higher-order shear deformation theory. Talha and Singh (2011) studied the large amplitude free flexural vibration analysis of shear deformable FGM plates based on the higher-order shear deformation theory using a C^0 continuous element with 13 dof at each node. Malekzadeh and Shojaee (2013) used an eight-nodded solid element along with the Newmark's time integration scheme to investigate the response of FGM plates based on the FSDT under arbitrary boundary conditions and subjected to moving heat source.

Reddy and Chin (1998) studied the dynamic response of FG cylinders and plates subjected to two different types of thermal loadings using the FSDT and the finite element method. A geometrically nonlinear analysis of FG shells was performed by Arciniega and Reddy (2007) using the FSDT and the finite element method. Naghdabadi and Kordkheili (2005) presented a finite element formulation for analysis of functionally graded plates and shells. Hosseini and Naghdabadi (2007) worked on geometrically non-linear thermoelastic analysis of functionally graded shells using finite element method. Santos et al. (2009) reported a semi-analytical finite element model for the analysis of cylindrical shells made of functionally graded materials. Recently, Ansari et al. (2018) worked on Static analysis of doubly curved singly ruled truncated FGM cone by using finite element method.

1.2.4.6 Experimental Investigation

Experimental investigations for FGM structures were found to be carried out by a limited number of researchers in the recent past. Watanabe et al. (1998) worked on control of composition gradient in a metal-ceramic functionally graded material manufactured by the

centrifugal method. Li et al. (2000) experimentally investigated of the quasi-static fracture of functionally graded materials. Bogdanski et al. (2002) showed the assessment of the biocompatibility of Ni–Ti alloys by in vitro cell culture experiments on a functionally graded Ni–NiTi–Ti material. On the other hand, Sadowski et al. (2007) theoretically predicted the temperature distribution in FGM cylindrical plates subjected to thermal shock and results were validated experimentally. Kapuria et al. (2008) experimentally validated the bending and free vibration response of layered functionally graded beams. Recently, Gunes et al. (2014) investigated the low velocity impact on functionally graded circular plates.

1.2.4.7 Other Different Methods

Other techniques exist for solving the vibration problem of FGM shells viz. finite differences, boundary element methods (BEM), point matching, Trefftz, differential quadrature etc. The relative ease, accuracy, and dependability of the Ritz method for linear analysis and the Galerkin method for nonlinear analysis have proved to be valuable. Differential quadrature was used to analyze thermo-mechanical vibration of FGM sandwich beam by Pradhan and Murmu (2009). Lanhe et al. (2007) used the same technique for dynamic stability analysis of FGM plates. Tornabene et al. (2009) used 2-D differential quadrature solution for vibration analysis of functionally graded conical, cylindrical shell and annular plate structures. Three-dimensional temperature dependent free vibration analysis of functionally graded material curved panels resting on two-parameter elastic foundation using a hybrid semi-analytic and differential quadrature method was perfomed by Farid et al. (2010). The weighted residuals method was applied by Sharafkhani et al. (2012) and Abbasnejad et al. (2013). Boundary domain elements were employed to analyze for transient heat conduction in functionally graded materials by Sutradhar and Paulino (2004). A spline strip method was used to analyze thick cylindrical shells by Foroughi and Azhari (2014), Mirsalehi et al. (2015) and Cheung et al. (1989). Norouzi and Alibeigloo (2017) used a state space differential quadrature method for three dimensional static analysis of viscoelastic FGM cylindrical panel. Fu et al. (2011) used hybrid-Trefftz finite element method for heat conduction in nonlinear functionally graded materials

1.2.5 REVIEW OF RECENT SHELL RESEARCH

For the last few years', versatile studies were carried out on shell research which includes the essential scope of shell research ranging from the applications of different shell theories, tools of analyses, mode of methods to several types of shell structures. It also

includes the study with different types of loading including effect of impact and different boundary conditions. In recent past, Bich et al. (2011) studied on shallow spherical shells made of functionally graded material (FGM) under uniform external pressure incorporating thermal effect. Su et al. (2014) presented a unified solution for vibration analysis of functionally graded cylindrical, conical shells and annular plates with general boundary conditions while Kaparia et al. (2015) developed a quadrilateral shallow shell element based on the third-order theory for functionally graded plates and shells and the inaccuracy of rule of mixtures. Beni et al. (2015) performed the free vibration analysis of size-dependent shear deformable functionally graded cylindrical shell on the basis of modified couple stress theory. Sofiyev (2015) studied the vibration and stability of shear deformable FGM truncated conical shells subjected to an axial load. Akbari et al. (2015) investigated on the thermal buckling of temperature-dependent FGM conical shells with arbitrary edge supports. Sofiyev and Kuruoglu (2016) showed the domains of dynamic instability of FGM conical shells under time dependent periodic loads while Sofiyev (2016) incorporated parametric vibration of FGM conical shells under periodic lateral pressure within the shear deformation theory. Van (2016) performed the nonlinear axisymmetric response of FGM shallow spherical shells with tangential edge constraints and resting on elastic foundations while Ayoubi and Alibeigloo (2017) solved a three-dimensional transient analysis problem of FGM cylindrical shell subjected to thermal and mechanical loading. Frikha et al. (2017) demonstrated a four-node shell element for geometrically nonlinear analysis of thin FGM plates and shells. Trabelsi et al. (2017) determined the post-buckling behavior of functionally graded material shell structures using FSDT. Sofiyev et al. (2017) analyzed thermoelastic buckling of FGM conical shells under non-linear temperature rise in the framework of the shear deformation theory. An analytical investigation on mechanical buckling of FGM truncated conical shells reinforced by orthogonal stiffeners carried out by Van and Chan (2017) based on FSDT. Duc et al. (2017) determined the thermal and mechanical stability of functionally graded carbon nanotubes (FG CNT)-reinforced composite truncated conical shells surrounded by the elastic foundations. Thermal buckling of thin conical shell subjected to uniform pressure and temperature reported by Liao et al. (2017). Chen et al. (2017) analyzed the free vibration characteristics of FGM sandwich doubly-curved shallow shell based on a new shear deformation theory with stretching effects. Han et al (2017) performed the vibration analysis of submerged orthogonally stiffened FGM cylindrical shells. Wang et al. (2018) investigated the effect of imperfection on thermal buckling of cylindrical shell with FGM coating. Mohammadimehr and Rostami (2018) worked on bending and vibration analyses of a

rotating sandwich cylindrical shell considering nanocomposite core and piezoelectric layers subjected to thermal and magnetic fields.

In the light of impact analysis, Ayoubi and Alibeigloo (2017) studied three-dimensional transient analysis of FGM cylindrical shell subjected to thermal and mechanical loading. Aizi et al. (2017) determined the low velocity impact response of laminated composite truncated sandwich conical shells with various boundary conditions using complete model and GDQ method while Khalili and Saeedi (2018) evaluated the dynamic response of laminated composite beam reinforced with shape memory alloy wires subjected to low velocity impact of multiple masses. Bandyopadhyay and Karmakar (2017) worked on low-velocity impact response of delaminated composite conical shells in hygrothermal environment due to time-delay. Gao et al. (2018) investigated the nonlinear dynamic stability of the orthotropic functionally graded cylindrical shell surrounded by Winkler-Pasternak elastic foundation subjected to a linearly increasing load. Najafi et al. (2017) determined nonlinear dynamic response of FGM beams with Winkler–Pasternak foundation subject to noncentral low velocity impact in thermal field

1.2.6 REVIEW OF POROUS FGM STRUCTUTRES

Production of porosity free FGM using available manufacturing technique is extremely difficult. Therefore, the effect of porosity factor on structural behavior of FGM components is essential to consider porosities in FGM. Porosities are of two kinds viz. even and uneven. The detailed theoretical formulation of even and uneven porosities was explained by Wang and Zu (2017). With the rapid progression of materials technology, structures with graded porosity can be considered as one of the latest developments in FGMs. The presence of porosity within the microstructures of such materials is taken into account by means of the local density of the material. The porous materials are composed of two elements, one of which is solid (body) and the other element is either liquid or gas that is frequently found in nature, such as wood, stone, and layers of dust. Presently researchers concentrates on the method of preparation of FGMs, which includes powder metallurgy (Khor and Gu, 2000), vapor deposition (Seifried et al., 2001), self-propagation (Liu et al., 2006), centrifugal casting (Watanabe et al., 1998, 2001) and magnetic separation (Song et al., 2007). However, these methods are costly and have their own technical complexities.

1.2.6.1 Causes and Types of Porosity in FGM

Earlier studies reveal that quite a few porosities can occur inside the materials during the FGM preparation process by the non-pressure sintering technique (Zhu et al. 2001), these porosities can weaken the strength of FGMs dramatically. Also, in the multi-step sequential infiltration technique, porosities are existing in the intermediate area of the FGMs. This phenomenon is due to the fact that it is hard to infiltrate the secondary material into the middle area perfectly, whereas it is easier to infiltrate the material into the top and bottom area, remaining less porosity in these two zones (Wattanasakulpong et al., 2012). In the light of existence of porosities in FGMs, it is essential to study the influence of porosity on the vibration characteristics of FGM structures. According to this work, it is important to take into consideration the porosity effect when designing and analyzing FGM structures. Studies on the vibration and impact responses of porous FGM structures, especially for shells, are still unexplored area.

1.2.6.2 Dynamic Analysis of Porous FGM

Wattanasakulpong and Ungbhakorn (2014) investigated the linear and nonlinear vibration of porous FGM beams with elastically restrained ends. Ebrahimi and Mokhtari (2015) studied vibration of rotating Timoshenko FG beams with porosities employing DT method. They reported that porosity volume fraction and type of porosity distribution have a significant impact on the vibrational response of the FGM beams. Also, Wattanasakulpong and Chaikittiratana (2015) predicted flexural vibration of porous FGM beams using Timoshenko beam theory. Moreover, the wave propagation of FG porous plates based on higher-order shear deformation theory was studied by Yahia et al. (2015). Ebrahimi and Zia (2015) investigated the large amplitude nonlinear vibration of porous FGM beams by utilizing Galerkin and multiple scales methods. Atmane et al. (2017) applied an efficient beam theory to study the effects of thickness stretching and porosity on mechanical responses of FGM beams resting on elastic foundation. They stated that the presence of porosities brings about two important consequences: reduction of both mass and strength of FG beams. Ebrahimi et al. (2016) investigated thermo-mechanical vibration response of temperature-dependent FGM beams having porosities. Recently, Mechab et al. (2016) developed a nonlocal elasticity model for free vibration of FG porous nanoplates resting on elastic foundations. Zare et al (2017) presented the free vibration analysis of functionally graded porous doubly-curved shells based on the first-order shear deformation theory.

1.2.7 CRITICAL DISCUSSION

There is a general trend among researchers observed in the research of FGM conical shell structures to include shear deformation and rotary inertia wherein the finite element methods are being employed in shell engineering. The pioneering work on FGM conical shell was carried out by Zhao and Liew (2011a) to find out the free vibration characteristics by a meshless method. Lee et al. (2009) exhibited the thermoelastic analysis of functionally graded plates using the element-free kp-Ritz method. While, Karmakar et al. (2005) analyzed the free vibration characteristics of delaminated composite rotating cantilever shallow shells. Sreenivasamurthy and Ramamurti (1981) investigated on the effect of Coriolis force on the vibration of flat rotating low aspect ratio cantilever plates. The basic finite element formulation was interpreted by Bathe (1990), Zienkiewicz (1979) and Cook et al. (1989) while the dynamic analysis of structures was explored by Meirovitch (1992). The mechanics of layered composite structures was provided by Jones (1975). On the other hand, the free vibration characteristics of delaminated composite pretwisted rotating shells were studied by Karmakar and Kishimoto (2006). Miyamoto et al. (2013) explained in detailed about the functionally graded materials: design, processing and applications. The pioneer work for theory and physical behaviour of colliding solids was reported by Goldsmith (1960). Gong et al. (1999) first determined the elastic response of functionally graded cylindrical shells subjected to low-velocity impact.

A new modified contact law for FGM was introduced by Larson and Palazotto (2006). Kiani et al. (2013) used that modified contact law for FGM structure to determine the low velocity impact response of the FGM structure for single impact problem. For the multiple impact problems no literature was reported till date considering the FGM shell or plate. The only work for the low velocity multiple-impact problem by Lam and Sathiyamoorthy (1999) is available, where the low-velocity multi-impact dynamics of a system of a laminated beam are considered. It is found that although FGM plates and shells have received some attention from researchers, studies on FGM pretwisted conical shells are absent in the literature in both areas of free vibration and transient response subjected to low velocity impact. To fulfill this apparent void, the object and scope of the present study is systematically presented in the successive topic.

1.3 OBJECTIVE AND SCOPE

It is observed from the exhaustive literature review that the studies carried out so far on FGM conical shells are very limited and scanty. Engineering analyses related to this specific structural element are reviewed based on available literature. Accordingly, the objective of the present research is aimed at investigating several aspects of the dynamic behaviour in terms of free vibration and low velocity impact performance of FGM pretwisted conical shells. A thorough literature review on shell elements with emphasis on the development work that took place in the field of FGM shell structures are provided in the previous Section 1.2. It is observed that dynamic behavior of FGM conical shell structures are promising area of research with application of mechanical structures of such shells. The next sub-section represents the appraisal of past work, gap analysis, the scope of the present work while the next section (1.4) provides the organization of this thesis.

1.3.1 APPRAISAL OF PAST WORK

The in-depth review of the open literature on pretwisted shells, in the context of the present work brings out the following facts:

(a) The pioneering investigation was carried out on FGM stationary and rotary plate and shell structures especially with reference to the vibration characteristics. Different methods were resorted to the vibration analyses of FGM plates and shells, which included broadly analytical, experimental and numerical methods. The finite element approach was adopted as numerical techniques in most of the analyses, because of its versatility, flexibility and capability to solve complicated problems by satisfying the compatibility requirements and boundary conditions. A shallow FGM shell element was proved to be highly useful in dealing with the vibration problems of turbomachinery blades.

(b) In comparison, studies dealing with FGM pretwisted shells subjected to dynamic behavior received appreciably less attention. The three dimensional shell elements for the analysis of FGM shallow conical shells was developed assuming that the Jacobian was independent of the linear coordinate in the thickness direction and accordingly explicit integration through the thickness was performed.

(c) The finite element technique employed for free vibration analyses of FGM structures considered only three-noded and six-noded triangular plate finite elements, and the Ritz method, Galarkin's method as well as exact solution techniques were adopted for determining natural frequencies of stationary FGM shells. The studies on rotating pretwisted FGM shells are rare in open literature. The effect of rotational speeds on natural frequencies was studied for composite cylindrical shells only in moderate rotational speed range. No investigations on pretwisted FGM conical shells under rotation have been considered for analysis.

(d) Investigation on the FGM structures subjected to low velocity impact was dealt with flat plates having simply supported and clamped free boundary conditions. Low velocity impact induced through-the-thickness stresses and strains were calculated for clamped plates using eight nodded brick finite elements. Low velocity impact response of FGM shallow conical shell is unexplored. The effect of rotational speeds, target displacement, impactor's displacement, impactor's initial velocity, mass of the impactor, shell thickness and location of the impact of the pretwisted FGM conical shells subjected to low velocity impact are yet to be explored.

(e) A wide range of work on shells was carried out both for steady state as well as transient response but limited to composite and FGM plates other than conical shells. There has been no study are taken into account for addressing the dynamic analysis of pretwisted FGM conical shells which could be idealized as turbomachinery blades.

1.3.2 GAP ANALYSIS

The fundamental approach for analyzing FGM structure should be macro-mechanical wherein each layer is to be considered as homogeneous. Subsequently, after reaching to essence of behaviour of FGM structure, micro-mechanical study should be conducted so that proper FGM laws with correct graded material property index can be chosen for its intended application. Macro-mechanical study should be given first priority to access the dynamic behaviour of FGM pretwisted cantilevered shallow conical shells. For dynamic behaviour of the same, it demands to bridge the gap of research identified from review of open literature.

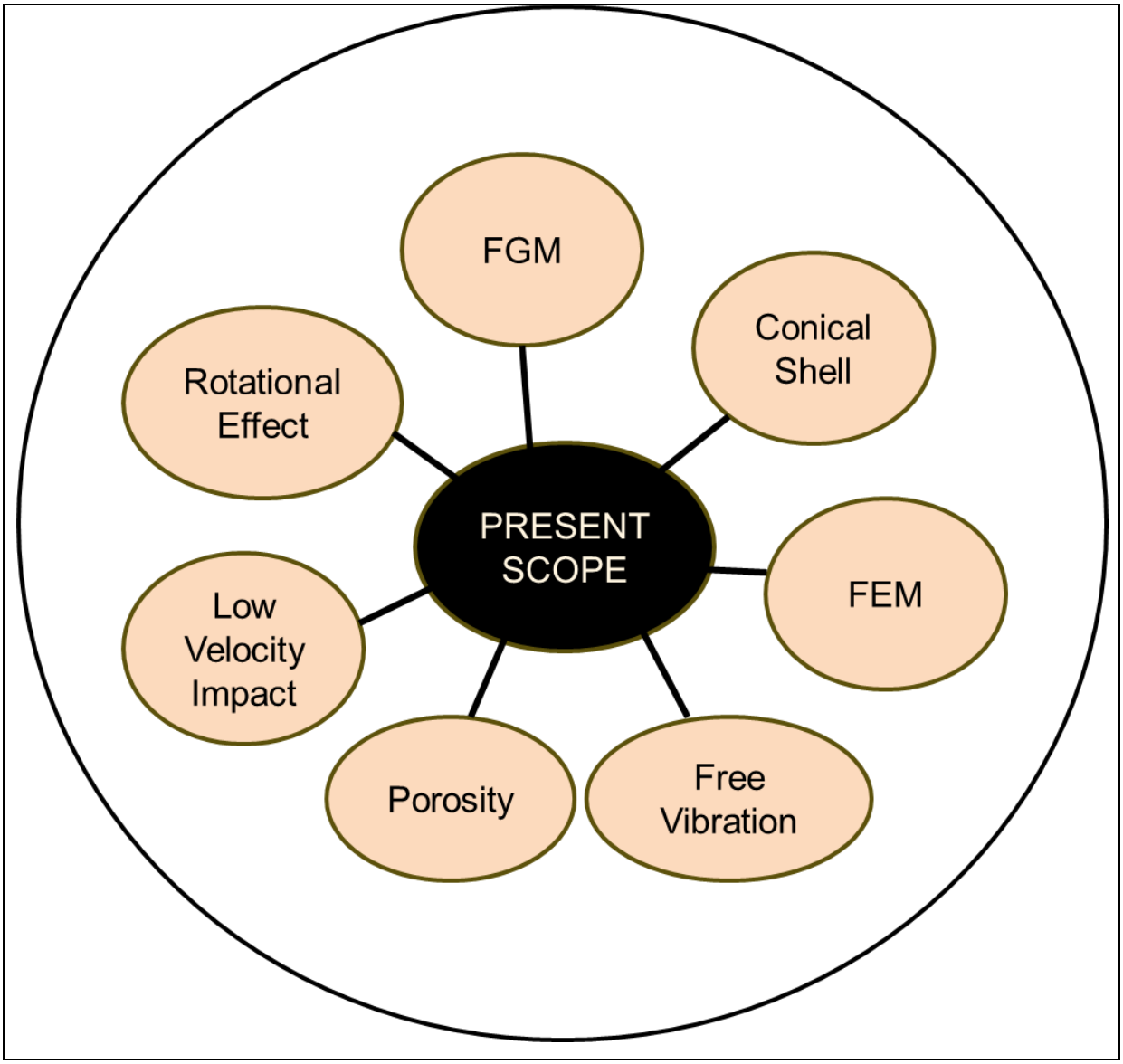

Figure. 1.5 Identified research Gap Captured

The entity of research gap is captured in Figure 1.5 wherein the outer circle indicates the universal set of FGM structure while the integral effect of seven distinct subset arenas namely, free vibration, low velocity impact, FGM, conical shell , FEM, rotational effect and porosity effect. These key areas are focused as the research gap which in turn portrayed as the manifestation of present scope. To the best of the authors' knowledge, there is no literature available which deals with free vibration and impact performance of pretwisted FGM shallow conical shells. To fill up this apparent void, the present analysis is considered to study the free vibration characteristics and low velocity impact performance of pretwisted FGM shallow conical shells employing finite element method.

1.3.3 SCOPE OF THE PRESENT WORK

The critical review of existing open literature explicitly indicates the research in the area of FGM pretwisted shells is far from completeness and there lies a wider scope of further research particularly in the field of dynamic analyses of FGM conical shells. In this respect a systematic study is needed to be carried out from the engineering point of view. The present study is aimed at investigating a few such problem areas so as to improve the understanding of the dynamic behaviour of pretwisted FGM conical shells. To fill the apparent void of the research as identified from the review of open literature, the present scope of work for this study is defined. Both perfect (porosity free) and porous (even and uneven) FGM conical shell structures are considered in the present analysis.

(a) A shallow conical shell element is established in a trapezoidal plan form. The turbomachinery blades can be suitably and accurately modelled as pretwisted shallow conical shell for compatibility with its geometrical complexity. The generalized dynamic equilibrium equation is derived from Lagrange's equation of motion neglecting the Coriolis effect for moderate rotational speeds. The analyses are carried out using an eight noded isoparametric shell bending element considering the effects of transverse shear deformation and rotary inertia based on Mindlin's theory. The FGMs layer along the thickness direction is modelled by varying the composition of the FGM constituent (ceramic and metal) based on different FGMs constituent laws. The numerical studies are carried out considering simple power law, sigmoidal law and exponential law of FGM constituents.

(b) Rotating pretwisted conical shells with low aspect ratio can be idealized as turbo-machinery blades. To ensure the compatibility of deformation and equilibrium of resultant forces and moments a layer wise isotropic material property is considered for calculating the element stiffness matrices. The QR iteration algorithm is utilized to solve the standard eigenvalue problem. A finite element based numerical technique is used to investigate dynamic analyses of pretwisted and untwisted FGM conical shells neglecting Coriolis effect for moderate rotational speed. Parametric studies are performed to obtain non-dimensional natural frequencies of FGM conical shells considering the prime parameters like twist angles, rotational speeds, material property graded index of different FGM constituent laws.

(c) An in-house computer code has been developed based on the present finite element formulation which is validated with the published results from the open literature. Numerical solutions are obtained in relation to dynamic analysis of pretwisted FGM shallow conical shells both free vibration characteristics as well as transient low velocity normal impact performance. Comparative studies are conducted for free vibration analysis with respect to stationary and rotating conditions both for twisted and untwisted FGM conical shells considering different FGM constituent laws. The deformed modes shapes for each vibrational case are furnished and proper justifications are made accordingly.

(d) Numerical investigation is carried out to study the low velocity normal impact performance of pretwisted and untwisted FGM shallow conical shells incorporating the effect of initial stress resulting from the centrifugal forces. In the context of the present work, dynamic response includes the computation of contact force, impactor displacement, impactor velocity and shell displacement with respect to time. The modified Hertzian contact law which accounts for permanent indentation is utilized to compute the contact force between the impactor and the shell for impact at different location of the FGM conical shells having moderate speeds of rotation. The time dependent equations are solved by Newmark's time integration algorithm (constant-average-acceleration method). Parametric studies are conducted in respect of velocity of impactor, mass of the impactor, location of the impactor, thickness of conical shell, angle of twist and various material property graded index of constituent laws for FGM conical shells subjected to low velocity normal impact. Possible reasons for variation in trends of dynamic parameters obtained from the present analysis are provided with suitable justification.

(e) The results are discussed in detail considering the effects of prime design parameters on the dynamic behaviour of pretwisted and untwisted FGM rotating conical shells. Based on the key identification and critical discussion, a set of significant conclusions are summarized. The scope for future research in the area is also addressed.

1.4 ORGANISATION OF THE THESIS

The present thesis comprises of five chapters. The first chapter contains the general introduction of the composite pretwisted shells along with its importance in relation to free vibration and transient dynamic analyses and finite element technique. A detailed review of

the existing literature is presented in this chapter with an emphasis on the aspects namely, shell theories, shell geometries, dynamic analyses of shells, method of analyses, recent research work on FGM shells structures and porous FGM structures. Based on literature review and addressing to appraisal of past work and gap analysis, the scope of the present work is also defined in Chapter 1.

Chapter 2 contains the theoretical formulation employed for the present analyses. The basic elastic equations of FGM conical shell model are discussed, followed by the derivation of governing equations for FGM shell material for perfect and porous FGM structures. The finite element model is based on Lagrange's equation of motion neglecting the Coriolis effect for moderate rotational speeds. An eight noded isoparametric quadratic shell element is employed in the finite element formulation. The standard eigenvalue problem is solved by applying the QR iteration algorithm. The modified Hertzian contact law is utilized to calculate the dynamic parameters like contact force between the impactor and the target shell, displacement of the target as well as imapctor and velocity of the impactor. The time-dependent equations of the target and impactor are solved by Newmark's time integration scheme.

The numerical results of free vibration analyses of FGM conical shell with and without pretwist are presented in Chapter 3. The computer codes are validated by comparing the results available in the open literature. A concise study of the influence of several triggering parameters like twist angle, rotational speeds, and material property graded index of different FGM constituent laws on natural frequencies is also reported in this chapter. The mode shapes of FGM conical pretwisted and untwisted shells of typical configuration are also depicted. The effects of porosity on the free vibration characteristics of FGM conical shell are also evaluated. In this chapter numerical results are generated considering different porosity factors both for even and uneven porous FGM shell structures. Comparative studies of free vibration characteristics between perfect FGM shell (without porosity) structures with two types of porous FGM shell structures are also portrayed in this chapter.

Chapter 4 deals with the transient low velocity impact performance of FGM shallow conical shells for both pretwisted and untwisted cases. To establish the validity of the present finite element formulation in respect of low velocity impact, some specific problems are also compared with those of earlier investigators. In this chapter numerical results are generated

for several cases and salient points are discussed to investigate the effects of different impact parameters like contact force, target displacement, impactor's displacement, impactor velocity, rotational speeds and material property graded index of different FGM constituent laws. The effects of porosity on the low velocity impact performances of FGM conical shell considering different even and uneven porosity factors are determined. In this chapter numerical results are generated and the effect of triggering parameters on the low velocity impact performances are analyzed and discussed. Comparative studies on low velocity impact performances for perfect (without porosity) and porous FGM shell structures are also portrayed in this chapter.

The important conclusions drawn based on the present investigation are systematically enumerated in Chapter 5. The major contribution of the present thesis is listed. The scope for future research in the context of present and the related problem areas is also summarized. The list of references that are cited in the present thesis is furnished at the end.

CHAPTER 2

THEORETICAL FORMULATION

2.1 INTRODUCTION

In this chapter a detailed theoretical formulation and solution techniques based on finite element method for the present analysis are provided. The basic elastic equations, relevant equations of conical shell model and the derivation of governing equations for the free vibration and low velocity impact problems are outlined. An eight nodded isoparametric quadratic shell bending element is considered for modeling the FGM shallow conical shell. The standard eigen value problem is solved by QR iteration algorithm for determining the natural frequencies while for determining the low velocity impact characteristics the Newmark's time integration scheme of constant-average-acceleration method is used. The details of finite element formulation based on it are presented. A modified Hertzian contact law considering permanent indentation is used to calculate the contact force along with other impact response parameters. The governing equations for different FGM constituent laws along with different porosity factors are portrayed.

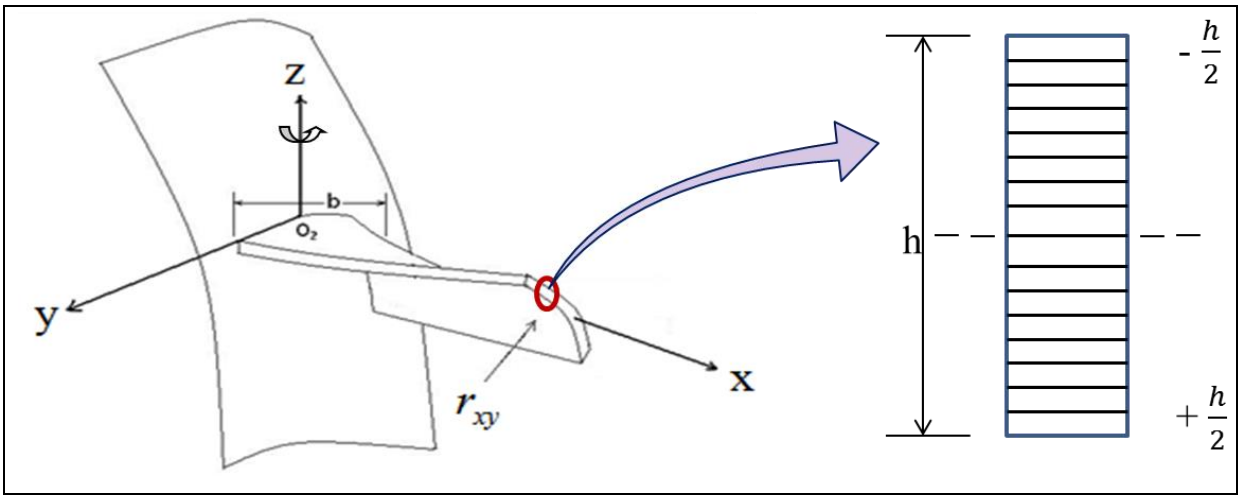

Figure 2.1 Co-ordinate system of conical shell blade and 16 layer gradation along thickness

2.2 GOVERNING EQUATION FOR CONICAL SHELL

A FGM shallow conical shell of uniform thickness is shown in figure 2.1. The principal material axes of each layer with respect to mid-plane of the shell are considered. If the mid-plane forms the x-y plane of the reference plane, then the displacements can be assumed as

$$u(x,y,z) = u^0(x,y) - z\,\theta_x(x,y)$$

$$v(x,y,z) = v^0(x,y) - z\,\theta_y(x,y) \tag{2.1}$$

$$w(x,y,z) = w^0(x,y) = w(x,y),$$

Assuming u, v and w are the displacement components in x, y-and z directions, respectively and u^0, v^0 and w^0 are the mid-plane displacements, and θ_x and θ_y are rotations of cross-sections along the x and y axes. The strain-displacement relationships for small deformations can be expressed as

$$\varepsilon_{xx} = \varepsilon_x^0 + z\kappa_x$$

$$\varepsilon_{yy} = \varepsilon_y^0 + z\kappa_y$$

$$\gamma_{xy} = \gamma_{xy}^0 + z\kappa_{xy} \tag{2.2}$$

$$\gamma_{xz} = w_{,x}^0 - \theta_x$$

$$\gamma_{yz} = w_{,y}^0 - \theta_y,$$

where mid-plane components are given by

$$\varepsilon_x^0 = u_x^0\ , \qquad \varepsilon_y^0 = u_y^0 + \frac{w}{R_y} \qquad \text{and} \qquad \gamma_{xy}^0 = u_y^0 + v_x^0 + \frac{2w}{R_{xy}} \tag{2.3}$$

and plate curvatures are expressed as

$$\kappa_x = -\theta_{x,x} = -w_{x,x} + \gamma_{xz,x}$$

$$\kappa_y = -\theta_{y,y} = -w_{y,y} + \gamma_{yz,y} \tag{2.4}$$

$$\kappa_{xy} = -(\theta_{x,y} + \theta_{y,x}) = -2w_{xy} + \gamma_{xz,y} + \gamma_{yz,x}$$

Therefore the strains in the k-th layer of the FGM shell can be expressed in the form

$$\begin{Bmatrix} \varepsilon_x \\ \varepsilon_y \\ \gamma_{xy} \end{Bmatrix}^k = \begin{Bmatrix} \varepsilon_x^0 \\ \varepsilon_y^0 \\ \gamma_{xy}^0 \end{Bmatrix} + z \begin{Bmatrix} \kappa_x \\ \kappa_y \\ \kappa_{xy} \end{Bmatrix} = \{\varepsilon^0\} + z\,\{\kappa\} \text{ and } \{\gamma\}^k = \begin{Bmatrix} \gamma_{xz}^0 \\ \gamma_{yz}^0 \end{Bmatrix} = \{\gamma\} \tag{2.5}$$

Combining all the stress terms it can be written as

$$\{\varepsilon\} = \begin{Bmatrix} \varepsilon_x \\ \varepsilon_y \\ \gamma_{xy} \\ \gamma_{xz} \\ \gamma_{yz} \end{Bmatrix} = \begin{Bmatrix} \varepsilon_x^0 \\ \varepsilon_y^0 \\ \gamma_{xy}^0 \\ \gamma_{xz}^0 \\ \gamma_{yz}^0 \end{Bmatrix} + z \begin{Bmatrix} \kappa_x \\ \kappa_y \\ \kappa_{xy} \\ 0 \\ 0 \end{Bmatrix} \tag{2.6}$$

In matrix form it can be written as

$$\{\varepsilon\} = \begin{bmatrix} 1 & 0 & 0 & z & 0 & 0 & 0 & 0 \\ 0 & 1 & 0 & 0 & z & 0 & 0 & 0 \\ 0 & 0 & 1 & 0 & 0 & z & 0 & 0 \\ 0 & 0 & 0 & 0 & 0 & 0 & 1 & 0 \\ 0 & 0 & 0 & 0 & 0 & 0 & 0 & 1 \end{bmatrix} \begin{Bmatrix} \varepsilon_x^0 \\ \varepsilon_y^0 \\ \gamma_{xy}^0 \\ \kappa_x \\ \kappa_y \\ \kappa_{xy} \\ \gamma_{xz}^0 \\ \gamma_{yz}^0 \end{Bmatrix} \tag{2.7}$$

In compact form the above equation can be expressed as

$$\{\varepsilon\} = [T]\{\varepsilon^*\} \tag{2.8}$$

Where, *[T]* is the thickness co-ordinate matrix and $\{\varepsilon^*\}$ is the mid-plane stress and curvature vectors.

FGM consists of a number of isotropic layers. Therefore the in-plane stress resultant $\{N\}$, the moment resultant $\{M\}$, and the transverse shear resultants $\{Q\}$ can be expressed as

$$\begin{Bmatrix} N_x \\ N_y \\ N_{xy} \end{Bmatrix} = \sum_{k=1}^{n=8} \left[Q_{ij} \right] \left\{ \int_{z_{k-1}}^{z_k} \begin{Bmatrix} \varepsilon_x^0 \\ \varepsilon_y^0 \\ \gamma_{xy}^0 \end{Bmatrix} dz + \int_{z_{k-1}}^{z_k} \begin{Bmatrix} \kappa_x \\ \kappa_y \\ \kappa_{xy} \end{Bmatrix} z dz \right\}, \qquad ...i, j = 1,2,6,$$

$$\begin{Bmatrix} M_x \\ M_y \\ M_{xy} \end{Bmatrix} = \sum_{k=1}^{n=8} \left[Q_{ij} \right] \left\{ \int_{z_{k-1}}^{z_k} \begin{Bmatrix} \varepsilon_x^0 \\ \varepsilon_y^0 \\ \gamma_{xy}^0 \end{Bmatrix} z dz + \int_{z_{k-1}}^{z_k} \begin{Bmatrix} \kappa_x \\ \kappa_y \\ \kappa_{xy} \end{Bmatrix} z^2 dz \right\}, \qquad ...i, j = 1,2,6, \tag{2.9}$$

$$\begin{Bmatrix} Q_x \\ Q_y \end{Bmatrix} = \sum_{k=1}^{n=8} \left[Q_{ij} \right] \left\{ \int_{z_{k-1}}^{z_k} \begin{Bmatrix} \gamma_{xz}^0 \\ \gamma_{yz}^0 \end{Bmatrix} dz \right\}, \qquad ...i, j = 4,5.$$

Where,

$$\overline{Q}_{ij} = \begin{bmatrix} Q_{11} & Q_{12} & 0 & 0 & 0 \\ Q_{12} & Q_{22} & 0 & 0 & 0 \\ 0 & 0 & Q_{66} & 0 & 0 \\ 0 & 0 & 0 & Q_{44} & 0 \\ 0 & 0 & 0 & 0 & Q_{55} \end{bmatrix} \tag{2.10}$$

$$Q_{11} = Q_{22} = \frac{E_{(z)}}{1-\nu_{(z)}^2},\ Q_{12} = \frac{\nu E_{(z)}}{1-\nu_{(z)}^2},\ Q_{33} = Q_{44} = Q_{55} = G_{(z)} \tag{2.11}$$

In a combined form the equation 2.9 one can expressed as,

$$\begin{Bmatrix} N_x \\ N_y \\ N_{xy} \\ M_x \\ M_y \\ M_{xy} \\ Q_x \\ Q_y \end{Bmatrix} = \begin{bmatrix} A_{11} & A_{12} & 0 & B_{11} & B_{12} & 0 & 0 & 0 \\ A_{12} & A_{11} & 0 & B_{12} & B_{11} & 0 & 0 & 0 \\ 0 & 0 & A_{66} & 0 & 0 & B_{66} & 0 & 0 \\ B_{11} & B_{12} & 0 & D_{11} & D_{12} & 0 & 0 & 0 \\ B_{12} & B_{11} & 0 & D_{12} & D_{11} & 0 & 0 & 0 \\ 0 & 0 & B_{66} & 0 & 0 & D_{66} & 0 & 0 \\ 0 & 0 & 0 & 0 & 0 & 0 & K^* A_{44} & 0 \\ 0 & 0 & 0 & 0 & 0 & 0 & 0 & K^* A_{55} \end{bmatrix} \begin{Bmatrix} \varepsilon_x^0 \\ \varepsilon_y^0 \\ \gamma_{xy}^0 \\ \kappa_x \\ \kappa_y \\ \kappa_{xy} \\ \gamma_{xz}^0 \\ \gamma_{yz}^0 \end{Bmatrix} \tag{2.12}$$

Where K^* is the shear correction factor, which is taken as 5/6 for the present analysis.

Thus, $$\{F\} = [D]\{\varepsilon^*\}. \tag{2.13}$$

where

$$[D] = \begin{bmatrix} A_{11} & A_{12} & 0 & B_{11} & B_{12} & 0 & 0 & 0 \\ A_{12} & A_{11} & 0 & B_{12} & B_{11} & 0 & 0 & 0 \\ 0 & 0 & A_{66} & 0 & 0 & B_{66} & 0 & 0 \\ B_{11} & B_{12} & 0 & D_{11} & D_{12} & 0 & 0 & 0 \\ B_{12} & B_{11} & 0 & D_{12} & D_{11} & 0 & 0 & 0 \\ 0 & 0 & B_{66} & 0 & 0 & D_{66} & 0 & 0 \\ 0 & 0 & 0 & 0 & 0 & 0 & K^* A_{44} & 0 \\ 0 & 0 & 0 & 0 & 0 & 0 & 0 & K^* A_{55} \end{bmatrix} \tag{2.14}$$

$$[F] = [N_x\ N_y\ N_{xy}\ M_x\ M_y\ M_{xy}\ Q_x\ Q_y]^T \tag{2.15}$$

$$\{\varepsilon^*\} = [\varepsilon_x^0\ \ \varepsilon_y^0\ \ \gamma_{xy}^0\ \ \kappa_x\ \ \kappa_y\ \ \kappa_{xy}\ \ \gamma_{xz}^0\ \ \gamma_{yz}^0]^T \tag{2.16}$$

where,

$$A_{ij} = \sum_{k=1}^{n} (Q_{ij})_k (z_k - z_{k-1}), \quad ...i, j = 1,2,6,$$

$$B_{ij} = \frac{1}{2} \sum_{k=1}^{n} (Q_{ij})_k (z_k^2 - z_{k-1}^2), \quad ...i, j = 1,2,6, \tag{2.17}$$

$$D_{ij} = \frac{1}{3} \sum_{k=1}^{n} (Q_{ij})_k (z_k^3 - z_{k-1}^3), \quad ...i, j = 1,2,6,$$

2.3 FINITE ELEMENT FORMULATION

An eight noded isoparametric shell element has been considered for finite element formulation, where each node is having five degrees of freedom (three translations and two rotations). In order to represent the displacement fields properly, shape functions or the interpolation functions are derived from an interpolation polynomial in terms of natural co-ordinates. In the case of a thin shell element, the interpolation polynomial is a function of ξ and η, expressed in the following form.

$$u(\xi, \eta) = C_0 + C_1\xi + C_2\eta + C_3\xi^2 + C_4\xi\eta + C_5\eta^2 + C_6\xi^2\eta + C_7\xi\eta^2 \tag{2.18}$$

Where, $C_0, C_1, C_2, C_3, C_4, C_5, C_6, C_7$ are the generalized degrees of freedom.

2.3.1 QUADRETIC ISOPARAMETRIC SHELEL EMENET

An isoparametric shell element with eight nodes has been considered, where each node is having five degrees of freedom as shown in Figure 2.2 and Figure 2.3. The displacements and rotations at each node are denoted as u, v, w and θ_x, θ_y respectively. The element geometry and displacement fields are expressed by quadratic shape function(S_i).

$$x = \sum_{i=1}^{8} S_i x_i \qquad y = \sum_{i=1}^{8} S_i y_i \tag{2.19}$$

Where, x_i and y_i are the coordinates at node "i".

The element displacements are expressed in terms of their nodal values using eight noded element shape function as given below,

$$u = \sum_{i=1}^{8} S_i u_i \qquad v = \sum_{i=1}^{8} S_i v_i \qquad w = \sum_{i=1}^{8} S_i w_i \tag{2.20}$$

Here, S_i 's are the shape functions which interpolate the generalized displacements u_i , v_i , w_i along x, y and z axis, respectively at i[th] node with in an element.

$$\theta_x = \sum_{i=1}^{8} S_i \theta_{xi} \qquad \theta_y = \sum_{i=1}^{8} S_i \theta_{yi} \tag{2.21}$$

Here, S_i 's are the shape functions which interpolate the generalized rotations θ_{xi} and θ_{yi} about *x*, and *y* axis, respectively at i[th] node with in an element.

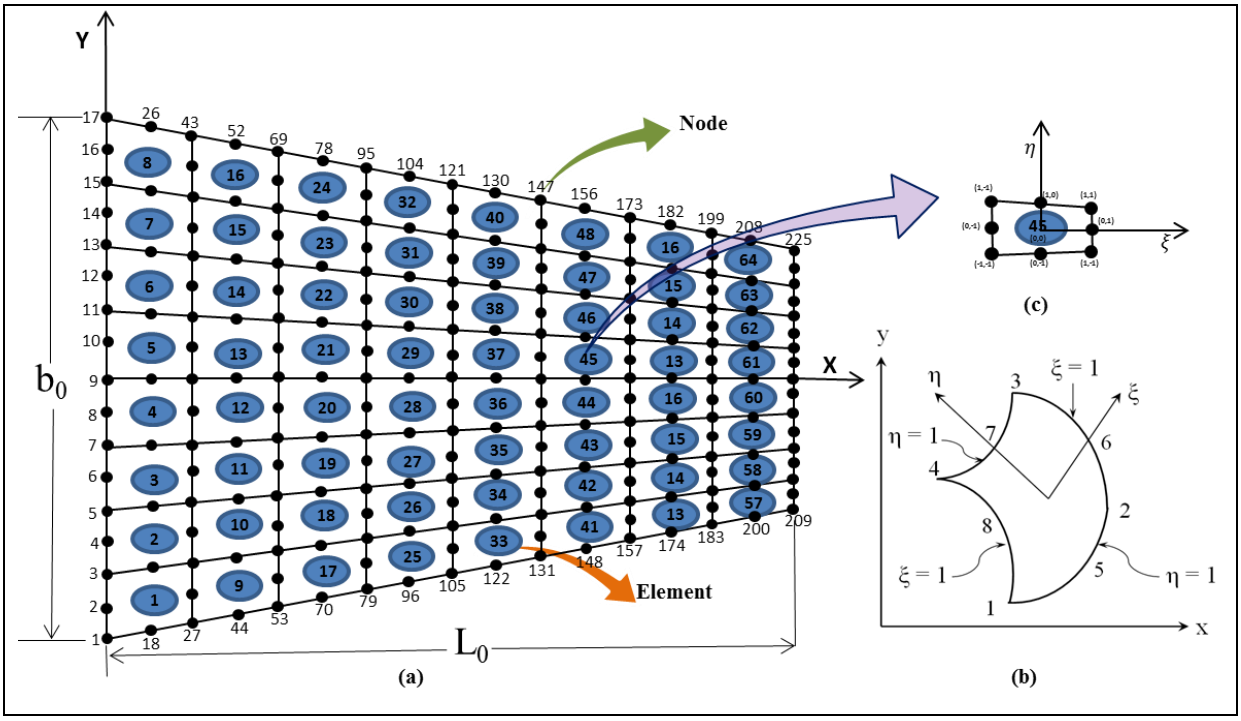

Figure 2.2 (a) Finite element discretization of (8 x 8) mesh on plan area with elements (b) node numbers and the natural coordinates considering isoparametric shell element. (c) Node numbers and natural coordinates in planner view.

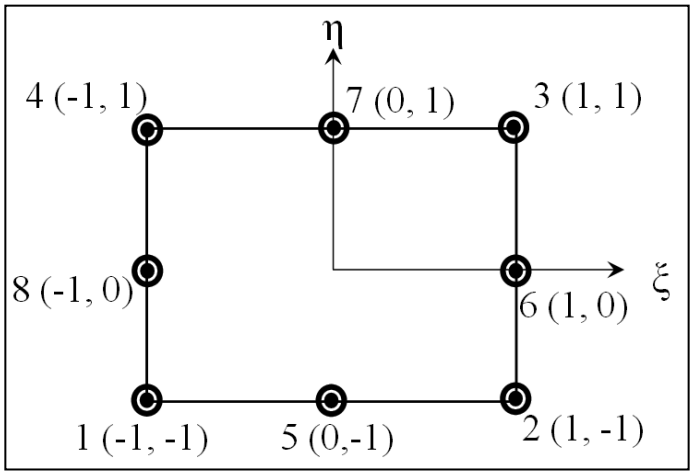

Figure 2.3 Element in the $\xi - \eta$ space coordinates

The shape function can be expressed as follows as given by (Bathe, 1990)

$$S_i = (1 + \xi\,\xi_i)(1 + \eta\,\eta_i)(\xi\,\xi_i + \eta\,\eta_i - 1)/4 \quad i = 1,2,3,4$$
$$S_i = (1 - \xi^2)(1 + \eta\,\eta_i)/2 \quad i = 5,7 \tag{2.22}$$
$$S_i = (1 - \eta^2)(1 + \xi\,\xi_i)/2 \quad i = 6,8$$

Where, the natural coordinate systems are denoted by ξ and η and ξ_i , η_i are the values at the i[th] node , the value of i ranging from 1 to 8.

$$\begin{bmatrix} S_{i,x} \\ S_{i,y} \end{bmatrix} = [J]^{-1} \begin{bmatrix} S_{i,\xi} \\ S_{i,\eta} \end{bmatrix} \tag{2.23}$$

$$[J] = \begin{bmatrix} x_\xi & y_\xi \\ x_\eta & y_\eta \end{bmatrix} \tag{2.24}$$

Here, $[J]$ is the Jacobian Matrix.

2.3.2 ELEMENT STIFFNESS MATRIX

The potential energy of the element due to deformation is expressed as

$$U_e = \frac{1}{2}\int_V \{\varepsilon\}^T \{\sigma\} dV = \frac{1}{2}\int_V [T]^T \{\varepsilon^*\}^T \left[Q_{ij}\right][T]\{\varepsilon^*\} dV \tag{2.25}$$

$$U_e = \frac{1}{2}\iint_A \{\varepsilon^*\}^T [D]\,\{\varepsilon^*\} dA \tag{2.26}$$

Where,

$$[D] = \int_{-\frac{h}{2}}^{\frac{h}{2}} [T]^T \left[Q_{ij}\right][T]\, dz \tag{2.27}$$

The strain displacement relation is given as follows,

$$\{\varepsilon^*\} = [B]\{\delta_e\} \tag{2.28}$$

Where, [B] is the strain displacement matrix.

$$\{\delta_e\} = \left\{u_1^0 \quad v_1^0 \quad w_1^0 \quad \theta_{x1}^0 \quad \theta_{y1}^0 \ldots\ldots\ldots u_8^0 \quad v_8^0 \quad w_8^0 \quad \theta_{x8}^0 \quad \theta_{y8}^0\right\}^T \tag{2.29}$$

Then,

$$U_e = \frac{1}{2}\int_{-a/2}^{a/2}\int_{-b/2}^{b/2}\{\delta_e\}^T[B]^T[D]\{\delta_e\}\,dx\,dy = \{\delta_e\}^T[K_e]\{\delta_e\} \tag{2.30}$$

Here,

$$[K_e] = \int_{-a/2}^{a/2}\int_{-b/2}^{b/2}[B]^T[D]\,[B]\,dx\,dy \tag{2.31}$$

The strain displacement matrix $[B_i]$ in the above equation is given by

$$[B_i] = \begin{bmatrix} S_{i,x} & 0 & 0 & 0 & 0 \\ 0 & S_{i,y} & \frac{S_i}{R_y} & 0 & 0 \\ S_{i,y} & S_{i,x} & \frac{2S_i}{R_{xy}} & 0 & 0 \\ 0 & 0 & 0 & 0 & S_{i,x} \\ 0 & 0 & 0 & -S_{i,y} & 0 \\ 0 & 0 & 0 & -S_{i,x} & -S_{i,y} \\ 0 & 0 & -S_{i,x} & S_i & 0 \\ 0 & 0 & -S_{i,y} & 0 & -S_i \end{bmatrix} \tag{2.32}$$

The element stiffness matrix $[K_e]$ can be expressed in local natural coordinates of the element as

$$[K_e] = \int_{-1}^{1}\int_{-1}^{1}[B]^T[D]\,[B][J]\,d\xi\,d\eta \tag{2.33}$$

Here, $[B]$, $[D]$, $[J]$ are the strain – displacement matrix, elasticity matrix and determinant of the Jacobian matrix respectively. 2 x 2 integration has been used in order to avoid shear locking.

2.3.3 ELEMENT MASS MATRIX

The element mass matrix is obtained from the following integral

$$[M_e] = \int_{-1}^{1}\int_{-1}^{1}[S]^T[P]\,[S][J]\,d\xi\,d\eta \tag{2.34}$$

Where,

$$[P] = [T_m]^T[P][T_m] \tag{2.35}$$

The transformation matrix T_m is given by

$$[T_m] = \begin{bmatrix} l_1 & m_1 & n_1 & 0 & 0 \\ l_2 & m_2 & n_2 & 0 & 0 \\ l_3 & m_3 & n_3 & 0 & 0 \\ 0 & 0 & 0 & m_2 & l_2 \\ 0 & 0 & 0 & m_1 & l_1 \end{bmatrix} \tag{2.36}$$

Here, *l*, *m* and *n* denote the direction cosines of the local frame of reference with respect to the global coordinate system. The inertia matrices $[P']$ and the shape function $[S_i]$ are given as follows,

$$[P'] = \begin{bmatrix} l_r & 0 & 0 & 0 & 0 \\ 0 & l_t & 0 & 0 & 0 \\ 0 & 0 & l_t & 0 & 0 \\ 0 & 0 & 0 & l_r & 0 \\ 0 & 0 & 0 & 0 & l_r \end{bmatrix}$$

$$[S_i] = \sum_{i=1}^{8} \begin{bmatrix} S_i & 0 & 0 & 0 & 0 \\ 0 & S_i & 0 & 0 & 0 \\ 0 & 0 & S_i & 0 & 0 \\ 0 & 0 & 0 & S_i & 0 \\ 0 & 0 & 0 & 0 & S_i \end{bmatrix} \tag{2.37}$$

Where, l_r and l_t represents the rotary and translator inertia terms respectively as given below.

$$l_r = \frac{1}{h}\sum_{k=1}^{n}\int_{Z_k}^{Z_{k-1}} \rho_k z^2 dz \tag{2.38}$$

$$l_t = \frac{1}{h}\sum_{k=1}^{n}\int_{Z_k}^{Z_{k-1}} \rho_k dz \tag{2.39}$$

Where, Z_k and Z_{k-1} are the distances of the top and bottom layer from the mid-plane of the FGM shell respectively and ρ_k denotes the mass density of the kth layer.

2.3.4 ELEMENT GEOMETRIC STIFFNESS MATRIX

Due to presence of in-plane stresses in mid-surface caused by rotation, the additional strain energy is stored in the element. This additional strain energy results in an increase in the stiffness of the element.

The geometric stiffness matrix due to rotation is given by (Sreenivasamurthy and Ramamurti, 1981)

$$[K_{\sigma e}] = \int_{\varphi} [G]^T [M_\sigma][G] d\varphi \tag{2.40}$$

where [G] consists of the derivatives of shape functions and [M_σ] is the matrix of initial in-plane stress resultant caused by rotation.

2.4 BASIC GOVERNING EQUATIONS

Under dynamic load the response pattern of structures are varies with time. The Lagrangian energy function is familiarized in deriving the equations of motion of the shell structure. The formulation considers both inertial frame of reference and the local coordinate axes. Newmark‘s constant-acceleration time integration technique is used for solving the time dependent equations of the shell and the impactor.

2.4.1 GENERAL DYNAMIC EQUILIBRIUM

Hamilton’s principle (Meirovitch, 1992) applied to the dynamic analysis of elastic bodies states that among all admissible displacements which satisfy the specific boundary conditions, the actual solution makes the functional $\int (T+W)\, dt$ stationary, where T and W are the kinetic energy and the work done by conservative and non-conservative forces, respectively. The stationary value is actually a minimum. In case of a dynamic problem without damping the conservative forces are the elastic forces developed within a deformed body and the non-conservative forces are the external force functions. The energy functional for Hamilton’s principle is the Lagrangian (L_f) which includes kinetic energy (T) in addition to potential strain energy (U) of an elastic body.

Two coordinate system (x', y', z') and (x, y, z) are used for modelling the rotating plate (Figure 2.4) where (x', y', z') is the inertial reference frame (absolute fixed system) and (x, y, z) is the plate coordinate system (local coordinate axes). Hamilton’s principle is used to derive Lagrange’s equation of motion which is employed for establishing the dynamic equilibrium equation for a finite element. The local kinetic energy of the rotating shell can be expressed as

$$T = \frac{1}{2}\int_{vol} \rho \vec{V}.\vec{V} d(vol) \tag{2.41}$$

where ρ is the mass density of the shell and $\vec{V}$ is the absolute velocity of an arbitrary point on the shell with respect to reference frames. It is assumed that

$$\vec{\Omega} = \Omega\,\hat{k}\ ,\ \text{about the z axis.}$$

The components of angular velocity with respect to the local co-ordinate system are given as

$$\{\Omega_x, \Omega_y, \Omega_z\} = \{0, 0, \Omega\} \tag{2.42}$$

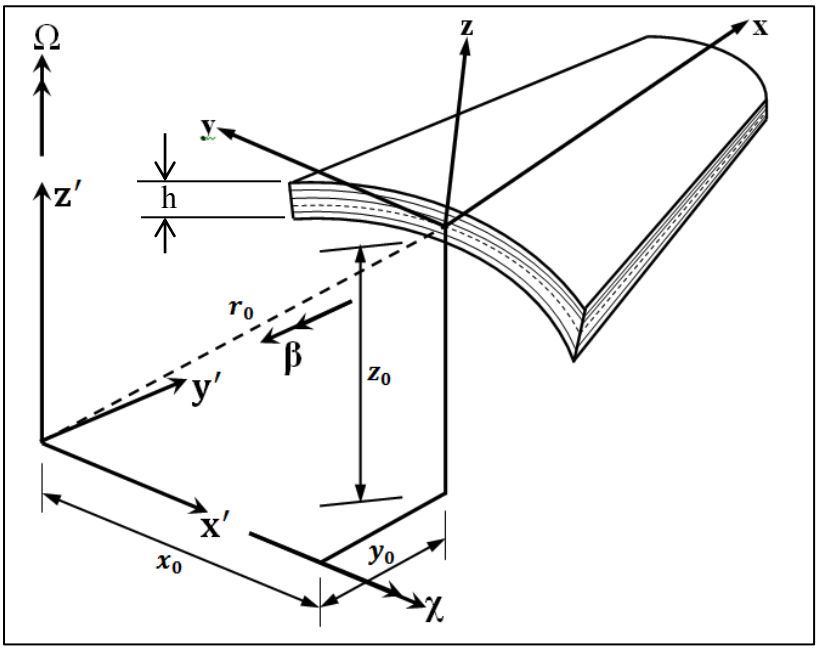

Figure 2.4 Rotational and translational offsets of rotating plate local axes from inertial axes.

According to Chasle's theorem

$$\vec{V} = \frac{d\vec{r}}{dt} + \left(\Omega\,\hat{k}\right) \times \vec{r} \tag{2.43}$$

Where $\vec{r}$ is the position vector from the local inertial reference frame to a vector of a point on the deformed shell. The position vector $\vec{r}$ and the angular velocity vector $\vec{\Omega}$ can be written as

$$\vec{r} = (x+u)i + (y+v)j + (z+w)k \tag{2.44}$$

and

$$\vec{\Omega} = \Omega\,\hat{k} = \Omega_x i + \Omega_y j + \Omega_z k \tag{2.45}$$

Where *(x, y, z)* are the co-ordinates of the point with respect to local coordinate axes. *(u,v,w)* are the elastic deflections of a point on the shell and $(\Omega_x, \Omega_y, \Omega_z)$ are the components of the angular velocity with respect to the local coordinate system. The velocity vector $\vec{V}$ is given by

$$\vec{V} = \left[\left(\dot{u} + \Omega_y\,(z+w) - \Omega_y\;(y+v)\right]\right)i + \left[(\dot{v} + \Omega_z\,(x+u) - \Omega_x\;(z+w)\right])j +$$

$$\left[\left(\dot{w} + \Omega_x\,(y+v) - \Omega_y\;(x+u)\right]\right)k \qquad (2.46)$$

In which the dot *(.)* represents derivative with respect to time and $\vec{V}.\,\vec{V} = \left|\vec{V}\right|^2$

Computing $\left|\vec{V}\right|^2$ (i.e $\vec{V}^T\vec{V}$) and cancelling the terms which give no contribution when Lagrange's equation of motion is applied and substituting the results in kinetic energy expression

$$T = \frac{1}{2}\int_{vol}\rho\begin{Bmatrix}\dot{u}\\ \dot{v}\\ \dot{w}\end{Bmatrix}^T\begin{Bmatrix}\dot{u}\\ \dot{v}\\ \dot{w}\end{Bmatrix}d(vol) + \frac{1}{2}\int_{vol}\rho\begin{Bmatrix}\dot{u}\\ \dot{v}\\ \dot{w}\end{Bmatrix}^T[A_1]\begin{Bmatrix}u\\ v\\ w\end{Bmatrix}d(vol)$$

$$+\tfrac{1}{2}\int_{vol}\rho\begin{Bmatrix}u\\ v\\ w\end{Bmatrix}^T[A_2]\begin{Bmatrix}u\\ v\\ w\end{Bmatrix}d(vol) + \int_{vol}\rho\begin{Bmatrix}x\\ y\\ z\end{Bmatrix}^T[A_2]\begin{Bmatrix}u\\ v\\ w\end{Bmatrix}d(vol) \qquad (2.47)$$

$$\text{Where } [A_1] = \begin{bmatrix}0 & -2\Omega_z & 2\Omega_y\\ 2\Omega_z & 0 & -2\Omega_x\\ -2\Omega_y & 2\Omega_x & 0\end{bmatrix}$$

$$\text{and } [A_2] = \begin{bmatrix}\Omega_y^2 + \Omega_z^2 & -\Omega_x\Omega_y & -\Omega_x\Omega_z\\ -\Omega_x\Omega_y & \Omega_x^2 + \Omega_z^2 & -\Omega_y\Omega_z\\ -\Omega_x\Omega_z & -\Omega_y\Omega_z & \Omega_x^2 + \Omega_y^2\end{bmatrix} \qquad (2.48)$$

The displacement vector *{d}* at any point in the element can be written as

$$\{d\} = [u, v, w]^T = [S]\{\delta_e\} \qquad (2.49)$$

Where *[S]* is the shape function matrix and $\{\delta_e\}$ is the element nodal displacement vector. Substituting the above relation the expression for kinetic energy of an element neglecting the coriolis matrix and the rotational stiffness matrix (for moderate rotational speed)

$$T = \tfrac{1}{2}\int_{vol}\rho\left\{\dot{\delta_e}\right\}^T[S]^T[S]\{\dot{\delta_e}\}d(vol) + \int_{vol}\rho\begin{Bmatrix}x\\ y\\ z\end{Bmatrix}^T[A_2][S]\{\delta_e\}d(vol) \qquad (2.50)$$

i.e $$T = \frac{1}{2}\{\dot{\delta}_e\}^T [M_e]\{\dot{\delta}_e\} + \{\dot{\delta}_e\}^T [F_{ce}] \quad (2.51)$$

Where *[M_e]* is the element mass matrix

$$[M_e] = \rho \int_v [S]^T [S]\, d(vol) \quad (2.52)$$

And the element centrifugal force vector is

$$\{F_{ce}\} = \rho \int_v [S]^T [A_2] \begin{Bmatrix} x \\ y \\ z \end{Bmatrix} d(vol) \quad (2.53)$$

The linear elastic strain energy of an element is given by

$$U_1 = \frac{1}{2}\int_{vol}\{\varepsilon\}^T \{\sigma\} d(vol) \quad (2.54)$$

The strain vector $\{\varepsilon\}$ and the stress vector $\{\sigma\}$ are expressed as

$$\{\varepsilon\} = [B]\{\delta_e\} \text{ and } \{\sigma\} = [D]\{\sigma\} \quad (2.55)$$

Where *[B]* is the strain displacement matrix and *[D]* is elasticity matrix.

Substituting the above equation U_1 becomes

$$U_1 = \frac{1}{2}\int_{vol}\{\delta_e\}^T \{B\}^T [D][B]\{\delta_e\} d(vol) \quad (2.56)$$

i.e $$U_1 = \frac{1}{2}\{\delta_e\}^T [K_e]\{\delta_e\} \quad (2.57)$$

Where the elastic stiffness matrix is

$$K_e = \frac{1}{2}\int_{vol}\{B\}^T [D][B] d(vol) \quad (2.58)$$

The non-linear strain components can be written as

$$\{\acute{\varepsilon}\} = \frac{1}{2}\begin{bmatrix} \theta_x^T & 0 & 0 \\ 0 & \theta_y^T & 0 \\ \theta_y^T & \theta_x^T & 0 \\ \theta_z^T & 0 & \theta_x^T \\ 0 & \theta_z^T & \theta_y^T \end{bmatrix} \begin{Bmatrix} \theta_x \\ \theta_y \\ \theta_z \end{Bmatrix} = \frac{1}{2}[A]\{\theta\} \quad (2.59)$$

Where,

$$\theta_x^T = \left[\frac{\partial u}{\partial x}, \frac{\partial v}{\partial x}, \frac{\partial w}{\partial x}\right],\ \theta_y^T = \left[\frac{\partial u}{\partial y}, \frac{\partial v}{\partial y} + \frac{w}{R_y}, \frac{\partial w}{\partial y} - \frac{v}{R_y}\right], \theta_z^T = \left[\frac{\partial u}{\partial z}, \frac{\partial v}{\partial z}, \frac{\partial w}{\partial z}\right] \quad (2.60)$$

Now, $$[\theta] = [G]\{\delta_e\} \quad (2.61)$$

where *[G]* represents the matrix of derivatives of the shape functions. The strain energy contribution from the initial stresses generated due to rotation is given by

$$U_2 = \frac{1}{2}\int_{vol}\{\acute{\varepsilon}\}^T \{\sigma_0\} d(vol) \quad (2.62)$$

Where σ_0 is the initial stress vector. From the above relation

$$U_2 = \frac{1}{2}\int_{vol}\{\theta\}^T [A]^T\{\sigma_0\}d(vol) \quad (2.63)$$

i.e $$U_2 = \frac{1}{2}\int_{vol}\{\delta_e\}^T[G]^T [A]^T\{\sigma_0\}d(vol) \quad (2.64)$$

Now, $$[A]^T\{\sigma_0\} = [M_\sigma]\{\theta\} = [M_\sigma][G]\{\delta_e\} \quad (2.65)$$

Where $[M_\sigma]$ is a matrix of initial stresses. So the additional strain energy stored in an element is given by,

$$U_2 = \frac{1}{2}\int_{vol}\{\delta_e\}^T[G]^T [M_\sigma][G]\{\delta_e\}d(vol) \quad (2.66)$$

i.e $$U_2 = \frac{1}{2}\{\delta_e\}^T[K_{\sigma e}]\{\delta_e\} \quad (2.67)$$

Where $[K_{\sigma e}]$ is element geometric stiffness matrix and is given by

$$[K_{\sigma e}] = \int_{vol}[G]^T [M_\sigma][G]d(vol) \quad (2.68)$$

Now, the potential strain energy *(U)* for an element of a rotating shell can be expressed as

$U = U_1 + U_2$

i.e $$U = \frac{1}{2}\{\delta_e\}^T[K_e]\{\delta_e\} + \frac{1}{2}\{\delta_e\}^T[K_{\sigma e}]\{\delta_e\} \quad (2.69)$$

Lagrange's equation of motion and is given by

$$\frac{d}{dt}\left(\frac{\partial L_f}{\partial \dot{\delta}_e}\right) - \left(\frac{\partial L_f}{\partial \delta_e}\right) = \{F_e\} \quad (2.70)$$

Where $\{F_e\}$ is the applied external force vector of an element and L_f is the Lagrangian function.

Replacing $L_f = U - T$ in Lagrange's equation incorporating the corresponding expressions for *T* and *U*, the dynamic equilibrium equation for each element can be expressed in following form (Karmakar and Sinha, 2001)

$$[M_e]\{\ddot{\delta}_e\} + ([K_e] + [K_{\sigma e}])\{\delta_e\} = \{F_{ce}\} + \{F_e\} \quad (2.71)$$

Where $[M_e]$, $[K_e]$ and $[K_{\sigma e}]$ represents element mass matrix, elastic stiffness matrix and geometric stiffness matrix, respectively. $\{F_{ce}\}$, $\{F_e\}$ and $\{\delta_e\}$ represents the element load

vector due to centrifugal force , element load vector due to externally applied load and element displacement vector respectively. After assembling all the element matrices and the force vectors with respect to the common global coordinates, the resulting equilibrium equation of the structure becomes

$$[M]\{\ddot{\delta}\} + ([K] + [K_\sigma])\{\delta\} = \{F(\Omega^2)\} + \{F\} \qquad (2.72)$$

Where *[M]*, *[K]* and $[K_\sigma]$ are the respective global matrices, $\{F(\Omega^2)\}$ is the vector of nodal equivalent centrifugal forces, *{F}* is the global vector of externally applied load and *{δ}* is the global displacement vector. Where $[K_\sigma]$ depends on initial stress distribution and is obtained by the iterative procedure upon solving

$$([K] + [K_\sigma])\{\delta\} = \{F(\Omega^2)\} \qquad (2.73)$$

The stress values are found to converge with three iterations. The equation (2.73) solved by Gauss elimination technique (Bathe, 1990).

From equation (2.72), for the single impact problem, {F} is given as

$$\{F\} = \{0\ 0\ 0 \ldots\ldots Fc \ \ldots\ldots 0\ 0\ 0\}^T \qquad (2.74)$$

Also From equation (2.72), for the multiple impact problem, {F} is given as

$$\{F_c\} = \{0\ 0\ 0 \ \ldots\ F_{cA} \ldots\ 0 \ \ldots F_{cB} \ \ldots 0\}^T \qquad (2.75)$$

Where, Fc_A and Fc_B are the contact forces at the nodes *A* and *B* where the impacts occur.

The equation of motion of the rigid impactor is obtained as

$$m_i\ddot{w}_i + \mathrm{F}_c = 0 \qquad (2.76)$$

Where m_i and $\ddot{w}_i$ are the mass and acceleration of the impactor, respectively. Newmark's time integration scheme (constant-average-acceleration method) is employed for solving the time dependent equations of the shell and the impactor.

2.5 FORMULATION OF CONICAL SHELL

A shallow shell is characterized by its middle surface, and it is defined by the equation 2.77 (Leissa et al., 1984)

$$z = -\frac{1}{2}\left[\frac{x^2}{r_x} + 2\frac{xy}{r_{xy}} + \frac{y^2}{r_y}\right] \tag{2.77}$$

Where, r_x, r_y and r_{xy} denote the radii of curvature in the x and y directions and the radius of twist, respectively. The radius of twist (r_{xy}), length (L_0) of the shell and twist angle (ψ) are related by the equation 2.78.

$$\tan\psi = -\frac{L_0}{r_{xy}} \tag{2.78}$$

A thin shallow conical shell with length L_0, reference width b_0, thickness h, vertex angle φ_{ve} and base subtended angle of cone φ_0 is shown in Figure 2.5.

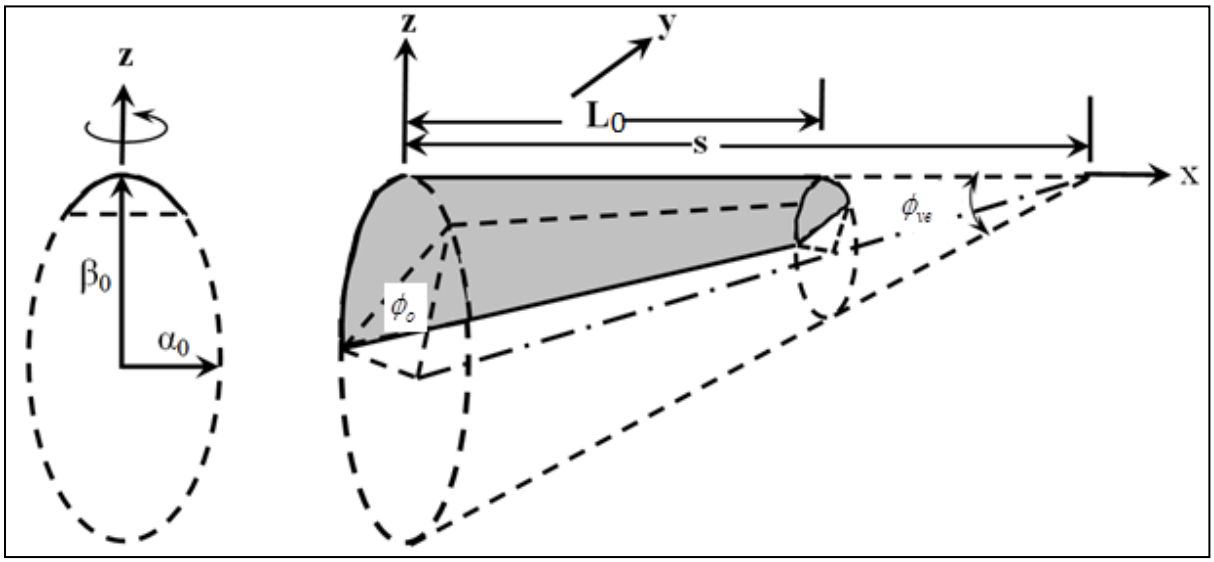

Figure 2.5 Geometry of cantilever shallow conical shell model

Since the conical shell is shallow, it may be assumed that the cross section in Figure 2.6 is elliptical. The component of radius of curvature in the chord wise direction $r_y(x, y)$is a parameter varying both in the x- and y-directions. The variation in the x-direction is linear. There is no curvature along the span wise direction$(r_x = \infty)$. The cantilever shell, clamped along x = 0, is pretwisted with radius of twist r_{xy} as shown in Figure 2.6.

Introducing the non-dimensional coordinate system,

$$\xi = \frac{x}{L_0} \;\; and \; \eta = \frac{y}{b_0} \tag{2.79}$$

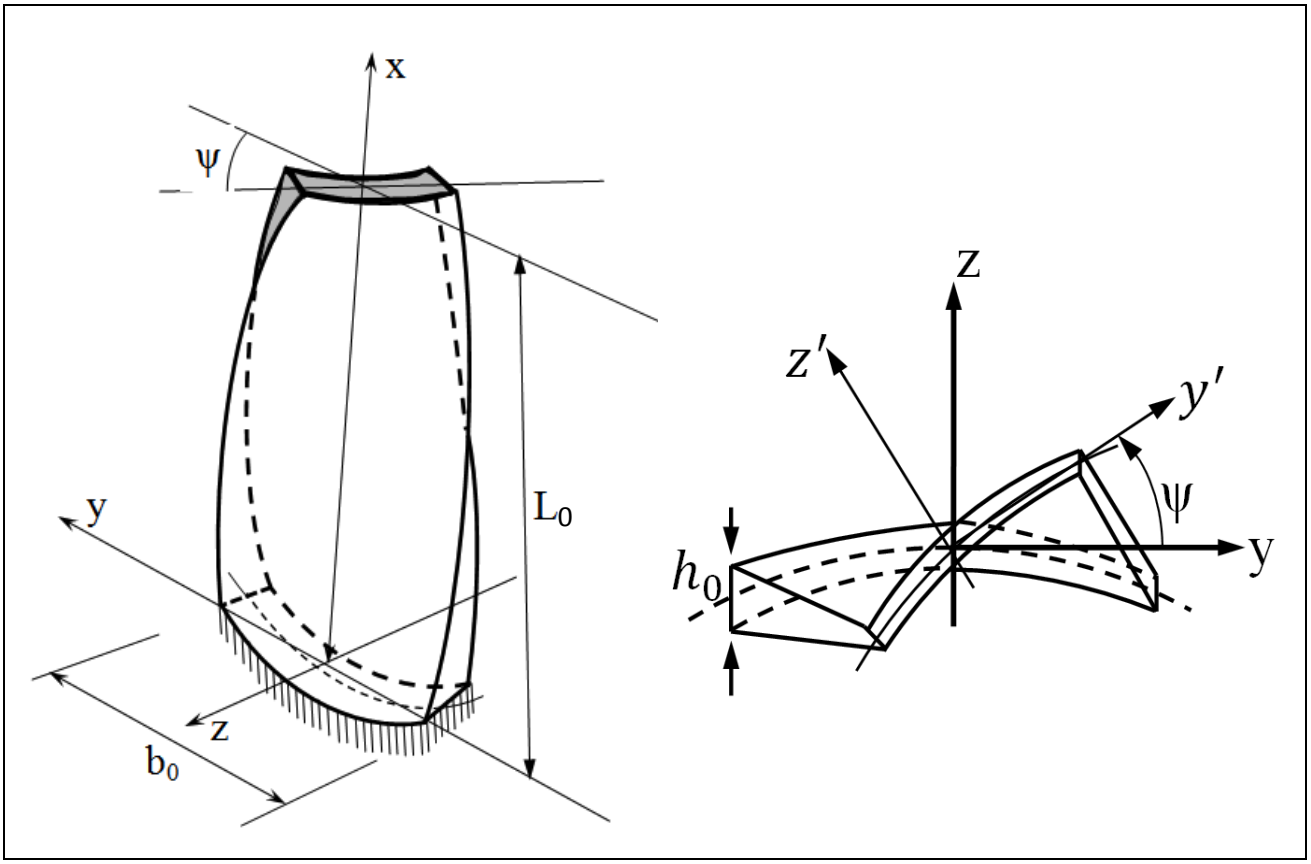

Figure 2.6 Geometry of pretwisted Conical Shell Model

Where, L_0 and b_0 are the length and reference width of the shell plan form as shown in Figure 2.6.

The varying radius of curvature can be expressed as per (Liew et al., 1994)

$$r_y(\xi,\eta) = \frac{\beta_0}{f(\xi,\eta)} \tag{2.80}$$

Where, β_o is the reference major radius as shown in Figure 2.5. Let β and α are the major and minor radius at any cross-section parallel to the reference ellipse and S the slant-length of the cone of the conical shell;

The function can be derived from the geometry of conical shell and is expressed as follows:

$$f(\xi,\eta) = tan(\theta_v/2)\frac{S}{r_y(\xi,\eta)} \tag{2.81}$$

$$\frac{r_y(\xi,\eta)}{S} = \left(\frac{\alpha_0}{S}\right)^2\left(\frac{\beta}{S}\right)^2\left\{\left(\frac{S}{\beta}\right)^2 + \eta^2\left(\frac{b_0}{S}\right)^2\left(\frac{S}{\alpha_0}\right)^2\left[\left(\frac{S}{\alpha_0}\right)^2 - \left(\frac{S}{\beta}\right)^2\right]\right\}^{3/2} \tag{2.82}$$

$$\frac{\alpha_0}{S} = \frac{(b/S)(\beta/S)\,tan(\theta_0/2)}{\sqrt{4(\beta/S)^2 tan^2(\theta_0/2) - (b/S)^2}} \tag{2.83}$$

$$\frac{\beta}{S} = \tan(\theta_v/2)\,[1 - (L/S)\xi] \tag{2.84}$$

$$\frac{b_0}{S} = \sin(\theta_v/2)\sqrt{\frac{tan^2(\theta_0/2)}{\cos(\theta_v/2) + tan^2(\theta_0/2)}} \tag{2.85}$$

$$\frac{b}{s} = \frac{b_0}{s}\,[1 - (L/s)\xi] \tag{2.86}$$

2.5.1 FORMULATION OF FREE VIBRATION PROBLEM

The natural frequencies and eigenvectors are found about the deformed configuration. For the static analysis, the time-dependent terms are neglected and the form is obtained

$$([K] + [K_\sigma])\{\delta_s\} = \{F(\Omega^2)\} \tag{2.87}$$

where $\{\delta_s\}$ is the static equilibrium solution as a result of centrifugal force. For the dynamic analysis, both the static and the time-dependent components are considered where the displacement vector $\{\delta\}$ can be expressed as the sum of static and a dynamic terms [$\{\delta\}=\{\delta_s\} + \{\delta_p\}$, where $\{\delta_p\}$ is a small linear time dependent perturbation about the static displaced position $\{\delta_s\}$]. The equation of motion can be written as

$$[M]\{\ddot{\delta}\} + ([K] + [K_\sigma])(\{\delta_s\} + \{\delta_p\}) = \{F(\Omega^2)\} \tag{2.88}$$

Finally the equation of motion for free vibration is obtained in global form considering the null force vectors (for free vibration case)

$$[M]\{\ddot{\delta}\} + ([K] + [K_\sigma])\{\delta\} = \{F(\Omega^2)\} \tag{2.89}$$

In this Equation the displacement $\{\delta\}$ is a function of space and time. To solve the free vibration problem, the separation of space and time co-ordinates is done by the following substitution

$$\{\delta\} = A' e^{i\omega t}\{\varphi\} \tag{2.90}$$

Therefore,

$$\{\ddot{\delta}\} = -A'\omega^2 e^{i\omega t}\{\varphi\} \tag{2.91}$$

Substituting Equations (2.90) and (2.91) into Equation (2.89) one can get

$$A' e^{i\omega t}(-\omega^2[M]\{\varphi\} + ([K] + [K_\sigma])\{\varphi\}) = 0 \tag{2.92}$$

As $A' e^{i\omega t}$ cannot be zero, therefore

$$(-\omega^2[M]\{\varphi\} + ([K] + [K_\sigma])\{\varphi\}) = 0 \quad (2.93)$$

Or,

$$([K] + [K_\sigma])\{\varphi\} = \omega^2[M]\{\varphi\} \quad (2.94)$$

Hence, the natural frequencies (ω) are determined from the standard eigen value problem (Bathe, 1990) which is represented below and is solved by the QR iteration algorithm. By multiplying both sides of Equation (2.94) by $([K] + [K_\sigma])^{-1}$ the equation reduces to

$$\lambda\{\varphi\} = \omega^2([K] + [K_\sigma])^{-1}[M]\{\varphi\} \quad (2.95)$$

Or,

$$\lambda\{\varphi\} = A\{\varphi\} \quad (2.96)$$

Where,

$$([K] + [K_\sigma])^{-1}[M] = A \quad (2.97)$$

and

$$\lambda \ = \ 1 \ / \ \omega^2 \quad (2.98)$$

2.5.2 IMPACT MODELLING (SINGLE AND MULTIPLE)

A rigid spherical impactor with low velocity travels towards a functionally graded conical target and impacts on the top surface of the conical shell, where the top surface is ceramic-rich. The shell is initially at stationary and undeformed with one end clamped boundary condition that could be idealized as a turbo machinery blades (as shown in figure 2.7). The impactor is presumed to contribute no mass to the system that would affect the shell modes and combined response. Additionally, the impact is idealized by neglecting gravitational effects and assuming the impactor bounces off the shell instantaneously after impacting on the surface. The governing equations of low-velocity, low-energy impact phenomenon between a sphere and a plate have been defined by Goldsmith (1960). The formulation initiates by considering the pressure distribution from an impact incident can be resolved into a concentrated force of magnitude F. At impact, the projectile will deform the shell globally as well as a small localized area where the elastic sphere indents the shell. The impact force causing the localized deformation refers as indentation. Fc, is a contact force that may be expressed by the Hertzian contact formulation which is effective for a relatively low-velocity, low-energy impact where deformation between the impactor and target are elastic in nature. The validity of this assumption weakens for high velocity impact. Conway (1956) established a Hertzian-type contact force model which is appropriate for transversely isotropic materials.

This model has been used to state the contact between the impactor and FGM materials (Larson and Palazotto, 2006; Shariyat and Jafari, 2013). The apparent elasticity module of the shallow conical shell may be governed by

$$E_x = E_c V_{c,sum} + E_m V_{m,sum} \tag{2.99}$$

$$E_z = \left[\frac{V_{c,sum}.E_m + V_{m,sum}.E_c}{E_c E_m}\right]^{-1} \tag{2.100}$$

Where $V_{c,sum}$ and $V_{m,sum}$ are the sum of the volume fraction of ceramic and metal constituents along the thickness domain of the shell. The constituent material property distributed based on simple power law distribution and can be written as

$$V_{c,sum} = \frac{1}{h}\int_{-\frac{h}{2}}^{-\frac{h}{2}} V_c\, dz = \frac{1}{h}\int_{-\frac{h}{2}}^{-\frac{h}{2}} \left[\frac{2z+h}{2h}\right]^N dz = \frac{1}{N+1} \tag{2.101}$$

$$V_{m,sum} = 1 - V_{c,sum} = 1 - \frac{1}{N+1} = \frac{N}{N+1} \tag{2.102}$$

Following the equation (2.99) the apparent density ρ_x, Poisson's ratio υ_x and shear modulus G_x are defined using the rule of mixture approach as follows

$$\rho_x = \rho_c V_{c,sum} + \rho_m V_{m,sum} \tag{2.103}$$

$$\upsilon_x = \upsilon_c V_{c,sum} + \upsilon_m V_{m,sum} \tag{2.104}$$

$$G_x = \left[\frac{V_{c,sum}.G_m + V_{m,sum}.G_c}{G_c G_m}\right]^{-1} \tag{2.105}$$

For the modified Hertzian contact law, contact force (F_C) can be calculated during loading unloading cycle as (Larson and Palazotto, 2006)

$$F_c = K_{mod}\alpha^{1.5}\ ,\ 0 \le \alpha \le \alpha_{max} \tag{2.106}$$

Where, F_C is the contact forces at the nodes where the impacts occur. α =local indentation which is the change in distance between centre of the impactor and the mid-surface of target shell and α_{max}=maximum local indentation.

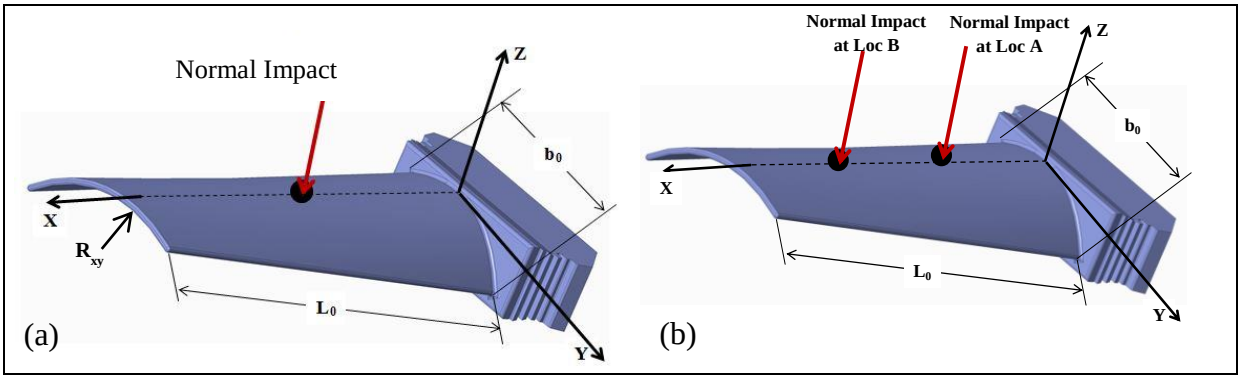

Figure. 2.7 (a) Single impact at centre on turbo-machinery pretwisted conical shells blade (b) Multiple impact on turbo-machinery pretwisted conical shells blade at location A and location B.

While $\{F_C\}$ is the global contact force vector resulting from single impacts and is given by

$$\{F_C\} = \{0\ 0\ 0\ \ldots\ldots F_C \ldots\ldots\ 0\ \ 0\ \ 0\}^T \tag{2.107}$$

While $\{F_C\}$ is the global contact force vector resulting from multiple impacts and is given by

$$\{F_c\} = \{0\ 0\ 0\ \ldots\ F_{cA} \ldots\ 0\ \ldots\ldots F_{cB}\ \ldots\ldots 0\}^T \tag{2.108}$$

Where, Fc_A and Fc_B are the contact forces at the nodes *A* and *B* where the impacts occur. The modified contact stiffness (K_{mod}) of the Hertzian contact law can be written as (Larson and Palazotto, 2006),

$$K_{mod} = \frac{16\sqrt{R_r}}{3\pi(K_{targ}+K_{impt})(\varepsilon)^{\frac{3}{2}}} \tag{2.109}$$

Where ε is a constant based on shape of the impactor and target surface. For the low velocity impact case, the value of this constant considered as 2 and this depends on contact behavior between a conical shell target and a spherical impactor. On the other hand R_r is a constant depending on the curvatures of both impactor and projectile and is expressed as

$$\frac{1}{R_r} = \frac{1}{R_x^{impt}} + \frac{1}{R_y^{impt}} + \frac{1}{R_x^{targ}} + \frac{1}{R_y^{targ}} \tag{2.110}$$

For spherical impactor, the principal radii R_x^{impt} and R_y^{impt} are equal.

The Stiffness K_{targ} of equation (2.109) is defined by following expression,

$$K_{targ} = \frac{\sqrt{A_{22}[(G_x+A_{11}A_{22})^2-(G_x+A_{12})^2]}}{\sqrt{G_x 4\pi^2}.(A_{11}A_{22}-A_{12}{}^2)} \tag{2.111}$$

Where G_x is defined in equation (2.105) and other parameters of the above expression are defined as follows

$$A_{11} = \frac{E_z(1-\upsilon_x)}{\left(1-\upsilon_x-2\upsilon_x^2\frac{E_x}{E_z}\right)}$$

$$A_{22} = \frac{E_x\left(1-\upsilon_x^2\frac{E_x}{E_z}\right)}{(1+\upsilon_x)\left(1-\upsilon_x-2\upsilon_x^2\frac{E_x}{E_z}\right)} \tag{2.112}$$

$$A_{12} = \frac{E_x\upsilon_x}{\left(1-\upsilon_x-2\upsilon_x^2\frac{E_x}{E_z}\right)}$$

Similar to the equation (2.111) the K_{impt} which is defined in equation (2.109) can also be determined. It can be noted that for the rigid impactor as in the present case, $K_{impt} = 0$.

The dynamic equilibrium equation with moderate rotational speeds is derived using Lagrange's equation of motion in global form neglecting Coriolis effect (Karmakar and Kishimoto, 2006).

$$[M]\{\ddot{\delta}\} + ([K_\sigma])\{\delta\} = \{F\} \tag{2.113}$$

Where {F} is the global vector of externally applied load and *{δ}* is the global displacement vector. For low velocity impact problem {F} can be expressed as

$$m_i\ddot{w}_i + F_c = 0 \tag{2.114}$$

Where mi and $\ddot{w}_i$ are the mass and acceleration of the impactor, respectively. Neglecting the contribution of plate displacements along global x and y directions, the indentation α can be written is (Karmakar and Kishimoto, 2006).

$$\alpha(t) = w_i(t) - w_p\,(x_c, y_c, t)\,Cos\Psi \tag{2.115}$$

Where w_i and w_p are displacement of impactor mass and target shell displacement along global z direction at the impact point (x_c, y_c), respectively and Ψ is the twist angle of the conical shell blade. The components of force at the impact point in global directions are given by

$$F_{ix} = 0, \quad F_{iy} = F_C\,Sin\Psi \;\; and \;\; F_{iz} = F_C\,Cos\Psi \tag{2.116}$$

2.5.3 TIME DELAYED MULTIPLE IMPACT

The contact force vector $\{F\}$ is given by

$$\{F_C\} = \{0\;0\;0\;\ldots\ldots\mathrm{F}_C\ldots\ldots\;0\;\;0\;\;0\}^T \qquad \textit{For single-site impact} \tag{2.117}$$

$$\{F_c\} = \{0\ 0\ 0\ \ldots\ F_{cA}\ \ldots\ 0\ \ldots.F_{cB}\ \ldots.0\}^T \quad \textit{For multi-site impact} \tag{2.118}$$

$$\{F_c\} = \{0\ 0\ 0\ \ldots\ F_{cA}.\ldots\ 0\ \ldots.F_{cdB}\ \ldots.0\}^T \textit{for multi-site delayed impact} \tag{2.119}$$

Where F_C is the contact force in case of single impact; $F_{cA}\ldots F_{cB}$ are the contact forces due to the simultaneous impact at location A and B while F_{cdB} is the contact forces due to the delayed impacts at specified nodes on the conical shell. The equation of motion for each rigid impactor is given by

$$m_i\ddot{w}_i + F_c = 0 \tag{2.120}$$

Where m_i and $\ddot{w}_i$ are the mass and acceleration of the impactor, respectively. The Newmark's time integration scheme (Bathe, 1990) of constant-average-acceleration method is used in solving the equations of motion of the shell and impactors.

2.5.4 NEWMARK'S TIME INTEGRATION SCHEME

The equilibrium equations (2.88) and (2.120) governing the linear dynamic response of the conical shell and the impactor involve the contact force F_c which is transient in character. These equations are regarded as a system of ordinary differential equations (ODE) with constant coefficients and are made to be satisfied at discrete time intervals Δt apart. Newmark's direct time integration scheme (constant-average-acceleration method) is considered to approximate the time derivatives and thereby to solve the forced vibration equations. Use of this unconditionally stable scheme to the equations (2.88) and (2.120) with time step Δt derive the following relations at time $t + \Delta t$

$$[\bar{K}]\{\delta\}^{t+\Delta t} = \{\bar{F}\}^{t+\Delta t} \tag{2.121}$$

$$\left[\bar{k}_{impt}\right]\left\{\omega_{impt}\right\}^{t+\Delta t} = \{\bar{F}_c\}^{t+\Delta t} \tag{2.122}$$

Where $[\bar{K}]$ and $\left[\bar{k}_{impt}\right]$ are the effective stiffness matrix of the target conical shell and the effective stiffness of the striker, respectively which are expressed as

$$[\bar{K}] = [K] + [K_\sigma] + a_0[M] \tag{2.123}$$

$$\left[\bar{k}_{impt}\right] = a_0 m_{impt} \tag{2.124}$$

Effective forces at time $t + \Delta t$ can be considered as

$$\{\bar{F}\}^{t+\Delta t} = \{F(\Omega^2)\} + \{F\}^{t+\Delta t} + [M]\left(a_0\{\delta\}^t + a_1\{\dot{\delta}\}^t + a_2\{\ddot{\delta}\}^t\right) \quad (2.125)$$

$$\{\bar{F}_c\}^{t+\Delta t} = \{F_c\}^{t+\Delta t} + m_{impt}\left(a_0{\omega_{impt}}^t + a_1{\dot{\omega}_{impt}}^t + a_2{\ddot{\omega}_{impt}}^t\right) \quad (2.126)$$

Velocity can be derived from displacement at time $t + \Delta t$ as

$$\{\dot{\delta}\}^{t+\Delta t} = \{\dot{\delta}\}^t + a_3\{\ddot{\delta}\}^t + a_4\{\ddot{\delta}\}^{t+\Delta t} \quad (2.127)$$

$${\omega_{impt}}^{t+\Delta t} = a_0\left[{\omega_{impt}}^{t+\Delta t} - {\omega_{impt}}^t\right] - a_1{\dot{\omega}_{impt}}^t - a_2{\ddot{\omega}_{impt}}^t \quad (2.128)$$

And the Acceleration can be derived from velocity at time $t + \Delta t$ as

$$\{\ddot{\delta}\}^{t+\Delta t} = a_0[\{\delta\}^{t+\Delta t} - \{\delta\}^t] - a_1\{\dot{\delta}\}^t - a_2\{\ddot{\delta}\}^t \quad (2.129)$$

$${\dot{\omega}_{impt}}^{t+\Delta t} = {\dot{\omega}_{impt}}^t + a_3{\ddot{\omega}_{impt}}^t + a_4{\ddot{\omega}_{impt}}^{t+\Delta t} \quad (2.130)$$

The initial boundary conditions as

$$\{\delta\} = \{\dot{\delta}\} = \{\ddot{\delta}\} = 0$$
$$\omega_{impt} = \ddot{\omega}_{impt} = 0 \quad \text{and} \quad \dot{\omega}_{impt} = VOI \quad (2.131)$$

Where, VOI is the initial velocity of the impactor or striker.

The integration constants can be calculated as

$$a_0 = \frac{1}{\beta'\Delta t^2}\ , a_1 = \frac{1}{\beta'\Delta t}\ , a_2 = \frac{1}{2\beta'} - 1\ , a_3 = (1-\alpha')\Delta t\ \ and\ a_4 = \alpha'\Delta t \quad (2.132)$$

The values of β' and $\alpha'$are taken as 0.25 and 0.5, respectively as per Newmark's constant-average-acceleration method. Equation (2.122) is analogous to equation (2.88) and is solved by the Gauss elimination technique to obtain the dynamic impact parameters at each time step.

2.5.5 GOVERNING EQUATIONS OF FUNCTIONALLY GRADED MATERIALS

FGMs are defined as a combination of two constituent materials, of which one side ceramic rich and another side metal rich. Most of the FGMs are in use at high-temperature

environments and many of the constituent materials may possess temperature-dependent properties.

$$P = P_0 + \frac{P_{-1}}{T} + 1 + P_1 T + P_2 T^2 + P_3 T^3 \tag{2.133}$$

Where P is the effective material properties of the FGM material and P_0, P_{-1}, P_1, P_2, P_3 are the temperature coefficients and T is the temperature in Kelvin scale.

2.5.5.1 SIMPLE POWER LAW

For the simple power law the ceramic volume fraction along the thickness direction is governed by the power law index.

$$V_c = \left[\frac{2z + h}{2h}\right]^N \tag{2.134}$$

Where N is the material property graded index which is a positive real number $(0 \leq N \leq 1)$ which determine the material distribution through the thickness of the beam. According to this distribution we have a fully metal beam for large value of N and when N equals to zero a fully ceramic beam remains and z is the distance (Figure 2.8) from the mid-plane of the graded beam. Figure 2.9 depicts the variation of ceramic volume fraction (V_c) and metallic volume fraction (V_m) along the non-dimensional thickness (z/h) direction for simple power law exponent (N). The material properties P of FGMs are a function of the material properties and volume fractions of the constituent materials, and are expressed as per equation 2.135.

$$P = \sum_{i=1}^{k} P_i \, V_{fi} \tag{2.135}$$

Where P_i and V_{fi} are the material property and volume fraction of the constituent material i, satisfying the volume fraction of all the constituent materials k is unity, i.e

$$\sum_{i=1}^{k} V_{fi} = \sum_{i=1}^{k} \left[\frac{2z + h}{2h}\right]^N = 1 \tag{2.136}$$

Where *N* is the material property graded index which is a positive real number *(0≤N≤1).* For FG conical shells the material properties vary continuously and smoothly along the thickness of the shell.

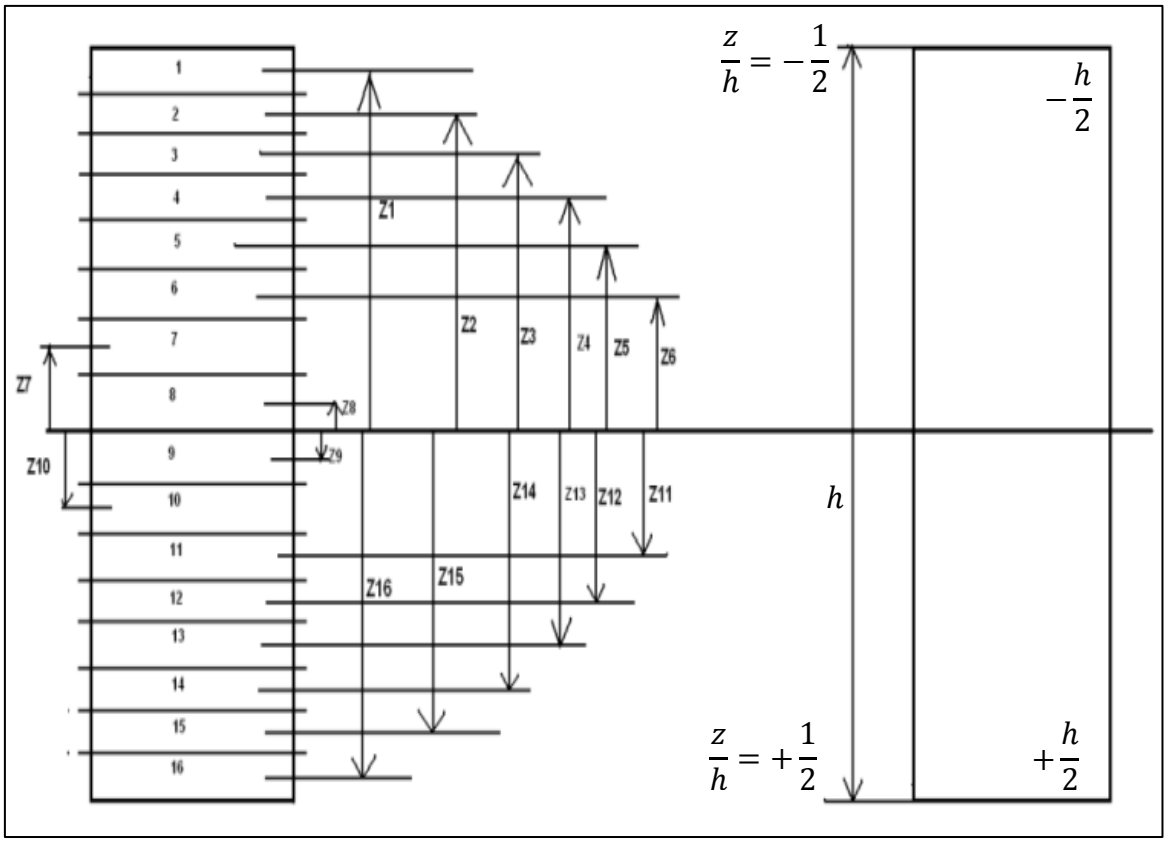

Figure 2.8 Graphical representation of z values for 16 Layer FGM material along the thickness direction

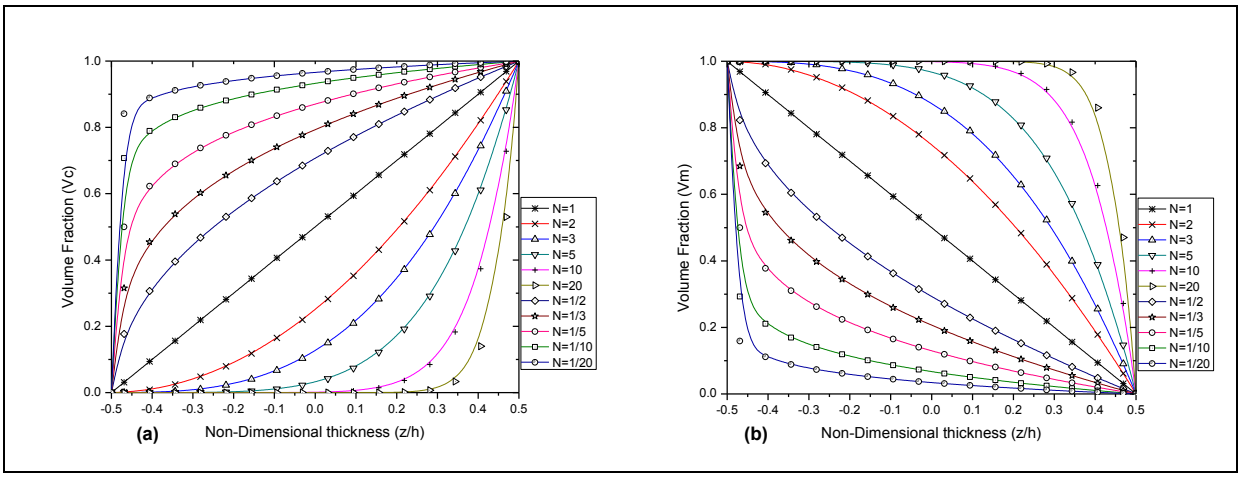

Figure 2.9 Ceramic (a) and metallic (b) volume fraction along the thickness of the shell for various power law index for P- FGM

The effective material properties are obtained using the power law distribution (Zhao and Liew, 2011a) and are expressed in the following

$$P_{eff}(z) = P_m + (P_c - P_m)\left[\frac{2z+h}{2h}\right]^N \tag{2.137}$$

$$E(z) = E_m + (E_c - E_m)\left[\frac{2z+h}{2h}\right]^N \tag{2.138}$$

$$\nu(z) = \nu_m + (\nu_c - \nu_m)\left[\frac{2z+h}{2h}\right]^N \tag{2.139}$$

$$\rho(z) = \rho_m + (\rho_c - \rho_m)\left[\frac{2z+h}{2h}\right]^N \tag{2.140}$$

$$G(z) = G_m + (G_c - G_m)\left[\frac{2z+h}{2h}\right]^N \tag{2.141}$$

E, υ and ρ denote Young's modulus, Poisson's ratio and mass density respectively where in suffix as '*c*' and '*m*' indicate the corresponding values at the outer surface (ceramic rich) and inner surface(metal rich) of the FG conical shell.

2.5.5.2 SIGMOIDAL POWER LAW

FGMs are defined as a combination of two or more constituent materials with smooth variation of the material properties along their thickness. The one surface is ceramic rich while the other surface is metal rich. Most of the FGMs are generally used in high-temperature locations and most of the constituent materials possess temperature-dependent mechanical and thermal properties.

The volume fraction 'V_c' of Sigmoidal FGM (S-FGMs) is expressed as (Jung and Han, 2015)

$$V_{c1}(z) = 1 - 0.5\left(1 - \frac{2z}{h}\right)^N \text{ For } 0 \le z \le h/2 \tag{2.142}$$

$$P_{eff}(z) = P_c V_{c1}(z) + P_m[1 - V_{c1}(z)] \text{ For } 0 \le z \le h/2 \tag{2.143}$$

Where *N* is the material property graded index, a positive real number ($0 \le N \le \infty$). h is the thickness of the shell. By using rule of mixture (ROM) the material property '*Peff*' for S-FGM are

$$P_{eff}(z) = P_m + (P_c - P_m)V_{c1}(z) \tag{2.144}$$

$$E(z) = E_m + (E_c - E_m)V_{c1}(z) \tag{2.145}$$

$$\nu(z) = \nu_m + (\nu_c - \nu_m)V_{c1}(z) \tag{2.146}$$

$$\rho(z) = \rho_m + (\rho_c - \rho_m)V_{c1}(z) \tag{2.147}$$

$$G(z) = G_m + (G_c - G_m)V_{c1}(z) \tag{2.148}$$

On the other hand the effective material properties for other half on the S-FGM can be written as.

$$P_{eff}(z) = P_c V_{c2}(z) + P_m[1 - V_{c2}(z)] \text{ For } -h/2 \leq z \leq 0 \tag{2.149}$$

$$P_{eff}(z) = P_m + (P_c - P_m)V_{c2}(z) \tag{2.150}$$

$$E(z) = E_m + (E_c - E_m)V_{c2}(z) \tag{2.151}$$

$$\nu(z) = \nu_m + (\nu_c - \nu_m)V_{c2}(z) \tag{2.152}$$

$$\rho(z) = \rho_m + (\rho_c - \rho_m)V_{c2}(z) \tag{2.153}$$

$$G(z) = G_m + (G_c - G_m)V_{c2}(z) \tag{2.154}$$

Where (P_{eff}) is material property and (V_{c1} and V_{c2}) are volume fraction of the constituent material (Jung and Han, 2015).

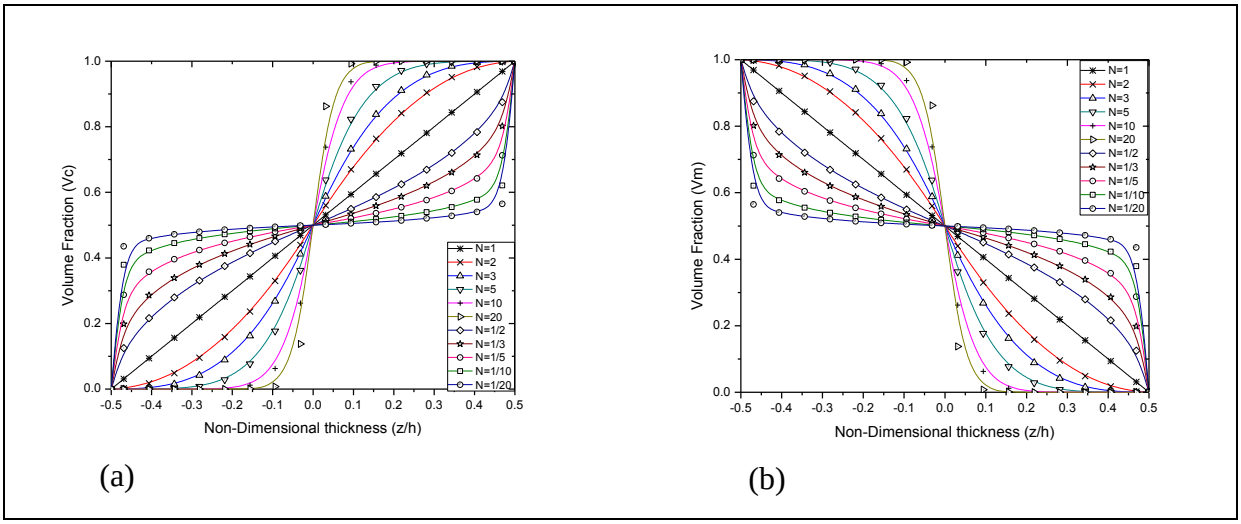

Figure 2.10 (a) Variation of Ceramic volume fraction (V_c) and (b) Metallic volume fraction (V_m) along the non-dimensional thickness direction for different values of N for S-FGM

The sum of the volume fractions for S-FGM for each layer is unity. Effective material properties such as E (Young's modulus), υ (Poisson's ratio) and ρ (mass density) can be calculated effectively with the help of equation 2.143 and 2.149 for each layer of the FGM shell. Figure 2.10 shows the variation of ceramic volume fraction (V_c) and metallic volume fraction (V_m) along the non-dimensional thickness (z/h) direction with sigmoidal power law exponent (N) of functionally graded material as furnished in equation 2.143 and 2.149. From

the Sigmoidal FGM properties, linear variation of volume fractions for both ceramic as well as metal constituents can only be observed for $N = 1$.

2.5.5.3 EXPONENTIAL POWER LAW

This particular idealization for *FGM* modeling is very common in the structural mechanics. For a perfect *FGM* (porosity free) shell structure with uniform thickness 'h', the typical material properties 'P_{eff}' at any point located at a distance 'z' from the reference surface (mid-surface along the thickness direction) is given by equation 2.155.

$$P_{eff} = P_m e^{\left\{\frac{1}{h}\left(\frac{P_c}{P_m}\right)\left(z+\frac{h}{2}\right)\right\}} \tag{2.155}$$

$$E(z) = E_m e^{\left\{\frac{1}{h}\left(\frac{E_c}{E_m}\right)\left(z+\frac{h}{2}\right)\right\}} \tag{2.156}$$

$$\nu(z) = \nu_m e^{\left\{\frac{1}{h}\left(\frac{\nu_c}{\nu_m}\right)\left(z+\frac{h}{2}\right)\right\}} \tag{2.157}$$

$$\rho(z) = \rho_m e^{\left\{\frac{1}{h}\left(\frac{\rho_c}{\rho_m}\right)\left(z+\frac{h}{2}\right)\right\}} \tag{2.158}$$

$$G(z) = G_m e^{\left\{\frac{1}{h}\left(\frac{G_c}{G_m}\right)\left(z+\frac{h}{2}\right)\right\}} \tag{2.159}$$

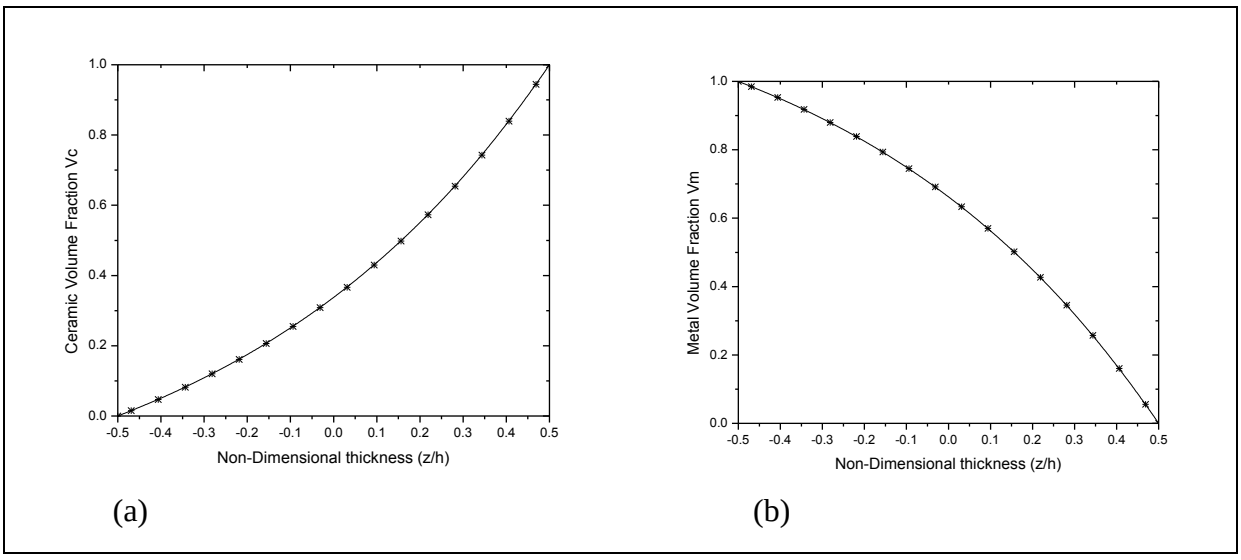

Figure 2.11 (a) Variation of Ceramic volume fraction (V_c) and (b) Metallic volume fraction (V_m) along the non-dimensional thickness direction for E-FGM

For the top surface and bottom surface of the conical shell the value of non-dimensional thickness (z/h) are considered to be -0.5 and 0.5, respectively. Figure 2.11 shows the variation

of ceramic volume fraction (V_c) and metallic volume fraction (V_m) along the non-dimensional thickness (z/h) direction for exponential power law.

2.5.6 FGM WITH POROSITY

Production of porosity free FGM is extremely difficult with the available manufacturing techniques. Porosities possibly occur inside functionally graded materials (FGMs) during fabrication because of technical constraints that lead to creation of micro-voids in these materials. So it is necessary to consider the effect of porosities on the free vibration behavior and low velocity impact characteristics of FGM shell in the present study. Imperfect FGM shell structure are assumed to have even and uneven distributions of porosities over the shell cross-section and material properties of FGM shell are supposed to vary in the z-axis direction based on modified power-law model (P-FGM) which approximate the porous material properties with even and uneven distributions of porous phases. Figure 2.12 represents the cross sectional view with even and uneven distribution of porosities.

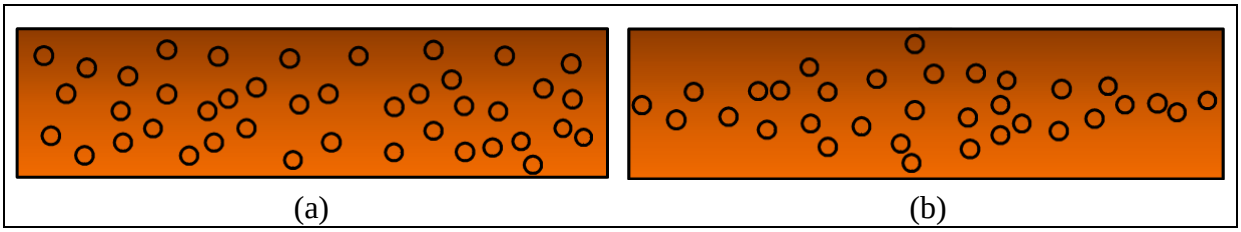

Figure. 2.12 Cross sectional view of (a) even and (b) uneven distributions of porosities

2.5.6.1 FGM WITH EVEN POROSITY

The effective material properties (P_{eff}) of FGM shell with even porosities distributed identically in two phases of ceramic and metal can be expressed by using the modified rule of mixture as (Wang and Zu, 2017)

$$P_{eff}(z) = \left(V_m - \frac{\alpha_{ep}}{2}\right) P_m + \left(V_c - \frac{\alpha_{ep}}{2}\right) P_c \tag{2.160}$$

Where α_{ep} denotes the volume fraction of even porosities($\alpha_{ep} \ll 1$). For perfect (without porosity) FGM α_{ep} is set to zero. P_m and P_c are the material properties of metal and ceramic, and V_m and V_c are the volume fraction of metal and ceramic, respectively.

SIMPLE POWER LAW

The effective material properties considering even porosity are obtained using the simple power law distribution (Wang and Zu, 2017) and are expressed in the following

$$P_{eff}(z) = P_m + (P_c - P_m)\left[\frac{2z+h}{2h}\right]^N - \frac{\alpha_{ep}}{2}(P_c + P_m) \tag{2.161}$$

$$E(z) = E_m + (E_c - E_m)\left[\frac{2z+h}{2h}\right]^N - \frac{\alpha_{ep}}{2}(E_c + E_m) \tag{2.162}$$

$$\nu(z) = \nu_m + (\nu_c - \nu_m)\left[\frac{2z+h}{2h}\right]^N - \frac{\alpha_{ep}}{2}(\nu_c + \nu_m) \tag{2.163}$$

$$\rho(z) = \rho_m + (\rho_c - \rho_m)\left[\frac{2z+h}{2h}\right]^N - \frac{\alpha_{ep}}{2}(\rho_c + \rho_m) \tag{2.164}$$

$$G(z) = G_m + (G_c - G_m)\left[\frac{2z+h}{2h}\right]^N - \frac{\alpha_{ep}}{2}(G_c + G_m) \tag{2.165}$$

E, υ and ρ denote Young's modulus, Poisson's ratio and mass density respectively where in suffix as '*c*' and '*m*' indicate the corresponding values at the outer surface (ceramic rich) and inner surface(metal rich) of the FG conical shell.

SIGMOIDAL POWER LAW

The effective material properties considering even porosity are obtained for the Sigmoidal FGM (S-FGMs) is expressed as (Wang and Zu, 2017a)

(For $0 \le z \le h/2$)

$$P_{eff}(z) = P_m + (P_c - P_m)V_{c1}(z) - \frac{\alpha_{ep}}{2}(P_c + P_m) \tag{2.166}$$

$$E(z) = E_m + (E_c - E_m)V_{c1}(z) - \frac{\alpha_{ep}}{2}(E_c + E_m) \tag{2.167}$$

$$\nu(z) = \nu_m + (\nu_c - \nu_m)V_{c1}(z) - \frac{\alpha_{ep}}{2}(\nu_c + \nu_m) \tag{2.168}$$

$$\rho(z) = \rho_m + (\rho_c - \rho_m)V_{c1}(z) - \frac{\alpha_{ep}}{2}(\rho_c + \rho_m) \tag{2.169}$$

$$G(z) = G_m + (G_c - G_m)V_{c1}(z) - \frac{\alpha_{ep}}{2}(G_c + G_m) \tag{2.170}$$

And, for $-h/2 \leq z \leq 0$ the effective material properties expressed as (Wang and Zu, 2017a)

$$P_{eff}(z) = P_m + (P_c - P_m)V_{c2}(z) - \frac{\alpha_{ep}}{2}(P_c + P_m) \tag{2.171}$$

$$E(z) = E_m + (E_c - E_m)V_{c2}(z) - \frac{\alpha_{ep}}{2}(E_c + E_m) \tag{2.172}$$

$$\nu(z) = \nu_m + (\nu_c - \nu_m)V_{c2}(z) - \frac{\alpha_{ep}}{2}(\nu_c + \nu_m) \tag{2.173}$$

$$\rho(z) = \rho_m + (\rho_c - \rho_m)V_{c2}(z) - \frac{\alpha_{ep}}{2}(\rho_c + \rho_m) \tag{2.174}$$

$$G(z) = G_m + (G_c - G_m)V_{c2}(z) - \frac{\alpha_{ep}}{2}(G_c + G_m) \tag{2.175}$$

EXPONENTIAL POWER LAW

The effective material properties considering even porosity are obtained for the Exponential FGM (E-FGMs) is expressed as

$$P_{eff}(z) = P_m e^{\frac{1}{h}\left(\frac{P_c}{P_m}\right)\left((z+\frac{h}{2})\right)} - \frac{\alpha_{ep}}{2}(P_c + P_m) \tag{2.176}$$

$$E(z) = E_m e^{\left\{\frac{1}{h}\left(\frac{E_c}{E_m}\right)\left((z+\frac{h}{2})\right)\right\}} - \frac{\alpha_{ep}}{2}(E_c + E_m) \tag{2.177}$$

$$\nu(z) = \nu_m e^{\left\{\frac{1}{h}\left(\frac{\nu_c}{\nu_m}\right)\left((z+\frac{h}{2})\right)\right\}} - \frac{\alpha_{ep}}{2}(\nu_c + \nu_m) \tag{2.178}$$

$$\rho(z) = \rho_m e^{\left\{\frac{1}{h}\left(\frac{\rho_c}{\rho_m}\right)\left((z+\frac{h}{2})\right)\right\}} - \frac{\alpha_{ep}}{2}(\rho_c + \rho_m) \tag{2.179}$$

$$G(z) = G_m e^{\left\{\frac{1}{h}\left(\frac{G_c}{G_m}\right)\left((z+\frac{h}{2})\right)\right\}} - \frac{\alpha_{ep}}{2}(G_c + G_m) \tag{2.180}$$

2.5.6.2 FGM WITH UNEVEN POROSITY

The equivalent material properties (P_{eff}) of FGM shell with uneven porosities in ceramic and metal are given by the modified rule of mixture (Wang and Zu, 2017) expressed as

$$P_{eff}(z) = \left(V_m - \frac{\alpha_{up}}{2}\right)\left(1 - \frac{2|z|}{h}\right)P_m + \left(V_c - \frac{\alpha_{up}}{2}\right)\left(1 - \frac{2|z|}{h}\right)P_c \tag{2.181}$$

Where α_{up} denotes the volume fraction of uneven porosities($\alpha_{up} \ll 1$). For perfect (without porosity) FGM α_{up} is set to zero. When uneven porosity is taken into account the effective material properties considering different FGM constituent laws are determined by the equation as described in the following.

SIMPLE POWER LAW

When uneven porosity is taken into account the effective material properties considering P-FGM constituent laws can be written as

$$P_{eff}(z) = P_m + (P_c - P_m)\left[\frac{2z+h}{2h}\right]^N - \frac{\alpha_{up}}{2}(P_c + P_m)\left(1 - \frac{2|z|}{h}\right) \tag{2.182}$$

$$E(z) = E_m + (E_c - E_m)\left[\frac{2z+h}{2h}\right]^N - \frac{\alpha_{up}}{2}(E_c + E_m)\left(1 - \frac{2|z|}{h}\right) \tag{2.183}$$

$$\nu(z) = \nu_m + (\nu_c - \nu_m)\left[\frac{2z+h}{2h}\right]^N - \frac{\alpha_{up}}{2}(\nu_c + \nu_m)\left(1 - \frac{2|z|}{h}\right) \tag{2.184}$$

$$\rho(z) = \rho_m + (\rho_c - \rho_m)\left[\frac{2z+h}{2h}\right]^N - \frac{\alpha_{up}}{2}(\rho_c + \rho_m)\left(1 - \frac{2|z|}{h}\right) \tag{2.185}$$

Figure 2.13 represents the variation of Young's Modulus and density along the non-dimensional thickness direction for different values of simple power law index (*N*). Porosity free FGM shows highest value of material properties and the material properties degrade with porosity percentage. Uneven porosity shows better mechanical property compare to even porosity for same porosity factor.

SIGMOIDAL POWER LAW

The effective material properties considering uneven porosity are obtained for the Sigmoidal FGM (S-FGMs) is expressed as (Wang and Zu, 2017a)

For $0 \le z \le h/2$

$$P_{eff}(z) = P_m + (P_c - P_m)V_{c1}(z) - \frac{\alpha_{up}}{2}(P_c + P_m)\left(1 - \frac{2|z|}{h}\right) \tag{2.186}$$

$$E(z) = E_m + (E_c - E_m)V_{c1}(z) - \frac{\alpha_{up}}{2}(E_c + E_m)\left(1 - \frac{2|z|}{h}\right) \tag{2.187}$$

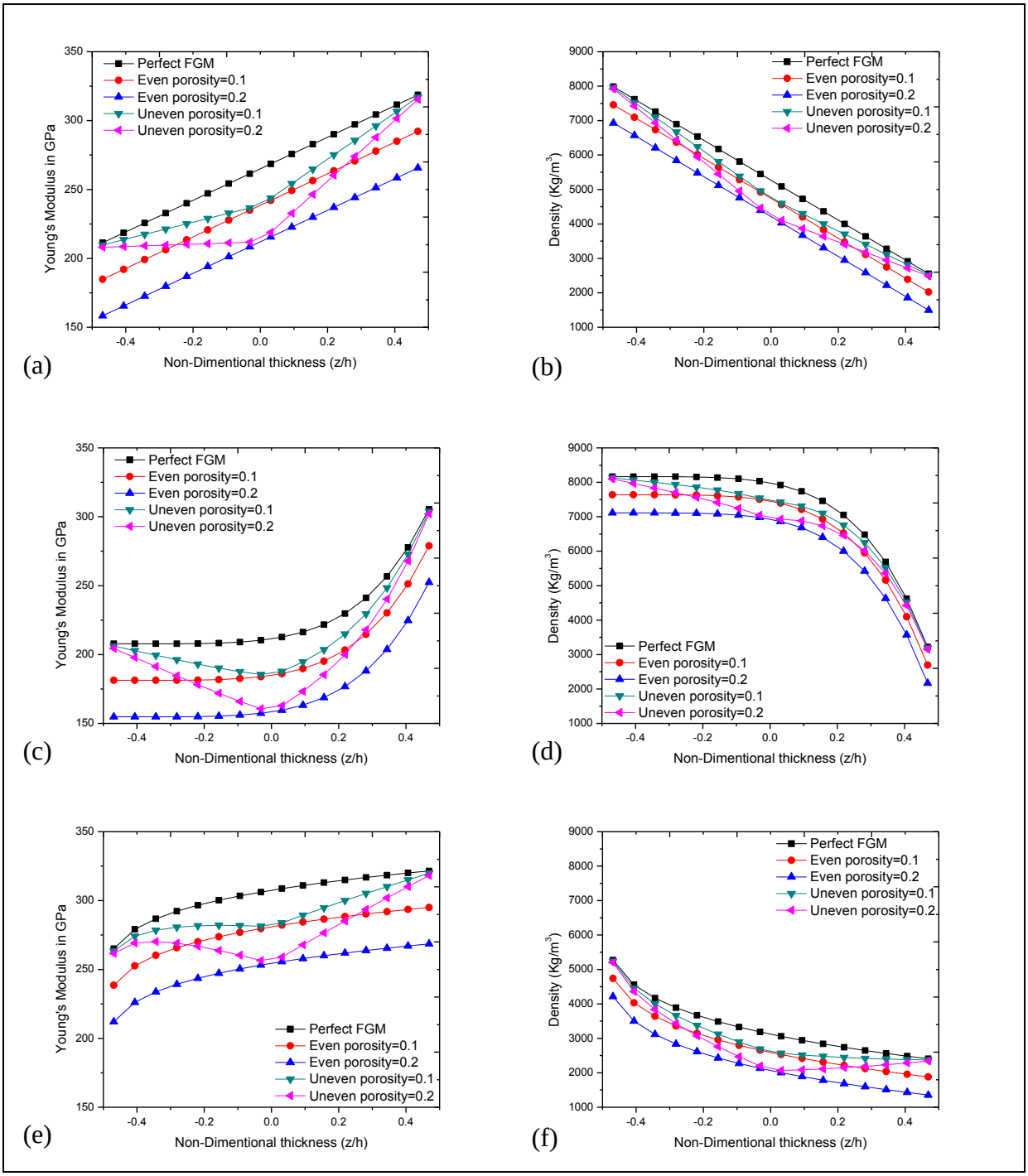

Figure. 2.13 Variation of Young's Modulus Density along the non-dimensional thickness direction for different values of N of SS-Si_3N_4 P-FGM (a, b for N=1), (c, d for N=5),(e, f for N=1/5)

$$\nu(z) = \nu_m + (\nu_c - \nu_m)V_{c1}(z) - \frac{\alpha_{up}}{2}(\nu_c + \nu_m)\left(1 - \frac{2|z|}{h}\right) \tag{2.188}$$

$$\rho(z) = \rho_m + (\rho_c - \rho_m)V_{c1}(z) - \frac{\alpha_{up}}{2}(\rho_c + \rho_m)\left(1 - \frac{2|z|}{h}\right) \tag{2.189}$$

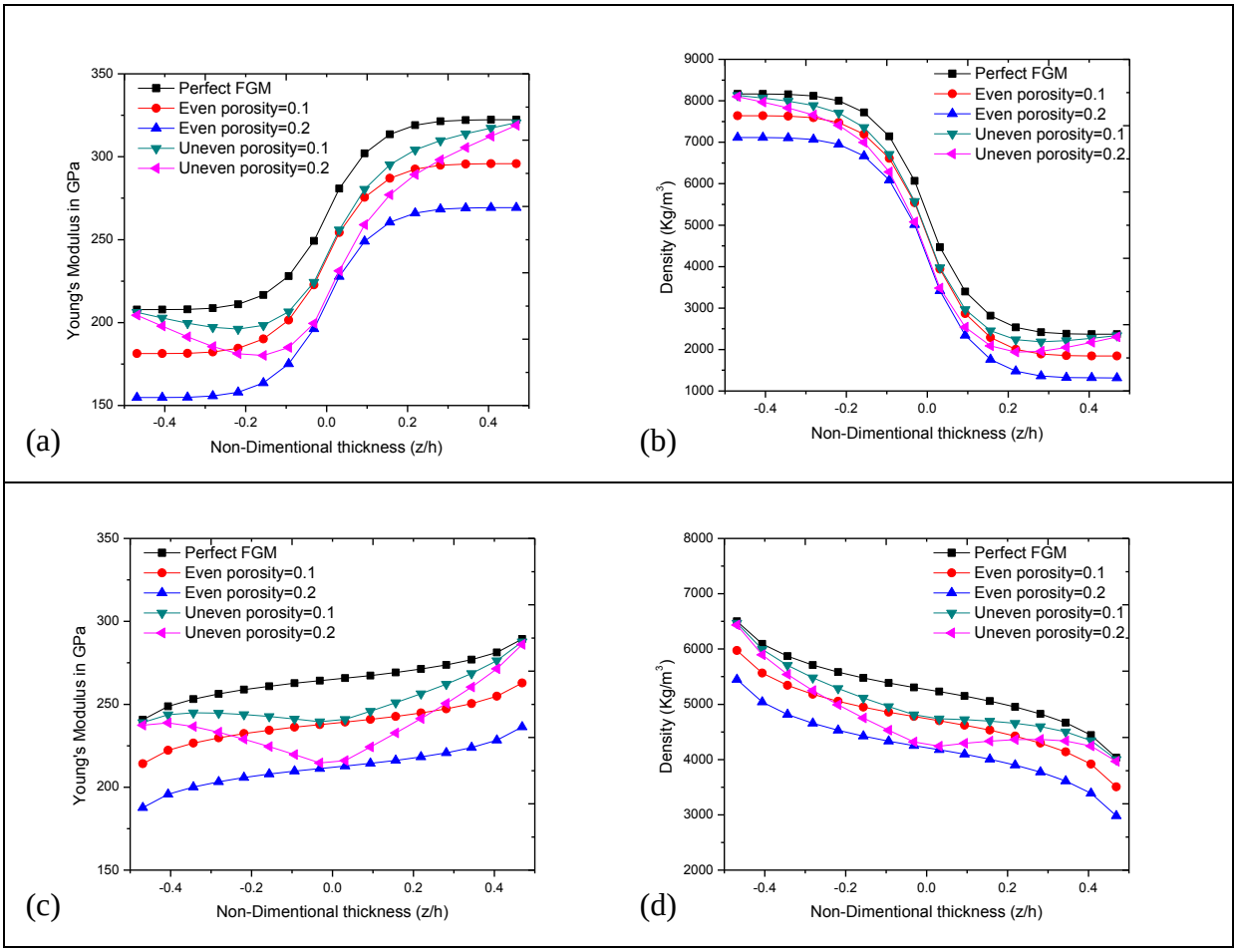

Figure. 2.14 Variation of Young's Modulus and Density along the non-dimensional thickness direction for different values of N of SS-Si_3N_4 S-FGM (a, b for N=5),(c, d for N=1/5)

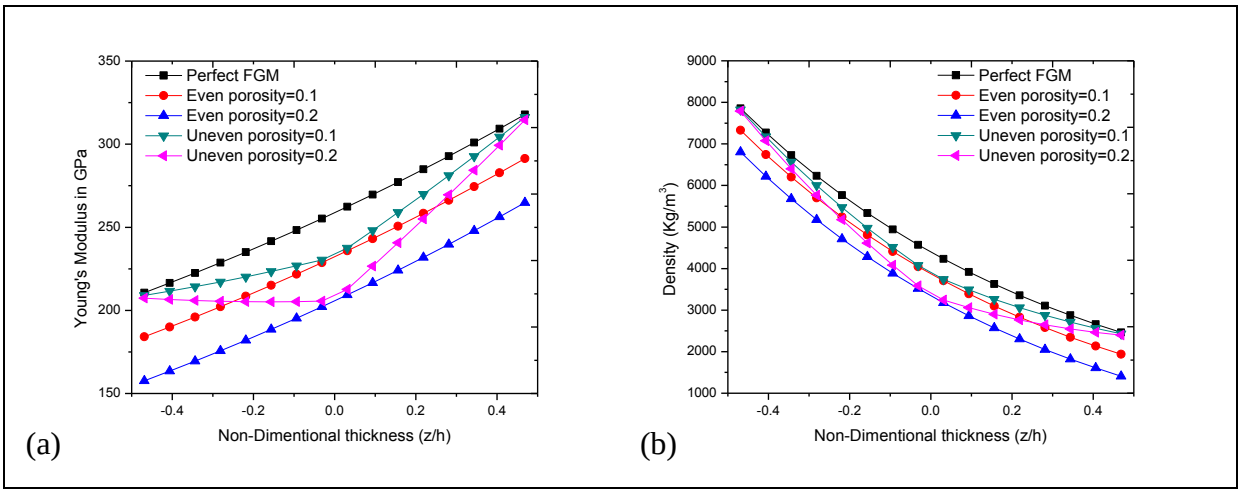

Figure. 2.15 (a) Variation of Young's Modulus (b) Density along the non-dimensional thickness direction for SS-Si_3N_4 E-FGM

$$G(z) = G_m + (G_c - G_m)V_{c1}(z) - \frac{\alpha_{up}}{2}(G_c + G_m)\left(1 - \frac{2|z|}{h}\right) \quad (2.190)$$

For $-h/2 \leq z \leq 0$

$$P_{eff}(z) = P_m + (P_c - P_m)V_{c2}(z) - \frac{\alpha_{up}}{2}(P_c + P_m)\left(1 - \frac{2|z|}{h}\right) \quad (2.191)$$

$$E(z) = E_m + (E_c - E_m)V_{c2}(z) - \frac{\alpha_{up}}{2}(E_c + E_m)\left(1 - \frac{2|z|}{h}\right) \quad (2.192)$$

$$\nu(z) = \nu_m + (\nu_c - \nu_m)V_{c2}(z) - \frac{\alpha_{up}}{2}(\nu_c + \nu_m)\left(1 - \frac{2|z|}{h}\right) \quad (2.193)$$

$$\rho(z) = \rho_m + (\rho_c - \rho_m)V_{c2}(z) - \frac{\alpha_{up}}{2}(\rho_c + \rho_m)\left(1 - \frac{2|z|}{h}\right) \quad (2.194)$$

$$G(z) = G_m + (G_c - G_m)V_{c2}(z) - \frac{\alpha_{up}}{2}(G_c + G_m)\left(1 - \frac{2|z|}{h}\right) \quad (2.195)$$

Figure 2.14 represents the variation of Young's Modulus and density along the non-dimensional thickness direction for different values of sigmoidal power law index (*N*). Uneven porosity shows intermediate property compare to perfect and even porosity.

EXPONENTIAL POWER LAW

This particular idealization for E-FGM modeling with porosity, the typical material properties 'P_{eff}' at any point located at a distance 'z' from the reference surface (mid-surface along the thickness direction) is given by equation 2.196.

$$P_{eff}(z) = P_m e^{\frac{1}{h}\left(\frac{P_c}{P_m}\right)\left((z+\frac{h}{2})\right)} - \frac{\alpha_{up}}{2}(P_c + P_m)\left(1 - \frac{2|z|}{h}\right) \quad (2.196)$$

$$E(z) = E_m e^{\left\{\frac{1}{h}\left(\frac{E_c}{E_m}\right)\left((z+\frac{h}{2})\right)\right\}} - \frac{\alpha_{up}}{2}(E_c + E_m)\left(1 - \frac{2|z|}{h}\right) \quad (2.197)$$

$$\nu(z) = \nu_m e^{\left\{\frac{1}{h}\left(\frac{\nu_c}{\nu_m}\right)\left((z+\frac{h}{2})\right)\right\}} - \frac{\alpha_{up}}{2}(\nu_c + \nu_m)\left(1 - \frac{2|z|}{h}\right) \quad (2.198)$$

$$\rho(z) = \rho_m e^{\left\{\frac{1}{h}\left(\frac{\rho_c}{\rho_m}\right)\left((z+\frac{h}{2})\right)\right\}} - \frac{\alpha_{up}}{2}(\rho_c + \rho_m)\left(1 - \frac{2|z|}{h}\right) \quad (2.199)$$

$$G(z) = G_m e^{\left\{\frac{1}{h}\left(\frac{G_c}{G_m}\right)\left((z+\frac{h}{2})\right)\right\}} - \frac{\alpha_{up}}{2}(G_c + G_m)\left(1 - \frac{2|z|}{h}\right) \quad (2.200)$$

Figure 2.15 represents the variation of Young's Modulus and density along the non-dimensional thickness direction for exponential FGM considering perfect and porous FGM shell. Even porosity with 0.2 porosity factor shows lowest material property while material property for uneven porosity shows in between the perfect and even porosity.

CHAPTER 3 FREE VIBRATION ANALYSIS OF FUNCTIONALLY GRADED SHALLOW CONICAL SHELLS

3.1 GENERAL

A pretwisted shallow conical shell with low aspect ratio can be idealized as turbomachinery blades. A deep knowledge of the dynamic performance of FGM pretwisted conical shells is very much important from designer's point of view in order to avoid the unsafe frequencies and escape the resonance zone by evaluating system response in respect of vibration frequency. FGM shell materials are advantageous in weight-sensitive and high thermal gradient applications such as aircraft engines, aero derivative gas turbines, windmills because of optimal weight, high stiffness, strength and ability to bear high thermal gradient without delamination like in composite materials. The properties of FGM could be tailored to realize high performance as layer of isotropic material with smooth variation by controlling the constituents' (ceramic and metal in the present case) volume fraction variations along the thickness directions. In typical situations, twisted conical shell structures have geometrical complexities arising due to their specific applications in various service environments. Certain dynamic parameters are also to be considered when these structural elements are rotating leading to initial stresses. Finite element method is an efficient tool to the design engineer for the dynamic analysis of such type of applications. The work herein involves numerical investigation of free vibration characteristics of FGM shallow conical shells. The benchmark problems are identified from available literature, within the scope of the present study (Section 3.2). These problems are solved using the present finite element approach and the results are compared with the published ones to check the validity of the present formulation. Sections 3.3 to 3.7 illustrate the additional examples of FGM conical shells with different practical parametric variations followed by the analyses of the results from different practical standpoints.

3.2 COMPARISON OF RESULTS

The numerical results obtained from the developed computer codes based on finite element method are compared and validated with those published in open literature (Zhao

and Liew 2011a, Sreenivasamurthy and Ramamurti 1981, Pradyumna and Bandyopadhyay 2008, Matsunaga 2008 and Ferreira et al. 2006) as furnished in Table 3.1, Table 3.2 and Table 3.3. Table 3.1 presents the validation of non-dimensional fundamental natural frequencies of functionally graded Al-ZrO_2 conical shells (Zhao and Liew 2011a), while Table 3.2 provides the comparison of the non-dimensional fundamental natural frequencies of an isotropic rotating cantilever plate (Sreenivasamurthy and Ramamurti 1981). The comparative study shows an excellent agreement with the formerly published results in the open literature. The predictive capability of the computer programs in respect of FG conical shells, rotating and twisted models is thus confirmed. Therefore it can be concluded that the developed computer code is capable enough to determine the numerical data accurately. Convergence studies are also performed to determine the converged mesh size as furnished in Table 3.1. It is observed from the convergence study that uniform mesh divisions of (6 x 6), (8 x 8) and (10 x 10) considering the complete planform of the shell provide nearly equal results with the difference being around one percent (1%). The lower mesh size (6 x 6) consisting of 36 elements and 133 nodes, has been used for the analysis due to computational efficiency. The total number of degrees of freedom involved in the computation is 600 [(133-13) x 5] as each node of the isoparametric element is having five degrees of freedom comprising of three translations, two rotations and the root of the blade consisting 13 element is fixed with the hub. Table 3.3 represents the non-dimensional fundamental natural frequencies of simply supported Aluminum-Zirconia functionally graded plate (Pradyumna and Bandyopadhyay 2008, Matsunaga 2008, Ferreira et al. 2006).

Table 3.1 Convergence study for NDFF [$\omega=\omega_n a^2\sqrt{(\rho_c/E_c h^2)} / 2\pi$, for the FGM Al-$ZrO_2$ conical shells, considering R_1=0.2 m, h=0.01 m, L_0=0.8 m, θ_v=30°, θ_o=120°.

N	Zhao and Liew (2011a)	Present FEM		
		6 x 6	8 x 8	10 x 10
0	1.3666	1.3608	1.3449	1.2356
0.5	1.2486	1.2387	1.2271	1.0848
1	1.1893	1.1792	1.1641	1.1038
5	1.0737	1.0578	1.0492	0.9910
10	1.0404	1.0222	1.0102	0.9566

Table 3.2 Non-dimensional fundamental natural frequencies [$\omega=\omega_n L^2 \sqrt{(\rho h/D)}$] of an isotropic rotating cantilever plate, $L/b=1$, h/L=0.12, $D=Eh^3/\{12(1-\nu^2)\}$, ν =0.3

Non-dimensional Speed (Ω)	Present FEM	Sreenivasamurthy and Ramamurti (1981)
0.0	3.4174	3.4368
0.2	3.4933	3.5185
0.4	3.7110	3.7528
0.6	4.0458	4.1287
0.8	4.4690	4.5678
1.0	4.9549	5.0916

Table 3.3 Non-dimensional fundamental natural frequencies [$\omega=\omega_n h^2 \sqrt{(\rho_m/E_m)}$] of simply supported aluminum–zirconia FG plate $a=b$=1 m, N=1 (For aluminum: E_m=70 GPa, ν_m=0.3,and ρ_m=2707 kg/m^3 and for zirconia: E_c=200 GPa, ν_c=0.3 and ρ_c=2702 kg/m^3)

a / h	Present FEM	Pradyumna and Bandyopadhyay (2008)	Matsunaga (2008)	Ferreira et al. (2006)
5	0.2235	0.2257	0.2285	0.2188
10	0.0608	0.0613	0.0618	0.0592
20	0.0156	0.0157	0.0158	0.0147

Material properties of the Al- ZrO_2 FGM material for the validation of the Zhao and Liew Liew (2011a) are considered as per the table 3.4.

Table 3.4 Material Properties of Al- ZrO_2 at 300 K

Material	Material Properties		
	E (N/m^2)	υ	ρ (Kg/m^3)
Aluminum (Al)	70.000 x 10^9	0.300000	2707
Zirconia (ZrO_2)	151.000 x 10^9	0.300000	3000

In the present study, Stainless Steel (SS)-Silicon Nitrite (Si_3N_4) FGM is considered for parametric analysis of free vibration conical shell, the material properties of FGM constituents' material are calculated as per equation 2.133 of chapter 2 as furnished in table 3.5.

Table 3.5 Temperature dependent material properties of the FGM constituent calculated at 300 K

	Material	P_{-1}	P_0	P_1	P_2	P_3	Effective property
E	SS	0	2.01E+11 N/m^2	3.08E-04	-6.53E-07	0	2.07788E+11 N/m^2
	Si_3N_4	0	3.48E+11 N/m^2	-3.07E-04	2.16E-07	-8.95E-11	3.22E+11 N/m^2
v	SS	0	0.326	-2.00E-04	3.80E-07	0	0.318
	Si_3N_4	0	0.24	0	0	0	0.24
ρ	SS	0	8166 kg/m^3	0	0	0	8166 kg/m^3
	Si_3N_4	0	2370 kg/m^3	0	0	0	2370 kg/m^3

3.3 PARAMTERIC CONFIGURATION OF FGM CONICAL SHELL

Parametric studies are carried out with respect to rotational speed and twist angle on natural frequencies of functionally graded shallow conical shells. Non-dimensional fundamental frequencies (NDFF) and Non-dimensional second frequencies (NDSF) for conical shells *(r_x = α)* having rectangular plan-form (L_o/b_o=5.59), curvature ratio (b_o/r_y) of 0.5 and thickness ratio *(s/h)* of 114 are obtained corresponding to non-dimensional speeds of rotation, $\Omega=(\Omega'/\omega_o)$=0.0, 0.25, 0.5, 0.75 and 1.0, considering three different angles of twist of conical shells, namely ψ = 15°, 30° and 45°, in addition to the untwisted one (ψ=0°). The variation of volume fractions (V_c, V_m) through the thickness direction are calculated based on different FGM power laws, namely simple power law FGM (P-FGM), sigmoidal power law FGM (S-FGM) and exponential power law FGM (E-FGM). Two types of porosity factors, namely even (α_{ep}) and uneven (α_{up}) factors along with perfect (without porosity) FGM conical shells are considered for the present analysis. The porosity factor 0.1 and 0.2 are considered for the present analysis. Porosity factor greater than 0.2 is not considered as beyond that factor the FGM shell structure will not viable to take the desired load.

3.4 SIMPLE POWER LAW FGM (P-FGM)

The parametric studies on the non-dimensional natural frequencies are conducted for SS-Si_3N_4 functionally graded conical shells for different twist angles both stationary as well as rotating condition for simple power law FGM. The effect of different parameters on natural frequencies and mode shape are illustrated below.

3.4.1 EFFECT OF SIMPLE POWER LAW INDEX (*N*)

The NDFF and NDSF for SS-Si_3N_4 functionally graded conical shell with different twist and rotation considering simple power law index (*N*) are furnished in table 3.6. The non-dimensional natural frequencies (NDFF and NDSF*)* are found to decrease with the increase of the simple power law index (*N*). This is due to the fact that the contribution of the metal part on FGM shell increases and the elastic stiffness matrix reduces with the increase of the material property graded index (*N*) which leads to decrease of the non-dimensional natural frequencies. At stationary condition, NDFF gives minimum value at *N*=100 while the maximum value is found at *N*=0 irrespective of angle of twist.

Therefore the material property graded index (*N*) has pronounced effect in non-dimensional natural frequencies. Figure 3.1 stipulates the decreasing trend of NDSF with increase of material property graded index (*N*) irrespective of the twist angles. The decreasing trend for NDFF with increase of N can also be observed from the table 3.6.

3.4.2 EFFECT OF TWIST ANGLE

Twist angle has pronounced effect on the natural frequencies of the FGM conical shell blade. Figure 3.2 depicts the variation of the NDFF for different twist angles. The fundamental natural frequencies and second natural frequencies are observed to increase with the increase of the twist angles. The increasing trend of NDFF with increase of twist angles are observed from the figure 3.2. Hence it leads to the fact that twisted conical shells, irrespective of the rotational speeds the fundamental natural frequencies and second natural frequencies are predominantly higher compared to untwisted cases and the natural frequencies are observed to increase with the twist angles. It is to be noted that the difference between maximum and minimum value of non-dimensional fundamental and second frequencies obtained from the analyses of four different twist angle for ψ=0°, 15°, 30° and 45° increases as the twist angle increases. For the FG conical shells, it is observed that the frequencies (NDFF and NDSF) at

Table 3.6 NDFF and NDSF $[\omega=\omega_n L_o^2\sqrt{(\rho/Eh^2)}]$ of rotating Stainless steel (SUS304)- Silicon nitride (Si_3N_4) functionally graded conical shells for various twist angles considering L_o/s=0.7, r_1=0.2 m, L_o=0.8 m, h=0.01 m, ϕ_o = 45º, ϕ_{ve} =20º considering P-FGM.

Twist Angle (Ψ)	Simple Power Law Index (N)	NDFF					*NDFF*				
		Ω=0	Ω=0.25	Ω=0.5	Ω=0.75	Ω=1.0	Ω=0	Ω=0.25	Ω=0.5	Ω=0.75	Ω=1.0
0^0	0	1.8700	1.9846	2.3279	2.8048	3.3407	4.8142	4.9804	5.4680	6.1894	7.0489
	1	1.1348	1.2364	1.6323	1.9234	2.3408	2.9190	3.0676	3.4365	4.1023	4.7699
	5	0.9217	0.9835	1.1724	1.4308	1.7169	2.3718	2.4619	2.7306	3.1236	3.5823
	10	0.8768	0.9327	1.1033	1.3386	1.6009	2.2565	2.3376	2.5796	2.9360	3.3556
	50	0.8228	0.8727	1.0249	1.2367	1.4743	2.1169	2.1890	2.4044	2.7239	3.1026
	100	0.8142	0.8632	1.0127	1.2211	1.4551	2.0945	2.1653	2.3769	2.6910	3.0637
15^0	0	1.9659	2.0875	2.4497	2.9486	3.5079	4.8147	4.9976	5.5321	6.3139	7.2355
	1	1.1947	1.3031	1.6186	2.0242	2.4595	2.9194	3.0835	3.5569	4.2125	4.9199
	5	0.9677	1.0333	1.2327	1.5025	1.8004	2.3719	2.4710	2.7652	3.1902	3.6803
	10	0.9204	0.9797	1.1595	1.4053	1.6785	2.2566	2.3457	2.6105	2.9958	3.4445
	50	0.8646	0.9175	1.0781	1.2996	1.5475	2.1170	2.1964	2.4326	2.7786	3.1841
	100	0.8557	0.9078	1.0656	1.2837	1.5278	2.0946	2.1726	2.4048	2.7452	3.1444
30^0	0	2.4269	2.5870	3.0445	3.6523	4.3251	4.7429	5.0191	5.7935	6.8594	8.0511
	1	1.4765	1.6235	2.0177	2.5030	3.0253	2.8758	3.1281	3.8057	4.6638	5.5282
	5	1.1861	1.2722	1.5225	1.8476	2.2026	2.3359	2.4841	2.9052	3.4737	4.0937
	10	1.1281	1.2058	1.4317	1.7283	2.0543	2.2223	2.3557	2.7351	3.2526	3.8235
	50	1.0644	1.1343	1.3371	1.6060	1.9031	2.0852	2.2051	2.5469	3.0165	3.5377
	100	1.0548	1.1236	1.3232	1.5882	1.8812	2.0632	2.1814	2.5181	2.9812	3.4952
45^0	0	3.2889	3.5506	4.2010	5.0063	5.8804	4.5963	5.0771	6.3121	7.8524	9.4422
	1	2.0019	2.2374	2.7760	3.4129	4.0893	2.7861	3.2228	4.2564	5.4481	6.5686
	5	1.5987	1.7396	2.0884	2.5132	2.9717	2.2597	2.5196	3.1797	3.9817	4.7944
	10	1.5207	1.6475	1.9640	2.3532	2.7744	2.1500	2.3834	2.9815	3.7180	4.4704
	50	1.4400	1.5546	1.8417	2.1967	2.5820	2.0190	2.2297	2.7740	3.4503	4.1450
	100	1.4282	1.5412	1.8244	2.1747	2.5549	1.9982	2.2060	2.7433	3.4115	4.0982

rotating condition (Ω=0.5 or 1.0) as well as at stationary condition (Ω=0.0)] the untwisted cases are mostly in the lower range compared to those of twisted ones and this has been depicted in figure 3.2.

3.4.3 EFFECT OF ROTATIONAL SPEEDS

For the FG conical shells, it is observed that the natural frequencies (NDFF and NDSF) at rotating condition (Ω=0.5 or 1.0) as well as at stationary condition (Ω=0.0)] the untwisted cases are mostly in the lower range compared to those of twisted ones and this has been depicted in figure 3.2. It can be conclude that the rotating effect is more pronounced for twisted shell in comparison to untwisted one. The centrifugal stiffening effect (i.e., increase of structural

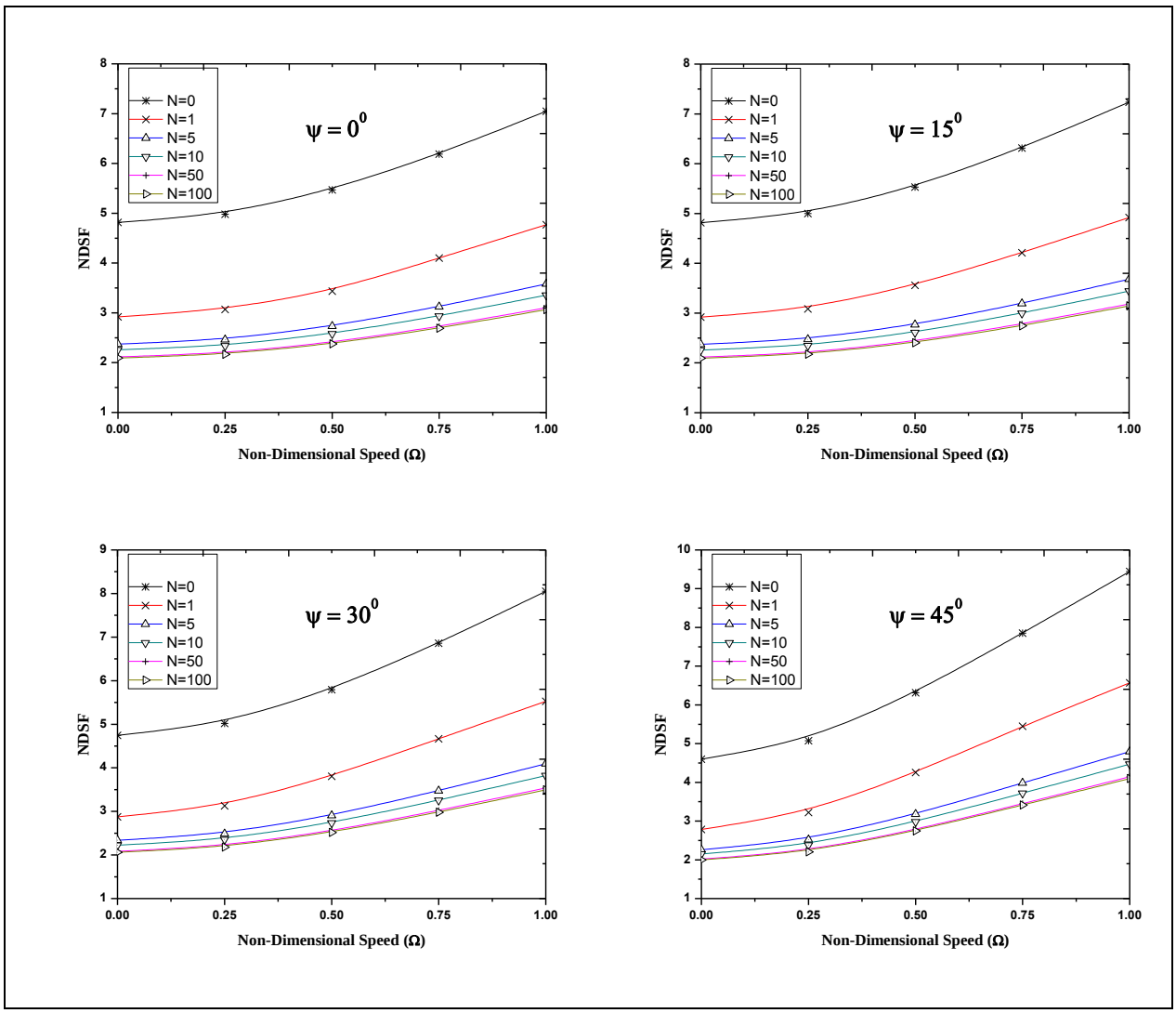

Figure 3.1 Variation of non-dimensional second natural frequencies (NDSF) with material property graded index (N) at (Ω=0.0, 0.25, 0.5, 0.75, 1.0) for Stainless steel (SUS304)- Silicon nitride (Si_3N_4) graded conical shells with various twist angles considering L_o/s=0.7, r_1=0.2 m, L_o=0.8 m, h=0.01 m, ϕ_o = 45º, θ_{ve}=20º

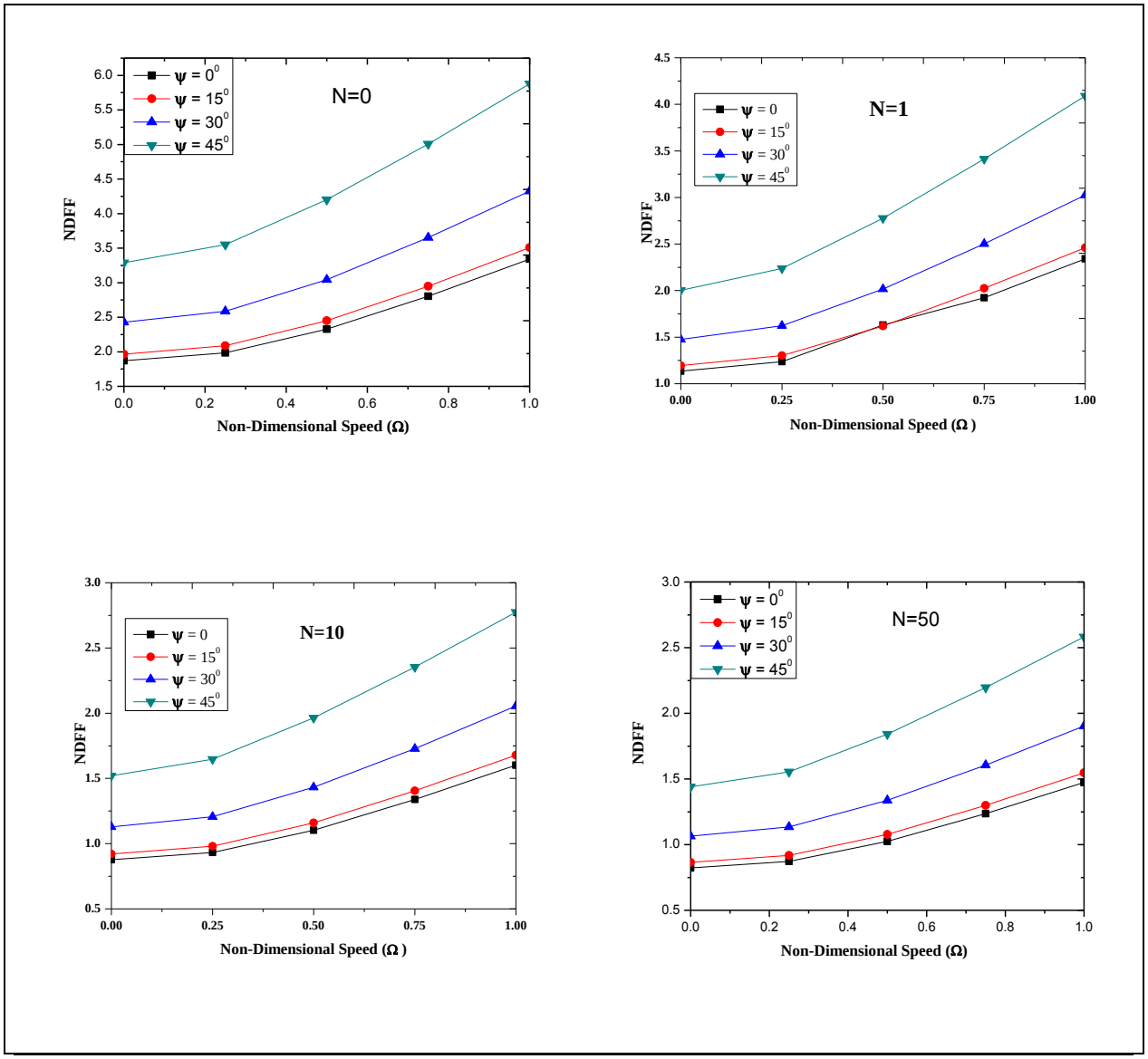

Figure.3.2 Variation of non-dimensional fundamental frequencies (NDFF) with various twist angles along with untwisted case with (Ω=0.0, 0.25, 0.5, 0.75 and 1.0) for SS- Si_3N_4 functionally graded conical shells for different values of N considering L_o/s=0.7, r_1=0.2 m, L_o=0.8 m, h=0.01 m, ϕ_o = 45º, ϕ_{ve} =20º.

stiffness with increase of rotational speeds) for NDFF and NDSF are observed for all the values of N irrespective of twist angle. This leads to the fact of increasing trend of the NDFF and NDSF with increase of rotational speed.

3.3.4 MODE SHAPES FOR SIMPLE POWER LAW

The mode shapes corresponding to the natural frequencies are furnished for various twist angles (ψ=0°, 15°, 30° and 45°) and non-dimensional rotational speeds (Ω=0.0, 0.5 and 1.0), for Stainless steel (SUS304)-Silicon nitride (Si_3N_4) FG conical shells. The mode shapes

corresponding to N=1 are shown in Figure 3.3 while the mode shapes corresponding to N=10 are shown in Figure 3.4. The fundamental frequency is observed to be the torsional mode at lower rotational speed for all cases. It is noted that for both the material property graded index (N=1 and N=10) the symmetry modes are absent for rotating pretwisted conical shells. Span wise bending is notified at higher rotational speeds (Ω=0.5 and 1.0) corresponding to both NDFF and NDSF, irrespective of twist angle. The first span wise bending is found for both NDFF and NDSF at higher rotational speeds (Ω= 0.5, 1.0) for both twisted and untwisted shells corresponding N=10. The first span wise bending is found for all values of N for both the NDFF and NDSF only at higher rotational speeds (Ω= 0.5, 1.0). Unlike the rotational shell the span wise bending mode is absent for the stationary shell for all values of twist angle irrespective of the (N). For stationary shell (Ω= 0) torsional mode is observed for all the cases irrespective of N.

Ψ	NDFF			NDSF		
	Ω=0.0	Ω=0.5	Ω=1.0	Ω=0.0	Ω=0.5	Ω=1.0
0°	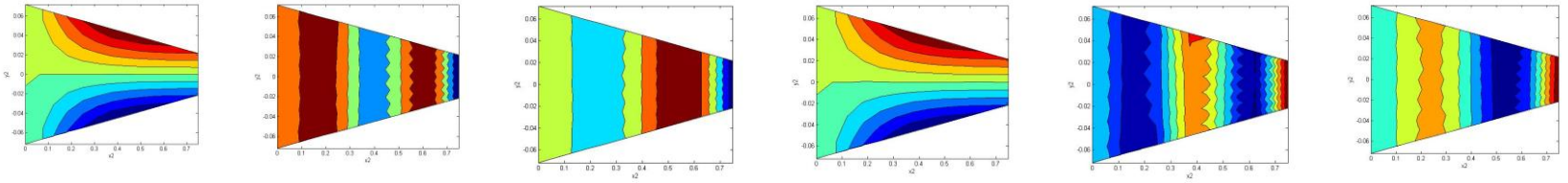					
15°	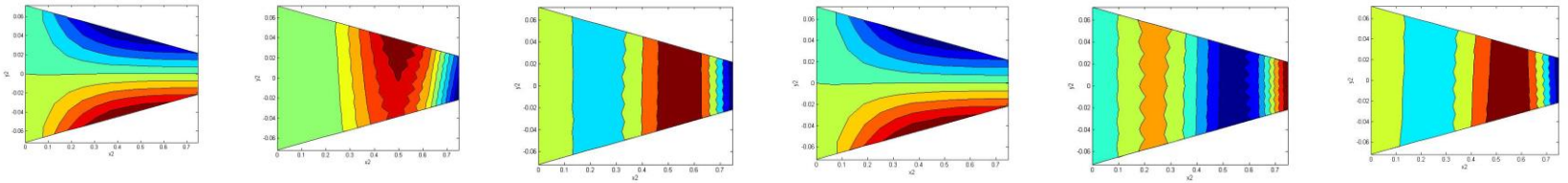					
30°	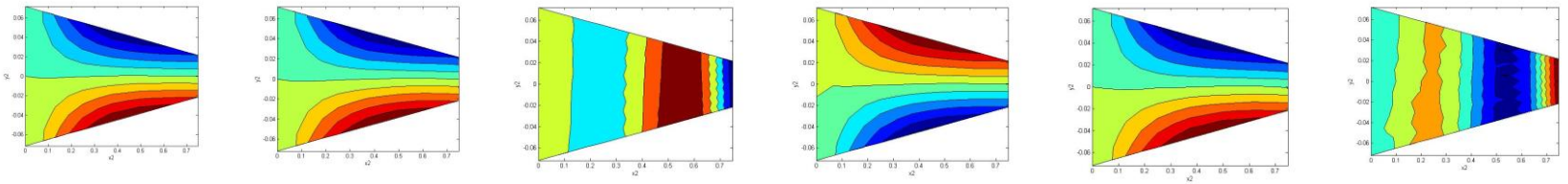					
45°	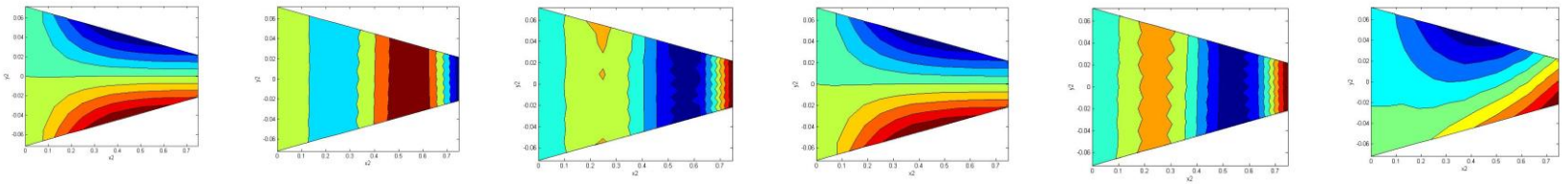					

Figure 3.3 Effect of twist and rotation on NDFF and NDSF for mode shapes for SS-Si_3N_4 P-FGM conical shells for different twist angles, considering r_1=0.2 m, h=0.01 m, N=1, s/h=114, L_o/s=0.7, ϕ_o = 45º, ϕ_{ve} = 20º.

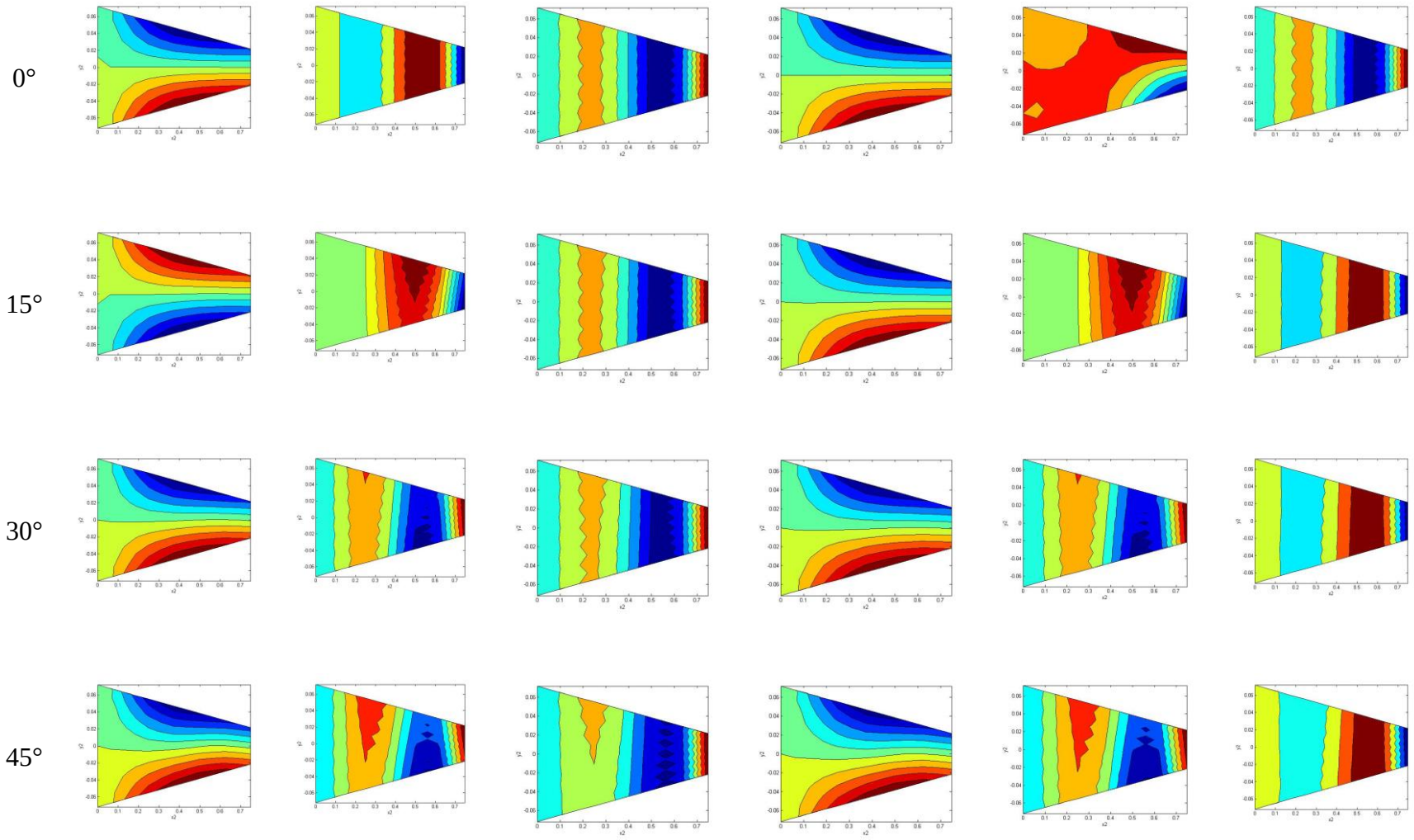

Figure.3.4 Effect of twist and rotation on NDFF and NDSF for mode shapes of SS-Si_3N_4 P-FGM conical shells for different twist angles, considering r_1=0.2 m, h=0.01 m, N=10, s/h=114, L_o/s=0.7, ϕ_o = 45º, ϕ_{ve} = 20º.

3.4 SIGMOIDAL POWER LAW FGM (S-FGM)

The parametric studies on the non-dimensional natural frequencies of SS-Si_3N_4 conical shells are conducted for different sigmoidal power law index and twist angles both stationary as well as rotating condition. The effect of different parameters on natural frequencies and mode shape are illustrated below.

3.5.1 EFFECT OF SIGMOIDAL POWER LAW INDEX (*N*)

The NDFF and NDSF for different values of twist and rotation are furnished in table 3.7 considering *N*=1, 5 and 10. Interestingly the NDFF and NDSF for different values of *N* are not varied and remain nearly same irrespective of the sigmoidal power law index. The natural frequencies is invariant with the sigmoidal power law index (*N*) for a given twist angle and rotational speed. This is due to the fact that total contribution of metal and ceramic parts remains unchanged irrespective of the *N* and this has been shown in the figure 2.10 in chapter 2. As the contribution of metal part and ceramic part remains same, therefore the total stiffness matrix and geometric mass matrix remains same for the structure hence the natural frequency remains unaltered. As the NDFF & NDSF are invariant with sigmoidal power law index "*N*" therefore sigmoidal power law will be more useful for designer to get the desired application arresting the variation of natural frequencies. But it can be noticed that higher values of *N* (>10) sharp change of material property will occur like composite material which may lead to delamination or debonding between the layers. Therefore a range of values (0.1 to 10) for *N* is preferred to consider during choosing of such FGM components.

3.5.2 EFFECT OF TWIST ANGLE

Twist angle has significant effect on the natural frequencies of the S-FGM conical shell also. Figure 3.5 depicts the variation of the NDFF and NDSF for different twist angles. The increasing trend of NDFF with increase of twist angles are observed while for the NDSF the increase of the frequencies with twist angle can distinctively observed for higher rotational speeds. In general, for untwisted conical shells the fundamental natural frequencies and second natural frequencies at twisted cases are predominantly higher compared to respective NDFF and NDSF values of untwisted cases. It is to be noted that the difference between maximum and minimum value of non-dimensional fundamental and second frequencies obtained from the analyses of four different twist angle for ψ=0°, 15°, 30° and 45° increases as the twist angle

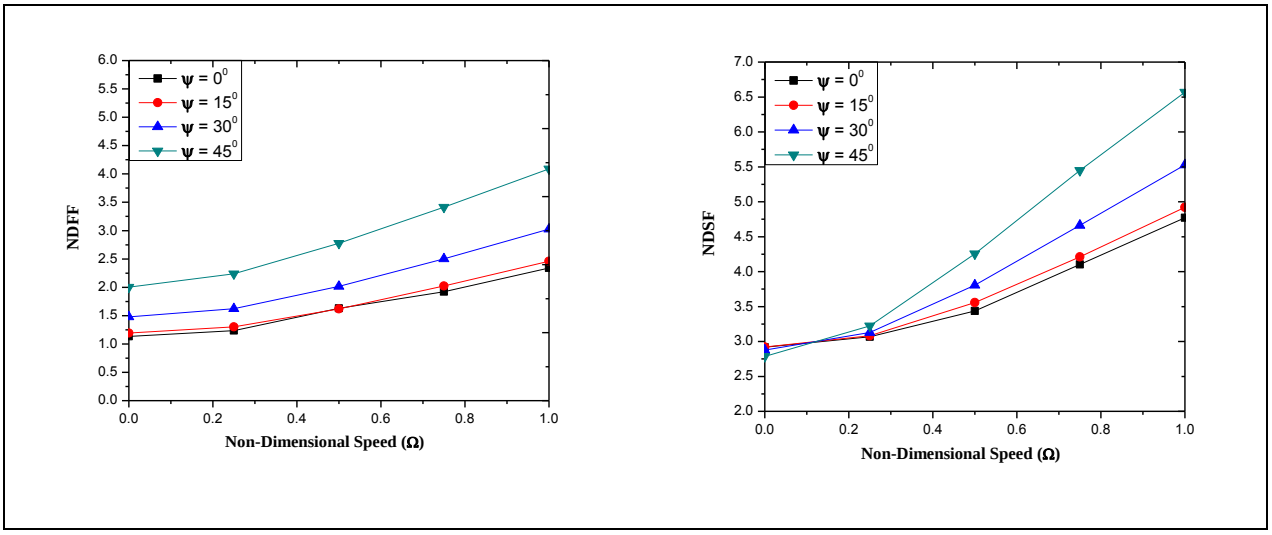

Figure.3.5 Variation of NDFF and NDSF with various twist angles along with untwisted case with (Ω=0.0, 0.25, 0.5, 0.75 and 1.0) for SS- Si_3N_4 functionally graded conical shells for S-FGM N=1, considering L_o/s=0.7, r_1=0.2 m, L_o=0.8 m, h=0.01 m, ϕ_o = 45º, ϕ_{ve} =20º.

increases. For the FG conical shells, it is observed that the frequencies (NDFF and NDSF) at rotating condition (Ω=0.5 or 1.0) as well as at stationary condition (Ω=0.0)] the untwisted cases are mostly in the lower range compared to those of twisted ones and this has been depicted in figure 3.5.

3.5.3 EFFECT OF ROTATIONAL SPEED

For the S-FMG conical shells, it is observed that the frequencies (NDFF and NDSF) at rotating condition (Ω=0.5 or 1.0) as well as at stationary condition (Ω=0.0) the untwisted cases are mostly in the lower range compared to those of twisted ones. This observation can be found depicted in figure 3.5. It can be conclude that the rotating effect is more pronounced for twisted shell in comparison to untwisted one. The centrifugal stiffening effect (i.e., increase of structural stiffness with increase of rotational speeds) for NDFF and NDSF are observed for all the values of sigmoidal power law index irrespective of twist angle. This leads to the fact of increasing trend of the NDFF and NDSF with increase of rotational speed.

3.5.4 MODE SHAPES FOR FGM SIGMOIDAL LAW

The mode shapes corresponding to the natural frequencies are furnished in Figure 3.6 for various twist angles (ψ=0°, 15°, 30° and 45°) and non-dimensional rotational speeds (Ω=0.0, 0.5 and 1.0), for Stainless steel (SUS304)-Silicon nitride (Si_3N_4) S-FGM considering N=1. As the fundamental natural frequencies are invariant with sigmoidal power law index N,

Table 3.7 NDFF and NDSF $[\omega=\omega_n L_o^2\sqrt{(\rho/Eh^2)}]$ of rotating Stainless steel (SUS304)- Silicon nitride (Si_3N_4) functionally graded conical shells for various twist angles considering L_o/s=0.7, r_1=0.2 m, L_o=0.8 m, h=0.01 m, ϕ_o = 45º, ϕ_{ve} =20º considering S-FGM.

Twist Angle (Ψ)	Sigmoidal Power Law Index (N)	NDFF					*NDFF*				
		Ω=0	Ω=0.25	Ω=0.5	Ω=0.75	Ω=1.0	Ω=0	Ω=0.25	Ω=0.5	Ω=0.75	Ω=1.0
0^0	1	1.1348	1.2364	1.6323	1.9234	2.3408	2.9190	3.0676	3.4365	4.1023	4.7699
	5	1.1327	1.2390	1.6327	1.9228	2.3440	2.9242	3.0730	3.4426	4.1095	4.7783
	10	1.1341	1.2364	1.6325	1.9238	2.3408	2.9186	3.0671	3.4360	4.1017	4.7692
15^0	1	1.1947	1.3031	1.6186	2.0242	2.4595	2.9194	3.0835	3.5569	4.2125	4.9199
	5	1.1948	1.3032	1.6187	2.0243	2.4596	2.9245	3.0890	3.5631	4.2200	4.9286
	10	1.1946	1.3040	1.6186	2.0240	2.4597	2.9189	3.0831	3.5563	4.2119	4.9191
30^0	1	1.4765	1.6235	2.0177	2.5030	3.0253	2.8758	3.1281	3.8057	4.6638	5.5282
	5	1.4766	1.6232	2.0178	2.5015	3.0254	2.8809	3.1336	3.8124	4.6721	5.5380
	10	1.4765	1.6235	2.0176	2.5030	3.0252	2.8754	3.1276	3.8051	4.6631	5.5274
45^0	1	2.0019	2.2374	2.7760	3.4129	4.0893	2.7861	3.2228	4.2564	5.4481	6.5686
	5	2.0017	2.2381	2.7778	3.4130	4.0910	2.7910	3.2285	4.2639	5.4577	6.5802
	10	2.0018	2.2377	2.7781	3.4128	4.0882	2.7857	3.2223	4.2557	5.4472	6.5676

Table 3.8 NDFF and NDSF $[\omega=\omega_n L_o^2\sqrt{(\rho/Eh^2)}]$ of rotating Stainless steel (SUS304)- Silicon nitride (Si_3N_4) functionally graded conical shells for various twist angles considering L_o/s=0.7, r_1=0.2 m, L_o=0.8 m, h=0.01 m, ϕ_o = 45º, ϕ_{ve} =20º considering E-FGM.

Twist Angle (Ψ)	NDFF					*NDFF*				
	Ω=0	Ω=0.25	Ω=0.5	Ω=0.75	Ω=1.0	Ω=0	Ω=0.25	Ω=0.5	Ω=0.75	Ω=1.0
0^0	1.1969	1.3163	1.6592	2.0959	2.5622	2.9190	3.0676	3.4365	4.1023	4.7699
15^0	1.2598	1.3870	1.7486	2.2044	2.6908	2.9194	3.0835	3.5569	4.2125	4.9199
30^0	1.5557	1.7258	2.1760	2.7215	3.3043	2.8758	3.1281	3.8057	4.6638	5.5282
45^0	2.1081	2.3807	2.9899	3.7030	4.4572	2.7861	3.2228	4.2564	5.4481	6.5686

Ψ	NDFF			NDSF		
	Ω=0.0	Ω=0.5	Ω=1.0	Ω=0.0	Ω=0.5	Ω=1.0
0°	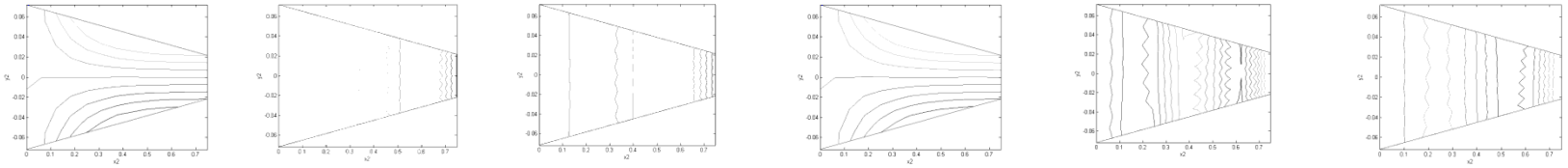					
15°	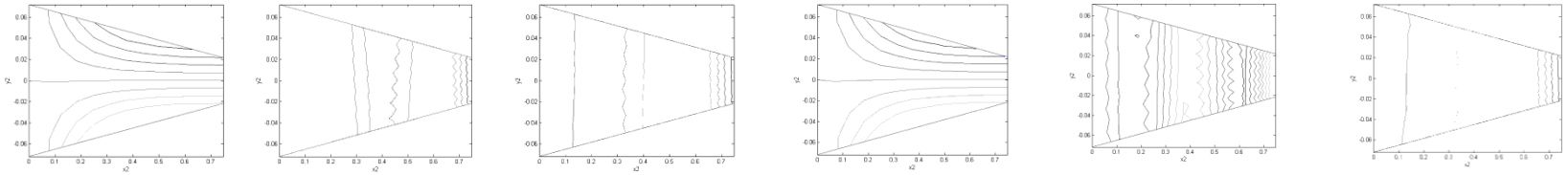					
30°	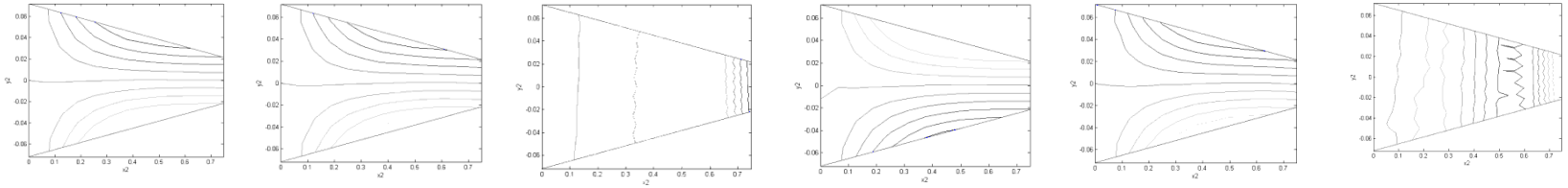					
45°	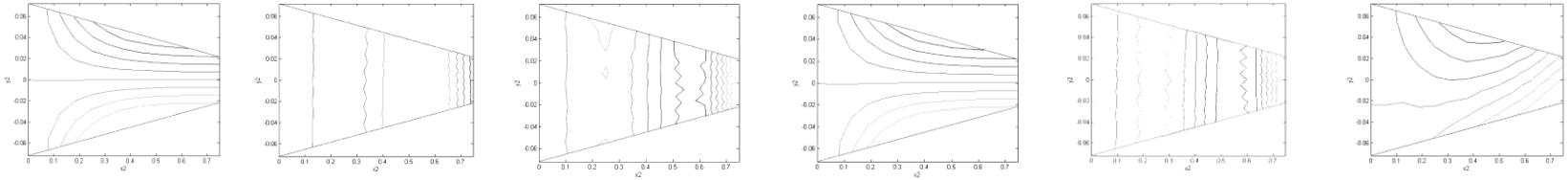					

Figure.3.6 Effect of twist and rotation on NDFF and NDSF for mode shapes of SS- Si_3N_4 S-FGM conical shells for different twist angles, considering r_1=0.2 m, h=0.01 m, N=1, s/h=114, L_o/s=0.7, ϕ_o = 45º, ϕ_{ve} = 20º.

therefore linear variation of material property (N=1) is consider for the mode shape evaluation. The fundamental frequency is observed to be the torsional mode at lower rotational speed for both NDFF and NDSF. Symmetry modes are absent for rotating pretwisted conical shells. Span wise bending is notified at higher rotational speeds (Ω=0.5 and 1.0) corresponding to both NDFF and NDSF, irrespective of twist angle. The first span wise bending is found for both the NDFF and NDSF only at higher rotational speeds (Ω= 0.5, 1.0). For stationary shell (Ω=0) torsional mode is observed for all the twist angles.

3.6 EXPONENTIAL POWER LAW FGM (E-FGM)

The parametric studies on the non-dimensional natural frequencies of SS-Si_3N_4 conical shells are conducted for exponential power law considering different twist angles both stationary as well as rotating condition. For the exponential power law the constituent material property is varied based on exponential law as per figure 2.11. Therefore for this law, the material property graded index is absent and it follows a single variation of the material property.

3.6.1 EFFECT OF TWIST ANGLE

The NDFF and NDSF for different values of twist and rotation for E-FGM conical shell are furnished in table 3.8. Twist angle has prominent effect on the natural frequencies of the E-FGM conical shell blade. Figure 3.7 represents the variation of the NDFF and NDSF with different rotational speeds for various twist angles. The increasing trend of NDFF with increase of twist angles for all rotational speed are observed while for the NDSF the increase of the frequencies with twist angle can distinctively observed for higher rotational speeds. In general, for twisted conical shells the fundamental natural frequencies and second natural frequencies are predominantly higher compared to respective NDFF and NDSF values of untwisted cases. It is to be noted that the difference between maximum and minimum value of non-dimensional fundamental and second frequencies obtained from the analyses of four different twist angle for ψ=0°, 15°, 30° and 45° increases as the twist angle increases. For the FG conical shells, it is observed that the frequencies (NDFF and NDSF) at rotating condition (Ω=0.5 or 1.0) as well as at stationary condition (Ω=0.0)] the untwisted cases are mostly in the lower range compared to those of twisted ones and this has been depicted in figure 3.7

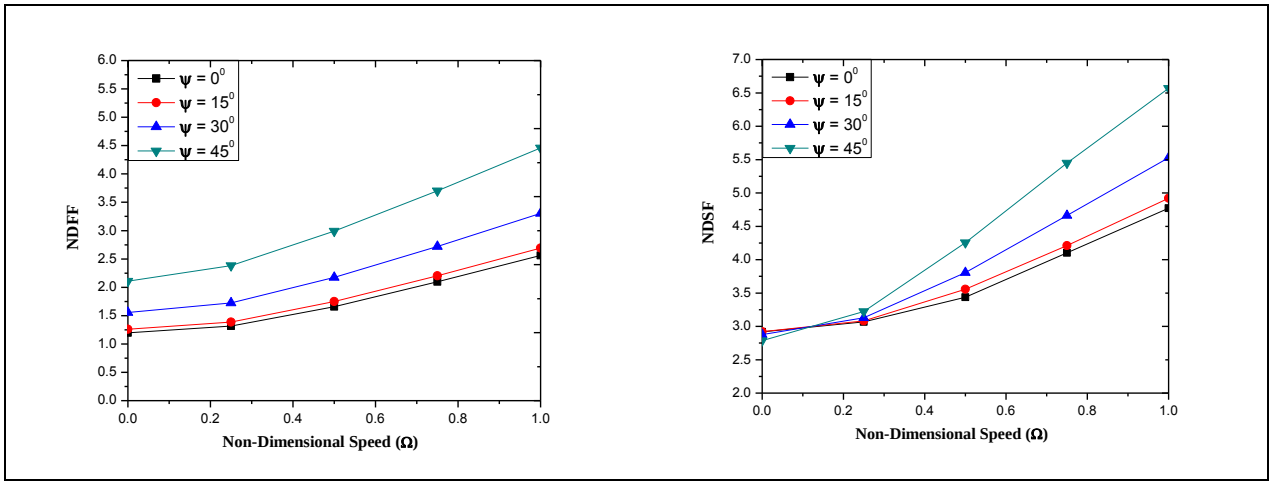

Figure.3.7 Variation of NDFF and NDSF with various twist angles along with untwisted case with (Ω=0.0, 0.25, 0.5, 0.75 and 1.0) for SS- Si_3N_4 functionally graded conical shells for E-FGM, considering L_o/s=0.7, r_1=0.2 m, L_o=0.8 m, h=0.01 m, ϕ_o = 45º, ϕ_{ve} =20º.

3.6.2 EFFECT OF ROTATIONAL SPEEDS

For the E-FGM conical shells, it is observed that the non-dimensional natural frequencies (NDFF and NDSF) at rotating condition (Ω=0.5 or 1.0) as well as at stationary condition (Ω=0.0) the untwisted cases are mostly in the lower range compared to those of twisted ones. This observation can be found depicted in figure 3.7. It can be conclude that the rotating effect is more pronounced for twisted shell in comparison to untwisted one. The centrifugal stiffening effect (i.e., increase of structural stiffness with increase of rotational speeds) for NDFF and NDSF are observed for E-FGM shell irrespective of twist angle. This leads to the fact of increasing trend of the NDFF and NDSF with increase of rotational speed.

3.6.3 MODE SHAPES FOR EXPONENTIAL LAW

The mode shapes corresponding to the natural frequencies are presented in Figure 3.8 for various twist angles (ψ=0°, 15°, 30° and 45°) and non-dimensional rotational speeds (Ω=0.0, 0.5 and 1.0), for Stainless steel (SUS304)-Silicon nitride (Si_3N_4) E-FGM conical shell. The fundamental natural frequencies are varied based on exponential variation of material property and the corresponding shape are evaluated. The non-dimensional fundamental natural frequency is observed to be the torsional mode at lower rotational speed. Symmetry modes are absent for rotating pretwisted conical shells. Span wise bending is notified at higher rotational speeds (Ω=0.5 and 1.0) corresponding to both NDFF and NDSF, irrespective of twist angle. The first span wise bending is found for both the NDFF and NDSF only at higher rotational speeds (Ω= 0.5, 1.0). For stationary shell (Ω=0) torsional mode is observed for all the twist angles.

Ψ	NDFF		
	Ω=0.0	Ω=0.5	Ω=1.0
0°	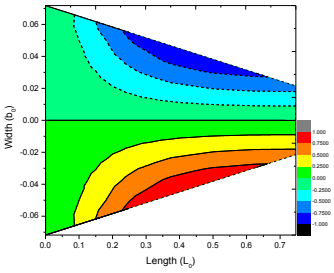	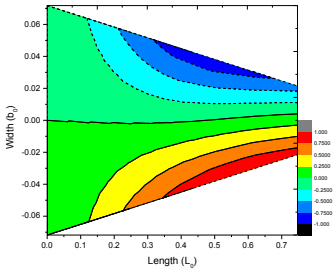	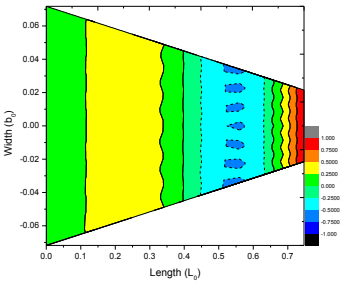
15°	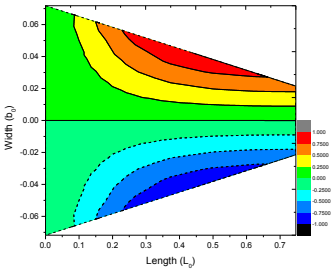	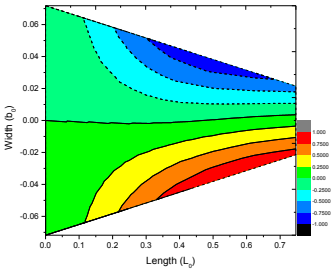	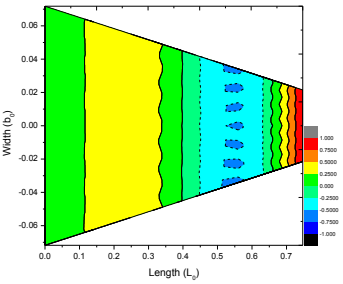
30°	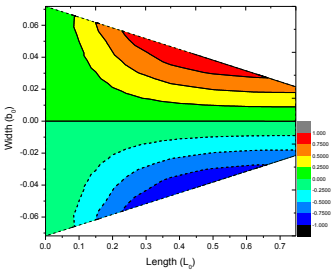	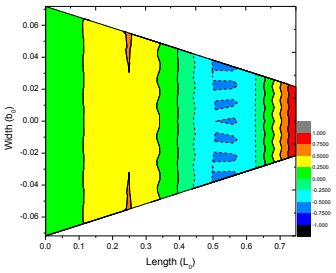	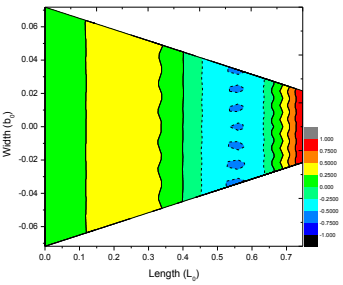
45°	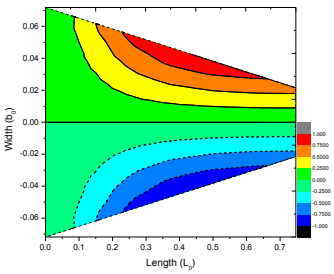	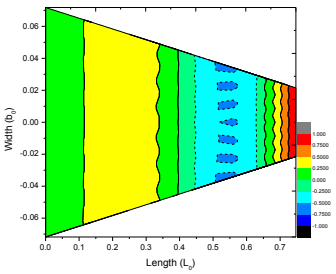	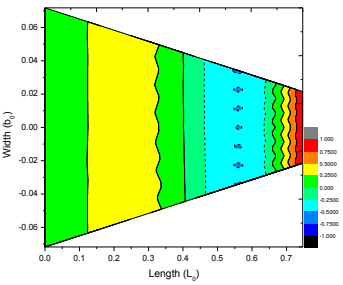

Figure 3.8 Mode shapes of Perfect (porosity free) SS-Si_3N_4 E-FGM conical shells considering r_1=0.2 m, h=0.01 m, s/h=114, L_o/s=0.7, ϕ_o = 45º, ϕ_{ve} = 20º.

3.7 POROUS FGM

Parametric studies are carried out for perfect (porous free) and porous (even and uneven porosity) FGM conical shell with respect to rotational speed and twist angle on natural frequencies of functionally graded shallow conical shells. Non-dimensional fundamental frequencies (NDFF) and Non-dimensional second frequencies (NDSF) for conical shells ($r_x = \alpha$) having rectangular plan-form (L_0/b_0=5.59), curvature ratio (b_0/r_y) of 0.5 and thickness ratio (s/h) of 114 are obtained corresponding to non-dimensional speeds of rotation, $\Omega=(\Omega'/\omega_o)$=0.0, 0.25, 0.5, 0.75 and 1.0, considering three different angles of twist of conical shells, namely ψ = 15°, 30° and 45°, in addition to the untwisted one (ψ=0°).

3.7.1 FGM WITH EVEN AND UNEVEN POROSITY

The parametric studies on the non-dimensional natural frequencies are conducted for SS-Si_3N_4 functionally graded conical shells with different twist angles for both stationary as well as rotating condition. The NDFF and NDSF for even porous, uneven porous P-FGM (N=5) are furnished in table 3.9 considering different porosity factors along with perfect FGM (porosity free) while the table 3.10 and 3.11 present the data for the S-FGM (N=1) and E-FGM, respectively. NDFF are found to decrease with increase of the porosity factor as the presence of porosity lowers the total stiffness of the shell. For even porosity the decrement of NDFF is higher than that of uneven case. The variation of the NDFF with twist angle for perfect and porous FGM shell considering different even and uneven porosity factors are shown graphically in the figure 3.9 (for P-FGM) , 3.11 (for S-FGM) and 3.13 (for E-FGM). On the other hand Figure 3.10 (for P-FGM) depicts the NDFF variation for different twist angles while Figure 3.12 (for S-FGM) and 3.14 (for E-FGM) represents the NDSF variation considering different twist angle and porosity factors. The NDFF is found to increase with the angle of twist irrespective of the porosity factor for all the cases. The maximum NDFF is found for twist angle of 45^0 for perfect FGM shell. NDFF is identified to attain lowest value for twist angle, ψ=0°and gradually increase to a maximum value for twist angle, ψ=45° for highest rotational speed for all the cases as depicted in Figure 3.9, 3.11 and 3.13. This is due to the fact that the geometric stiffness matrix has higher dominance at higher twist angle. For a typical FGM configuration the perfect FGM predicts highest non-dimensional natural frequencies and the non-dimensional natural frequencies are observed to reduce with increase of the porosity factor. For the same porosity factor the even porous FGM shell predicts lower natural frequencies than that of corresponding uneven porous FGM shell.

Table 3.9. NDFF and NDSF $[\omega=\omega_n L_o^2\sqrt{(\rho/Eh^2)}]$ of rotating Stainless steel (SUS304)- Silicon nitride (Si_3N_4) functionally graded conical shells for various twist angles considering L_o/s=0.7, r_1=0.2 m, L_o=0.8 m, h=0.01 m, ϕ_o = 45º, ϕ_{ve} =20º for P-FGM Shell, N=5

Twist Angle (Ψ)	Porosity Factor	NDFF					*NDSF*				
		Ω=0	Ω=0.25	Ω=0.5	Ω=0.75	Ω=1.0	Ω=0	Ω=0.25	Ω=0.5	Ω=0.75	Ω=1.0
0^0	Perfect FGM ($\alpha_{ep}=\alpha_{up}$= 0)	0.9217	0.9835	1.1724	1.4308	1.7169	2.3718	2.4619	2.7306	3.1236	3.5823
	Even Porous (α_{ep} =0.1)	0.8903	0.9451	1.1158	1.3329	1.6053	2.2910	2.3781	2.6376	3.0173	3.4603
	Uneven Porous (α_{up}=0.1)	0.8369	0.8884	1.0488	1.2529	1.5090	2.1536	2.2354	2.4794	2.8362	3.2527
	Even Porous (α_{ep} =0.2)	0.8921	0.9529	1.1350	1.3839	1.6601	2.2971	2.3852	2.6444	3.0241	3.4725
	Uneven Porous (α_{up}=0.2)	0.8826	0.9376	1.1087	1.3466	1.6120	2.2717	2.3520	2.5935	2.9532	3.3838
15^0	Perfect FGM ($\alpha_{ep}=\alpha_{up}$= 0)	0.9677	1.0333	1.2327	1.5025	1.8004	2.3719	2.4710	2.7652	3.1902	3.6803
	Even Porous (α_{ep} =0.1)	0.9347	0.9981	1.1907	1.4513	1.7391	2.2911	2.3869	2.6710	3.0815	3.5550
	Uneven Porous (α_{up}=0.1)	0.8786	0.9382	1.1192	1.3642	1.6347	2.1536	2.2437	2.5107	2.8966	3.3417
	Even Porous (α_{ep} =0.2)	0.9351	0.9994	1.1908	1.4505	1.7379	2.3619	2.4181	2.7329	3.1304	3.5868
	Uneven Porous (α_{up}=0.2)	0.9260	0.9844	1.1647	1.4131	1.6894	2.1985	2.3131	2.5789	2.9771	3.4748
30^0	Perfect FGM ($\alpha_{ep}=\alpha_{up}$= 0)	1.1861	1.2722	1.5225	1.8476	2.2026	2.3359	2.4841	2.9052	3.4737	4.0937
	Even Porous (α_{ep} =0.1)	1.1457	1.2288	1.4707	1.7847	2.1276	2.2563	2.3995	2.8062	3.3554	3.9543
	Uneven Porous (α_{up}=0.1)	1.0770	1.1551	1.3824	1.6776	1.9999	2.1209	2.2555	2.6378	3.1541	3.7171
	Even Porous (α_{ep} =0.2)	1.1397	1.2231	1.4605	1.7737	2.1145	2.2371	2.3682	2.4199	3.2688	3.8642
	Uneven Porous (α_{up}=0.2)	1.1324	1.2091	1.4343	1.7346	2.0631	2.1197	2.2390	2.2803	3.0719	3.6364
45^0	Perfect FGM ($\alpha_{ep}=\alpha_{up}$= 0)	1.5987	1.7396	2.0884	2.5132	2.9717	2.2597	2.5196	3.1797	3.9817	4.7944
	Even Porous (α_{ep} =0.1)	1.5443	1.6804	2.0173	2.4276	2.8705	2.1827	2.4338	3.0714	3.8461	4.6311
	Uneven Porous (α_{up}=0.1)	1.4516	1.5796	1.8962	2.2819	2.6982	2.0517	2.2877	2.8871	3.6153	4.3533
	Even Porous (α_{ep} =0.2)	1.5300	1.6630	1.9958	2.4024	2.8410	2.1859	2.4294	3.0531	3.8167	4.6129
	Uneven Porous (α_{up}=0.2)	1.5238	1.6482	1.9660	2.3572	2.7810	2.1633	2.3917	2.9907	3.7328	4.5127

Table 3.10. NDFF and NDSF $[\omega=\omega_n L_o^2\sqrt{(\rho/Eh^2)}]$ of rotating Stainless steel (SUS304)- Silicon nitride (Si_3N_4) functionally graded conical shells for various twist angles considering L_o/s=0.7, r_1=0.2 m, L_o=0.8 m, h=0.01 m, ϕ_o = 45º, ϕ_{ve} =20º for S-FGM Shell, N=1.

Twist Angle (Ψ)	Porosity Factor	NDFF					*NDSF*				
		Ω=0	Ω=0.25	Ω=0.5	Ω=0.75	Ω=1.0	Ω=0	Ω=0.25	Ω=0.5	Ω=0.75	Ω=1.0
0^0	Perfect FGM ($\alpha_{ep}=\alpha_{up}$= 0)	1.1341	1.2364	1.5600	1.9800	2.3408	2.9242	3.0730	3.4426	4.1095	4.7783
	Even Porous (α_{ep} =0.1)	1.0955	1.1882	2.0844	2.0988	2.1887	2.8246	2.9683	3.3254	3.9696	4.6156
	Uneven Porous (α_{up}=0.1)	1.0297	1.1169	1.9594	1.9729	2.0574	2.6551	2.7902	3.1258	3.7314	4.3387
	Even Porous (α_{ep} =0.2)	1.0978	1.1980	2.1205	2.1791	2.2634	2.8320	2.9772	3.3339	3.9786	4.6319
	Uneven Porous (α_{up}=0.2)	1.0860	1.1788	2.0712	2.1203	2.1978	2.8008	2.9357	3.2697	3.8853	4.5136
15^0	Perfect FGM ($\alpha_{ep}=\alpha_{up}$= 0)	1.1946	1.3040	1.6186	2.0240	2.4597	2.9189	3.0831	3.5563	4.2119	4.9191
	Even Porous (α_{ep} =0.1)	1.1539	1.2596	1.5635	1.9551	2.3759	2.8195	2.9781	3.4352	4.0684	4.7516
	Uneven Porous (α_{up}=0.1)	1.0847	1.1840	1.4697	1.8378	2.2334	2.6503	2.7994	3.2291	3.8243	4.4665
	Even Porous (α_{ep} =0.2)	1.1543	1.2611	1.5637	1.9540	2.3743	2.9067	3.0170	3.5148	4.1330	4.7941
	Uneven Porous (α_{up}=0.2)	1.1431	1.2422	1.5293	1.9036	2.3081	2.7055	2.8861	3.3167	3.9306	4.6444
30^0	Perfect FGM ($\alpha_{ep}=\alpha_{up}$= 0)	1.4765	1.6235	2.0176	2.5030	3.0252	2.8758	3.1281	3.8057	4.6638	5.5282
	Even Porous (α_{ep} =0.1)	1.4262	1.5682	1.9489	2.4178	2.9222	2.7779	3.0215	3.6761	4.5050	5.3399
	Uneven Porous (α_{up}=0.1)	1.3407	1.4741	1.8320	2.2727	2.7468	2.6112	2.8402	3.4555	4.2347	5.0195
	Even Porous (α_{ep} =0.2)	1.4188	1.5608	1.9354	2.4030	2.9042	2.7543	2.9822	3.1701	4.3888	5.2183
	Uneven Porous (α_{up}=0.2)	1.4096	1.5431	1.9008	2.3499	2.8337	2.6097	2.8195	2.9872	4.1244	4.9106
45^0	Perfect FGM ($\alpha_{ep}=\alpha_{up}$= 0)	2.0018	2.2377	2.7781	3.4128	4.0882	2.7857	3.2223	4.2557	5.4472	6.5676
	Even Porous (α_{ep} =0.1)	1.9336	2.1615	2.6835	3.2966	3.9490	2.6908	3.1126	4.1108	5.2617	6.3439
	Uneven Porous (α_{up}=0.1)	1.8176	2.0318	2.5225	3.0988	3.7120	2.5294	2.9258	3.8641	4.9460	5.9633
	Even Porous (α_{ep} =0.2)	1.9158	2.1392	2.6549	3.2623	3.9084	2.6947	3.1070	4.0863	5.2215	6.3190
	Uneven Porous (α_{up}=0.2)	1.9080	2.1201	2.6152	3.2010	3.8258	2.6669	3.0589	4.0027	5.1067	6.1817

Table 3.11. NDFF and NDSF $[\omega=\omega_n L_o^2\sqrt{(\rho/Eh^2)}]$ of rotating Stainless steel (SUS304)- Silicon nitride (Si_3N_4) functionally graded conical shells for various twist angles considering L_o/s=0.7, r_1=0.2 m, L_o=0.8 m, h=0.01 m, ϕ_o = 45º, ϕ_{ve} =20º for E-FGM Shell

Twist Angle (Ψ)	Porosity Factor	NDFF					*NDSF*				
		Ω=0	Ω=0.25	Ω=0.5	Ω=0.75	Ω=1.0	Ω=0	Ω=0.25	Ω=0.5	Ω=0.75	Ω=1.0
0^0	Perfect FGM ($\alpha_{ep}=\alpha_{up}$= 0)	1.1969	1.3163	1.6592	2.0959	2.5622	3.0788	3.2526	3.7499	4.4354	5.1730
	Even Porous (α_{ep} =0.1)	1.1561	1.2649	1.5790	1.9525	2.3957	2.9739	3.1418	3.6222	4.2843	4.9968
	Uneven Porous (α_{up}=0.1)	1.0867	1.1890	1.4843	1.8353	2.2519	2.7955	2.9533	3.4048	4.0272	4.6970
	Even Porous (α_{ep} =0.2)	1.1585	1.2754	1.6063	2.0271	2.4774	2.9818	3.1512	3.6315	4.2940	5.0145
	Uneven Porous (α_{up}=0.2)	1.1461	1.2549	1.5690	1.9725	2.4057	2.9489	3.1073	3.5616	4.1933	4.8864
15^0	Perfect FGM ($\alpha_{ep}=\alpha_{up}$= 0)	1.2598	1.3870	1.7486	2.2044	2.6908	4.8147	4.9976	5.5321	6.3139	7.2355
	Even Porous (α_{ep} =0.1)	1.2168	1.3398	1.6890	2.1293	2.5992	2.9194	3.0835	3.5569	4.2125	4.9199
	Uneven Porous (α_{up}=0.1)	1.1438	1.2594	1.5877	2.0016	2.4432	2.3719	2.4710	2.7652	3.1902	3.6803
	Even Porous (α_{ep} =0.2)	1.2173	1.3414	1.6893	2.1282	2.5974	2.2566	2.3457	2.6105	2.9958	3.4445
	Uneven Porous (α_{up}=0.2)	1.2054	1.3213	1.6521	2.0733	2.5250	2.1170	2.1964	2.4326	2.7786	3.1841
30^0	Perfect FGM ($\alpha_{ep}=\alpha_{up}$= 0)	1.5557	1.7258	2.1760	2.7215	3.3043	4.7429	5.0191	5.7935	6.8594	8.0511
	Even Porous (α_{ep} =0.1)	1.5027	1.6671	2.1019	2.6288	3.1918	2.8758	3.1281	3.8057	4.6638	5.5282
	Uneven Porous (α_{up}=0.1)	1.4125	1.5670	1.9758	2.4711	3.0003	2.3359	2.4841	2.9052	3.4737	4.0937
	Even Porous (α_{ep} =0.2)	1.4949	1.6592	2.0873	2.6127	3.1721	2.2223	2.3557	2.7351	3.2526	3.8235
	Uneven Porous (α_{up}=0.2)	1.4852	1.6403	2.0500	2.5551	3.0951	2.0852	2.2051	2.5469	3.0165	3.5377
45^0	Perfect FGM ($\alpha_{ep}=\alpha_{up}$= 0)	2.1081	2.3807	2.9899	3.7030	4.4572	4.5963	5.0771	6.3121	7.8524	9.4422
	Even Porous (α_{ep} =0.1)	2.0363	2.2996	2.8881	3.5769	4.3054	2.7861	3.2228	4.2564	5.4481	6.5686
	Uneven Porous (α_{up}=0.1)	1.9141	2.1617	2.7148	3.3623	4.0471	2.2597	2.5196	3.1797	3.9817	4.7944
	Even Porous (α_{ep} =0.2)	2.0175	2.2759	2.8573	3.5397	4.2612	2.1500	2.3834	2.9815	3.7180	4.4704
	Uneven Porous (α_{up}=0.2)	2.0093	2.2556	2.8146	3.4732	4.1712	2.0190	2.2297	2.7740	3.4503	4.1450

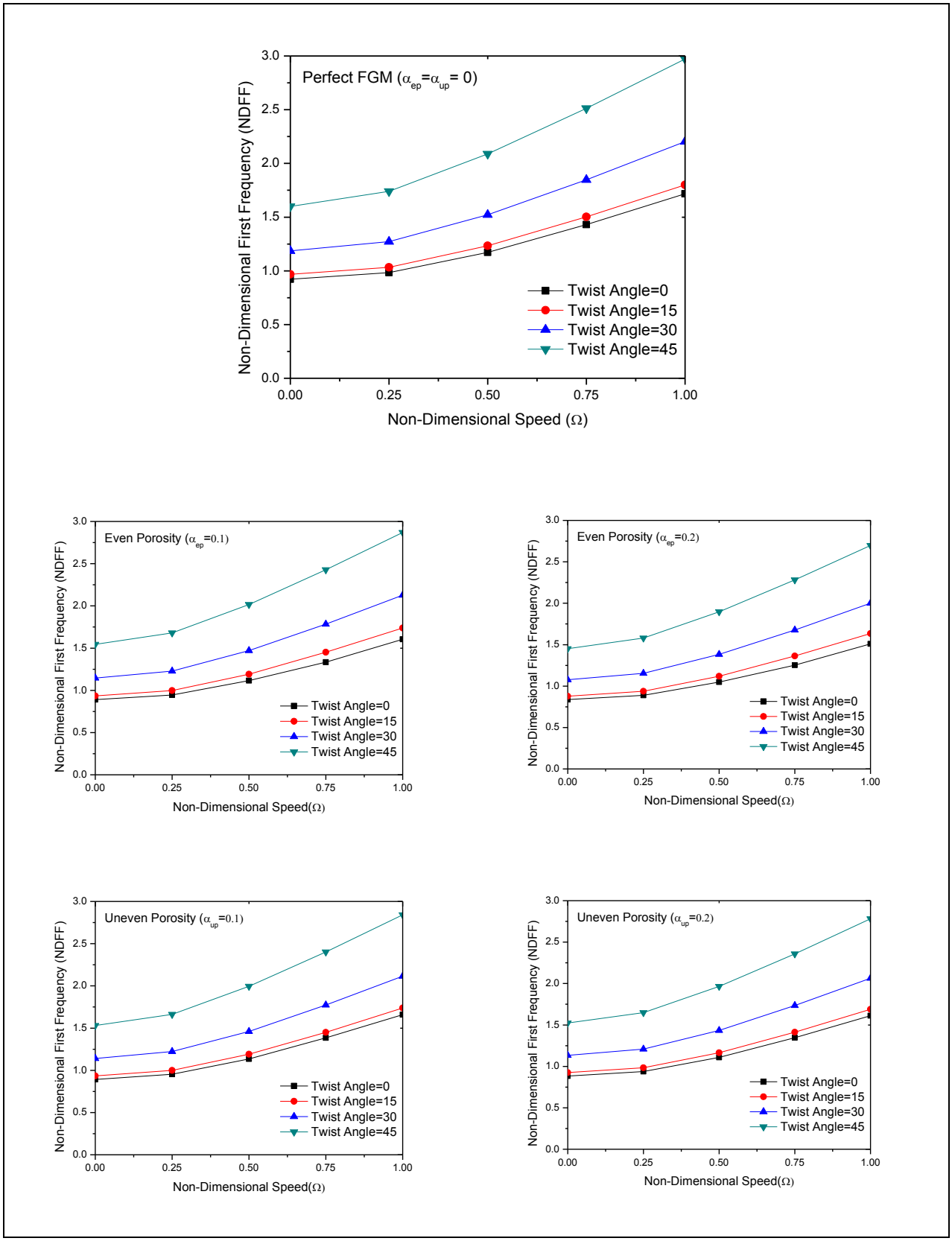

Figure 3.9 Variation of NDFF with non-dimensional speed of rotation (Ω=0.0, 0.25, 0.5, 0.75, 1.0) for various twist angle considering different even and uneven porosity factor along with perfect Stainless steel (SUS304)- Silicon nitride (Si_3N_4) graded conical shells (L_0/s=0.7, r_1=0.2 m, L_0=0.8 m, h=0.01 m, ϕ_o = 45º, ϕ_{ve} =20º), P-FGM, N=5.

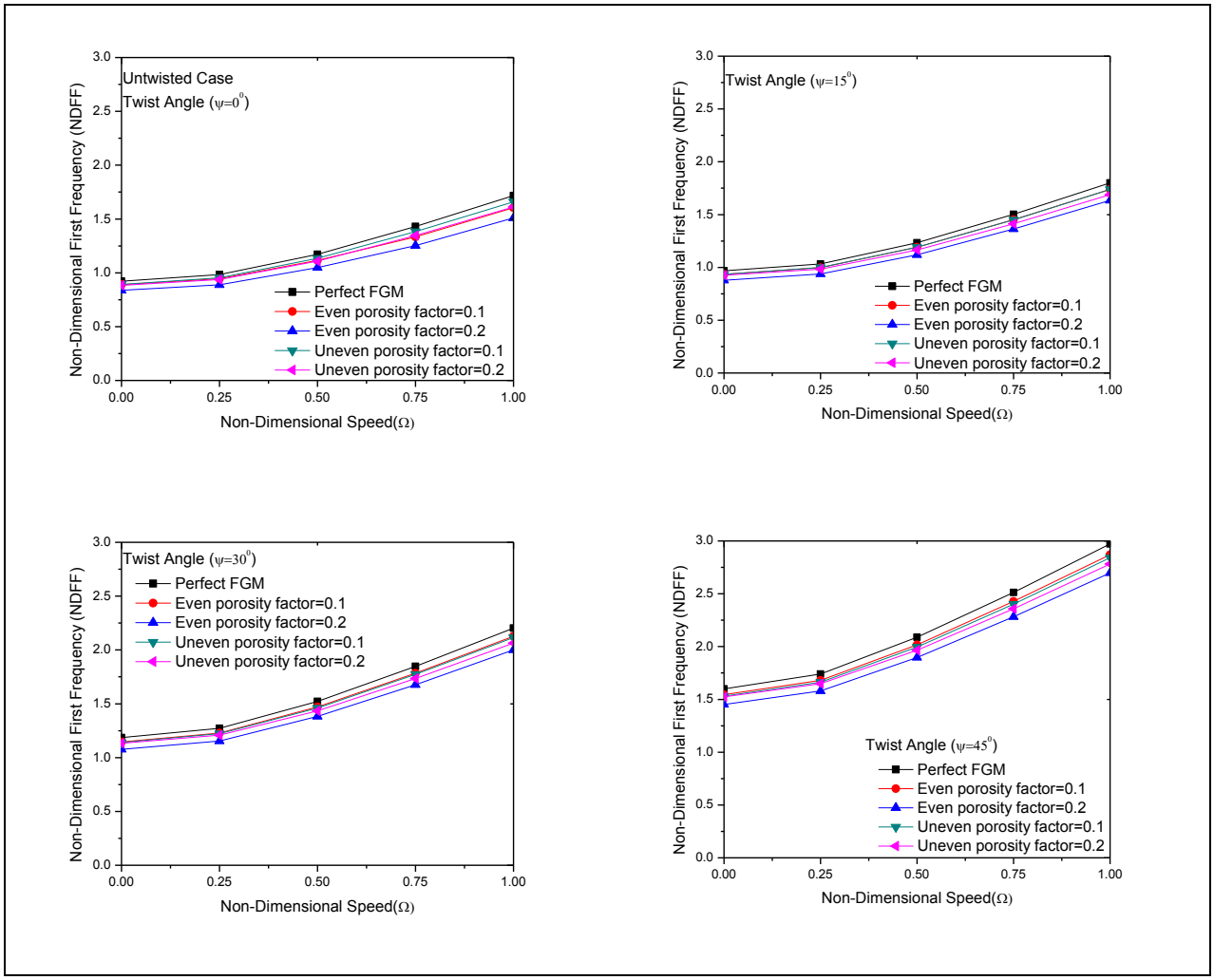

Figure 3.10 Variation of NDFF with non-dimensional speed of rotation (Ω=0.0, 0.25, 0.5, 0.75, 1.0) for different even and uneven porosity factor along with perfect Stainless steel (SUS304)-Silicon nitride (Si_3N_4) graded conical shells (r_1=0.2 m, h=0.01 m, s/h=114, L_o/s=0.7, ϕ_o = 45º, ϕ_{ve} =20º) P-FGM, N=5.

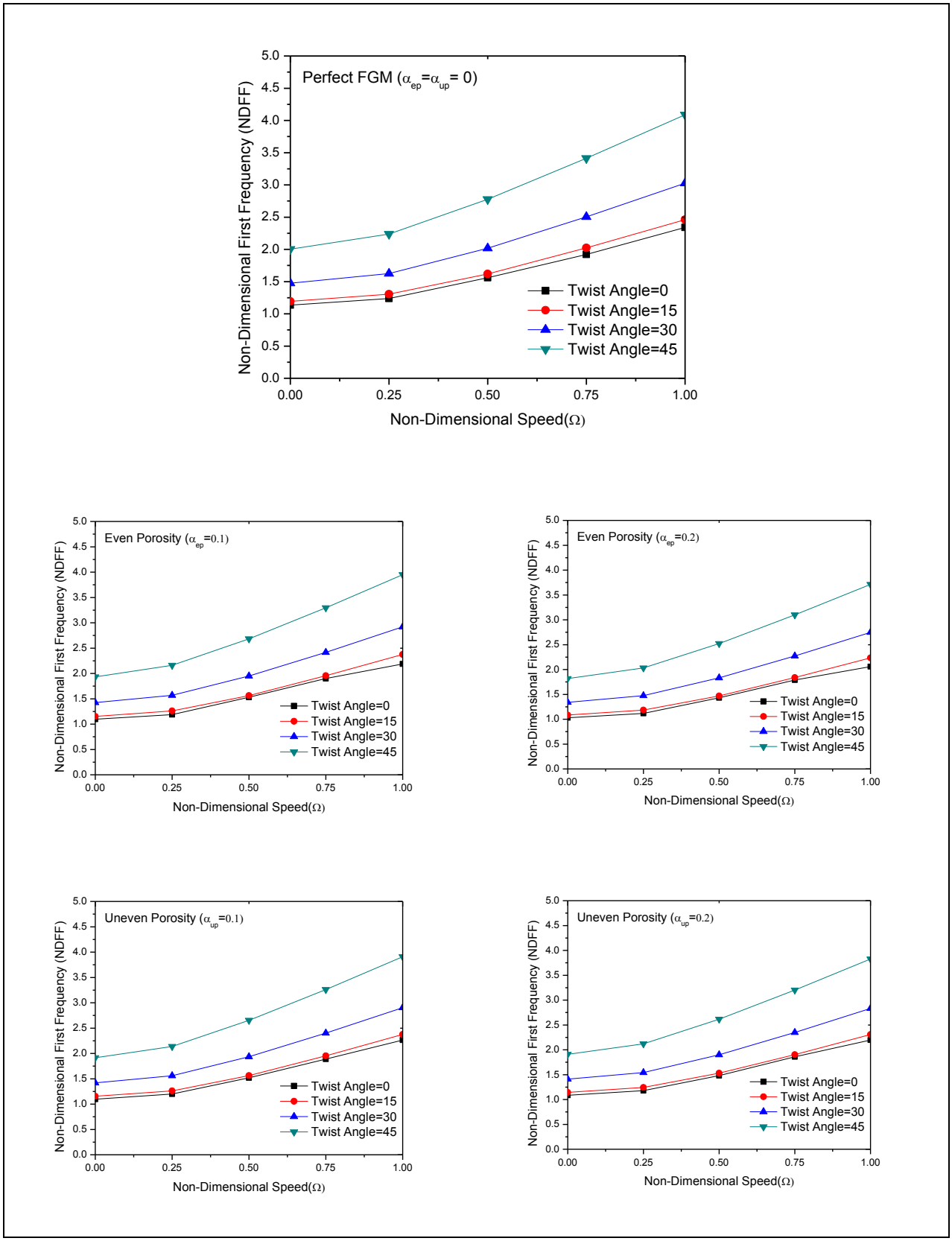

Figure 3.11 Variation of NDFF with non-dimensional speed of rotation (Ω=0.0, 0.25, 0.5, 0.75, 1.0) for various twist angle considering different even and uneven porosity factor along with perfect Stainless steel (SUS304)- Silicon nitride (Si_3N_4) graded conical shells (L_0/s=0.7, r_1=0.2 m, L_0=0.8 m, h=0.01 m, ϕ_o = 45º, ϕ_{ve} =20º), S-FGM, N=1.

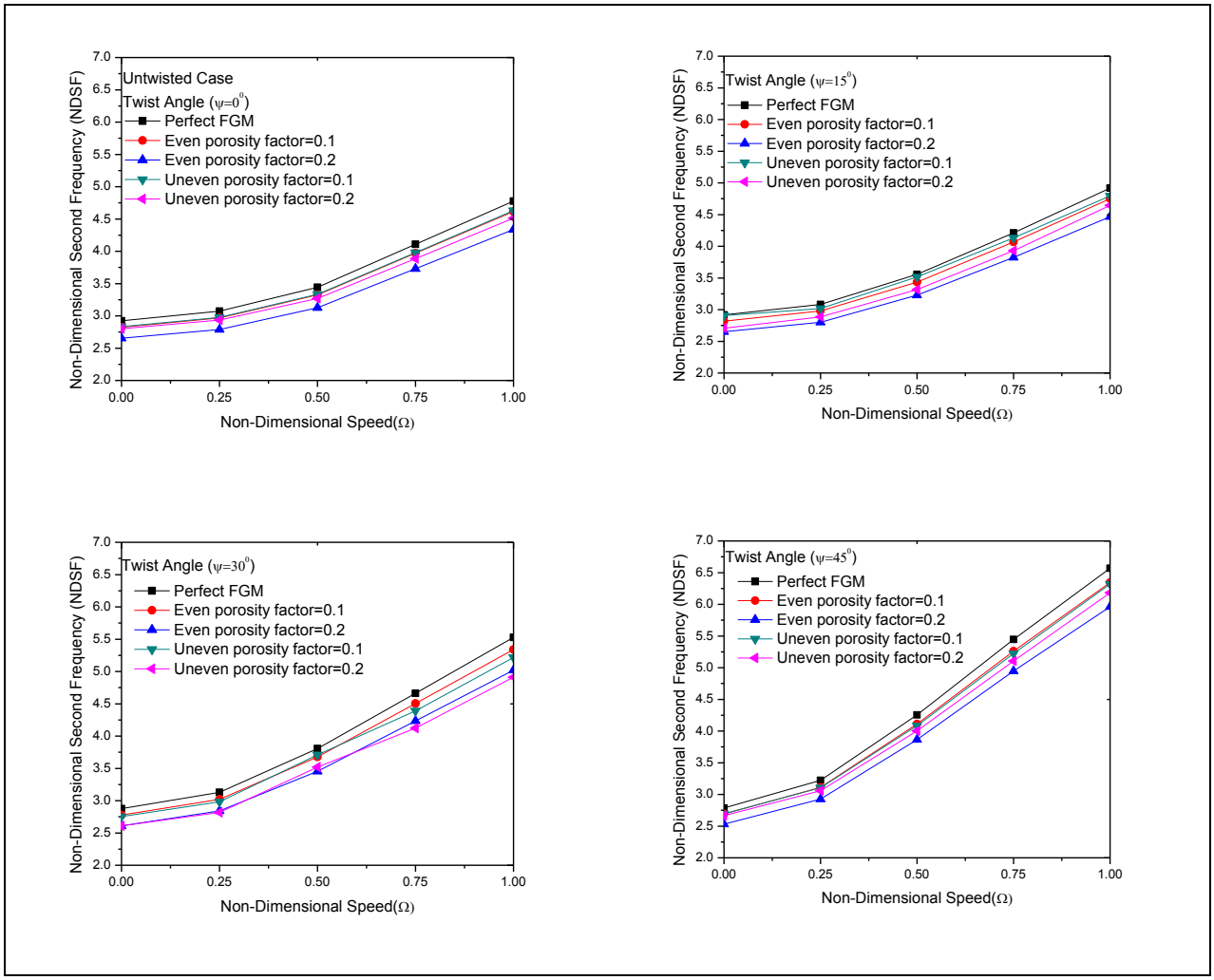

Figure 3.12 Variation of NDSF with non-dimensional speed of rotation (Ω=0.0, 0.25, 0.5, 0.75, 1.0) for various twist angle considering different even and uneven porosity factor along with perfect Stainless steel (SUS304)- Silicon nitride (Si_3N_4) graded conical shells (r_1=0.2 m, h=0.01 m, s/h=114, L_o/s=0.7, ϕ_o = 45º, ϕ_{ve} = 20º.) S-FGM, N=1.

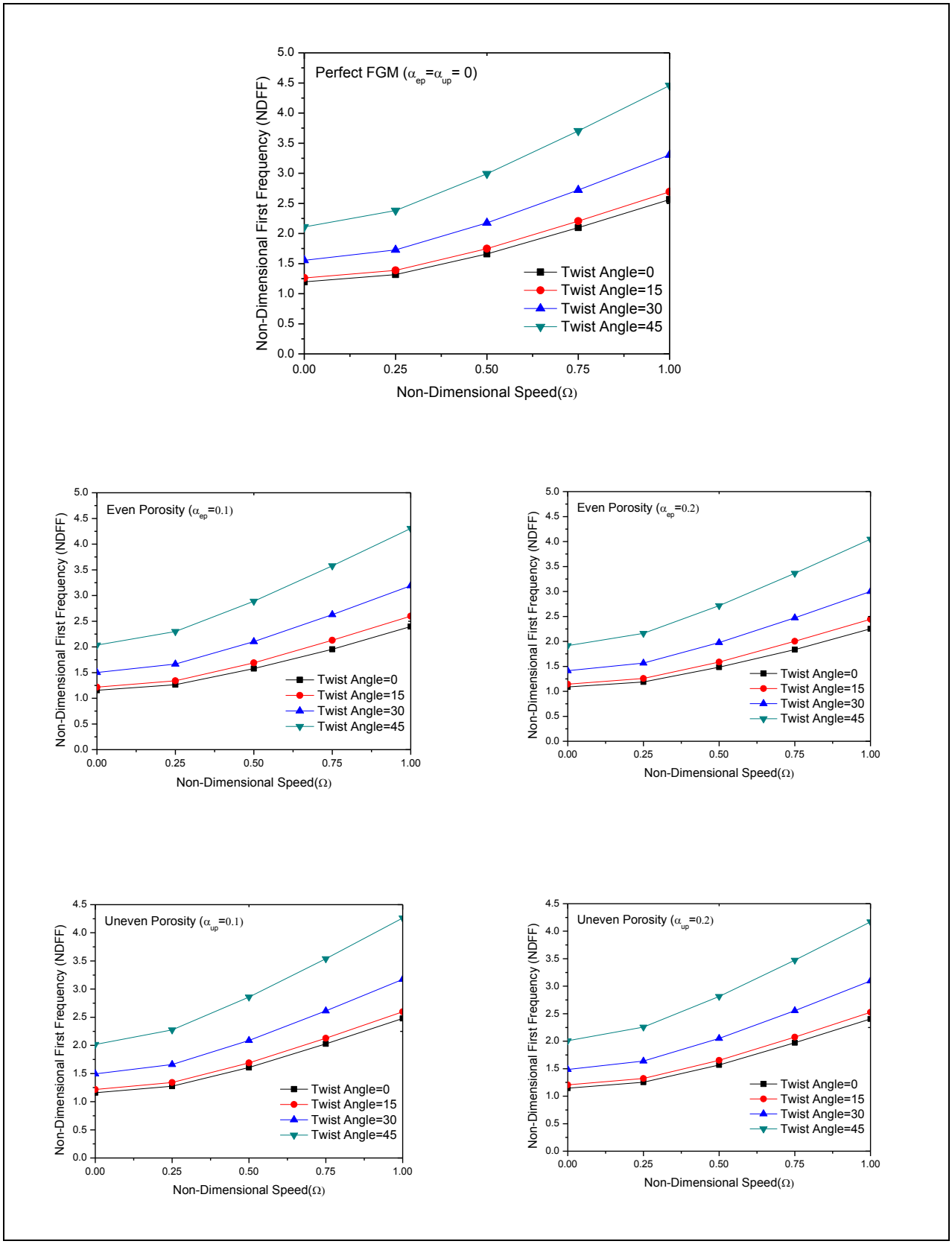

Figure 3.13 Variation of NDFF with non-dimensional speed of rotation (Ω=0.0, 0.25, 0.5, 0.75, 1.0) for various twist angle considering different even and uneven porosity factor along with perfect Stainless steel (SUS304)- Silicon nitride (Si_3N_4) graded conical shells (L_0/s=0.7, r_1=0.2 m, L_0=0.8 m, h=0.01 m, ϕ_o = 45º, ϕ_{ve} =20º), E-FGM

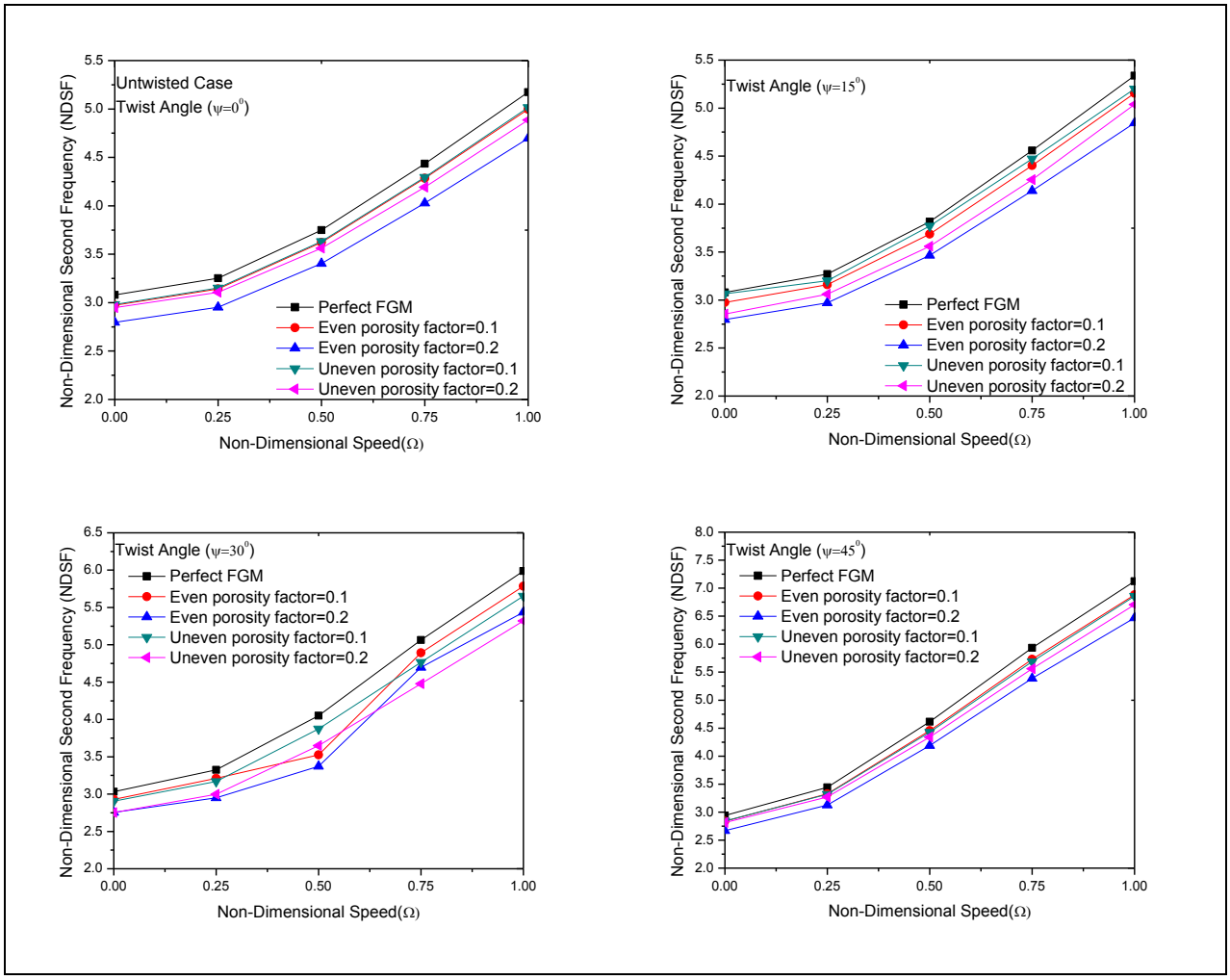

Figure 3.14 Variation of NDSF with non-dimensional speed of rotation (Ω=0.0, 0.25, 0.5, 0.75, 1.0) for various twist angle considering different even and uneven porosity factor along with perfect Stainless steel (SUS304)- Silicon nitride (Si_3N_4) graded conical shells (r_1=0.2 m, h=0.01 m, s/h=114, L_o/s=0.7, ϕ_o = 45º, ϕ_{ve} = 20º.) E-FGM

3.7.2 MODE SHAPES WITH POROUS FGM CONICAL SHELL

Mode shapes corresponding to the first natural frequencies are furnished in figure 3.15 for various twist angles (ψ=0°, 15°, 30° and 45°) and non-dimensional rotational speeds (Ω=0.0, 0.5 and 1.0) for porous ($\alpha_{ep} = 0.2$) SS-Si_3N_4 E-FGM conical shells. The dotted line represents the deflection in negative direction (negative z direction) while the firm line shows the deflection in positive direction (positive z direction) of the conical shell. The first frequency is found to be the torsional mode at stationary condition irrespective of the twist angle. Torsional modes are also observed with Ω=0.5 for untwisted and lower twist angle (15^0), but the torsional mode reversal along the longitudinal axis is observed for ψ=30°, 45°. The torsional symmetry modes are not observed for other twist angle under rotation. Bending mode along the longitudinal direction is

Ψ	NDFF		
	Ω=0.0	Ω=0.5	Ω=1.0
0°	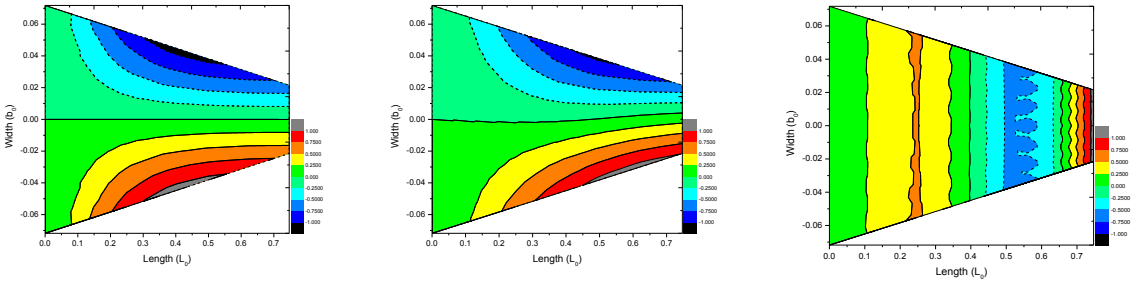		
15°	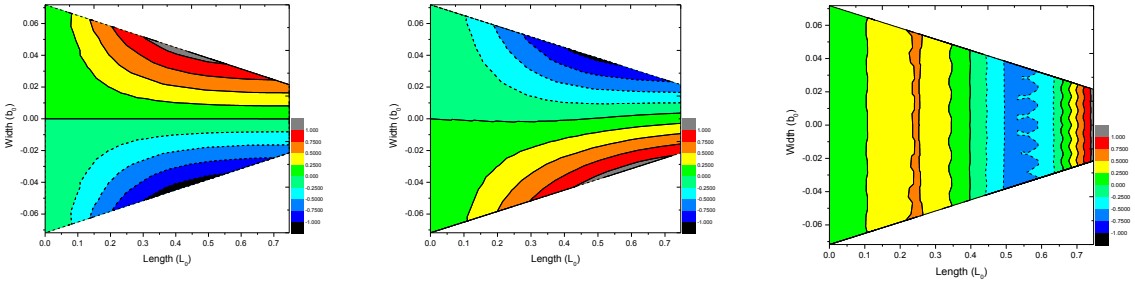		
30°	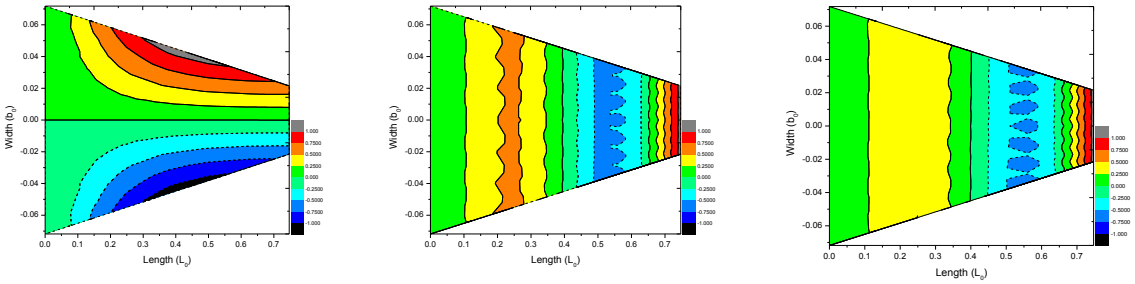		
45°	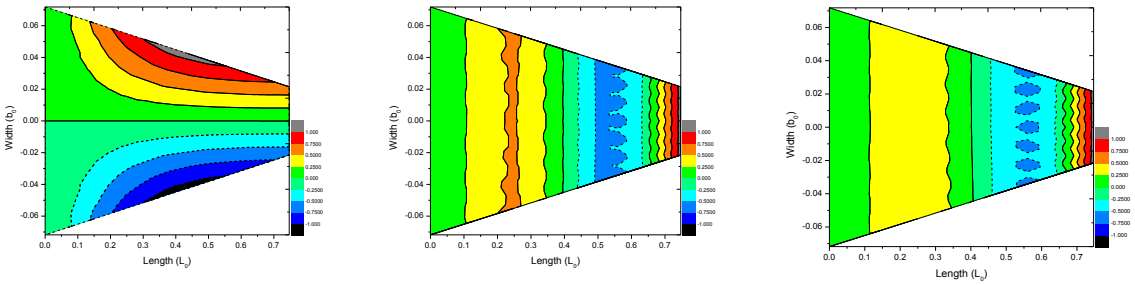		

Figure 3.15. Mode shapes of Porous SS-Si_3N_4 E-FGM conical shells (even porosity factor, $\alpha_{ep} = 0.2$) considering r_1=0.2 m, h=0.01 m, s/h=114, L_o/s=0.7, ϕ_o = 45º, ϕ_{ve} = 20º

observed for those cases. Bending mode is also observed at rotational speed Ω=1 for twisted and untwisted cases. For the porous FGM conical shell the deflection is higher compared to that of

perfect FGM shell. The deflection is proportional to the percentage of porosity. The Figure 3.15 of mode shapes show the relative non-dimensional deflection (calculated based on perfect FGM) considering the even porosity factor 0.2 and the corresponding mode shapes of the figure show higher deflection compared to perfect FGM. The mode shapes for the intermediate percentage of porosity have same basic nature of deflection with higher deflection compared to perfect FGM shell. Maximum deflection is observed for the even porous FGM shell considering porosity factor 0.2.

CHAPTER 4

LOW VELOCITY IMPACT RESPONSE OF FUNCTIONALLY GRADED SHALLOW CONICAL SHELLS

4.1 GENERAL

For low velocity impact problems penetrations is not happening due to the low energy of the impact. Though the penetration is not happening still the structure may be damaged severely due to the cascading effect of low energy and low velocity impact. The transient dynamic analysis for low velocity impact response of FGM materials subjected to localized contact loading is of significant concern in many advanced engineering structures and components, such as the leading edge of an aircraft wing, fan blades in a jet engine or the protruded sections of machinery blade and other areas where these materials are used extensively. Recent widespread applications of FGM conical shells are facing with the situations wherein the shells are impacted by foreign bodies of arbitrary shapes moving at relatively low velocities (typically less than 10m/s). Impact of masses moving at relatively low velocities with underwater vehicles, windmill blades, automobile or aircraft bodies, steam turbine blades or spaceships is quite common in actual practice. Low-velocity impact may also occur during manufacturing, processing, maintenance or transportation of the FGM structures as in tool drop or rough handling. Micro-voids or porosity may present due to manufacturing discrepancy of the FGM materials. An impact with a foreign mass may result in the coalescence of such micro-voids or porosity at different location of the FGM shells structures. The turbomachinery blades are under a preload originated from the centrifugal forces resulting in initial stresses which may aggravate the damage due to impact especially in the presence of porosity. In most practical applications as in hailstorm or ballistic attacks, impact on FGM shell structure is never a localized phenomenon and the loading and unloading cycles of multiple impactors can greatly influence the contact force and displacement. Thus an analytical method to predict the dynamic response of FGM conical shells under single, multiple and time delayed multiple impact is very helpful in most practical applications. Hence, attention is needed for in-depth study of transient impact performance of pretwisted and untwisted FGM conical shells subjected to low velocity normal impact. Numerical results are obtained for FGM shells impacted centrally and at

location away from the centre. Parametric studies are performed in respect of angle of twist, rotational speeds, velocity of the impactor, location of the impact, thickness of conical shell and different FGM power laws and material property graded index. This chapter presents a finite element based numerical study for transient dynamic impact performance of FGM conical shells.

4.2 LOW VELOCITY NORMAL IMPACT

The centrifugal forces arising out of rotation induce the initial stresses in FGM conical shells. The pretwist of the FGM shell also causes coupling in both bending directions. Moreover, the pretwisted FGM conical shells are prone to incur damage by impacts especially those normal to the shell surface. Hence, reliable and accurate prediction of normal impact response of delaminated composite pretwisted conical shells covers a wide range of parameters. The analyses herein are concerned with some important aspects in this context. The investigation primarily concentrates upon the low velocity normal impact which is said to occur for impactor speeds less than 10 m/sec. A modified Hertzian contact law considering permanent indentation is used to calculate the contact force along with other impact response parameters. Using the Newmark's time integration scheme (constant average acceleration method) the time dependent equations are solved. Parametric studies are performed to study the effect of prime parameters like initial velocity of impactor, mass of the impactor, twist angle, location of the impact and material property garded index through different FGM constituent laws.

4.3 CONTACT PHENOMENON AND INDENTATION

The contact force depends on a contact law which relates the contact force with the indentation. The present study considers FGM conical shells having a large ratio of the radius of curvature to its thickness as well as a high value of width to thickness ratio. Conway (1956) established a Hertzian-type contact force model which is appropriate for transversely isotropic materials. Yang and Sun (1982) proposed a power law based on static indentation tests using steel balls as indentors. The Hertzian-type contact model has been used to state the contact between the impactor and FGM materials by Larson and Palazotto (2006). The indentation parameter α depends on the difference of the displacements of the impactor and the target structure at any instant of time, and so also the contact force. The values of α are changing with time because of time varying displacements of both the rigid impactor and the

target structure. So at an instant the maximum indentation takes place and as a result the maximum contact force is also obtained. At this instant the displacement of the impactor also attains the maximum value. Thereafter, the displacement of the impactor gradually decreases, but the target point displacement keeps on changing and finally increases to a maximum value and at some point of time these two displacements become equal. This leads to zero value of indentation and eventually the contact force becomes zero. At this instant the impactor looses contact with the target. The process after attaining the maximum contact force till the reduction of contact force to zero value is essentially referred to as unloading. An elastic spherical mass impact on top surface of a functionally graded conical shell as shown in figure 4.5, where the top surface is ceramic-rich and bottom surface is metal rich. The shell is initially at rest and undeformed with one end clamped boundary condition that could be idealized as a turbo machinery blade. The spherical impactor is assumed to add no mass to the system that would affect the modes and net response. Furthermore, the contact phenomenon is idealized by neglecting gravitational effect and assuming the impactor bounces off the shell structure immediately after impact. The governing equations of low-velocity, low-energy impact event between a sphere and a plate have been defined by Goldsmith (1960). The formulation initiates by considering the pressure distribution from an impact event which can be resolved into a concentrated force of magnitude F. At impact, the projectile will deform the shell globally as well as a small localized area where the elastic sphere indents the shell. The impact force causes the localized deformation on the shell. F_c, is a contact force that can be expressed by the Hertzian contact formulation which is valid for a relatively low-velocity, low-energy impact where deformation between the impactor and target are elastic in nature. For the high velocity impact this assumption does not hold good, and in the present analysis the low velocity impact is considered

4.4 COMPARISON OF RESULTS

In order to validate the computer codes developed for the transient dynamic analysis of FGM conical shells under low velocity single impact, the results obtained on the basis of present finite element modelling are compared with those of the reference solutions published in the open literature for low velocity impact model. The present finite element formulation for impact response a computation study has been carried out with 15 mm thick isotropic FGM beam that could be idealized for the present conical shell formulation with $r_x=r_y$=infinity and a rectangular planner form. In this context, essentially two important

aspects namely, analytical solution and finite element treatment have been taken into account. The results of Kiani et al. (2013) are compared considering a simply supported boundary condition of 153.5 mm length (L_0), 10mm width (b) and 15 mm thick (h) FGM beam impacted centrally by an steel sphere of 12.7 mm radius and 10 gm mass with initial velocity of impactor (VOI) 2.0 m/sec which provides solution of an integral equation for a modified Hertzian contact law expressed as in equation 2.106. Figure 4.1 depicts the comparisons of time histories of contact force ,indentation, shell displacement and impactor velocity obtained from present FEM and that of Kiani et al. (2013). This shows a good match between the present FEM analysis and the reference (Kiani et al., 2013) results. The slight differences in the present results can be attributed to the fact that Kiani et al. (2013) used energy method.

From the comparison as per Figure 4.1 it can be seen that the nature of variation is similar and the present FEM formulation can be acceptable for carrying out these analysis with FGM conical shell considering single impact problem.

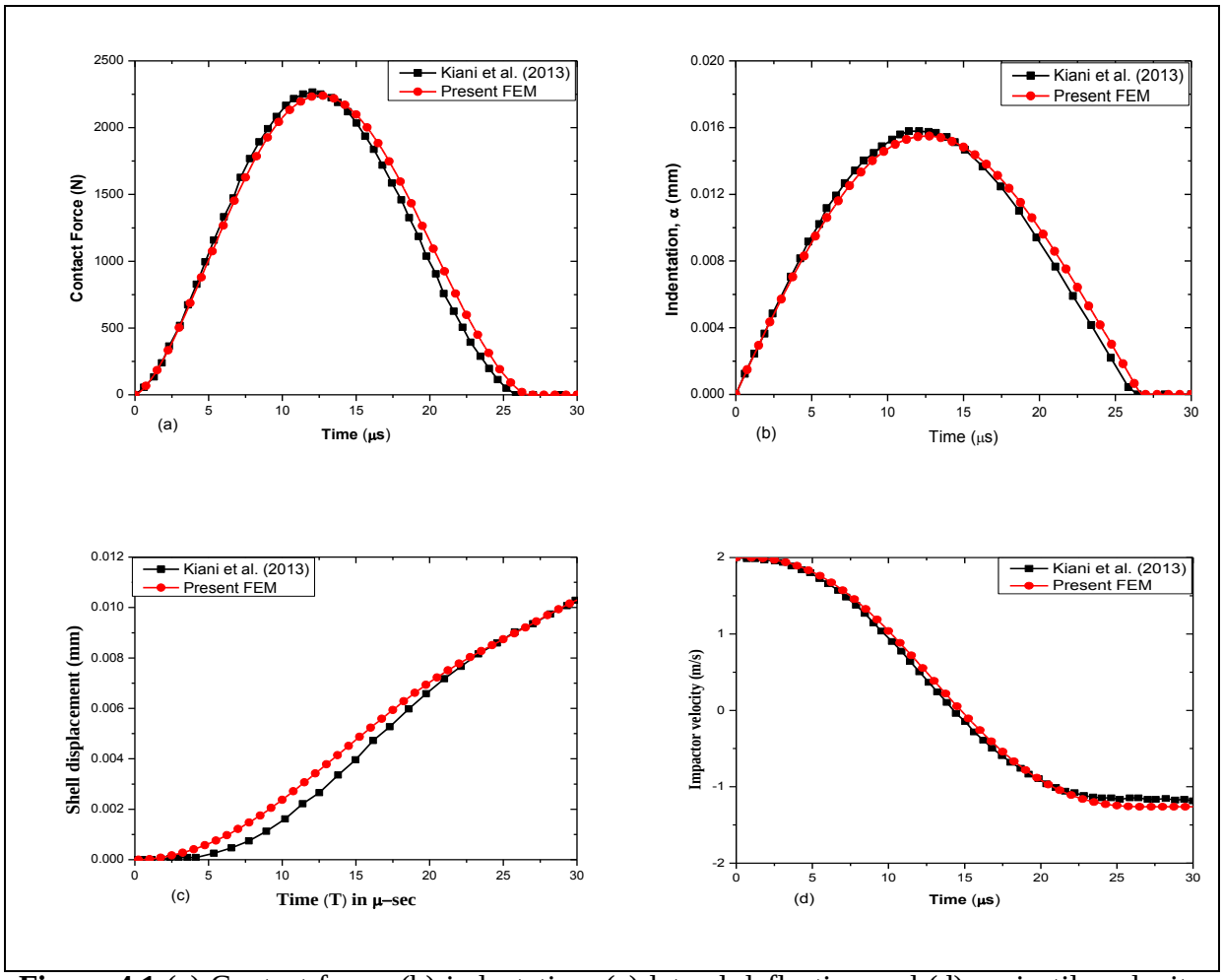

Figure 4.1 (a) Contact force, (b) indentation, (c) lateral deflection and (d) projectile velocity histories of an FGM beam clamped at both ends with immovable in-plane boundary conditions. L_0 = 153.5 mm, b_0 = 10 mm, h = 15 mm, Mass of impactor (M_0)= 10 gm, r_i = 12.7 mm, VOI = 2 m/s, FGM power law index (N) =5.0

To validate the present finite element formulation for the transient dynamic analysis of FGM conical shells under low velocity multi impact response, computation has been carried out for 10 mm thick isotropic FGM beam that could be idealized for the conical shell formulation with $r_x=r_y=\infty$ and a rectangular planner form. In this context, essentially two important aspects namely, analytical solution and finite element treatment have been taken into account. The results of Lam and Sathiyamoorthy (1999) are compared considering a clamped-free boundary condition of 300 mm length (L_0), 10mm width (b_0) and 10 mm thick (h) FGM beam simultaneously impacted at location 1 ($L/6$, $b/2$) and location 2 ($5L/6$,$b/2$) by two steel sphere of 10 mm radius and 10 gm mass with initial velocity of both the impactors 2.0 m/sec which provides solution of an integral equation for a modified Hertzian contact law expressed as in equation 2.106. Figure 4.2 depicts the comparisons of time histories of Contact force and deflection obtained from present FEM and that of Lam and Sathiyamoorthy (1999). This shows a good agreement between the present FEM analysis and the reference (Lam and Sathiyamoorthy, 1999) results. The slight differences in the present results can be attributed to the fact that Lam and Sathiyamoorthy used energy method. From the comparison as per figure 4.2 it is observed that the nature of variation is similar and the present FEM formulation can be acceptable for carrying out these analysis with FGM conical shell for multiple impact problem.

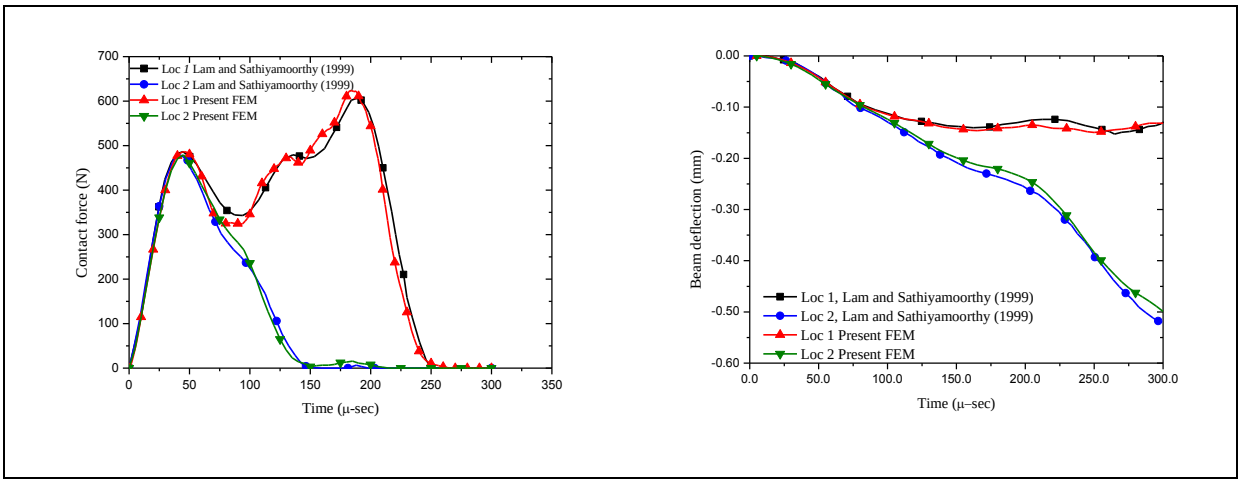

Figure.4.2 Contact force and beam displacement histories of a cantilever composite ($[0^0/90^0/90^0/0^0]$) beam at Loc *1* and *2*. L= 0.3 m, b=0.01m, h=0.01m, $r_{i1}= r_{i2}$= 0.01m, $v_{i1} = v_{i2}$=2.0 m/s, E_1= 144.80 GPa, E_2 = 9.65 GPa, G_{12} = G_{13} =4.14 GPa, G_{23}=3.45 GPa, ν_{12} = 0.30, ρ = 1389.23 kg/m^3. *Loc 1* (L/6, b/2), *Loc2* (5L/6,b/2)

The present study for low velocity impact performance of FGM conical shell is carried out to investigate the effect of initial velocity of impactor, mass of the impactor twist angle, location of the impact and material property garded index through different FGM constituent laws. Accordingly the dimensions of length (L_0) and width (b_0) are taken as 0.8m and 0.143m respectively. The other parameters of the conical shells ($r_x = \alpha$) having rectangular plan-form (L_o/b_o) of=5.59, curvature ratio (b_o/r_y) of 0.5 and aspect ratio (L_o/s) of 0.7 are considered. Considering the complete planform of the shell a uniform mesh division of 8 × 8 has been used for the analyses. For all the cases shells are impacted at centre as well as other locations by a spherical steel ball of 0.0127 m diameter with differnt initial velocity of 1 m/s, 3 m/s, 5 m/s and 10 m/s. The material property used for the present analysis are are considerd as per table 3.5. Figure 4.3 and 4.4 represnts the time step convergence study for both end clamped and one end clamped condistion respectively. It has been observed that the time step beyond 1 µ-sec the impact parametsrs remains almost same, therefore the time step has not much influence on the impact parameters. A converged optimum value of time step (1.0 µ-sec) and mesh size of 8x8 is considered for the further analysis.

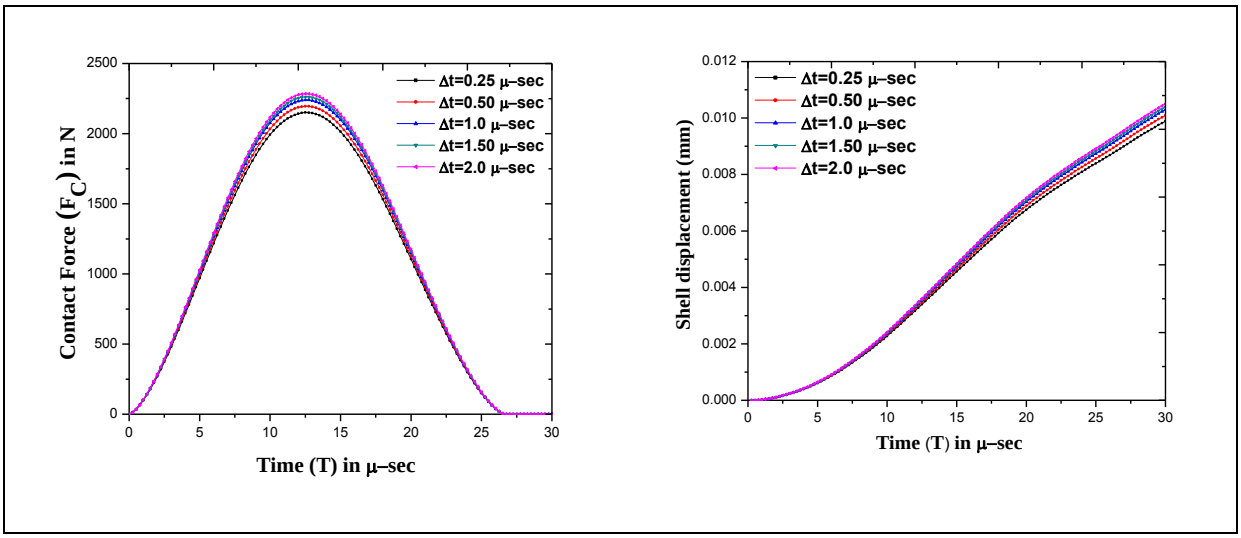

Figure.4.3 Time convergence study for histories of contact force (Fc) and shell displacement of FGM beam clamped at both ends with immovable in-plane boundary conditions. L_0 = 153.5 mm, b_0 = 10 mm, h = 15 mm, Mass of impactor (M_0)= 10 gm, r_i = 12.7 mm, v_0 = 2 m/s, FGM power law index (N) =5.0

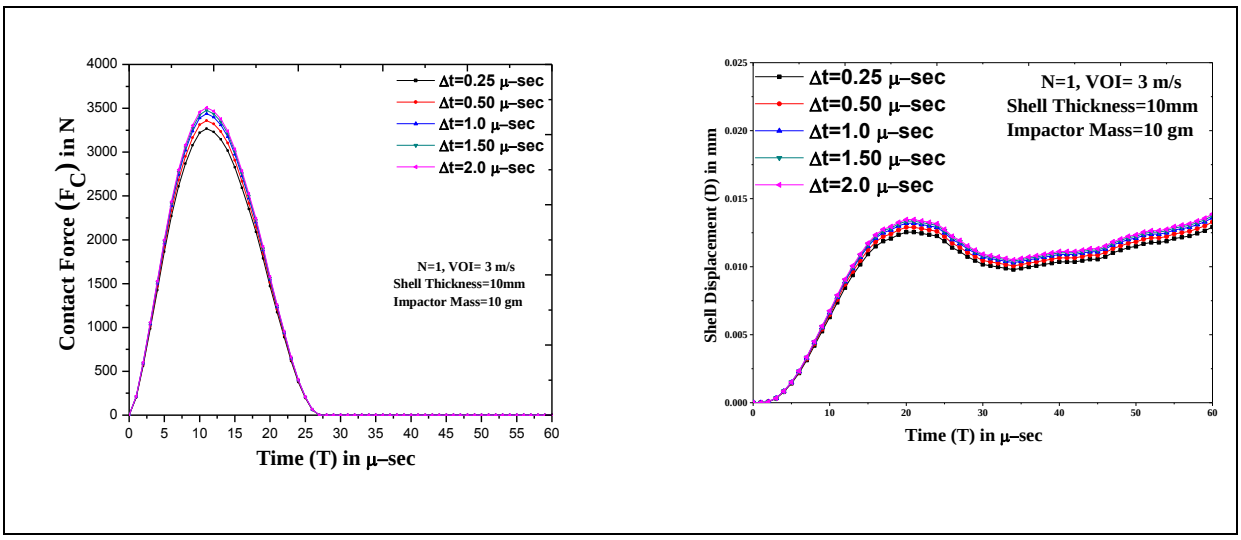

Figure.4.4 Time convergence study for histories of contact force (Fc) and shell displacement of FGM cantilevered conical shell clamped at one ends. Length=0.8m, width=0.143m, thickness=0.01 m, mass of the impactor (M_0)=0.01 Kg. , h = 0.01m, r_i = 12.7 mm, VOI = 3 m/s, FGM power law index (N) =1.0

4.5 RESULTS AND DISCUSSION

4.5.1 SINGLE IMPACT

The conical shell are impacted at centre ($L_0/2$,$b_0/2$) [denoted by "H" in the figure 4.5] of the shell for single impact problem with different initial velocities of 1m/s, 2m/s, 3m/s, 4m/s and 5m/s. The impact parameters are varied to see the effect on the single impact response and these are described below.

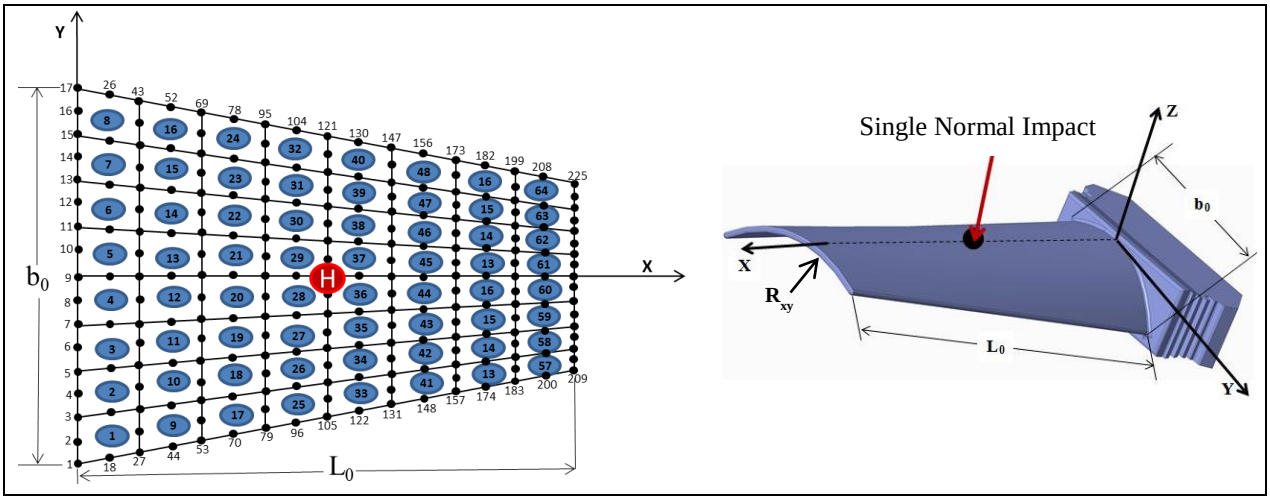

Figure. 4.5 Location (H) and node number (113) for the single normal impact problem

4.5.1.1 EFFECT OF INITIAL VELOCITY OF THE IMPACTOR

Design of an impact mitigating system is very essential for the turbomachinery blade to avoid catastrophic failure during operation. The initial velocity of the impactor is an important factor affecting the various impact responses. The effect of initial velocity of impactor (VOI) for simple power law index N=1 are furnished in Figure 4.6. The peak value of contact force is found to increase with increase of initial velocity of impactor as per Figure 4.6 (a). It is also observed that the contact duration reduces with the increase of VOI. The impactor's displacement curve is observed to increase during loading and after reaching the peak value, it is found to decrease with a slope which is proportional to initial velocity of impactor. From

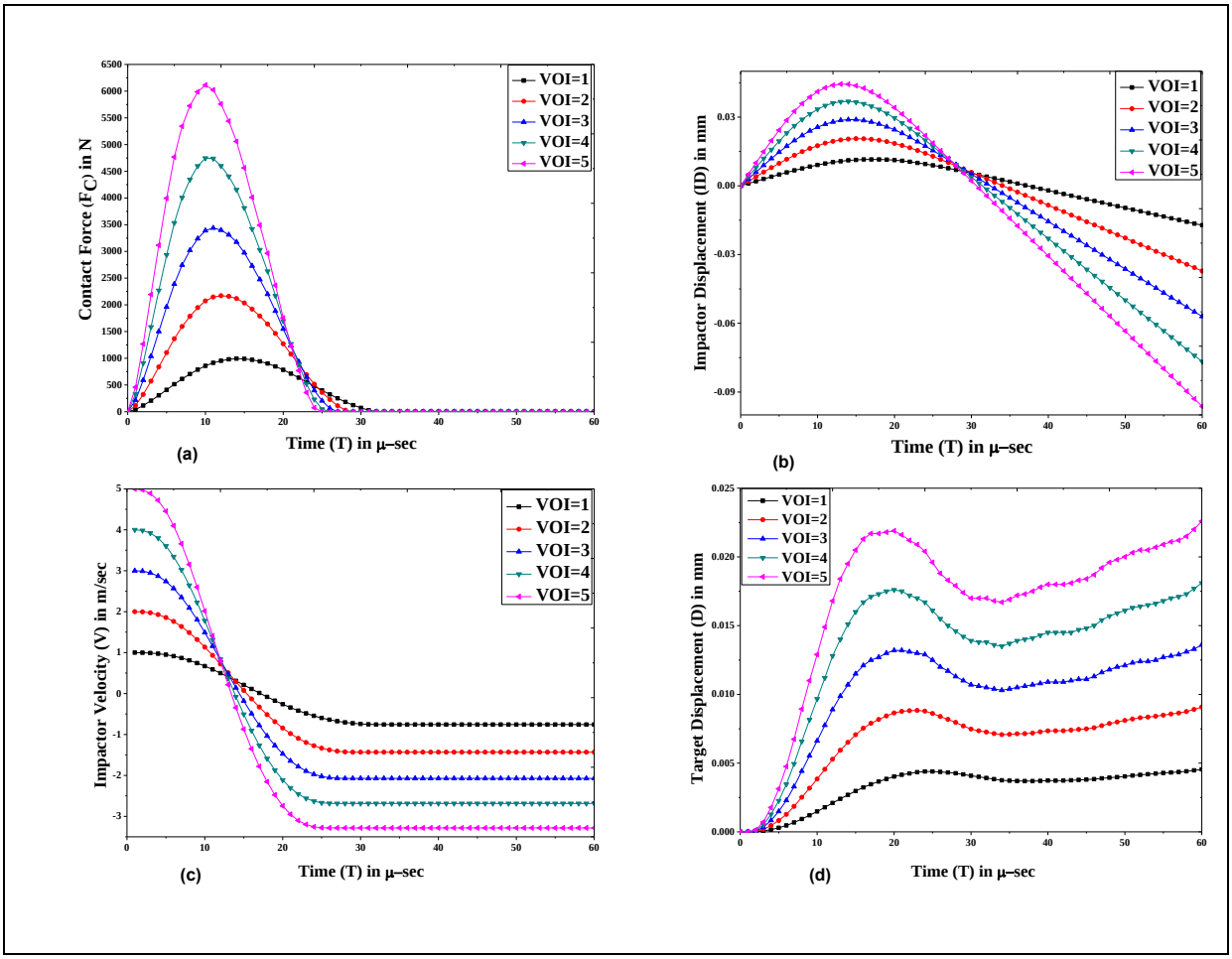

Figure. 4.6 (a) Contact Force, (b) Impactor displacement, (c) Impactor velocity, (d) Target displacement for N=1 with respect to time for SS-Si_3N_4 FG conical shell impacted at the center of top surface. Length=0.8m, width=0.143m, thickness=0.01 m, time step=1.0 μ-sec, mass of the impactor (M_0)=0.01 Kg.

Figure 4.6 (b) it is to be noted that the negative value of impactor's displacement indicates the situation when the impactor bounces back from the target after hitting the target surface. The contact duration has inverse relationship with initial velocity of impactor while the time

of attaining the peak value of contact force is found to reduce with the increase of initial velocity of impactor. The variation of the indentation is similar to the contact force with respect to initial velocity of the impactor. The slope of time history curves for velocity of impactor (from Figure 4.6.c) is found to be maximum value for VOI=5 m/sec, followed by VOI=4 m/sec, VOI=3 m/sec, VOI=2 m/sec and VOI=1 m/sec, respectively. It is also to be noted that the velocity of the impactor comes down to zero value at the end of contact duration and subsequently it falls down to negative value wherein null value of contact force is observed. Figure 4.6.d shows the increasing trend of shell displacement with increase of VOI.

4.5.1.2 EFFECT OF MASS OF THE IMPACTOR

Like initial velocity of the impactor, the mass of the impactor also plays a significant role affecting the impact responses and designer must be aware of the effect of impactor mass for the low impact phenomenon. Based on the mass of the outside/inside debris or small torn out objects from the turbo machines which impacts on the turbomachinery blade the impact performance varies. The impact characteristics greatly influenced by the mass of the impactor and it is obvious that the contact force as well as the impactor displacement, shell displacement and indentation will have basic similar nature with variation of mass. The figure 4.7 (a), 4.7 (b), 4.7 (c) and 4.7 (d) represents the contact Force, impactor displacement, impactor velocity and target displacement respectively considering initial velocity of the impactor 3 m/s for the power law index N=1. From figure 4.7 (a) it is observed that with higher the mass of the impactor the contact force is higher and the longer contact duration is observed with higher mass of the impactor. This trend can also be observed irrespective of the initial velocity of the impactor and the power laws index (N). The time of attaining peak value of the contact force is found to be lower for light mass of the impactor. Figure 4.7 (b) reveals the fact that the impactor displacement is higher for the higher mass of the impactor. It can also observed form the same figure that impactor displacement reaches quickly to the null value for lower mass of the impactor compared to the higher mass and the former one bounces back with higher displacement. Though the contact force is higher for heavier mass of the impactor but the impator bounces back with lesser velocity after hitting the target surface compared to lower mass of the impactor because the heavier mass has to overcome greater gravitational force while bouncing upward direction. Figure 4.7 (c) indicates this trend. The shell or target displacement is proportional to the mass of the impactor. Figure 4.7 (d) shows the predicted shell displacement enhances with increment of the impactor mass.

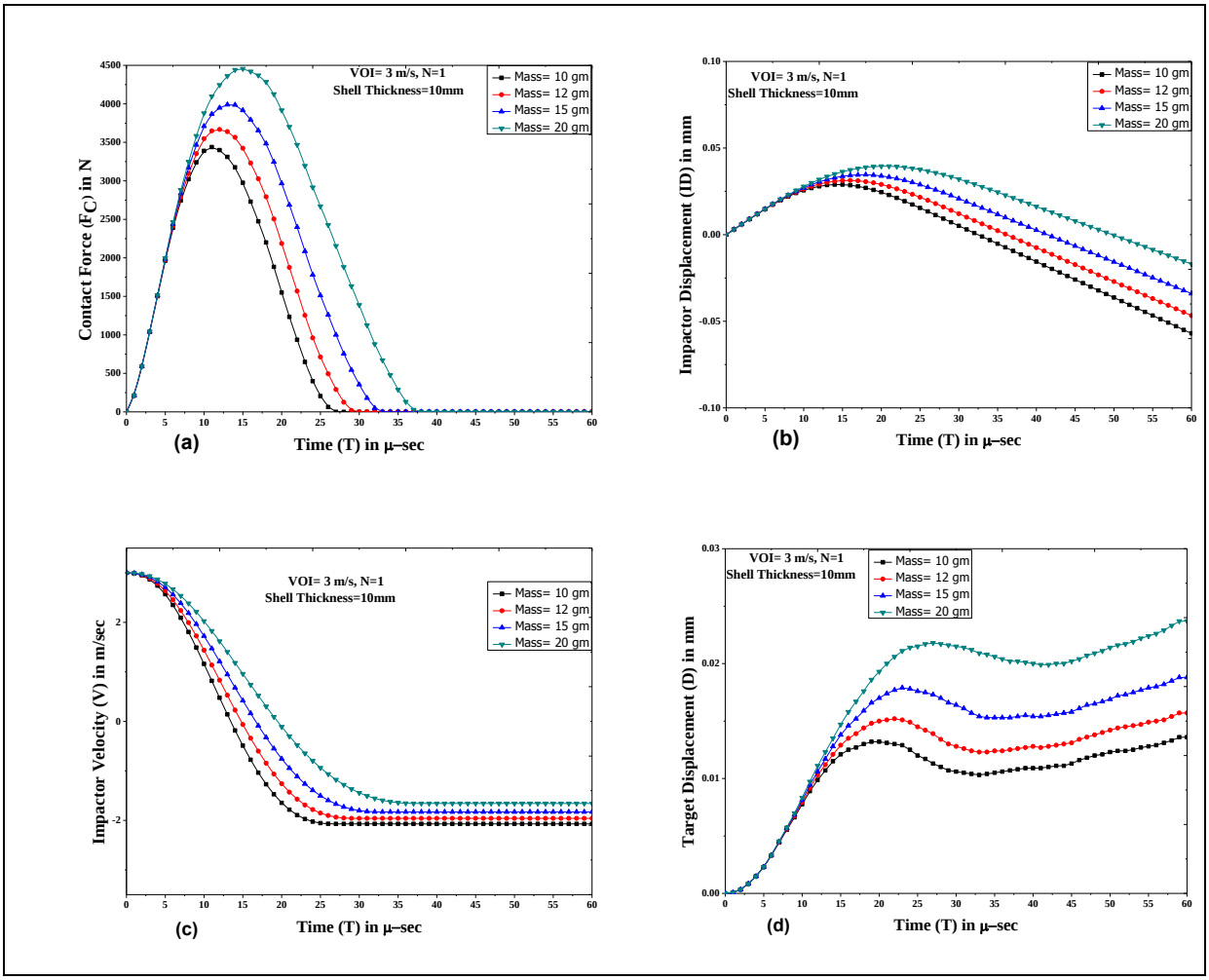

Figure. 4.7 (a) Contact Force, (b) Impactor displacement, (c) Impactor velocity, (d) Target displacement for *N*=1 with respect to time for SS-Si_3N_4 FG conical shell impacted at the center of top surface. Length=0.8m, width=0.143m, thickness=0.01 m, time step=1.0 μ-sec, VOI= 3m/s

4.5.1.3 EFFECT OF LOCATION OF IMPACT

The point hitting by the spherical impactor on the target surface of functionally graded conical shell plays significant role on the impact characteristics. The different locations on the conical shell on which the impactor is hitting are shown in Figure 4.8. diagonal direction as Point 1-2-3-C-4-5-6-7, in axial direction as Point 8-9-10-C-11-12-13-14 and transverse direction as Point 15-16-17-18-C-19-20-21-22 . The point C represents the centre of the conical shell along the axial and transverse direction. The variation of location of hitting point is observed to affect in the variation of effective elastic stiffness. The effective elastic stiffness is higher near the fixed end of the blade while the effective elastic stiffness reduces towards the free end of the blade. Due to this reason the peak value of the contact force is found to be maximum at point 8 and minimum at point 14 along axial (span wise) direction as shown in Figure 4.9. Due the same reason the maximum value of contact force obtained at point 1 and the lowest value of contact force is observed at point 7 as furnished in Figure 4.9

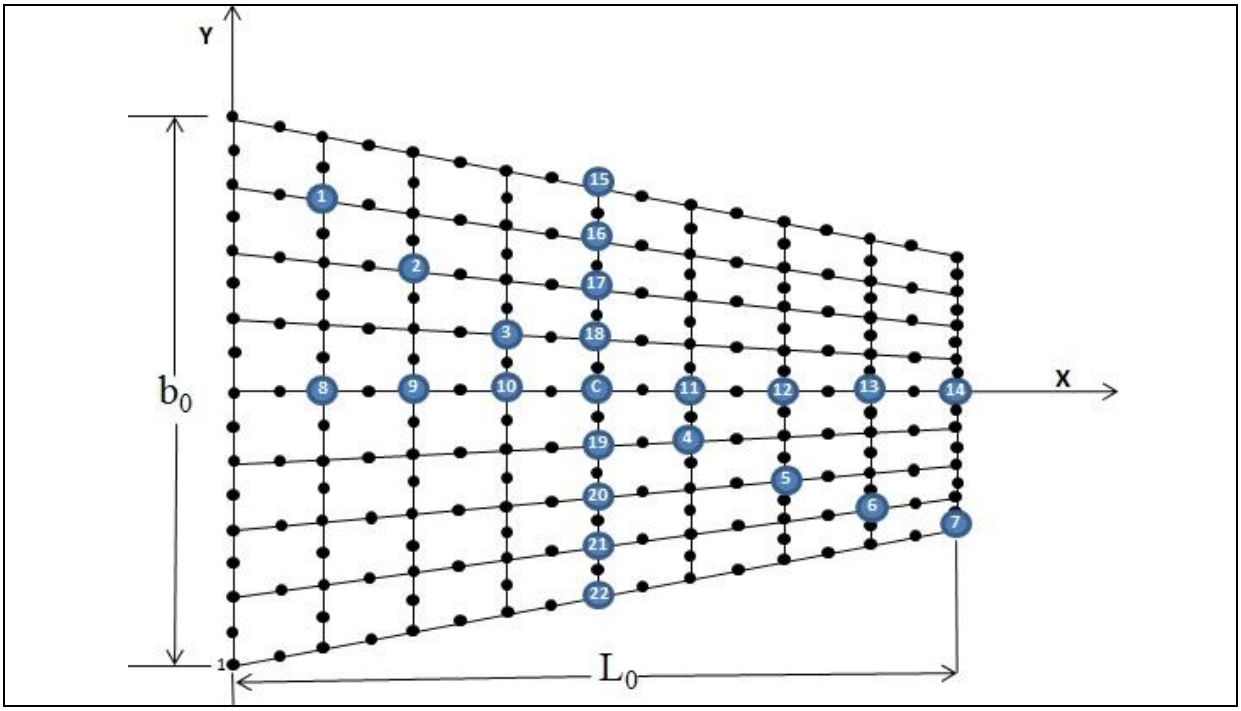

Figure. 4.8 Planner view of location of impact on top surface of the conical shell in axial, transverse and diagonal direction

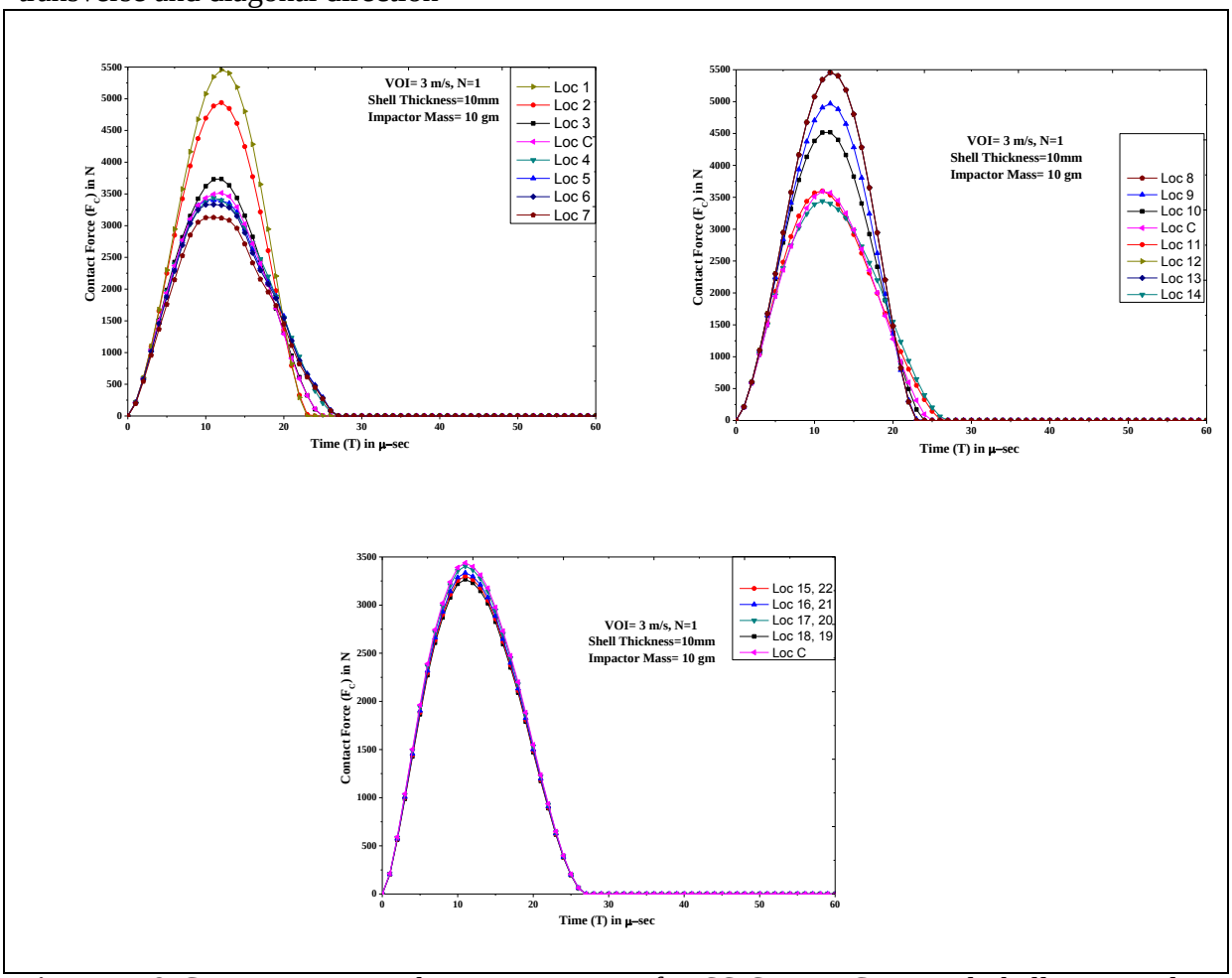

Figure. 4.9 Contact Force with respect to time for SS-Si_3N_4 FG conical shell impacted at different location on the top of the conical shell surface. Length=0.8m, width=0.143m, N=1, VOI=3m/s, time step=1.0 μ-sec, mass of the impactor (M_0)=0.01 Kg.

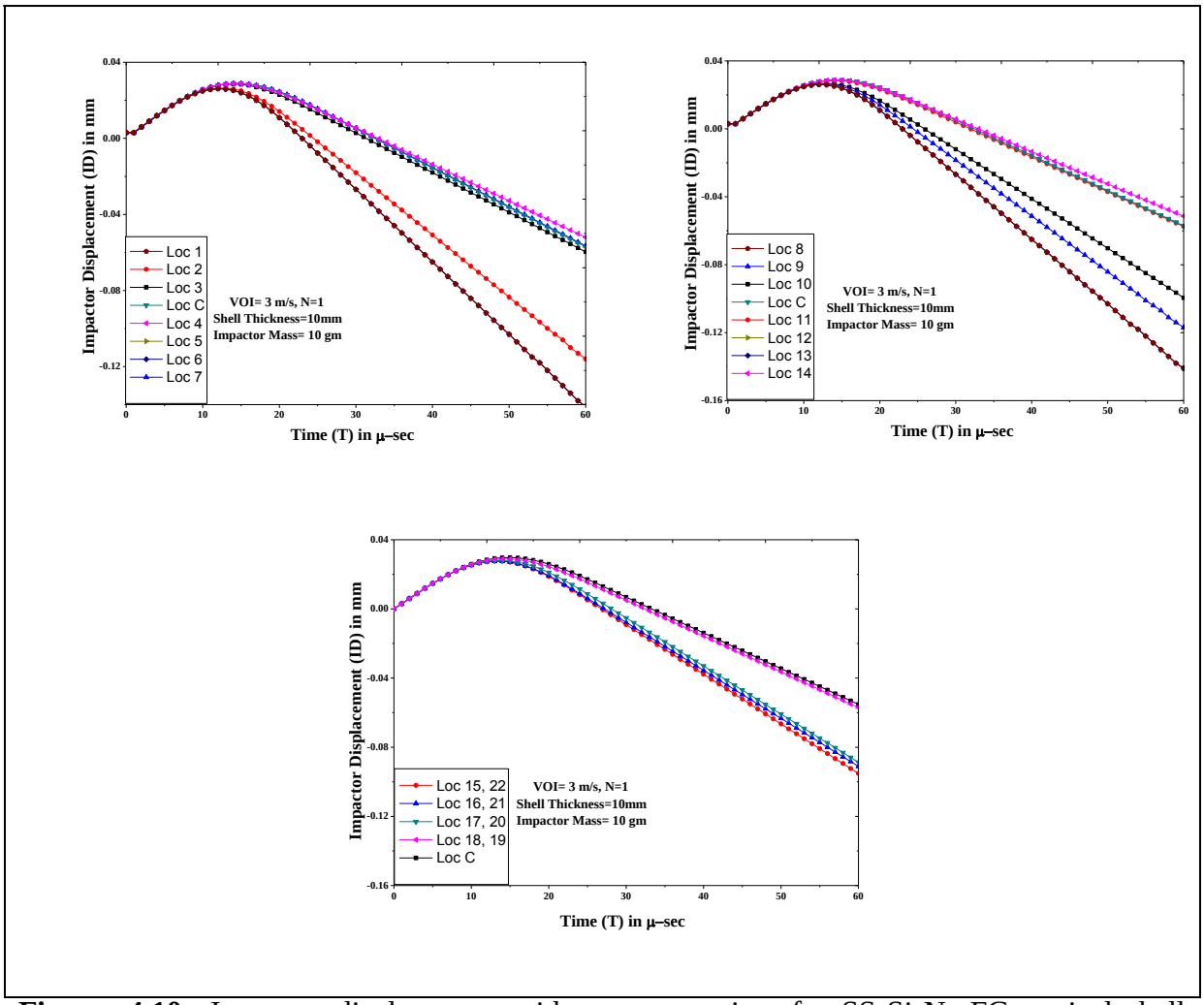

Figure. 4.10 Impactor displacement with respect to time for SS-Si_3N_4 FG conical shell impacted at different location on the top of the conical shell surface. Length=0.8m, width=0.143m, N=1, VOI=3m/s, time step=1.0 μ-sec, mass of the impactor (M_0)=0.01 Kg.

Hence, in case of span wise direction (point 8 to point 14), the peak value of contact force is found to decrease as the point of hitting moves from bottom (fixed end) to the tip (free end) of the functionally graded conical shells blade wherein the time duration of contact is found to increase from bottom of the blade to tip of the blade. In the similar way along the diagonal direction, maximum value of contact force is found at fixed diagonal end (i.e, at point 1) and reduces as it moves diagonally from fixed end to free end (i.e, at point 7) while the total contact duration is found to increase gradually from point 1 to point 7, which means the time duration of the contact is found to reduce from free end to fixed end. The contact force along the transverse direction is also shown in figure 4.9. The contact force for point 15 and 22 are same in nature as these two points are symmetric from central point. The similar nature is observed for other symmetrical points along the transverse direction i.e. point (15, 22), (16, 21), (17, 20) and (18, 19). The centre point (C) has the minimum contact force and gradually it increases towards the both end along the transverse direction. Figure 4.10 revels the fact

that the impactor bounces back with higher velocity when the impactor hits near the fixed end of the blade compared to the tip of the blade both for axial and diagonal direction while for the transverse direction the impactor bounces back with higher velocity when it hits

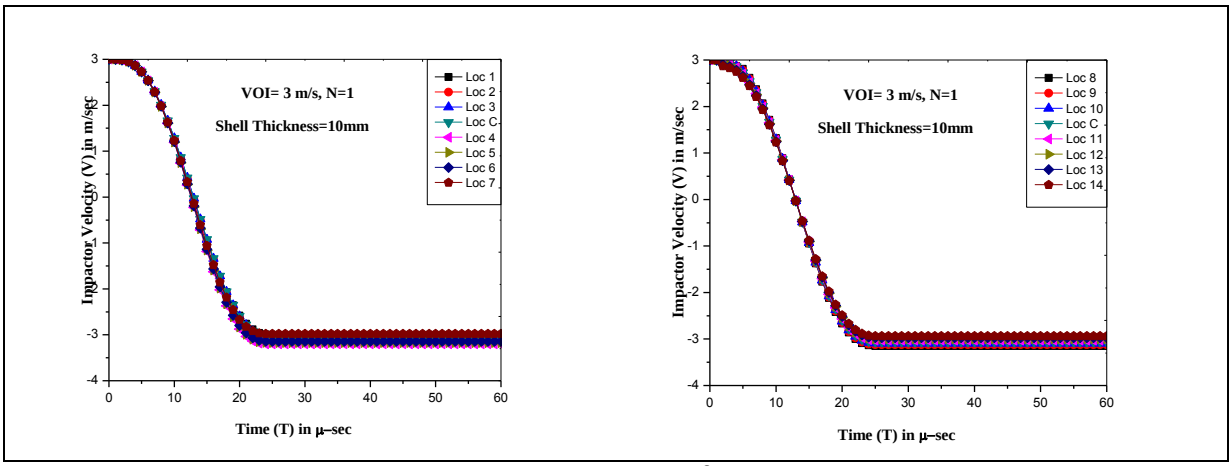

Figure. 4.11 Impactor velocity with respect to time for SS-Si_3N_4 FG conical shell impacted at different axial and diagonal location on the top of the conical shell surface. Length=0.8m, width=0.143m, N=1, VOI=3m/s, time step=1.0 µ-sec, mass of the impactor (M_0)=0.01 Kg.

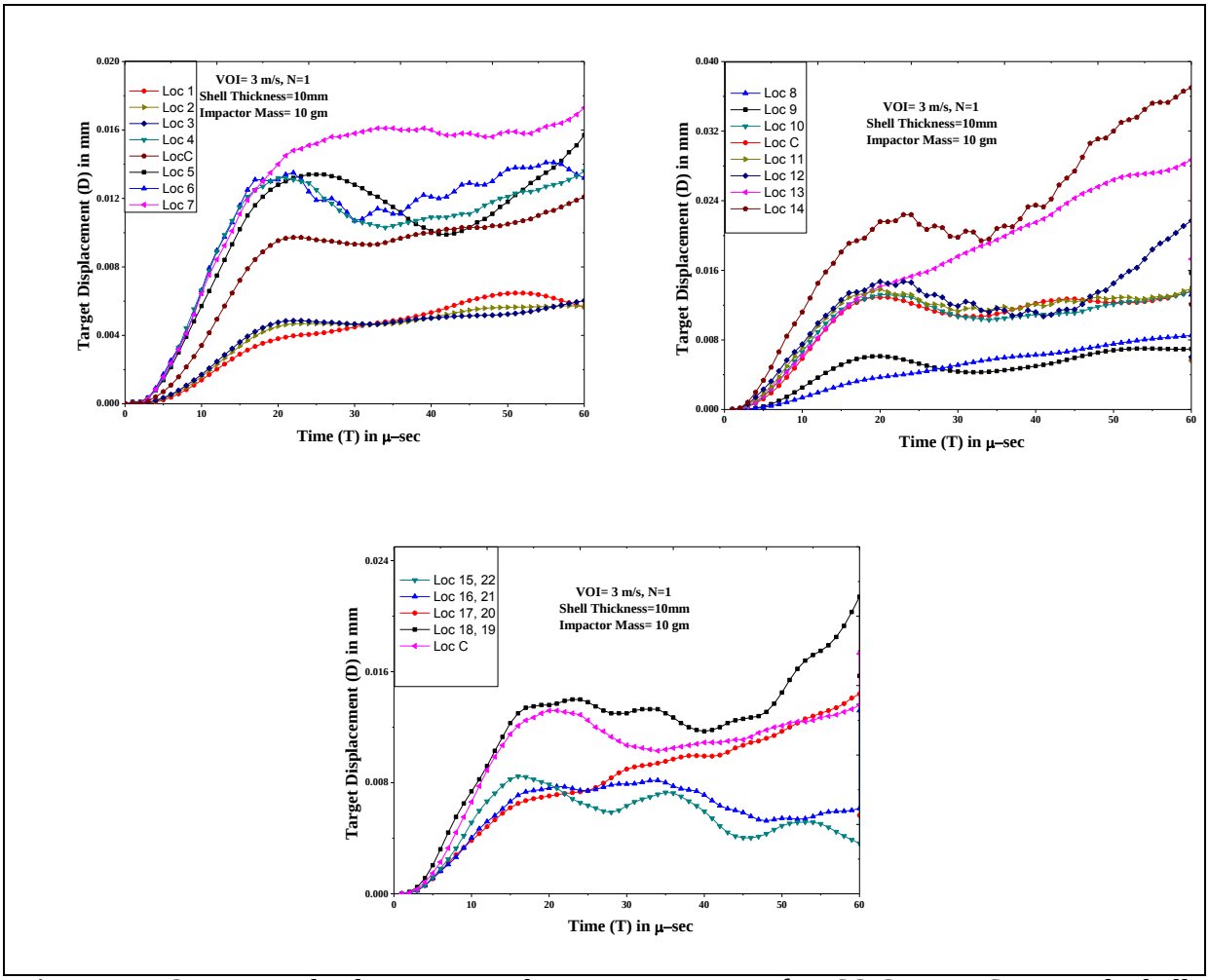

Figure. 4.12 Target displacement with respect to time for SS-Si_3N_4 FG conical shell impacted at different location on the top of the conical shell surface. Length=0.8m, width=0.143m, *N*=1, VOI=3m/s, time step=1.0 µ-sec, mass of the impactor (M_0)=0.01 Kg.

on the centre compared to the side of the blade. Impactor velocity has not much effect on the location of the impact. The nature of the impactor velocity shows is similar trend irrespective of the location of the impact. However it is observed from the figure 4.11 that the fixed end of the blade has slight higher velocity of the impact while returning after hitting the surface compared to the free end of the blade. From the figure 4.12 it can be seen that the shell or target displacement is maximum towards the tip of the blade compared to the fixed end of the blade both for the axial and diagonal direction. Also for the transverse direction the maximum shell displacement is observed towards the side of the blade compared to the centre of the blade. From the above discussion it can be conclude that for low velocity impact of FG conical shell in axial direction could be severe compared to the diagonal or transverse direction as location 14 has higher contact force compared to location 7. In other words, the FG conical shell subjected to low velocity impact which is safe in axial direction, subsequently will also be safe in design along the diagonal or transverse direction.

4.5.1.4 EFFECT OF THICKNESS OF THE CONICAL SHELL

The effect of thickness of the conical shell on the impact performance for power law index N=1 are furnished in Figure 4.13 (a-d). The peak value of contact force is found to increase with increase of conical shell thickness. It is also observed from figure 4.13 (a) that the contact duration reduces with the increase shell thickness. The impactor's displacement curve of figure 4.13 (b) is observed to lower during loading and after reaching the peak value, it is found to decrease with a higher slope for higher thickness of the shell. From Figure 4.13 (c) it is to be noted that the higher impactor's displacement is observed after bouncing from the shell. This indicates that the striker bounces back from the target surface with higher velocity for the thicker shell compared to thinner shell. The contact duration has inverse relationship with the shell thickness for same velocity of impactor while the time at which peak value of contact force is found to be unaltered with shell thickness. The unloading time for thicker shell is found to be less than that of thicker shell as the contact duration is lower for the former case. The slope of time history curves of velocity of impactor is found to be maximum value for highest thickness of the shell and minimum for the lowest thickness of the shell. It is also to be noted that the velocity of the impactor comes down to zero value at a faster rate for thicker shell and subsequently it falls down to maximum negative value while there is no contact force observed during that period. As the shell becomes thick the elastic stiffness of the shell becomes higher, hence the target/shell displacement is higher for the thinner shell compared to the thicker shell as depicted in figure 4.13 (d).

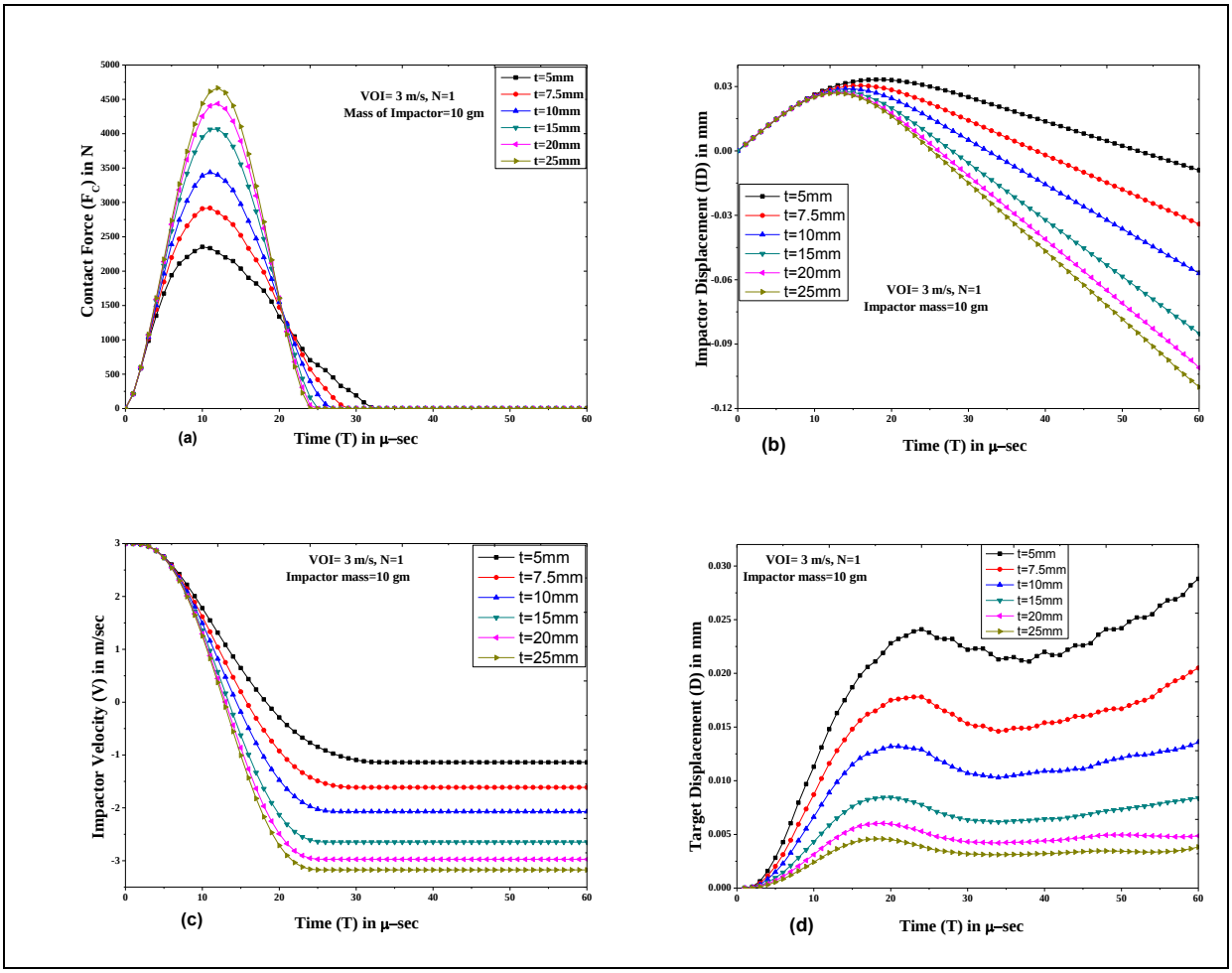

Figure. 4.13 (a) Contact Force, (b) Impactor displacement, (c) Impactor velocity, (d) Target displacement for *N*=1 with respect to time for SS-Si3N4 FG conical shell impacted at the center of top surface. Length=0.8m, width=0.143m, VOI=3m/s, time step=1.0 μ-sec, mass of the impactor (M_0)=0.01 Kg.

4.5.1.5 EFFECT OF TWIST ANGLE

For a particular value of material property graded index, the peak value of contact force is found to enhance slightly as the twist angle increases. The trend of contact force histories for different VOI with different twist angles has been furnished in Figure 4.14 (a), 4.14 (b), 4.14 (c) and 4.14 (d) for the contact force, impactor displacement, target displacement and impactor velocity histories, respectively. The increasing trend of contact force histories observed due to the fact that the coupling effect at higher twist angle enhances the stiffness which helps to raise the maximum contact force. The contact duration for twisted cases reduces marginally than that of untwisted cases irrespective of material property graded index and mass of the impactor. The time of attaining the peak value of contact force is found to be unaltered with the rise twist angle. Hence, it can be inferred that the effect of twist angle has significant impact on contact force and has marginal impact on contact duration but has no impact on time of attaining the peak value. The unloading time for untwisted cases is

observed to be higher than that of twisted cases while the contact force is found to increase minutely as the twist angle increases. The slope of time history curves of velocity of impactor is found to be maximum value for highest angle of twist and minimum for the untwisted shell. It is also to be noted that the velocity of the impactor comes down to zero value at a faster rate for higher angle of twist. Also it can be observed that for the higher twist angle the impactor bounces back from target after hitting the target surface with higher velocity following the stiffer slope. From Figure 4.14 (d) it can be observed that the target or shell displacement for the untwisted case is found to be less compared to the twisted case and the shell displacement value rises with the increase of angle of twist. This trend is observed due to the fact that, as the angle of twist increases the geometric stiffness matrix rises which results the shell to become more stiff and it gives more resistance to the shell displacement for higher twist angle compared to the lower twist angle or untwisted case.

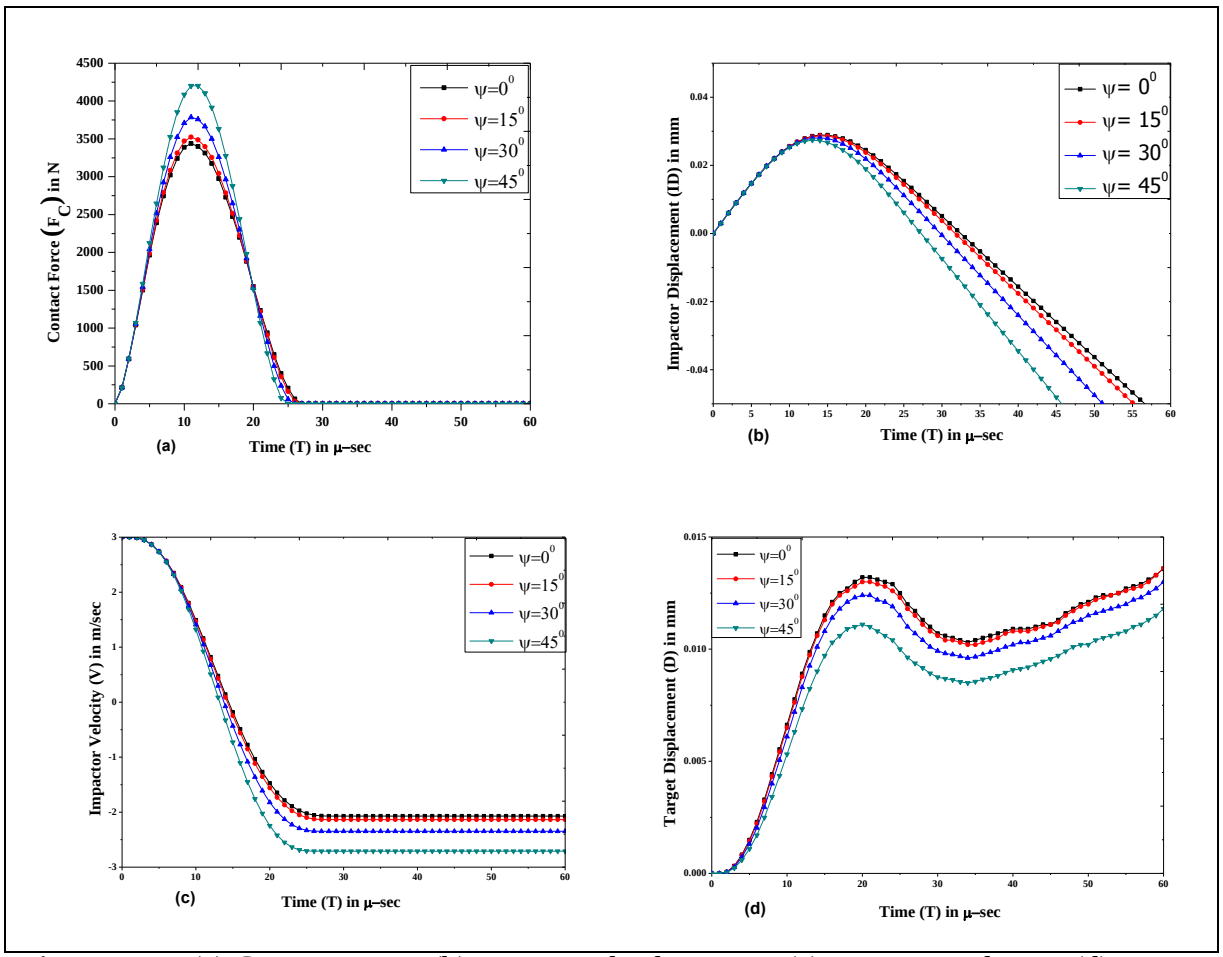

Figure. 4.14 (a) Contact Force, (b) Impactor displacement, (c) Impactor velocity, (d) Target displacement for untwisted (Ψ=0°) and twisted (Ψ=15°,30°and 45°) conical shell with respect to time for SS-Si_3N_4 FG conical shell impacted normally at the center of top surface. Length=0.8m, width=0.143m, thickness=0.01 m, time step=1.0 μ-sec, N=5, VOI=3m/s, mass of the impactor (M_0)=0.01 Kg.

4.5.1.6 EFFECT OF MATERIAL PROPERTY GRADED INDEX (*N*)

The variation of properties profile is studied to enumerate its effect on impact parameters. It is observed that the impact parameters like contact force, target (shell) displacement, impactor's displacement, velocity of the impactor with respect to time have notable change with the variation of material property graded index of functionally graded shallow conical shells irrespective of twist angle. For $N<1$ (i.e ceramic rich FGM structure) the contact force is higher compared to $N>1$ (for metal rich FGM structure) and for $N=1$ (i.e equal volume fraction of ceramic and metal mixture) the contact force lies in between the above two cases. This can be attributed to the fact that ceramic material has higher values of Youngs's modulus (E) than that of metal hence the total contact stiffness of the FGM shell for lower values of N is higher compared to the higher values of N. Therefore in general it can be conclude that the contact force decreases with increase of the material property graded index and contact duration of the loading-unloading cycle increases with N as shown in figure 4.15

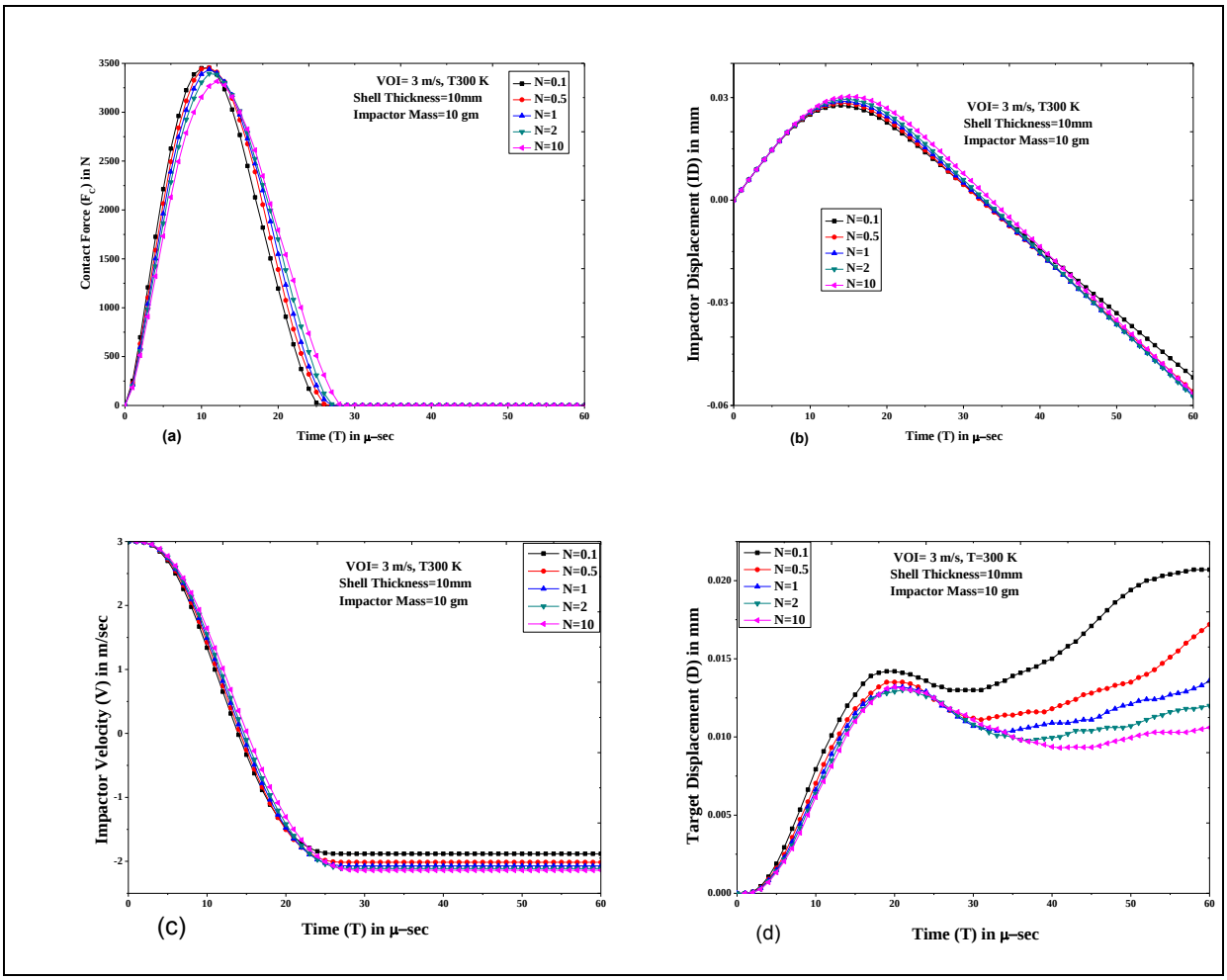

Figure. 4.15 (a) Contact Force, (b) Impactor displacement, (c) Impactor velocity, (d) Target displacement with respect to time for SS-Si_3N_4 FG conical shell impacted at the center of top surface for different values of N. Length=0.8m, width=0.143m, thickness=10mm, VOI=3m/s, time step=1.0 μ-sec, mass of the impactor (M_0)=0.01 Kg.

(a). Interestingly, it is to be noted that the contact force histories are identical in nature for the five different power law index cases. When the material property graded index increases, the shell displacement reduces (shown in figure 4.15 (d)) which is expected since the functionally graded conical shell becomes harder as the material property graded index increases up. The indentation parameter will also show the similar trend as that of shell displacement with the variation of *N*. However this observation is specific to the combination of FGM constituent materials where the ceramic constituent are harder than the metal constituent. But for the other combination where the metal constituent is harder than the corresponding ceramic constituent this trend will be reverse (i.e contact force and shell displacement will be higher for higher values of *N*).

4.5.2 MULTIPLE IMPACTS

The FGM conical shell are impacted at location A (Node 61) and location B (Node 165) simultaneously (as shown in figure 4.16) by a different spherical impactor of mass 10 gm, 15gm and 20gm with different initial velocities of 1m/s, 3m/s and 5m/s. The various power law exponents (*N*=0.1, 1 and 10) are considered for the analysis to see the effect of constituent volume fraction on the impact response of the shallow conical shell. The impact parameters are varied to see the effect on the multiple impact response and these are described below.

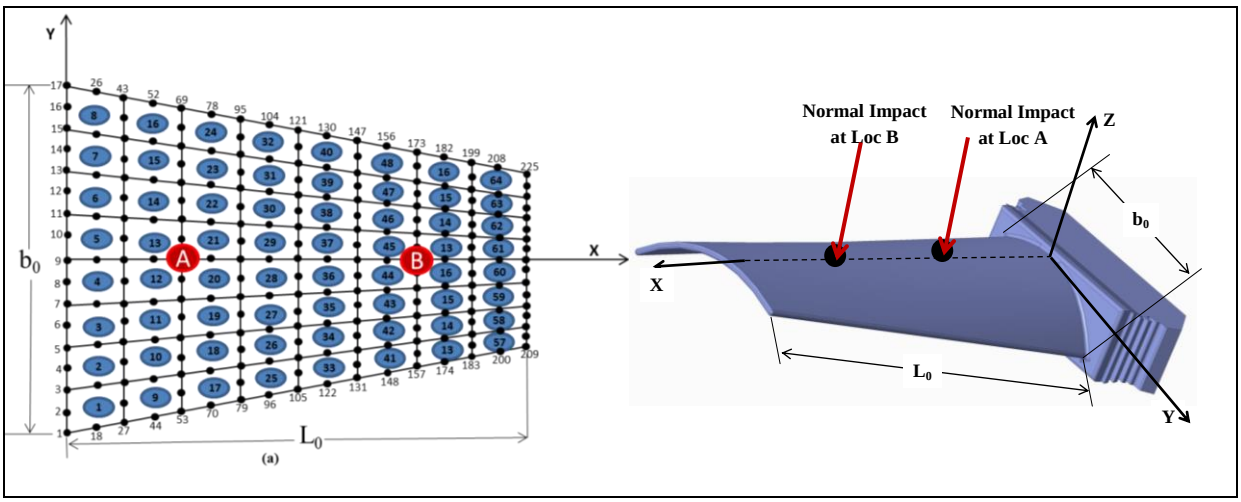

Figure. 4.16 Location (A and B) and node number (61 and 165) for the simultaneous multiple impact problem

4.5.2.1 VARIATION OF THE INITIAL VELOCITY OF THE IMPACTOR

Design of an impact alleviating system is vital for the turbomachinery blade to avoid catastrophic failure during operation. The initial velocity of the impactor is a significant

factor affecting the various impact response. The effect of initial velocity of impactor (VOI) for power law index N=1 is provided in Figure 4.17. Irrespective of the power law index and twist angle the peak value of contact force is found to increase with increase of initial velocity of impactor for both the location A and location B. The contact force (Figure 4.17.a) for location A is always higher than the corresponding location B however the contact duration for location A is slightly shorter than that of corresponding location B. It is also observed that the contact duration increases with the decrease of VOI. The impactor's displacement value is observed to increase during loading and after attaining a peak value, it is found to decrease with a slope which is proportional to VOI. From Figure 4.17 (b) it is also noted that the negative value of impactor's displacement shows the situation when the impactor bounces back from target after hitting the target surface. The shell displacement (Figure 4.17.d) is proportional to the VOI till it reaches to the peak value of the contact force, thereafter the trend becomes constant. Shell displacement shows higher trend for location A

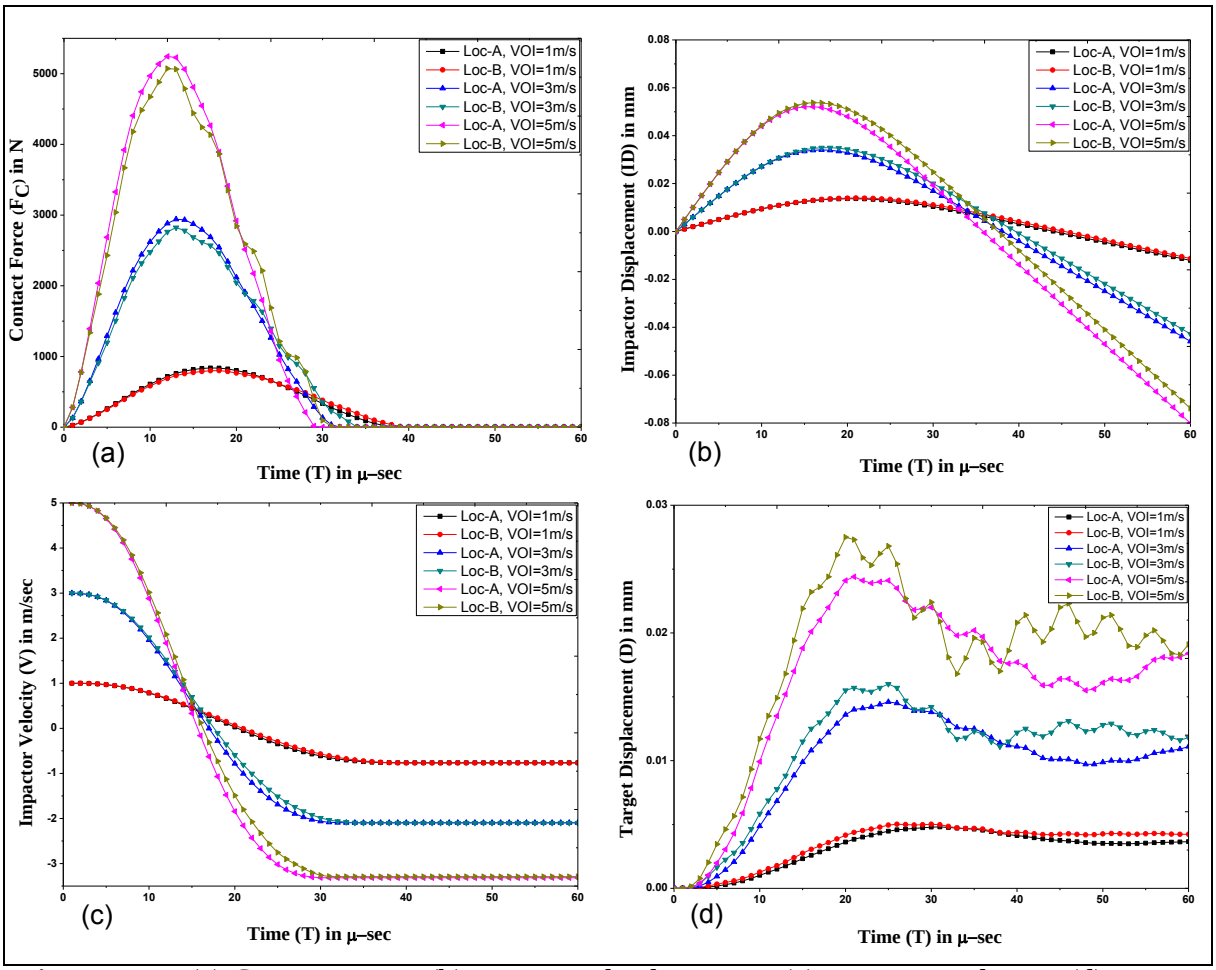

Figure. 4.17 (a) Contact Force, (b) Impactor displacement, (c) Impactor velocity, (d) Target displacement for N=1 with respect to time for SS-Si_3N_4 FG conical shell impacted at the center of top surface. Length=0.8m, width=0.143m, thickness=0.01 m, time step=1.0 μ-sec, mass of the impactor (M_0)=0.01 Kg.

compared to location B for all the cases because the contact force is always higher for the later one. The slope of the impactor velocity (Figure 4.17.c) for location A is stiffer than that of location B for all the cases. The slope of time history curves of velocity of impactor is found to be maximum value for the VOI=5 m/sec, followed by VOI=3 m/sec and VOI=1 m/sec respectively. It is also to be noted that the velocity of the impactor comes down to zero value at the end of contact duration and subsequently it falls down to negative value wherein null value of contact force is observed.

4.5.2.2 EFFECT OF MASS OF THE IMPACTOR

Like initial velocity of the impactor, the mass of the impactor also plays a significant role affecting the impact response and designer must be aware of the effect of impactor mass for the low velocity impact phenomenon. The impact characteristics greatly influenced by the mass of the impactor and it is obvious that the contact force as well as the impactor displacement, shell displacement and indentation will have basic similar nature.

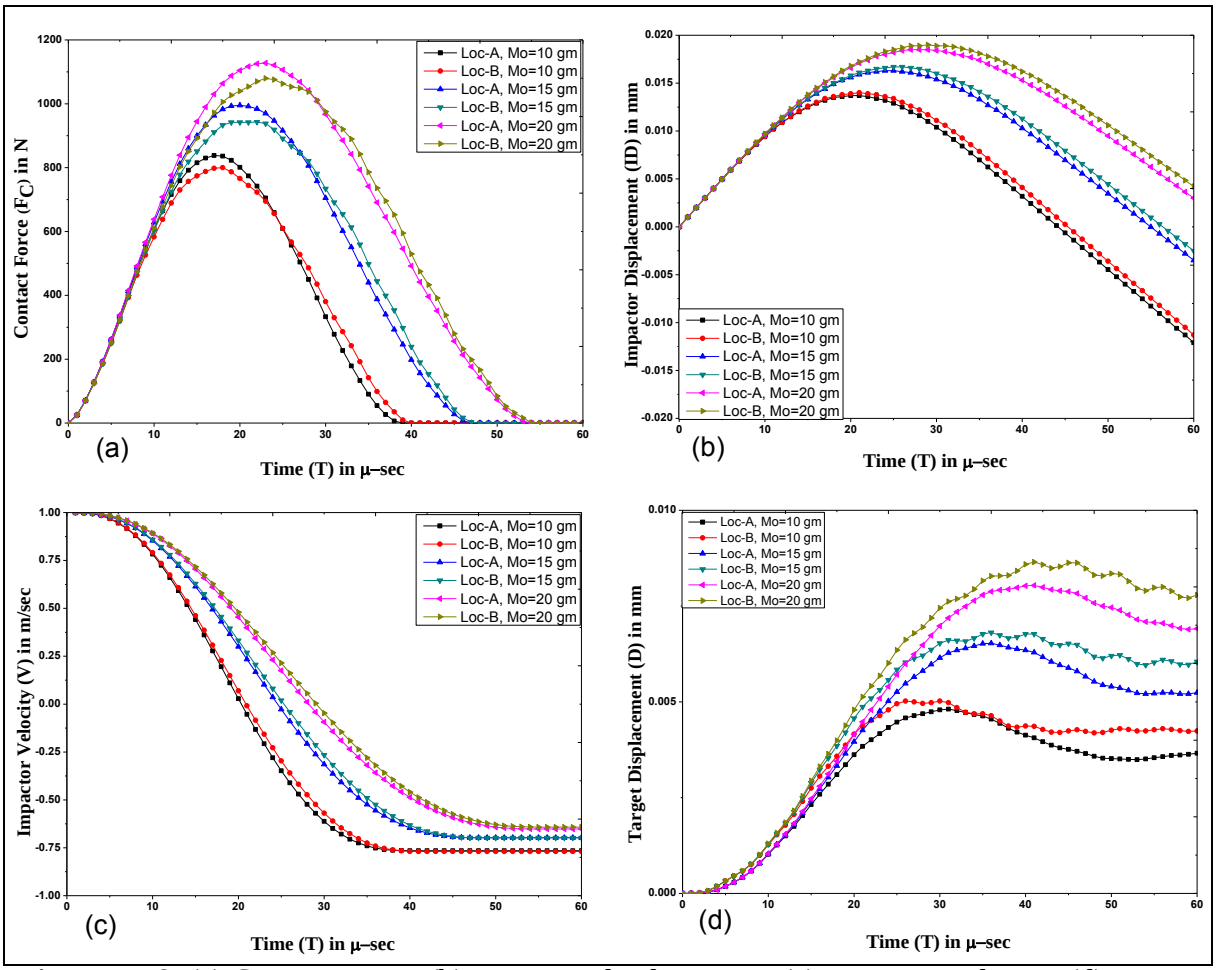

Figure 4.18 (a) Contact Force, (b) Impactor displacement, (c) Impactor velocity, (d) Target displacement for N=1 with respect to time for SS-Si_3N_4 FG conical shell impacted at the center of top surface. Length=0.8m, width=0.143m, thickness=0.01 m, time step=1.0 μ-sec, mass of the impactor (M_0)=0.01 Kg.

Figure. 4.18 (a, b, c, d) illustrates the effect of impactor mass on low velocity multi-impact problem for the different values for sigmoidal power law index N =1. The contact force increases with the increase of mass of the impactor and the time for attaining the peak value of the contact force becomes more with higher mass of the impactor. Target displacement also increases with higher mass of the impactor, but for the location B higher shell displacement is found compared to location A for all the cases. Impactor velocity curve is stiffer for lower mass of the impactor while the location A shows slightly lower trend compared to location B.

4.5.2.3 EFFECT OF TWIST ANGLE

For a particular value of material property graded index, the peak value of contact force is found to enhance slightly as the twist angle increases. The trend of contact force histories for different twist angles with VOI=5 m/s has been furnished in Figure 4.19 (a), 4.19 (b), 4.19 (c), and 4.19 (d) for the impactor displacement, target displacement and impactor velocity histories, respectively. The increasing trend of contact force histories observed due to the fact that the coupling effect at higher twist angle enhances the stiffness which helps to raise the

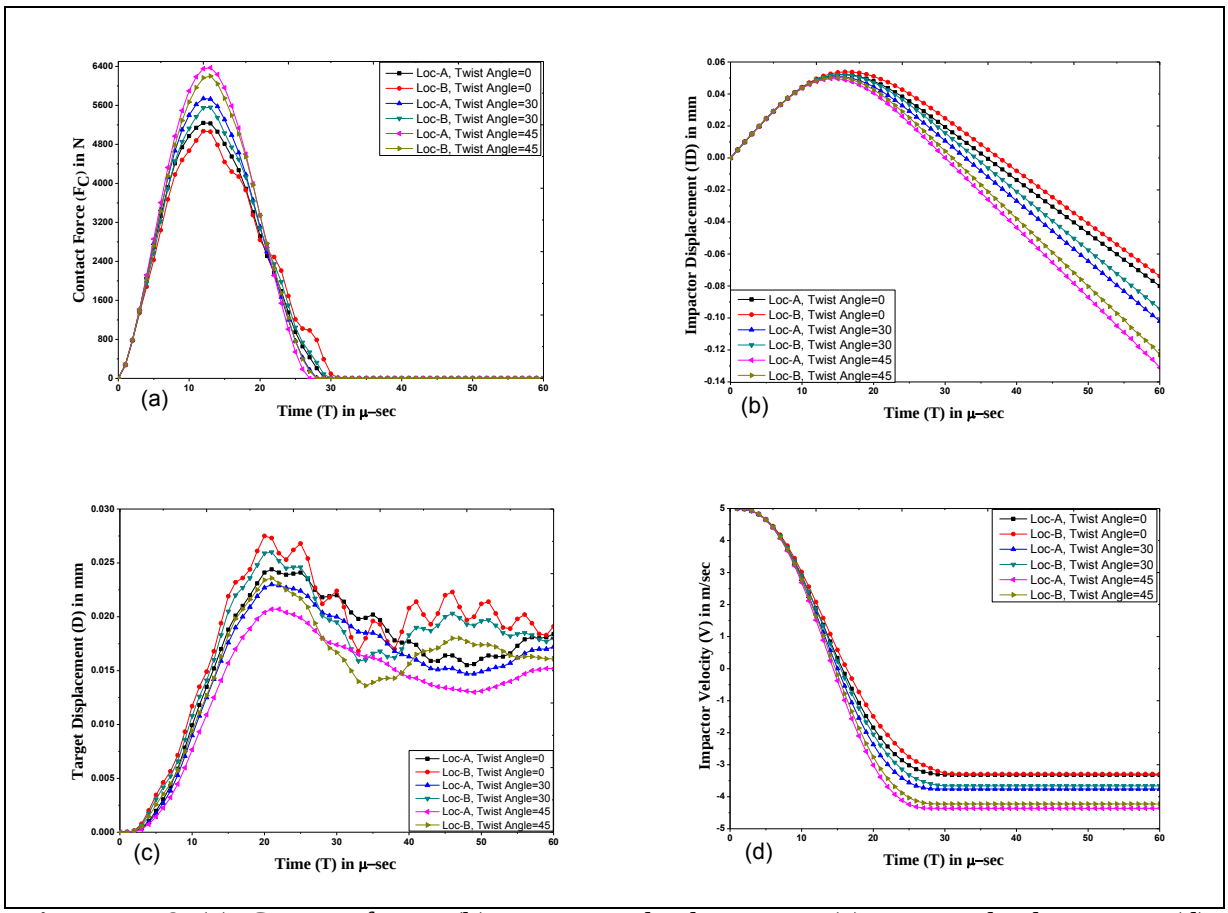

Figure 4.19 (a) Contact force, (b) Impactor displacement, (c) Target displacement, (d) Impactor Velocity histories of SS-Si_3N_4 FGM conical shell for various angle of twist (Ψ), VOI=5, L_0 = 0.8m, b_0 = 0.143m, h = 0.01m, Mass of impactor (M_0) = 10 gm, r_i = 12.7 mm, N=1.

maximum contact force. Also it can be noted from Figure 4.19 (a) that the contact force for location A is always higher compared to corresponding location B. The contact duration for twisted cases reduces marginally than that of untwisted cases irrespective of material property graded index and mass of the impactor. The time at which peak value of contact force occurs is found to be unaltered with the rise in twist angle. Hence, it can be inferred that the effect of twist angle has significant impact on contact force and has marginal impact on contact duration but has no impact on the time of achieving the peak value.

4.5.2.4 EFFECT OF POWER LAW INDEX (*N*)

The variation of the contact force, impactor displacement, target displacement and impactor velocity histories of FGM conical shell for various power law index (*N*) are depicted in the Figure 4.20 (a), 4.20 (b), 4.20 (c), and 4.20 (d) respectively. The contact force increases with the increase of power law index (*N*) but the contact duration reduces. The peak value of the contact force decreases considerably with the increase of *N*. Also it is noted that the

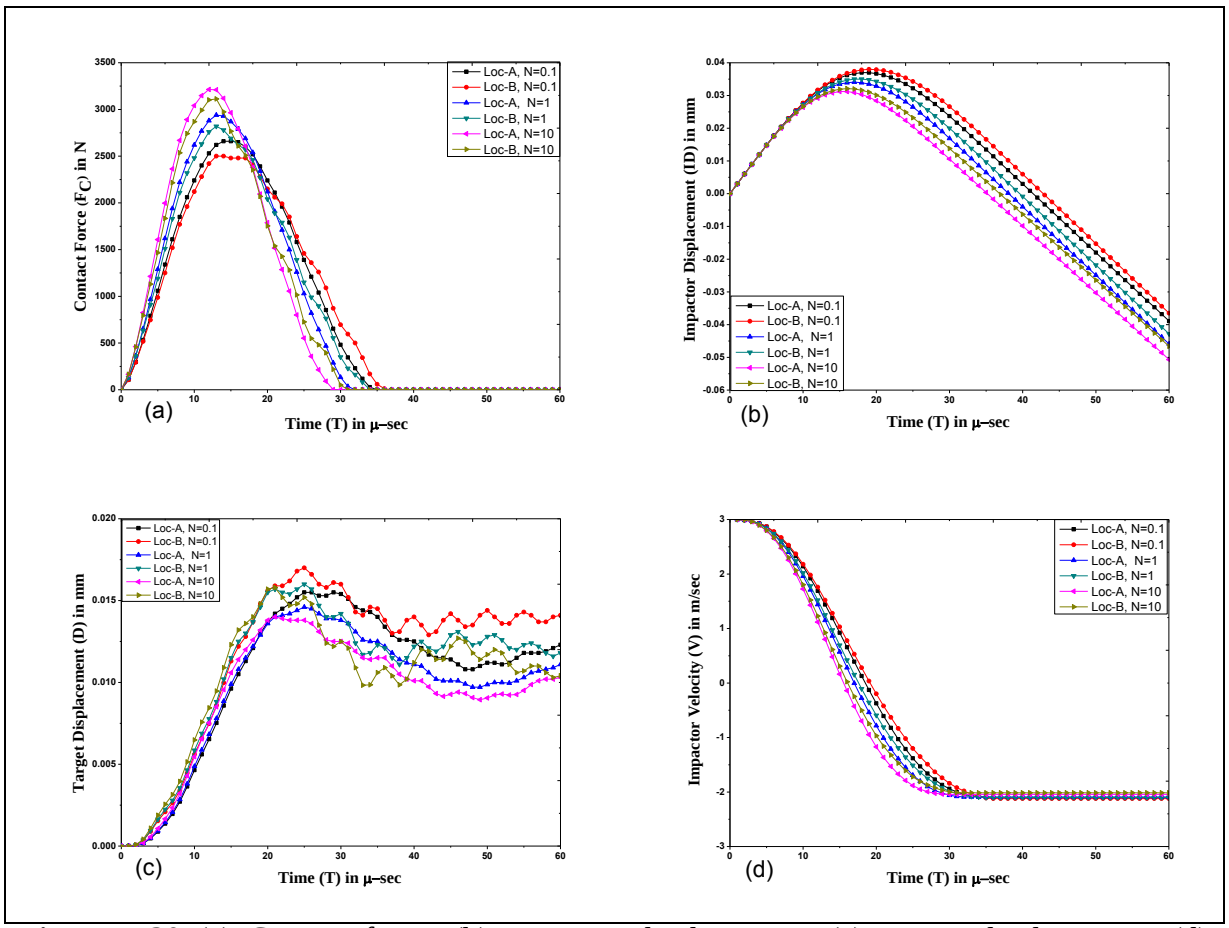

Figure 4.20 (a) Contact force, (b) Impactor displacement, (c) Target displacement, (d) Impactor Velocity histories of SS-Si_3N_4 FGM conical shell for various power law index(*N*), VOI=3, L_0 = 0.8m, b_0 = 0.143m, h = 0.01m, Mass of impactor (M_0) = 10 gm, r_i = 12.7 mm.

corresponding time for attaining peak contact force decreases with *N*. The peak value of the contact force always predicts higher for location A compared to location B for all the cases. Higher impactor displacement is observed for the lower values of *N* and also it can be noted that the location B predicts the higher impactor displacement compared to location A. Impactor velocity curve is almost similar in nature for all the values of *N* but for the higher values of *N* the curve has higher slope which signifies that for higher values of *N* the time taken to bounce back is lower and gradually it increases with the increase of *N*.

4.5.3 TIME DELAYED MULTIPLE IPACT

The FGM conical shell are first impacted at location A (Node 61) and after a time delay second impact is ocuured at location B (Node 165) with different initial velocities of 1m/s, 3m/s and 5m/s. The time delay for second impact at location B are considered 25 μ-sec and 50 μ-sec on the impact response of the shallow conical shell. The impact parameters are varied to see the effect on the multiple impact response and these are descriebed in the following.

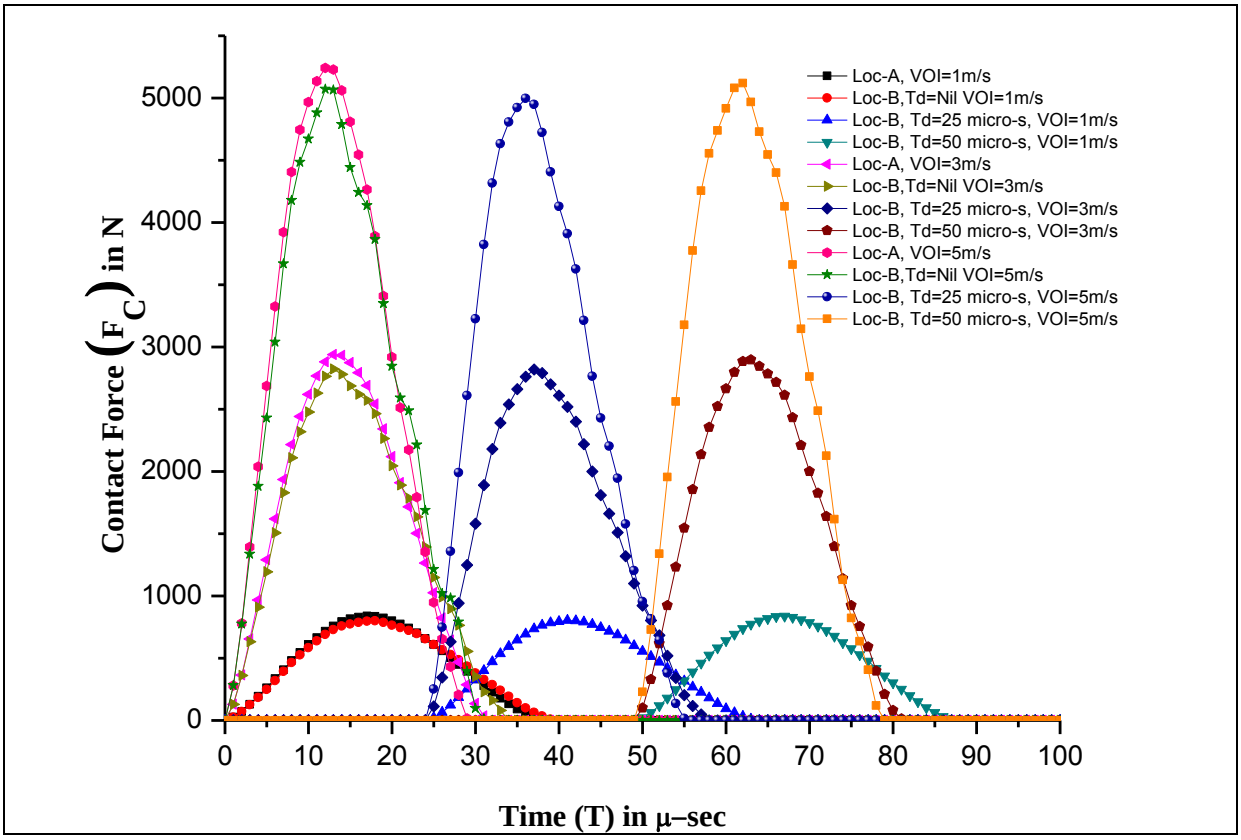

Figure 4.21 Contact force histories of SS-Si_3N_4 FGM conical shell considering time delayed multiple impact problem for various VOI and time delay, L_0 = 0.8m, b_0 = 0.143m, h = 0.01m, Mass of impactor (M_0) = 10 gm, r_i = 12.7 mm.

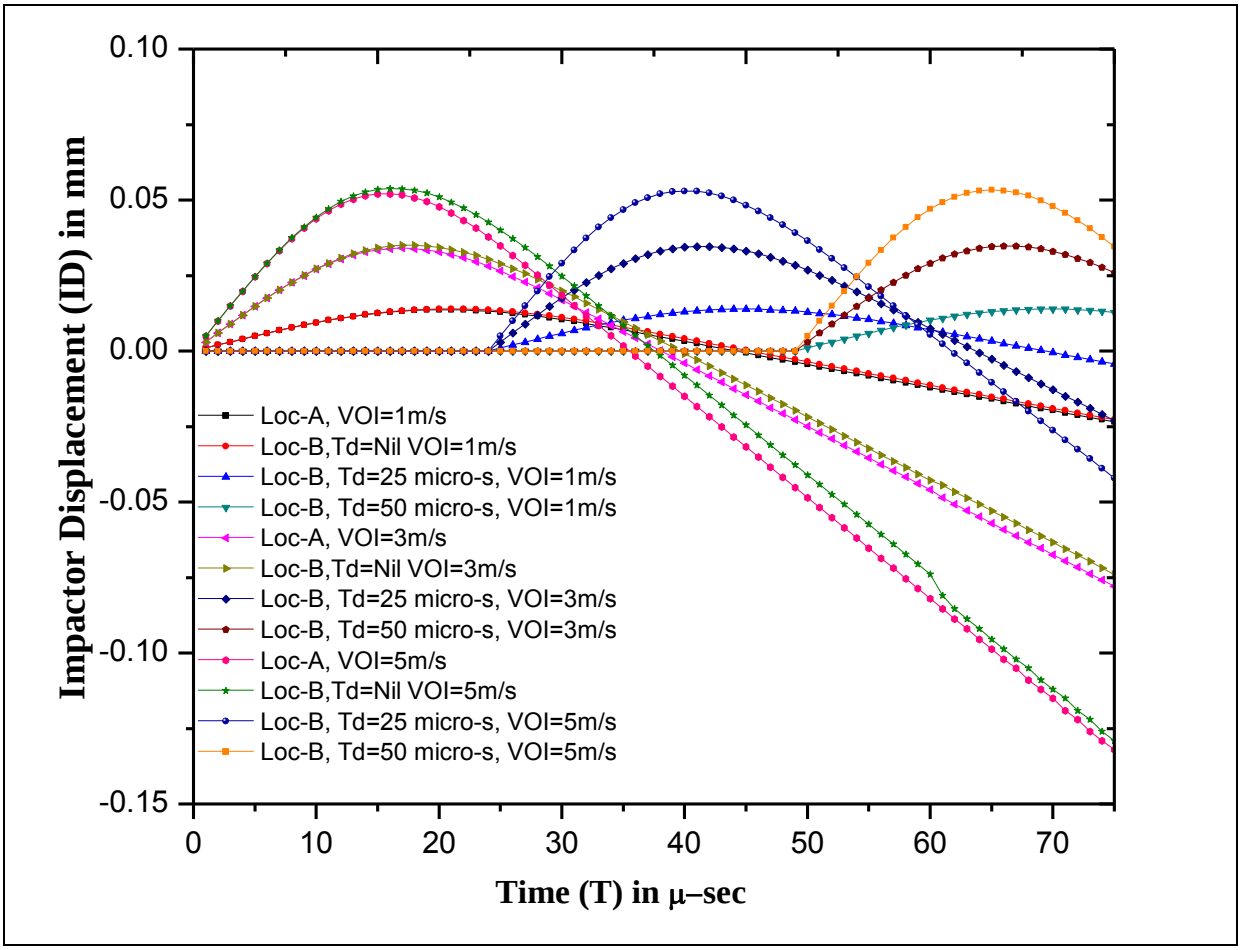

Figure 4.22 Impactor displacement curve of SS-Si_3N_4 FGM conical shell considering time delayed multiple impact problem for various VOI and time delay, L_0 = 0.8m, b_0 = 0.143m, h = 0.01m, Mass of impactor (M_0) = 10 gm, r_i = 12.7 mm.

Figure 4.21 represnts the contact force histories for multiple impact cases considering simultaneous (time delay, Nil) , 25 μ-sec and 50 μ-sec time delay for impact at location B with respect to location A. It is observed that the location B predicts lower contact force than that of location A for simultaneous impact irrespective of VOI. On the other hand, location B predicts further lower contact force with time delay for a given VOI if the contact at location B occurs during the time duration of location A. The contact force at location B regains to the actual values, as per the simultaneous multiple impact cases, if the impact on location B occurs after the time duration of impact of location A. From Figure 4.22 higher impactor displacement is observed at location B than that of location A and with time delay the impactor displacement at location B further increases. Figure 4.23 represents the impactor velocity curve for simultaneous and time delayed impact for different VOI. For simultaneous impact the impactor velocity curve for location B is slightly stiffer than that of location A irrespective of the VOI. For the time delayed impact case the impactor velocity at location B

is observed to be in lower range while returning after hitting the surface than that of simultaneous impact. Figure 4.24 represents the target/shell displacement histories for simultaneous and time delayed impact considering different VOI. For simultaneous impact the maximum value of the target/shell displacement is observed at a time when the contact force achieve its peak value. For a given VOI, the maximum value of the target/shell displacement is observed at location B than that of location A. For the time delayed impact case the target/shell displacement at location B is observed to be in lower range compared to simultaneous impact. As the time delay increases target/shell displacement at location B reduces further.

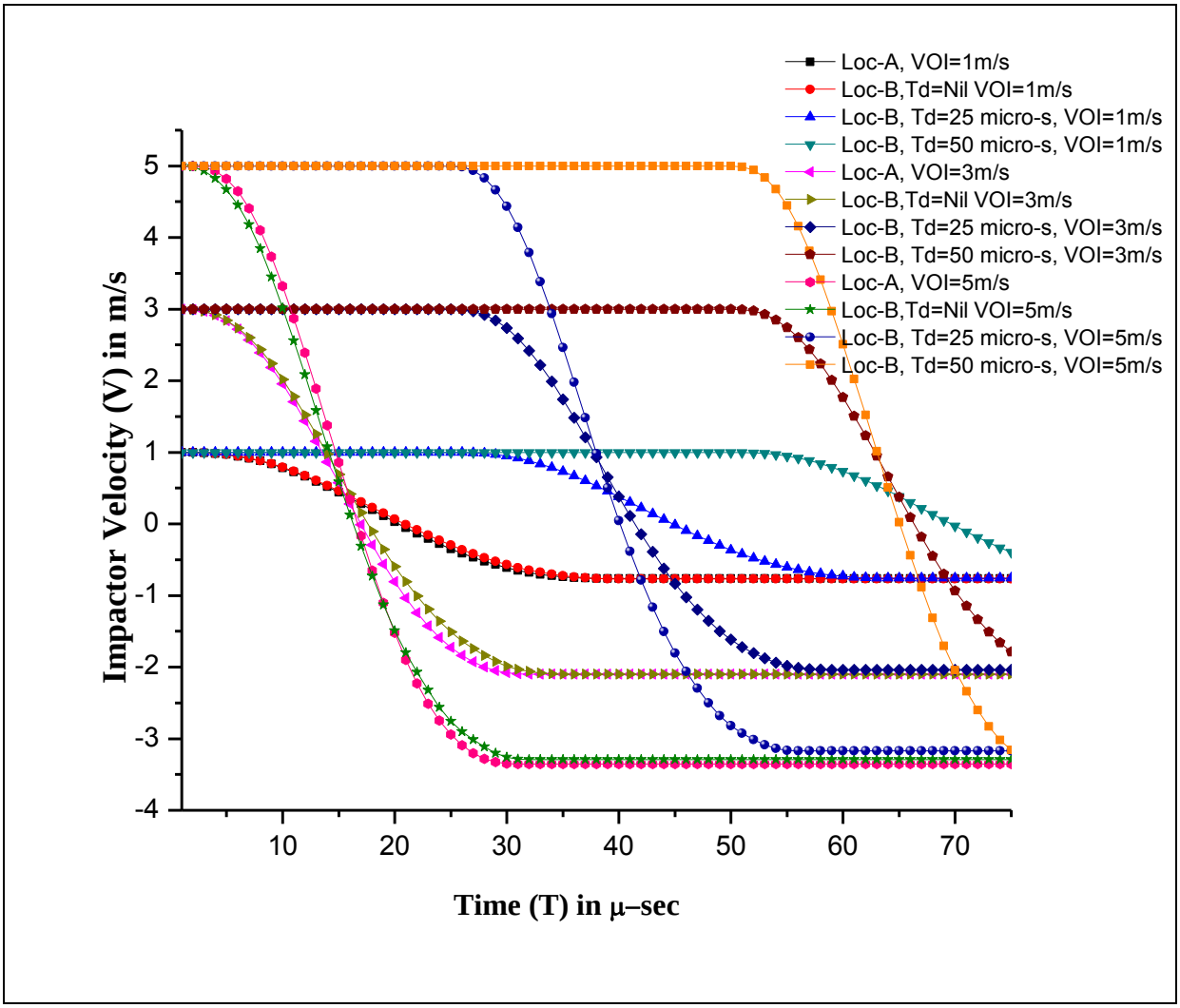

Figure 4.23 Impactor velocity curve of SS-Si_3N_4 FGM conical shell considering time delayed multiple impact problem for various VOI and time delay, L_0 = 0.8m, b_0 = 0.143m, h = 0.01m, Mass of impactor (M_0) = 10 gm, r_i = 12.7 mm.

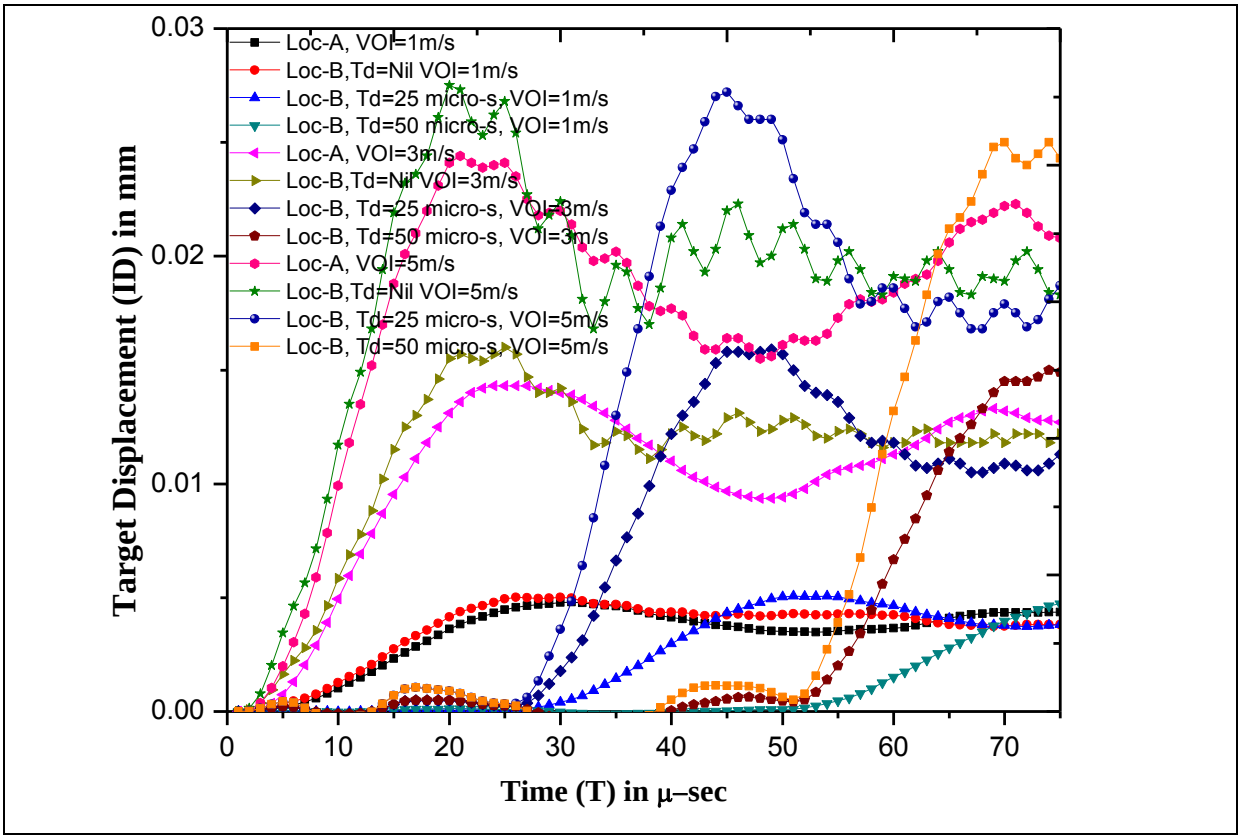

Figure 4.24 Shell displacement histories of SS-Si_3N_4 FGM conical shell considering time delayed multiple impact problem for various VOI and time delay, L_0 = 0.8m, b_0 = 0.143m, h = 0.01m, Mass of impactor (M_0) = 10 gm, r_i = 12.7 mm.

4.5.4 IMPACT PERFORMANCES CONSIDERING POROSITY

Transient dynamic analysis for single and multiple impact problems for SS-Si_3N_4 functionally graded shallow conical shells are carried out considering different VOI, mass of the impactor, different porosity factor for twisted as well as untwisted shell. Porosity factor 0.1 and 0.2 are considered for the even porous (α_{ep}) and uneven porous (α_{up}) FGM conical shells subjected to low velocity impact. Porosity factor greater than 0.2 is not considered as beyond that factor the FGM shell structure will loose its structural integrity to take the desired load for intendent application. The different spherical impactor of mass 10gm and 20gm with different porosity factors are considered.

4.5.4.1 EFFECT OF POROSITY FOR SINGLE IMPACT

Figure 4.25 depicts the impact response histories for perfet (porosity free) and porous (even and uneven) for different VOI. From figure 4.25 (a), it can be noted that even porous FGM shell predicts lower contact force than that of corresponding uneven porous FGM shell

for a given VOI. Maximum value of the contact force is found for perfect (porosity free) FGM shell while the peak value of the contact force decreases with the increase of the porosity factor. Uneven porous FGM shell predicts higher contact force than that of even porous FGM shell for a given porosity factor. This may be attributed to the fact that with the increase of porosity factor the stiffness of the shell material decreases, hence it predicts the lower contact force. The time at which peak value of contact force is obtained and the total contact duration is found to be unaltered with the increase of the porosity factor. From Figure 4.25 (b) it is to be noted that the negative value of impactor's displacement indicates the situation when the impactor bounces back from target after hitting the target surface. The contact duration has inverse relationship with initial velocity of impactor while the time at which peak value of contact force is achieved, is found to reduce with the increase of initial velocity of impactor. The slope of time history curves for velocity of impactor (from Figure 4.25.c) is found to be maximum value for VOI=5 m/sec and the slope decreases with lower

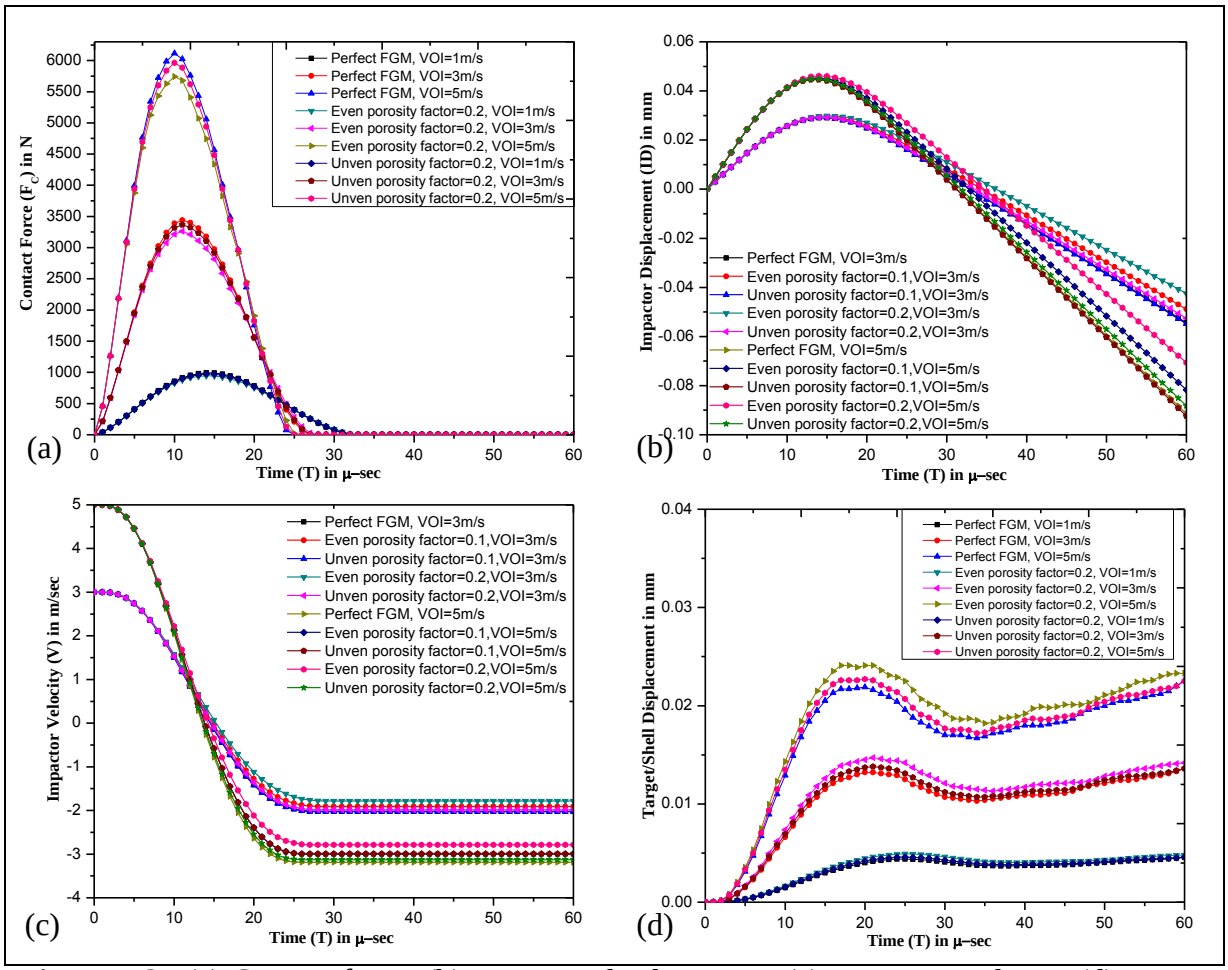

Figure 4.25 (a) Contact force, (b) Impactor displacement, (c) Impactor Velocity (d) Target displacement, histories of SS-Si_3N_4 porous FGM conical shell for various power law index(N), VOI=3, L_0 = 0.8m, b_0 = 0.143m, h = 0.01m, Mass of impactor (M_0) = 10 gm, r_i = 12.7 mm.

values of VOI. It is also to be noted that the velocity of the impactor comes down to zero value at the end of contact duration and subsequently it falls down to negative value wherein null value of contact force is observed. Figure 4.25 (d) shows the increasing trends of shell displacement with time. It can also be noted that the maximum shell displacement is found for even porous FGM shell with porosity factor 0.2 ($\alpha_{ep} = 0.2$). Shell displacement is lowest for perfect FGM shell, maximum for even porous ($\alpha_{ep} = 0.2$) FGM shell while the uneven porous ($\alpha_{up} = 0.2$) FGM shell predicts the intermediate shell displacements.

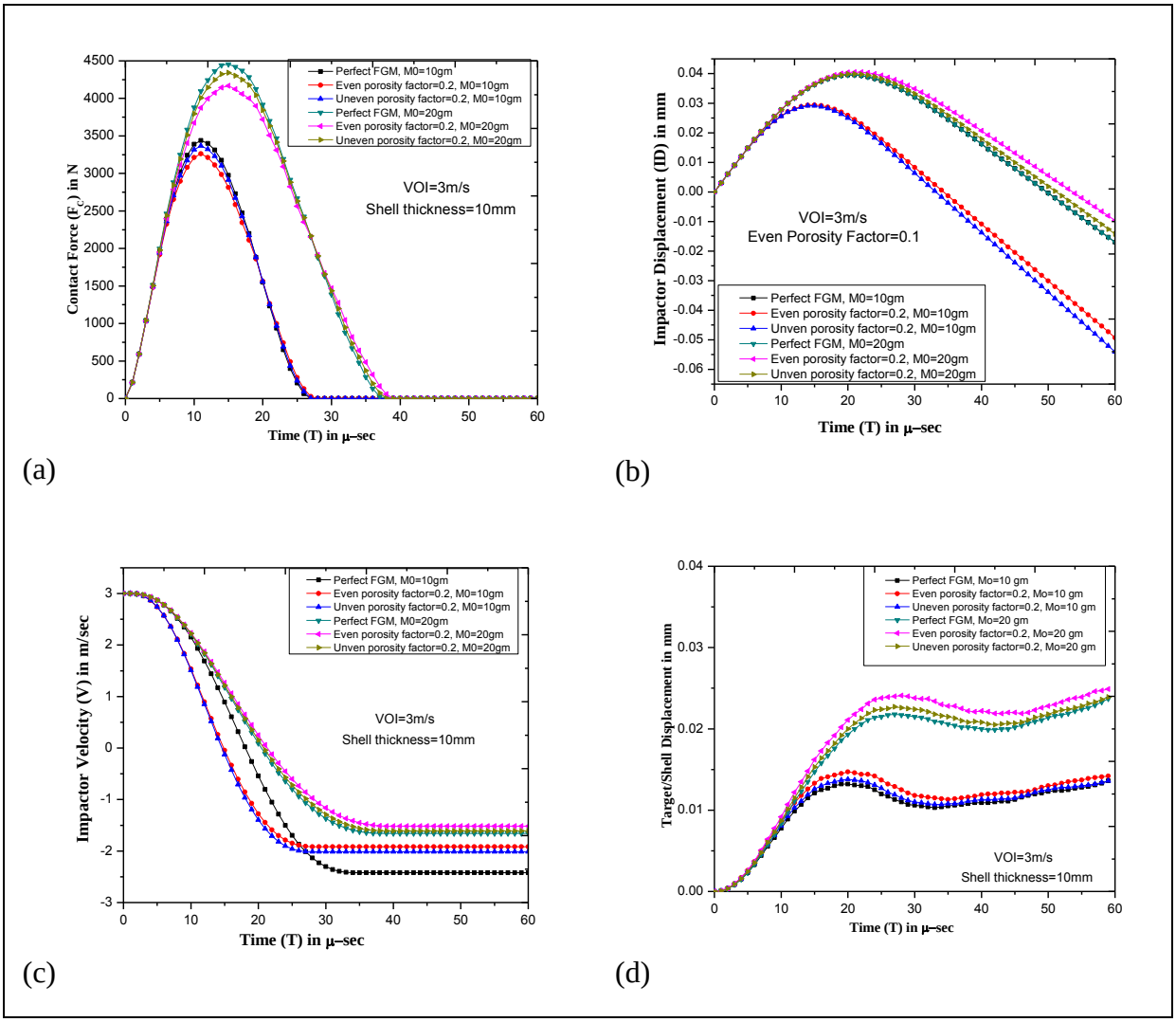

Figure 4.26 (a) Contact force, (b) Impactor displacement, (c) Impactor Velocity and (d) Target displacement, histories of SS-Si_3N_4 E-FGM untwisted conical shell for different mass of the impactor and porosity factor, VOI=3 m/s, L_0 = 0.8m, b_0 = 0.143m, h = 0.01m, M_0 = 10 gm, r_i = 12.7 mm.

The impact characteristics greatly influenced by the mass of the impactor (M_0) and it is obvious that the contact force as well as the impactor displacement, shell displacement and indentation will vary with M_0. Figure. 4.26 (a, b, c, d) illustrate the effect of impactor mass

on low velocity (VOI=3m/s) impact performance. The contact force increases with the increase of mass of the impactor also the time of achieving the peak value of the contact force increases with higher M_0 (shown in Figure 4.26.a). Even porous FGM shell predicts lower contact force than that of uneven porous FGM shell while perfect FGM shell shows maximum contact force for a given M_0. Impactor displacement (as per Figure 4.26.b) enhances with M_0 while the slope of the impactor velocity curve (shown in Figure 4.26.c) is stiffer for lower M_0 than that of higher M_0 for a given VOI.Shell displacement (shown in Figure 4.26.d) shows increasing trend with higher M_0, where perfect FGM predicts lowest shell displacement and even porous FGM shell predicts highest shell displacement.

4.5.4.2 EFFECT OF POROSITY FOR MULTIPLE IMPACT

For the multiple impact problems the impact performance are shown graphically in Figure 4.27. From Figure 4.27 (a), it is observed that the higher peak value of contact force

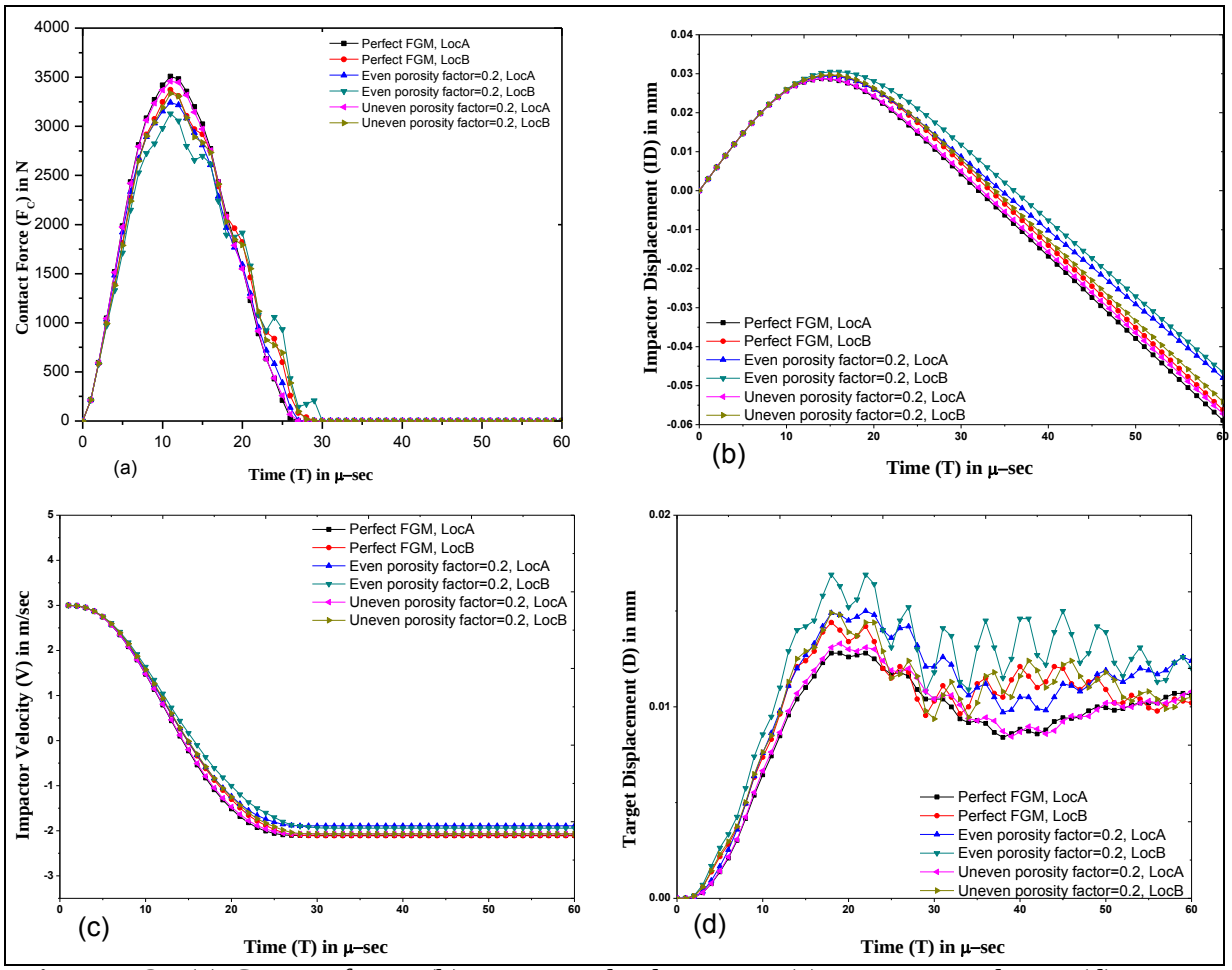

Figure 4.27 (a) Contact force, (b) Impactor displacement, (c) Impactor Velocity (d) Target displacement, histories of SS-Si_3N_4 porous FGM conical shell for various power law index(N), VOI=3, L_0 = 0.8m, b_0 = 0.143m, h = 0.01m, Mass of impactor (M_0) = 10 gm, r_i = 12.7 mm.

and lower contact duration are predicted at location A (near the fixed end) than that of location B (near the free end). Lower peak value of the contact force is observed for even porous case compared to uneven porous case. As depicted in figure 4.27 (b), higher impactor displacements are observed at location B compared to the location A. Higher impactor velocity is observed for location A than that of location B (as per figure 4.27.c). Impactor velocity is found to decrease with the increase of the porosity factor. Figure 4.27 (d) depicts higher value of shell displacement for location B than that of location A.

For a particular value of initial velocity of impactor, the peak value of contact force is found to increaes slightly as the twist angle increases. The trend of contact force histories with different angle of twist with 0.1 even porous FGM shell for VOI=3m/s, has been furnished in Figure 4.28 (a) while Figure 4.28 (b), 4.28 (c) and 4.28 (d) corresponding to the impactor displacement, impactor velocity and target displacement histories, respectively at

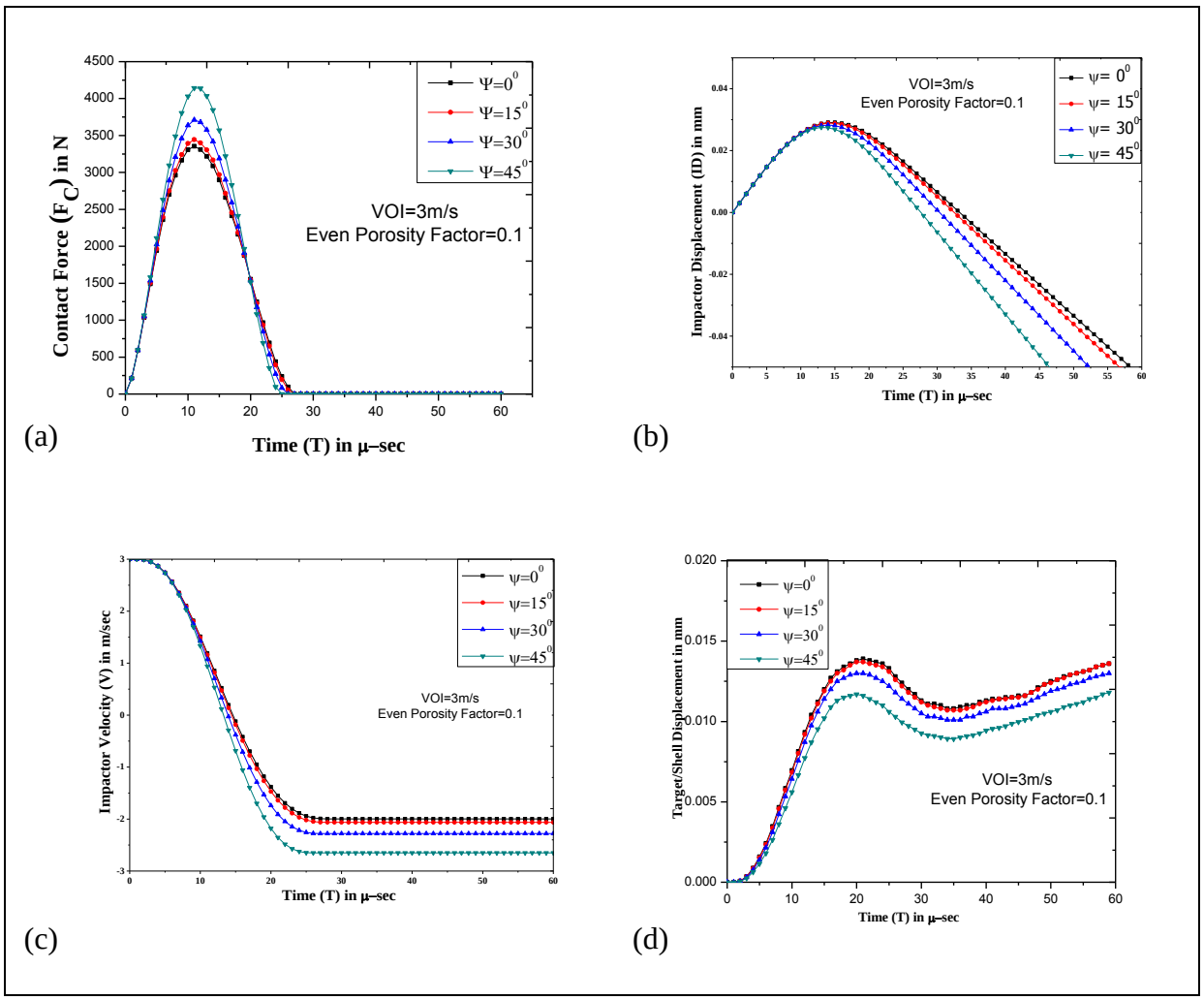

Figure 4.28 (a) Contact force, (b) Impactor displacement, (c) Impactor Velocity and (d) Target displacement, histories of SS-Si_3N_4 E-FGM porous conical shell for different angle of twist, VOI=3 m/s, L_0 = 0.8m, b_0 = 0.143m, h = 0.01m, Mass of impactor (M_0)= 10 gm, r_i = 12.7 mm. Even porosity factor (α_{ep})=0.1.

different twist angles. The increasing trend of contact force histories observed due to the fact that the coupling effect at higher twist angle increases the stiffness which consequentlyhelps to raise the maximum contact force. The time for attaining the peak value of contact force is found to be unaltered with the rise in twist angle. Hence, it can be inferred that the effect of twist angle has significant impact on contact force and has marginal effect on contact duration but has no effect on time of achieving peak value. Impactor displacement shows (Figure 4.28.b) decreasing trend with the increase of twist angle.

CHAPTER 5

CONCLUSIONS

5.1 INTRODUCTION

The outcome of the results in the form of tables and graphs for free vibration characteristics and low velocity impact response of FGM conical shell within the present scope of work is summarized in this chapter. The finite element based computer codes are developed to obtain numerical results for free vibration characteristics and low velocity transient impact performance of FGM conical shell. The convergence studies of the finite element solution method are obtained by varying mesh sizes for free vibration analysis. Also the convergence studies are performed varying mesh sizes and time steps for the case of transient response. The present analysis is carried out to investigate the effect of various triggering parameters on free vibration characteristics and transient low velocity impact performance of FGM shallow conical shells. Parametric studies are carried out for both free vibration and transient dynamic impact response reported in previous Chapter 3 and Chapter 4, respectively. The significant conclusions extracted from the present analysis are enumerated in this chapter. The results obtained are the first identified results of the type of analyses carried out in the present analysis and serve as benchmark solutions for future investigators. The future scope for extension of the present study or new study related to the similar type of problem areas is also listed in this chapter.

5.2 GENERAL

(a) In this present work numerical studies are performed for the dynamic characteristics in respect of free vibration and low velocity impact performance of FGM conical shells. The present model of FGM shallow conical shell can be idealized as rotating turbomachinery blades which can be employed in different application in mechanical and aviation field.

(b) The governing dynamic equilibrium equation is derived from Lagrange's equation of motion neglecting the Coriolis effect (Sreenivasamurthy and Ramamurti, 1981) for moderate rotational speeds.

(c) The effect of transverse shear deformation and rotary inertia are incorporated in the present finite element formulation. The present finite element method is versatile in analyzing shells of complex geometry and is sufficiently accurate, covering a wide range of span or width to thickness ratios.

(d) Convergence studies in terms of mesh sizes of (6 x 6), (8 x 8) and (10 x 10) are performed. The results are found to be nearly equal for (6 x 6) and (8 x 8) with the percentage difference less than 1% while the higher mesh size (10 x 10) predicts slight higher percentage difference than 1%. To avoid ill-conditioning of the numerical eigen value problem (Sreenivasamurthy and Ramamurti, 1981) lower mesh size of (6x6) has been adopted instead of (8x8) for the analysis without sacrificing computer accuracy and efficiency. But for the transient impact response, FEM results are generated using converged mesh size of (8 x 8) which also used to determine the converged value of time step for each parametric case.

5.3 FREE VIBRATION ANALYSIS

Based on the study on free vibration characteristics of pretwisted FGM shallow conical shells considering different FGM constituent's law varying the material property graded index and porosity factors for porous FGM shells the following important observations are found:

5.3.1 SIMPLE POWER LAW FGM (P-FGM)

(a) The non-dimensional natural frequencies (NDFF and NDSF*)* are found to decrease with the increase of the simple power law index (*N*). This is due to the fact that the contribution of the metal part on FGM shell increases and the elastic stiffness matrix reduces with the increase of the material property graded index (*N*) which leads to decrease of the non-dimensional natural frequencies.

(b) The fundamental natural frequencies and second natural frequencies are observed to increase with the increase of the twist angles irrespective of the rotational speed. The centrifugal stiffening effect (i.e., increase of structural stiffness with increase of rotational speeds) for NDFF and NDSF is also observed for all the values of *N* irrespective of twist

angle. This leads to the fact of increasing trend of the NDFF and NDSF for conical shell with increase of rotational speed and twist angle.

(c) The natural frequencies (NDFF and NDSF) at rotating condition (Ω=0.5 or 1.0) as well as at stationary condition (Ω=0.0), the untwisted cases are mostly in the lower range compared to those of twisted ones

(e) The fundamental frequency is observed to be the torsional mode at lower rotational speed for all cases. The symmetry modes are absent for rotating pretwisted conical shells. Span wise bending is notified at higher rotational speeds (Ω=0.5 and 1.0) corresponding to both NDFF and NDSF, irrespective of twist angle. The first span wise bending is found for both NDFF and NDSF at higher rotational speeds (Ω= 0.5, 1.0) for both twisted and untwisted shells. Unlike the rotational shell the span wise bending mode is absent for the stationary shell for all values of twist angle irrespective of the (*N).*

5.3.2 SIGMOIDAL POWER LAW FGM (S-FGM)

(a) The natural frequencies is invariant with the sigmoidal power law index (*N*) for a given twist angle and rotational speed. This is due to the fact that total contribution of metal and ceramic parts remains unchanged irrespective of the *N* and therefore, the total stiffness matrix and mass matrix remains same for the structure. Hence the sigmoidal power law will be more useful for designer to get the desired application arresting the variation of natural frequencies.

(b) The centrifugal stiffening effect (i.e., increase of structural stiffness with increase of rotational speeds) for NDFF and NDSF is also observed for all the values of sigmoidal power law index irrespective of twist angle. This leads to the fact of increasing trend of the NDFF and NDSF with increase of rotational speed. In addition increase of twist angle has also rising trend on the natural frequencies of S-FGM conical shell.

(c) As the fundamental natural frequencies are invariant with sigmoidal power law index *N*, therefore only linear variation of material property (*N*=1) is sufficient for the mode shape evaluation. Fundamental frequency is observed to be the torsional mode at lower rotational speed for both NDFF and NDSF. Symmetry modes are absent for rotating

pretwisted conical shells. Span wise bending is notified at higher rotational speeds (Ω=0.5 and 1.0) corresponding to both NDFF and NDSF, irrespective of twist angle.

5.3.3 EXPONENTIAL POWER LAW FGM (E-FGM)

(a) Twist angle has prominent effect on the natural frequencies of the E-FGM conical shell. The increasing trend of NDFF with increase of twist angles for all rotational speeds are observed while for the NDSF the increase of the frequencies with twist angle can distinctively observed for higher rotational speeds. The rotating effect is more pronounced for twisted shell in comparison to untwisted one and frequency increases with the increase in rotational speed as in the case of P-FGM and S-FGM.

(b) The non-dimensional fundamental natural frequency is observed to be the torsional mode at lower rotational speed. Symmetry modes are absent for rotating pretwisted conical shells. Span wise bending is notified at higher rotational speeds (Ω=0.5 and 1.0) corresponding to both NDFF and NDSF, irrespective of twist angle.

5.3.4 FREE VIBRATION CHARACTERISTICS CONSIDERING POROSITY

(a) Non-dimensional natural frequencies for Stainless steel (SUS304) - Silicon nitride (Si_3N_4) FG conical shells are consistently observed to decrease with the increase of the porosity factor as the presence of porosity lowers the total stiffness of the shell. For the uneven FGM conical shell the decrement of natural frequency (considering perfect FGM) is less compared to even porous FGM conical shell. For a typical FGM configuration the perfect FGM predicts highest non-dimensional natural frequencies. The NDFF is found to increase with the angle of twist irrespective of the porosity factor for all the cases.

(b) The first frequency is found to be the torsional mode at stationary condition irrespective of the twist angle. Torsional modes are also observed with Ω=0.5 for untwisted and lower twist angle (15^0), but the torsional mode reversal along the longitudinal axis are observed for the latter case. The torsional symmetry modes are not observed for other twist angle for rotating shells. Bending mode along the longitudinal direction is observed for those cases. For mode shapes with even porosity factor 0.2, the relative non-dimensional deflection (calculated based on perfect FGM) shows higher value compared to perfect FGM and mode shapes for the intermediate percentage of porosity have same basic nature of deflection.

5.4 TRANSIENT IMPACT ANALYSIS

Transient impact analyses of pretwisted FGM shallow conical shells subjected to low velocity normal impact are investigated by varying initial velocity of the impactor, rotational speeds, location of impact, angle of twist, thickness of shell, different FGM power law graded index and porosity factors. The significant observations from the present analysis are outlined below:

5.4.1 SINGLE IMPACT PROBLEM

In the present analysis, the computer code is authenticated with the benchmark problems of open literature. The developed computer code can be utilized to numerically predict the low velocity impact performance of other type of functionally graded shallow conical shells considering different FGM power law exponent. The following conclusions can be drawn from the present analysis.

a) Peak value of contact force is proportional with initial velocity of impactor, but contact duration shows inverse relation with the VOI and the shell displacement is proportional to the VOI till it reaches to the peak value of the contact force.
b) The maximum value of the contact force decreases considerably with the increase of the *N* and the corresponding time for attaining the peak value of contact force increases with *N*. This is because of the fact that for higher value of *N* the elastic stiffness matrix of the shell becomes lower.
c) Contact force as well as indentation is proportional to the mass of the impactor while the contact duration shows inverse relation with the mass of the impactor.
d) Contact force is found to increase with the increase of twist angles. The shell displacement value has inverse relationship with angle of twist. The time to attain peak value of contact force is found to be unaltered with the rise twist angle.

5.4.2 MULTIPLE IMPACT PROBLEM

a) Higher peak value of contact force and lower contact duration are observed at location A (near the fixed end) than that of location B (near the free end) and shell displacement shows higher value for location B than that of location A.

b) Slope of the impactor velocity curve for location A is stiffer than that of location B for all the cases

5.4.3 TIME DELAYED MULTIPLE IMPACT PROBLEM

a) For delayed multi impact problem the contact force at location B reduces with increase in time delay if the impact on location B occurs during the time duration of impact for the location A. The contact force at location B regains to the actual values, as per the simultaneous multiple impact cases, if the impact on location B occurs after the time duration of impact of location A.
b) Time duration of impact at location A persists for longer period for lower VOI, but corresponding contact force at location B shows lower trend for a particular value of time delay.

5.4.4 EFFECT OF POROSITY ON IMPACT RESPONSE

a) Contact force for perfect FGM (porosity free) shell is higher than that of porous FGM shell, also the contact force has inverse relation with the porosity factor but the shell displacement has proportional relationship with porosity factor.
b) Even porous FGM shell predicts lower contact force but higher shell displacement than that of uneven porous FGM for a given porosity factor.
c) Twisted shell shows higher contact force but lower shell displacement than that of untwisted one for a given porosity factor.

5.5 CONTRIBUTION OF THE THESIS

The contribution of the present work and the objective assessment of the thesis are presented as follows:

a) The finite element based numerical analysis program for determining the free vibration characteristics and low velocity impact (single, multiple and time delayed) response of functionally graded conical shell structures are developed and validated with benchmark solutions. The programs are so general that it can be used for other types of shallow shell geometry with different boundary conditions. This generic computer code can also be used to draw the mode shapes.

b) Natural frequencies are found to increase with the increase of power law exponent as well as with the twist angle of the FG conical shell blade. The rotating effect is found to be more pronounced for twisted FG conical shells compared to untwisted one for free vibration characteristics. It is identified that torsional mode is observed for untwisted conical shell with lower rotational speed but for twisted conical shell torsional symmetric modes are observed only at stationary condition and spanwise bending modes are observed for rotating case.

c) Natural frequencies are consistently observed to decrease with the increase of the porosity factor but for the uneven porous FGM the decrement of natural frequency is less compared to even porous FGM conical shell. Both the natural frequencies (NDFF and NDSF) increase with the rise of rotational speed irrespective of twist angle and porosity factor. For the mode shape the deflection is proportional to the percentage of porosity present in the shell.

d) Moderate rotational speeds have negligible effect on the impact response of FGM conical shells for low velocity impact (single, multiple and time delayed impact).

e) Contact force decreases considerably with the increase of the FGM material property graded index.

f) Contact force for perfect FGM (porosity free) shell is higher than that of porous FGM shell, also the contact force has inverse relation with the porosity factor. Even porous FGM shell predicts lower contact force but higher shell displacement than that of uneven porous FGM for a given porosity factor. Irrespective of the percentage of porosity present in the conical shell, twisted shell always shows higher contact force but lower shell displacement than that of untwisted one.

5.6 FUTURE SCOPE OF WORK

In this present study some important aspects of FGM conical shell have been attempted and solved. But due to technical significance and demand further research is needed for diverge applications of FGM pretwisted conical shells in relation to design, analysis, modeling and manufacturing. Further research can be carried out to completely explore the dynamic behaviour of these specialized FGM structures to provide broader scope of extension of the present work or as a new set of problems. Several potential areas to which the present work can be extended are mentioned as follows:

(i) The present shallow conical shell geometry of with open conical shell can be altered with closed conical shells having moderate thickness and can also be extended to incorporate the structural damping.

(ii) The effect of low-velocity impact for transient dynamic analysis may be extended to include oblique impact.

(iii) The extension of the present work can be made to analyze the conical shell structure considering the hydrothermal (combined effect of moisture and temperature) effect.

(iv) The present analysis can be extended considering the stiffened shells or shells with different sizes of cutouts.

(v) CNTs-reinforced shallow conical shell can be used for higher structural stiffness.

(vi) Functionally graded graphene reinforced cylindrical or conical shell can be considered for free vibration and low velocity impact problems.

REFERENCES

1. Abali BE, Völlmecke C, Woodward B, Kashtalyan M, Guz I, Müller WH. Three-dimensional elastic deformation of functionally graded isotropic plates under point loading. Composite Structures. 2014; 118:367-76.
2. Abbasnejad B, Rezazadeh G, Shabani R. Stability analysis of a capacitive FGM micro-beam using modified couple stress theory. Acta Mechanica Solida Sinica. 2013;26(4):427-40.
3. Abdelaziz HH, Atmane HA, Mechab I, Boumia L, Tounsi A, El Abbas AB. Static analysis of functionally graded sandwich plates using an efficient and simple refined theory. Chinese journal of aeronautics. 2011; 24(4):434-48.
4. Abrate S. Impact on composite structures. Cambridge university press; 2005.
5. Ahmad M, Naeem MN. Vibration characteristics of rotating FGM circular cylindrical shells using wave propagation method. European Journal of Scientific Research. 2009;36(2):184-235.
6. Ahmed Houari MS, Benyoucef S, Mechab I, Tounsi A, Adda Bedia EA. Two-variable refined plate theory for thermoelastic bending analysis of functionally graded sandwich plates. Journal of Thermal Stresses. 2011;34(4):315-34.
7. Akbari M, Kiani Y, Eslami MR. Thermal buckling of temperature-dependent FGM conical shells with arbitrary edge supports. Acta Mechanica. 2015;226(3):897.
8. Alibeigloo A. Exact solution for thermo-elastic response of functionally graded rectangular plates. Composite structures. 2010;92(1):113-21.
9. Alijani F, Amabili M, Karagiozis K, Bakhtiari-Nejad F. Nonlinear vibrations of functionally graded doubly curved shallow shells. Journal of Sound and Vibration. 2011;330(7):1432-54.
10. Alijani F, Amabili M. Non-linear vibrations of shells: A literature review from 2003 to 2013. International Journal of Non-Linear Mechanics. 2014; 58:233-57.
11. Ansari MI, Kumar A, Chakrabarti A. Static analysis of doubly curved singly ruled truncated FGM cone. Composite Structures. 2018; 184:523-35.
12. Ansari R, Darvizeh M. Prediction of dynamic behaviour of FGM shells under arbitrary boundary conditions. Composite Structures. 2008; 85(4):284-92.
13. Arciniega RA, Reddy JN. Large deformation analysis of functionally graded shells. International Journal of Solids and Structures. 2007; 44(6):2036-52.

14. Arshad SH, Naeem MN, Sultana N. Frequency analysis of functionally graded material cylindrical shells with various volume fraction laws. Proc Inst Mech Eng, Part C: J Mech Eng Sci 2007; 221(12):1483–95.
15. Asemi K, Akhlaghi M, Salehi M. Dynamic analysis of thick short length FGM cylinders. Meccanica. 2012; 47(6):1441-53.
16. Asnafi A, Abedi M. A comparison between the dynamic stability of three types of nonlinear orthotropic functionally graded plates under random lateral loads. Journal of Vibration and Control. 2017;23(15):2520-37.
17. Atmane HA, Tounsi A, Bernard F. Effect of thickness stretching and porosity on mechanical response of a functionally graded beams resting on elastic foundations. International Journal of Mechanics and Materials in Design. 2017;13(1):71-84.
18. Ayoubi P, Alibeigloo A. Three-dimensional transient analysis of FGM cylindrical shell subjected to thermal and mechanical loading. Journal of Thermal Stresses. 2017;40(9):1166-83.
19. Azizi A, Khalili S, Malekzadeh Fard K. Low velocity impact response of laminated composite truncated sandwich conical shells with various boundary conditions using complete model and GDQ method. Journal of Applied and Computational Mechanics. 2017;3(1):1-5.
20. Bandyopadhyay T, Karmakar A. Low-velocity impact response of delaminated composite conical shells in hygrothermal environment due to time-delay. Procedia Engineering. 2017;173:463-70.
21. Barati MR, Shahverdi H. Aero-hygro-thermal stability analysis of higher-order refined supersonic FGM panels with even and uneven porosity distributions. Journal of Fluids and Structures. 2017;73:125-36.
22. Barbosa JA, Ferreira AJ. Geometrically nonlinear analysis of functionally graded plates and shells. Mechanics of Advanced Materials and Structures. 2009;17(1):40-8.
23. Bathe K. J., Finite Element Procedures in Engineering Analysis, *Prentice Hall Inc.*, New Delhi, 1990
24. Batra RC, Jin J. Natural frequencies of a functionally graded anisotropic rectangular plate. Journal of Sound and Vibration. 2005;282(1):509-16.
25. Behjat B, Salehi M, Sadighi M, Armin A, Abbasi M. Static, dynamic, and free vibration analysis of functionally graded piezoelectric panels using finite element method. Journal of Intelligent Material Systems and Structures. 2009;20(13):1635-46.

26. Belabed Z, Houari MS, Tounsi A, Mahmoud SR, Bég OA. An efficient and simple higher order shear and normal deformation theory for functionally graded material (FGM) plates. Composites Part B: Engineering. 2014;60:274-83.
27. Beldjelili Y, Tounsi A, Mahmoud SR. Hygro-thermo-mechanical bending of S-FGM plates resting on variable elastic foundations using a four-variable trigonometric plate theory. Smart Structures and Systems. 2016;18(4):755-86.
28. Benachour A, Tahar HD, Atmane HA, Tounsi A, Ahmed MS. A four variable refined plate theory for free vibrations of functionally graded plates with arbitrary gradient. Composites Part B: Engineering. 2011;42(6):1386-94.
29. Beni NN, Dehkordi MB. An extension of Carrera unified formulation in polar coordinate for analysis of circular sandwich plate with FGM core using GDQ method. Composite Structures. 2018;185:421-34.
30. Beni YT, Mehralian F, Razavi H. Free vibration analysis of size-dependent shear deformable functionally graded cylindrical shell on the basis of modified couple stress theory. Composite Structures. 2015;120:65-78.
31. Bennoun M, Houari MS, Tounsi A. A novel five-variable refined plate theory for vibration analysis of functionally graded sandwich plates. Mechanics of Advanced Materials and Structures. 2016;23(4):423-31.
32. Bessaim A, Houari MS, Tounsi A, Mahmoud SR, Bedia EA. A new higher-order shear and normal deformation theory for the static and free vibration analysis of sandwich plates with functionally graded isotropic face sheets. Journal of Sandwich Structures & Materials. 2013;15(6):671-703.
33. Bhangale RK, Ganesan N, Padmanabhan C. Linear thermoelastic buckling and free vibration behavior of functionally graded truncated conical shells. Journal of Sound and Vibration. 2006;292(1):341-71.
34. Bharti I, Gupta N, Gupta KM. Novel applications of functionally graded nano, optoelectronic and thermoelectric materials. Int J Mater Mech Manuf 2013; 1:221–4.
35. Bich DH, Nam VH, Phuong NT. Nonlinear postbuckling of eccentrically stiffened functionally graded plates and shallow shells. Vietnam Journal of Mechanics. 2011;33(3):131-47.
36. Bich DH, Van Dung D, Nam VH. Nonlinear dynamic analysis of eccentrically stiffened imperfect functionally graded doubly curved thin shallow shells. Composite Structures. 2013;96:384-95.

37. Bich DH, Van Dung D. Nonlinear static and dynamic buckling analysis of functionally graded shallow spherical shells including temperature effects. Composite Structures. 2012;94(9):2952-60.
38. Bich DH, Van Tung H. Non-linear axisymmetric response of functionally graded shallow spherical shells under uniform external pressure including temperature effects. International Journal of Non-Linear Mechanics. 2011;46(9):1195-204.
39. Birman V, Byrd LW. Modeling and analysis of functionally graded materials and structures. Applied mechanics reviews. 2007;60(5):195-216.
40. Birman V. Stability of functionally graded hybrid composite plates. Composites Engineering. 1995;5(7):913-21.
41. Bogdanski D, Köller M, Müller D, Muhr G, Bram M, Buchkremer HP, Stöver D, Choi J, Epple M. Easy assessment of the biocompatibility of Ni–Ti alloys by in vitro cell culture experiments on a functionally graded Ni–NiTi–Ti material. Biomaterials. 2002;23(23):4549-55.
42. Bohidar SK, Sharma R, Mishra PR. Functionally graded materials: A critical review. Int J Res 2014; 1:289–301.
43. Bouderba B, Houari MS, Tounsi A. Thermomechanical bending response of FGM thick plates resting on Winkler-Pasternak elastic foundations. Steel and Composite Structures. 2013;14(1):85-104.
44. Bouiadjra MB, Ahmed Houari MS, Tounsi A. Thermal buckling of functionally graded plates according to a four-variable refined plate theory. Journal of Thermal Stresses. 2012;35(8):677-94.
45. Bourada M, Tounsi A, Houari MS, Bedia EA. A new four-variable refined plate theory for thermal buckling analysis of functionally graded sandwich plates. Journal of Sandwich Structures & Materials. 2012;14(1):5-33.
46. Brischetto S. A 3D layer-wise model for the correct imposition of transverse shear/normal load conditions in FGM shells. International Journal of Mechanical Sciences. 2018;136:50-66.
47. Byun C, Kapania RK. Nonlinear transient response of imperfect hyperbolic shells using a reduction method. Computers & structures. 1992;44(1-2):255-62.
48. Carrera E, Brischetto S, Nali P. Plates and shells for smart structures: classical and advanced theories for modeling and analysis. John Wiley & Sons; 2011.
49. Carrera E, Cinefra M, Petrolo M, Zappino E. Finite element analysis of structures through unified formulation. John Wiley & Sons; 2014.

50. Carrera E, Giunta G, Petrolo M. Beam structures: classical and advanced theories. John Wiley & Sons; 2011a.
51. Carrera E. A class of two-dimensional theories for anisotropic multilayered plates analysis. Atti della accademia delle scienze di Torino. Classe di scienze fisiche matematiche e naturali. 1995;19:1-39.
52. Carter RL, Robinson AR, Schnobrich WC. Free vibrations of hyperboloidal shells of revolution. Journal of the Engineering Mechanics Division. 1969;95(5):1033-52.
53. Chai GB, Zhu S. A review of low-velocity impact on sandwich structures. Proceedings of the Institution of Mechanical Engineers, Part L: Journal of Materials: Design and Applications. 2011;225(4):207-30.
54. Chakravorty D, Bandyopadhyay JN, Sinha PK. Finite element free vibration analysis of doubly curved laminated composite shells. Journal of Sound and Vibration. 1996;191(4):491-504.
55. Chakravorty D, Bandyopadhyay JN, Sinha PK. Free vibration analysis of point-supported laminated composite doubly curved shells—A finite element approach. Computers & structures. 1995;54(2):191-8.
56. Chapelle D, Bathe KJ. Fundamental considerations for the finite element analysis of shell structures. Computers & Structures. 1998;66(1):19-36.
57. Chen H, Wang A, Hao Y, Zhang W. Free vibration of FGM sandwich doubly-curved shallow shell based on a new shear deformation theory with stretching effects. Composite Structures. 2017;179:50-60.
58. Chen WQ, Bian ZG, Ding HJ. Three-dimensional vibration analysis of fluid-filled orthotropic FGM cylindrical shells. International Journal of Mechanical Sciences. 2004;46(1):159-71.
59. Cheng ZQ, Batra RC. Three-dimensional thermoelastic deformations of a functionally graded elliptic plate. Composites Part B: Engineering. 2000;31(2):97-106.
60. Cheung YK, Li WY, Tham LG. Free vibration analysis of singly curved shell by spline finite strip method. Journal of Sound and Vibration. 1989;128(3):411-22.
61. Choi CK. A conoidal shell analysis by modified isoparametric element. Computers & structures. 1984;18(5):921-4.
62. Choi IH. Finite element analysis of low-velocity impact response of convex and concave composite laminated shells. Composite Structures. 2018;186:210-20.

63. Chorfi SM, Houmat A. Non-linear free vibration of a functionally graded doubly-curved shallow shell of elliptical plan-form. Composite Structures. 2010;92(10):2573-81.
64. Cinefra M, Carrera E, Brischetto S, Belouettar S. Thermo-mechanical analysis of functionally graded shells. Journal of Thermal Stresses. 2010;33(10):942-63.
65. Cinefra M, Carrera E, Della Croce L, Chinosi C. Refined shell elements for the analysis of functionally graded structures. Composite Structures. 2012;94(2):415-22.
66. Cong PH, Khanh ND, Khoa ND, Duc ND. New approach to investigate nonlinear dynamic response of sandwich auxetic double curves shallow shells using TSDT. Composite Structures. 2018;185:455-65.
67. Conway H.D., Analytical model for delamination growth during small mass impact on plates. ZAMP, (1956), 7 (1), pp. 80-85.
68. Cook R. D., Malkus D. S. and Plesha M. E., Concepts and Applications of Finite Element Analysis, John Wiley & Sons, New York, 1989.
69. Dai HL, Guo ZY, Yang L. Nonlinear dynamic response of functionally graded materials circular plates subject to low-velocity impact. Journal of Composite Materials. 2013;47(22):2797-807.
70. Dai KY, Liu GR, Han X, Lim KM. Thermomechanical analysis of functionally graded material (FGM) plates using element-free Galerkin method. Comput Struct 2005;83(17–18):1487–502.
71. Darabi M, Darvizeh M, Darvizeh A. Non-linear analysis of dynamic stability for functionally graded cylindrical shells under periodic axial loading. Composite Structures. 2008;83(2):201-11.
72. Das AK, Bandyopadhyay JN. Theoretical and experimental studies on conoidal shells. Computers & structures. 1993;49(3):531-6.
73. Dey A, Bandyopadhyay JN, Sinha PK. Finite element analysis of laminated composite conoidal shell structures. Computers & structures. 1992;43(3):469-76.
74. Du C, Li Y, Jin X. Nonlinear forced vibration of functionally graded cylindrical thin shells. Thin-Walled Structures. 2014;78:26-36.
75. Du C, Li Y. Nonlinear resonance behavior of functionally graded cylindrical shells in thermal environments. Composite Structures. 2013;102:164-74.
76. Duc ND, Cong PH, Tuan ND, Tran P, Van Thanh N. Thermal and mechanical stability of functionally graded carbon nanotubes (FG CNT)-reinforced composite truncated

conical shells surrounded by the elastic foundations. Thin-Walled Structures. 2017;115:300-10.

77. Duc ND, Quan TQ, Luat VD. Nonlinear dynamic analysis and vibration of shear deformable piezoelectric FGM double curved shallow shells under damping-thermo-electro-mechanical loads. Composite Structures. 2015;125:29-40.
78. Duc ND, Quan TQ. Nonlinear dynamic analysis of imperfect functionally graded material double curved thin shallow shells with temperature-dependent properties on elastic foundation. Journal of Vibration and Control. 2015;21(7):1340-62.
79. Duc ND, Quan TQ. Nonlinear stability analysis of double-curved shallow FGM panels on elastic foundations in thermal environments. Mechanics of Composite Materials. 2012;48(4):435-48.
80. Duc ND, Thang PT, Dao NT, Van Tac H. Nonlinear buckling of higher deformable S-FGM thick circular cylindrical shells with metal–ceramic–metal layers surrounded on elastic foundations in thermal environment. Composite Structures. 2015;121:134-41.
81. Ebrahimi F, Ghasemi F, Salari E. Investigating thermal effects on vibration behavior of temperature-dependent compositionally graded Euler beams with porosities. Meccanica. 2016;51(1):223-49.
82. Ebrahimi F, Mokhtari M. Transverse vibration analysis of rotating porous beam with functionally graded microstructure using the differential transform method. Journal of the Brazilian Society of Mechanical Sciences and Engineering. 2015;37(4):1435-44.
83. Ebrahimi F, Zia M. Large amplitude nonlinear vibration analysis of functionally graded Timoshenko beams with porosities. Acta Astronautica. 2015;116:117-25.
84. Ebrahimi MJ, Najafizadeh MM. Free vibration analysis of two-dimensional functionally graded cylindrical shells. Applied Mathematical Modelling. 2014;38(1):308-24.
85. El Meiche N, Tounsi A, Ziane N, Mechab I. A new hyperbolic shear deformation theory for buckling and vibration of functionally graded sandwich plate. International Journal of Mechanical Sciences. 2011;53(4):237-47.
86. Etemadi E, Khatibi AA, Takaffoli M. 3D finite element simulation of sandwich panels with a functionally graded core subjected to low velocity impact. Composite Structures. 2009;89(1):28-34.
87. Farid M, Zahedinejad P, Malekzadeh P. Three-dimensional temperature dependent free vibration analysis of functionally graded material curved panels resting on two-parameter elastic foundation using a hybrid semi-analytic, differential quadrature method. Materials & Design. 2010;31(1):2-13.

88. Ferreira AJ, Batra RC, Roque CM, Qian LF, Jorge RM. Natural frequencies of functionally graded plates by a meshless method. Composite Structures. 2006;75(1-4):593-600.
89. Foroughi H, Azhari M. Mechanical buckling and free vibration of thick functionally graded plates resting on elastic foundation using the higher order B-spline finite strip method. Meccanica. 2014;49(4):981-93.
90. Frikha A, Trabelsi S, Zghal S. A Four-Node Shell Element for Geometrically Nonlinear Analysis of Thin FGM Plates and Shells. InInternational Conference Design and Modeling of Mechanical Systems 2017 pp. 209-215. Springer, Cham.
91. Frikha A, Zghal S, Dammak F. Dynamic analysis of functionally graded carbon nanotubes-reinforced plate and shell structures using a double directors finite shell element. Aerospace Science and Technology. 2018;78:438-51.
92. Fu ZJ, Qin QH, Chen W. Hybrid-Trefftz finite element method for heat conduction in nonlinear functionally graded materials. Engineering Computations. 2011;28(5):578-99.
93. Ganapathi M. Dynamic stability characteristics of functionally graded materials shallow spherical shells. Composite structures. 2007;79(3):338-43.
94. Gao K, Gao W, Wu D, Song C. Nonlinear dynamic stability of the orthotropic functionally graded cylindrical shell surrounded by Winkler-Pasternak elastic foundation subjected to a linearly increasing load. Journal of Sound and Vibration. 2018;415:147-68.
95. Garhwal A, Kaushik Y, Singh SM. Finite Element Analysis of Hyperbolic Paraboloid Composite Shells for Static Analysis Under Uniform Pressure. InProceedings of the International Conference on Modern Research in Aerospace Engineering 2018 (pp. 189-201). Springer, Singapore.
96. Gasik MM. Functionally graded materials: bulk processing techniques. Int J Mater Prod Technol 2010; 39:20–9.
97. Ghosh B, Bandyopadhyay JN. Approximate bending analysis of conoidal shells using the Galerkin method. Computers & Structures. 1990;36(5):801-5.
98. Ghosh B, Bandyopadhyay JN. Bending analysis of conoidal shells using curved quadratic isoparametric element. Computers & structures. 1989;33(3):717-28.
99. Giannakopoulos AE, Suresh S. Indentation of solids with gradients in elastic properties: Part I. Point force. International Journal of Solids and Structures. 1997;34(19):2357-92.
100. Goldsmith W. Impact: the theory and physical behaviour of colliding solids. 1960. Edward Arnold, London.

101. Gong SW, Lam KY, Reddy JN. The elastic response of functionally graded cylindrical shells to low-velocity impact. International Journal of Impact Engineering. 1999;22(4):397-417.
102. Gunes R, Aydin M, Apalak MK, Reddy JN. Experimental and numerical investigations of low velocity impact on functionally graded circular plates. Composites Part B: Engineering. 2014;59:21-32.
103. Gunes R, Aydin M, Apalak MK, Reddy JN. The elasto-plastic impact analysis of functionally graded circular plates under low-velocities. Composite Structures. 2011;93(2):860-9.
104. Gunes R, Aydin M. Elastic response of functionally graded circular plates under a drop-weight. Composite Structures. 2010;92(10):2445-56.
105. Gupta A, Talha M. Recent development in modeling and analysis of functionally graded materials and structures. Progress in Aerospace Sciences. 2015;79:1-4.
106. Haddadpour H, Mahmoudkhani S, Navazi HM. Free vibration analysis of functionally graded cylindrical shells including thermal effects. Thin-walled structures. 2007;45(6):591-9.
107. Hadid, H. A., An analytical and experimental investigation into the bending theory of elastic conoidal shells, Ph.D. Thesis, 1964, University of Southampton, UK.
108. Hadji L, Atmane HA, Tounsi A, Mechab I, Bedia EA. Free vibration of functionally graded sandwich plates using four-variable refined plate theory. Applied Mathematics and Mechanics. 2011;32(7):925-42.
109. Hajlaoui AB, Triki EM, Frikha AH, Wali MO, Dammak FA. Nonlinear Dynamics Analysis of FGM Shell Structures with a Higher Order Shear Strain Enhanced Solid-Shell Element. Latin American Journal of Solids and Structures. 2017;14(1):72-91.
110. Han Y, Zhu X, Li T, Yu Y. Vibration analysis of submerged orthogonally stiffened FGM cylindrical shells. InINTER-NOISE and NOISE-CON Congress and Conference Proceedings 2017,(Vol. 255, No. 4, pp. 3355-3363). Institute of Noise Control Engineering.
111. Hebali H, Tounsi A, Houari MS, Bessaim A, Bedia EA. New quasi-3D hyperbolic shear deformation theory for the static and free vibration analysis of functionally graded plates. Journal of Engineering Mechanics. 2014;140(2):374-83.
112. Heydarpour Y, Aghdam MM, Malekzadeh P. Free vibration analysis of rotating functionally graded carbon nanotube-reinforced composite truncated conical shells. Composite structures. 2014;117:187-200.

113. Heydarpour Y, Malekzadeh P, Haghighi MG, Vaghefi M. Thermoelastic analysis of rotating laminated functionally graded cylindrical shells using layerwise differential quadrature method. Acta Mechanica. 2012;223(1):81-93.
114. Hong Cong P, Anh VM, Dinh Duc N. Nonlinear dynamic response of eccentrically stiffened FGM plate using Reddy's TSDT in thermal environment. Journal of Thermal Stresses. 2017;40(6):704-32.
115. Hosseini Kordkheili SA, Naghdabadi R. Geometrically nonlinear thermoelastic analysis of functionally graded shells using finite element method. International journal for numerical methods in Engineering. 2007;72(8):964-86.
116. Inala R, Mohanty SC. Flap wise bending vibration and dynamic stability of rotating functionally graded material plates in thermal environments. Proceedings of the Institution of Mechanical Engineers, Part G: Journal of Aerospace Engineering. 2017;231(2):203-17.
117. Ip KH, Chan WK, Tse PC, Lai TC. Vibration analysis of orthotropic thin cylindrical shells with free ends by the Rayleigh-Ritz method. Journal of sound and vibration. 1996;195(1):117-35.
118. Isvandzibaei MR, Jamaluddin H, Raja Hamzah RI. Vibration analysis of supported thick-walled cylindrical shell made of functionally graded material under pressure loading. Journal of Vibration and Control. 2016;22(4):1023-36.
119. Javaheri R, Eslami MR. Buckling of Functionally Graded Plates under In-plane Compressive Loading. ZAMM-Journal of Applied Mathematics and Mechanics/Zeitschrift für Angewandte Mathematik und Mechanik. 2002;82(4):277-83.
120. Jha DK, Kant T, Singh RK. A critical review of recent research on functionally graded plates. Composite Structures. 2013;96:833-49.
121. Jones R. M., Mechanics of composite materials, Scripta Book Co., 1975.
122. Jung WY, Han SC. Static and eigenvalue problems of sigmoid functionally graded materials (S-FGM) micro-scale plates using the modified couple stress theory. Applied Mathematical Modelling. 2015;39(12):3506-24.
123. Kamarian S, Sadighi M, Shakeri M, Yas MH. Free vibration response of sandwich cylindrical shells with functionally graded material face sheets resting on Pasternak foundation. Journal of Sandwich Structures & Materials. 2014;16(5):511-33.
124. Kant T, Khare RK. A higher-order facet quadrilateral composite shell element. International Journal for Numerical Methods in Engineering. 1997;40(24):4477-99.

125. Kapuria S, Bhattacharyya M, Kumar AN. Bending and free vibration response of layered functionally graded beams: a theoretical model and its experimental validation. Composite Structures. 2008;82(3):390-402.
126. Kapuria S, Patni M, Yasin MY. A quadrilateral shallow shell element based on the third-order theory for functionally graded plates and shells and the inaccuracy of rule of mixtures. Eur J Mech A Solids 2015;49:268–82.
127. Kar VR, Mahapatra TR, Panda SK. Effect of different temperature load on thermal postbuckling behaviour of functionally graded shallow curved shell panels. Composite Structures. 2017;160:1236-47.
128. Karmakar A, Kishimoto K. Free Vibration Analysis of Delaminated Composite Pretwisted Rotating Shells─ A Finite Element Approach. JSME International Journal Series A Solid Mechanics and Material Engineering. 2006;49(4):492-502.
129. Karmakar A, Sinha PK. Failure analysis of laminated composite pretwisted rotating plates. Journal of reinforced plastics and composites. 2001;20(14-15):1326-57.
130. Karmakar AM, Mishra TK, Kishimoto K. Free vibration characteristics of delaminated composite rotating cantilever shallow shells. InICF11, Italy 2005, 5185.
131. Kashtalyan M, Menshykova M. Three-dimensional elasticity solution for sandwich panels with a functionally graded core. Composite Structures. 2009;87(1):36-43.
132. Kashtalyan M. Three-dimensional elasticity solution for bending of functionally graded rectangular plates. European Journal of Mechanics-A/Solids. 2004;23(5):853-64.
133. Khalili SM, Malekzadeh K, Gorgabad AV. Low velocity transverse impact response of functionally graded plates with temperature dependent properties. Composite Structures. 2013;96:64-74.
134. Khalili SM, Saeedi A. Dynamic response of laminated composite beam reinforced with shape memory alloy wires subjected to low velocity impact of multiple masses. Journal of Composite Materials. 2018;52(8):1089-101.
135. Khor KA, Gu YW. Effects of residual stress on the performance of plasma sprayed functionally graded ZrO2/NiCoCrAlY coatings. Materials Science and Engineering: A. 2000;277(1-2):64-76.
136. Kiani Y, Eslami MR. Thermal buckling and post-buckling response of imperfect temperature-dependent sandwich FGM plates resting on elastic foundation. Arch Appl 2012;82(7):891–905.

137. Kiani Y, Sadighi M, Salami SJ, Eslami MR. Low velocity impact response of thick FGM beams with general boundary conditions in thermal field. Composite Structures. 2013;104:293-303.
138. Kiani Y, Shakeri M, Eslami MR. Thermoelastic free vibration and dynamic behaviour of an FGM doubly curved panel via the analytical hybrid Laplace–Fourier transformation. Acta Mechanica. 2012;223(6):1199-218.
139. Kieback B, Neubrand A, Riedel H. Processing techniques for functionally graded materials. Mater Sci Eng A 2003; 362:81–105.
140. Kim JH, Paulino GH. Isoparametric graded finite elements for nonhomogeneous isotropic and orthotropic materials. Journal of applied mechanics. 2002;69(4):502-14.
141. Kim SE, Thai HT, Lee J. Buckling analysis of plates using the two variable refined plate theory. Thin-Walled Structures. 2009;47(4):455-62.
142. Kirchoff G. Uber das Gleichgewicht und die Bewegung einer elastischen Scheibe. Journal fur die reine und angewandte Mathematik (Crelle's Journal). 1850;40:51-88.
143. Kohli GS, Singh T. Review of functionally graded materials. J Prod Eng 2015; 18:1–4.
144. Krivoshapko SN. Static, vibration, and buckling analyses and applications to one-sheet hyperboloidal shells of revolution. Applied Mechanics Reviews. 2002;55(3):241-70.
145. Kubair DV, Lakshmana BK. Cohesive modeling of low-velocity impact damage in layered functionally graded beams. Mechanics Research Communications. 2008;35(1):104-14.
146. Lam KY, Hua L. Influence of boundary conditions on the frequency characteristics of a rotating truncated circular conical shell. Journal of Sound and Vibration. 1999;223(2):171-95.
147. Lam KY, Sathiyamoorthy TS. Response of composite beam under low-velocity impact of multiple masses. Composite structures. 1999;44(2-3):205-20.
148. Lanhe W, Hongjun W, Daobin W. Dynamic stability analysis of FGM plates by the moving least squares differential quadrature method. Composite Structures. 2007;77(3):383-94.
149. Larson RA, Palazotto A. Low velocity impact analysis of functionally graded circular plates. InProceedings of IMECE 2006 ASME international mechanical engineering congress and exposition, Chicago, Illinois, USA, 2006, (pp. 5-10).
150. Larson RA, Palazotto AN, Gardenier HE. Impact Response of titanium and titanium boride monolithic and functionally graded composite plates. AIAA journal. 2009;47(3):676.

151. Larson RA, Palazotto AN. Property estimation in FGM plates subject to low-velocity impact loading. Journal of Mechanics of Materials and Structures. 2009;4(7):1429-51.
152. Lee CY, Kim JH. Degradation of thermal postbuckling behaviors of functionally graded material in aero-hygrothermal environments. Composite Structures. 2014;118:228-33.
153. Lee CY, Kim JH. Hygrothermal postbuckling behavior of functionally graded plates. Composite Structures. 2013;95:278-82.
154. Lee YY, Zhao X, Liew KM. Thermoelastic analysis of functionally graded plates using the element-free kp-Ritz method. Smart Materials and Structures. 2009;18(3):035007.
155. Lee YY, Zhao X, Reddy JN. Postbuckling analysis of functionally graded plates subject to compressive and thermal loads. Computer Methods in Applied Mechanics and Engineering. 2010;199(25):1645-53.
156. Lei ZX, Zhang LW, Liew KM, Yu JL. Dynamic stability analysis of carbon nanotube-reinforced functionally graded cylindrical panels using the element-free kp-Ritz method. Composite Structures. 2014;113:328-38.
157. Leissa A.W., Vibration of shells, NASA SP388, The Government Printing Office, Washington DC, 1973.
158. Leissa AW, Lee JK, Wang AJ. Vibrations of twisted rotating blades. Journal of vibration, acoustics, stress, and reliability in design. 1984;106(2):251-7.
159. Levinson M. An accurate, simple theory of the statics and dynamics of elastic plates. Mechanics Research Communications. 1980;7(6):343-50.
160. Levy M. Mémoire sur la théorie des plaques élastiques planes. Journal de mathématiques pures et appliquées. 1877:219-306.
161. Li H, Lambros J, Cheeseman BA, Santare MH. Experimental investigation of the quasi-static fracture of functionally graded materials. International Journal of Solids and Structures. 2000;37(27):3715-32.
162. Li L, Li H, Pang F, Wang X, Du Y, Li S. The modified fourier-ritz approach for the free vibration of functionally graded cylindrical, conical, spherical panels and shells of revolution with general boundary condition. Mathematical Problems in Engineering. 2017.
163. Li Y, Yang C, Zhao H, Qu S, Li X, Li Y. New developments of Ti-based alloys for biomedical applications. Materials (Basel) 2014; 7:1709–800.
164. Liao YF, Chen LI, Miao YN, Feng QL. Thermal buckling of thin conical shell subjected to uniform pressure and temperature. DEStech Transactions on Engineering and Technology Research. 2017.

165. Librescu L, Khdeir AA, Frederick D. A shear deformable theory of laminated composite shallow shell-type panels and their response analysis I: free vibration and buckling. Acta Mechanica. 1989;76(1):1-33.
166. Librescu L, Oh SY, Song O, Kang HS. Dynamics of advanced rotating blades made of functionally graded materials and operating in a high-temperature field. Journal of Engineering Mathematics. 2008;61(1):1-6.
167. Liew KM, Lei ZX, Zhang LW. Mechanical analysis of functionally graded carbon nanotube reinforced composites: a review. Composite Structures. 2015;120:90-7.
168. Liew KM, Lim CW, Ong LS. Vibration of pretwisted cantilever shallow conical shells. International Journal of Solids and structures. 1994;31(18):2463-76.
169. Liew KM, Ng TY, Zhao X. Free vibration analysis of conical shells via the element-free kp-Ritz method. Journal of Sound and Vibration. 2005;281(3):627-45.
170. Liew KM, Zhao X, Ferreira AJ. A review of meshless methods for laminated and functionally graded plates and shells. Composite Structures. 2011;93(8):2031-41.
171. Liu CS, Fang JC, Chen QC. Fabrication and Performance Evaluation of Functionally Graded Materials. Materials for Mechanical Engineering. 2006;10:001.
172. Loy CT, Lam KY, Reddy JN. Vibration of functionally graded cylindrical shells. International Journal of Mechanical Sciences. 1999;41(3):309-24.
173. Makwana AB, Panchal KC. A review of stress analysis of functionally graded material plate with cut-out. Int J Eng Res Technol 2014;3: 2020–5.
174. Malekzadeh P, Heydarpour Y. Free vibration analysis of rotating functionally graded truncated conical shells. Composite structures. 2013;97:176-88.
175. Malekzadeh P, Heydarpour Y. Free vibration analysis of rotating functionally graded cylindrical shells in thermal environment. Composite Structures. 2012;94(9):2971-81.
176. Malekzadeh P, Shojaee SA. Dynamic response of functionally graded plates under moving heat source. Composites Part B: Engineering. 2013;44(1):295-303.
177. Mantari JL, Granados EV, Hinostroza MA, Soares CG. Modelling advanced composite plates resting on elastic foundation by using a quasi-3D hybrid type HSDT. Composite Structures. 2014;118:455-71.
178. Mantari JL, Granados EV. Thermoelastic analysis of advanced sandwich plates based on a new quasi-3D hybrid type HSDT with 5 unknowns. Composites Part B: Engineering. 2015;69:317-34.

179. Mantari JL, Oktem AS, Soares CG. Bending and free vibration analysis of isotropic and multilayered plates and shells by using a new accurate higher-order shear deformation theory. Composites Part B: Engineering. 2012;43(8):3348-60.
180. Mantari JL, Oktem AS, Soares CG. Bending response of functionally graded plates by using a new higher order shear deformation theory. Composite Structures. 2012a;94(2):714-23.
181. Mantari JL, Soares CG. A trigonometric plate theory with 5-unknowns and stretching effect for advanced composite plates. Composite Structures. 2014;107:396-405.
182. Mao YQ, Fu YM, Chen CP, Li YL. Nonlinear dynamic response for functionally graded shallow spherical shell under low velocity impact in thermal environment. Applied Mathematical Modelling. 2011;35(6):2887-900.
183. Matsunaga H. Free vibration and stability of functionally graded shallow shells according to a 2D higher-order deformation theory. Composite structures. 2008;84(2):132-46.
184. Matsunaga H. Free vibration and stability of functionally graded circular cylindrical shells according to a 2D higher-order deformation theory. Composite Structures. 2009;88(4):519-31.
185. Mechab I, Atmane HA, Tounsi A, Belhadj HA. A two variable refined plate theory for the bending analysis of functionally graded plates. Acta Mechanica Sinica. 2010;26(6):941-9.
186. Mechab I, Mechab B, Benaissa S, Serier B, Bouiadjra BB. Free vibration analysis of FGM nanoplate with porosities resting on Winkler Pasternak elastic foundations based on two-variable refined plate theories. Journal of the Brazilian Society of Mechanical Sciences and Engineering. 2016;38(8):2193-211.
187. Mechab I, Mechab B, Benaissa S. Static and dynamic analysis of functionally graded plates using four-variable refined plate theory by the new function. Composites Part B: Engineering. 2013;45(1):748-57.
188. Meirovitch L. Principles and techniques of vibrations. New Jersey: Prentice Hall; 1997.
189. Meirovitch L., Dynamics and Control of Structures, John Wiley & Sons, New York, 1992.
190. Mian MA, Spencer AJ. Exact solutions for functionally graded and laminated elastic materials. Journal of the Mechanics and Physics of Solids. 1998;46(12):2283-95.
191. Mindlin RD. Influence of rotatory inertia and shear on flexural motions of isotropic, elastic plates. J. appl. Mech.. 1951;18:31.

192. Mirsalehi M, Azhari M, Amoushahi H. Stability of thin FGM microplate subjected to mechanical and thermal loading based on the modified couple stress theory and spline finite strip method. Aerospace Science and Technology. 2015;47:356-66.
193. Miyamoto Y, Kaysser WA, Rabin BH, Kawasaki A, Ford RG. Functionally graded materials: design, processing and applications. Springer Science & Business Media; 2013.
194. Mohammadimehr M, Rostami R. Bending and vibration analyses of a rotating sandwich cylindrical shell considering nanocomposite core and piezoelectric layers subjected to thermal and magnetic fields. Applied Mathematics and Mechanics. 2018:1-22.
195. Mollarazi HR, Foroutan M, Moradi-Dastjerdi R. Analysis of free vibration of functionally graded material (FGM) cylinders by a meshless method. Journal of Composite Materials. 2012;46(5):507-15.
196. Moradi-Dastjerdi R, Foroutan M, Pourasghar A. Dynamic analysis of functionally graded nanocomposite cylinders reinforced by carbon nanotube by a mesh-free method. Materials & Design. 2013;44:256-66.
197. Mungan I. Buckling stresses of stiffened hyperboloidal shells. Journal of the Structural Division. 1979;105(8):1589-604.
198. Naeem MN, Arshad SH, Sharma CB. The Ritz formulation applied to the study of the vibration frequency characteristics of functionally graded circular cylindrical shells. Proceedings of the Institution of Mechanical Engineers, Part C: Journal of Mechanical Engineering Science. 2010;224(1):43-54.
199. Naghdabadi R, Kordkheili SH. A finite element formulation for analysis of functionally graded plates and shells. Archive of applied mechanics. 2005;74(5-6):375-86.
200. Naj R, Boroujerdy MS, Eslami MR. Thermal and mechanical instability of functionally graded truncated conical shells. Thin-Walled Structures. 2008;46(1):65-78.
201. Najafi F, Shojaeefard MH, Googarchin HS. Nonlinear dynamic response of FGM beams with Winkler–Pasternak foundation subject to noncentral low velocity impact in thermal field. Composite Structures. 2017;167:132-43.
202. Najafizadeh MM, Eslami MR. Buckling analysis of circular plates of functionally graded materials under uniform radial compression. International Journal of Mechanical Sciences. 2002;44(12):2479-93.
203. Najafizadeh MM, Heydari HR. An exact solution for buckling of functionally graded circular plates based on higher order shear deformation plate theory under uniform radial compression. International Journal of Mechanical Sciences. 2008;50(3):603-12.

204. Najafizadeh MM, Isvandzibaei MR. Vibration of functionally graded cylindrical shells based on higher order shear deformation plate theory with ring support. Acta Mechanica. 2007;191(1-2):75-91.
205. Nasir AM, Thambiratnam DP, Butler D, Austin P. Dynamics of axisymmetric hyperbolic shell structures. Thin-walled structures. 2002;40(7):665-90.
206. Nath Y, Alwar RS. Non-linear static and dynamic response of spherical shells. International Journal of Non-Linear Mechanics. 1978;13(3):157-70.
207. Nayak AN, Bandyopadhyay JN. Free vibration analysis and design aids of stiffened conoidal shells. Journal of engineering mechanics. 2002;128(4):419-27.
208. Neves AM, Ferreira AJ, Carrera E, Cinefra M, Roque CM, Jorge RM, Soares CM. Free vibration analysis of functionally graded shells by a higher-order shear deformation theory and radial basis functions collocation, accounting for through-the-thickness deformations. European Journal of Mechanics-A/Solids. 2013;37:24-34.
209. Ng TY, Hua LI, Lam KY, Loy CT. Parametric instability of conical shells by the generalized differential quadrature method. International Journal for Numerical Methods in Engineering. 1999;44(6):819-37.
210. Ng TY, Lam KY, Liew KM, Reddy JN. Dynamic stability analysis of functionally graded cylindrical shells under periodic axial loading. International Journal of Solids and Structures. 2001;38(8):1295-309.
211. Nguyen DD, Tran QQ. Nonlinear postbuckling of imperfect eccentrically stiffened P-FGM double curved thin shallow shells on elastic foundations in thermal environments. Compos Struct 2013;106:590–600.
212. Nguyen Dinh D, Nguyen PD. The dynamic response and vibration of functionally graded carbon nanotube-reinforced composite (FG-CNTRC) truncated conical shells resting on elastic foundations. Materials. 2017;10(10):1194.
213. Norouzi H, Alibeigloo A. Three dimensional static analysis of viscoelastic FGM cylindrical panel using state space differential quadrature method. European Journal of Mechanics-A/Solids. 2017;61:254-66.
214. Oktem AS, Mantari JL, Soares CG. Static response of functionally graded plates and doubly-curved shells based on a higher order shear deformation theory. European Journal of Mechanics-A/Solids. 2012;36:163-72.
215. Omurtag MH, Aköz AY. Hyperbolic paraboloid shell analysis via mixed finite element formulation. International journal for numerical methods in engineering. 1994;37(18):3037-56.

216. Panc V. Theories of elastic plates. Springer Science & Business Media; 1975.
217. Pang F, Li H, Wang X, Miao X, Li S. A semi analytical method for the free vibration of doubly-curved shells of revolution. Computers & Mathematics with Applications. 2018;75(9):3249-68.
218. Park T, Kim K, Han S. Linear static and dynamic analysis of laminated composite plates and shells using a 4-node quasi-conforming shell element. Composites Part B: Engineering. 2005;37(2-3):237-48.
219. Patel BP, Gupta SS, Loknath MS, Kadu CP. Free vibration analysis of functionally graded elliptical cylindrical shells using higher-order theory. Composite structures. 2005;69(3):259-70.
220. Pelletier JL, Vel SS. An exact solution for the steady-state thermoelastic response of functionally graded orthotropic cylindrical shells. International Journal of Solids and Structures. 2006;43(5):1131-58.
221. Pitkäranta J, Matache AM, Schwab C. Fourier mode analysis of layers in shallow shell deformations. Computer methods in applied mechanics and engineering. 2001;190(22-23):2943-75.
222. Pompe W, Worch H, Epple M, Friess W, Gelinsky M, Greil P, Hempel U, Scharnweber D, Schulte K. Functionally graded materials for biomedical applications. Materials Science and Engineering: A. 2003;362(1-2):40-60.
223. Pradhan SC, Loy CT, Lam KY, Reddy JN. Vibration characteristics of functionally graded cylindrical shells under various boundary conditions. Applied Acoustics. 2000;61(1):111-29.
224. Pradhan SC, Murmu T. Thermo-mechanical vibration of FGM sandwich beam under variable elastic foundations using differential quadrature method. Journal of Sound and Vibration. 2009;321(1):342-62.
225. Pradyumna S, Bandyopadhyay JN. Dynamic instability of functionally graded shells using higher-order theory. Journal of engineering mechanics. 2009;136(5):551-61.
226. Pradyumna S, Bandyopadhyay JN. Free vibration analysis of functionally graded curved panels using a higher-order finite element formulation. Journal of Sound and Vibration. 2008;318(1):176-92.
227. Pradyumna S, Bandyopadhyay JN. Free vibration and buckling of functionally graded shell panels in thermal environments. International Journal of Structural Stability and Dynamics. 2010;10(05):1031-53.

228. Pradyumna S, Nanda N. Geometrically nonlinear transient response of functionally graded shell panels with initial geometric imperfection. Mechanics of Advanced Materials and Structures. 2013;20(3):217-26.
229. Punera D, Kant T. Free vibration of functionally graded open cylindrical shells based on several refined higher order displacement models. Thin-Walled Structures. 2017;119:707-26.
230. Qatu MS. Natural vibration of free, laminated composite triangular and trapezoidal shallow shells. Composite structures. 1995;31(1):9-19.
231. Qu Y, Long X, Yuan G, Meng G. A unified formulation for vibration analysis of functionally graded shells of revolution with arbitrary boundary conditions. Composites Part B: Engineering. 2013;50:381-402.
232. Rao JS. Turbomachine blade vibration. New Age International; 1991.
233. Reddy JN, Cheng ZQ. Three-dimensional thermomechanical deformations of functionally graded rectangular plates. European Journal of Mechanics-A/Solids. 2001;20(5):841-55.
234. Reddy JN, Chin CD. Thermomechanical analysis of functionally graded cylinders and plates. Journal of thermal Stresses. 1998;21(6):593-626.
235. Reddy JN. A simple higher-order theory for laminated composite plates. Journal of applied mechanics. 1984;51(4):745-52.
236. Reddy JN. Mechanics of laminated composite plates and shells: theory and analysis. CRC Press; 2004.
237. Reissner E. On bending of elastic plates. Q Appl Math 1947;5(1):55–68.
238. Reissner E. The effect of transverse shear deformation on the bending of elastic plates. J Appl Mech 1945;12(2):69–72.
239. Richardson MO, Wisheart MJ. Review of low-velocity impact properties of composite materials. Composites Part A: Applied Science and Manufacturing. 1996;27(12):1123-31.
240. Rotter JM. Shell structures: the new European standard and current research needs. Thin-walled structures. 1998;31(1-3):3-23.
241. Sadowski T, Boniecki M, Librant Z, Nakonieczny K. Theoretical prediction and experimental verification of temperature distribution in FGM cylindrical plates subjected to thermal shock. International Journal of Heat and Mass Transfer. 2007;50(21):4461-7.

242. Sahmani S, Ansari R, Gholami R, Darvizeh A. Dynamic stability analysis of functionally graded higher-order shear deformable microshells based on the modified couple stress elasticity theory. Composites Part B: Engineering. 2013;51:44-53.
243. Santos H, Soares CM, Soares CA, Reddy JN. A semi-analytical finite element model for the analysis of cylindrical shells made of functionally graded materials. Composite Structures. 2009;91(4):427-32.
244. Seifried S, Winterer M, Hahn H. Nanocrystalline gradient films through chemical vapor synthesis. Scripta materialia. 2001;44(8-9):2165-8.
245. Senthilnathan NR, Lim SP, Lee KH, Chow ST. Buckling of shear-deformable plates. AIAA journal. 1987;25(9):1268-71.
246. Shah AG, Mahmood T, Naeem MN. Vibrations of FGM thin cylindrical shells with exponential volume fraction law. Applied Mathematics and Mechanics. 2009;30(5):607-15.
247. Shahsiah R, Eslami MR, Naj R. Thermal instability of functionally graded shallow spherical shell. Journal of Thermal Stresses. 2006;29(8):771-90.
248. Shahsiah R, Eslami MR. Functionally graded cylindrical shell thermal instability based on improved Donnell equations. AIAA journal. 2003;41(9):1819-26..
249. Shahsiah R, Eslami MR. Thermal buckling of functionally graded cylindrical shell. Journal of Thermal Stresses. 2003a;26(3):277-94.
250. Sharafkhani N, Rezazadeh G, Shabani R. Study of mechanical behavior of circular FGM micro-plates under nonlinear electrostatic and mechanical shock loadings. Acta Mechanica. 2012;223(3):579-91.
251. Shariat BS, Javaheri R, Eslami MR. Buckling of imperfect functionally graded plates under in-plane compressive loading. Thin-walled structures. 2005;43(7):1020-36.
252. Shariyat M, Farzan F. Nonlinear eccentric low-velocity impact analysis of a highly prestressed FGM rectangular plate, using a refined contact law. Archive of Applied Mechanics. 2013:1-9.
253. Shariyat M, Jafari R. Nonlinear low-velocity impact response analysis of a radially preloaded two-directional-functionally graded circular plate: A refined contact stiffness approach. Composites Part B: Engineering. 2013;45(1):981-94.
254. Shariyat M. Vibration and dynamic buckling control of imperfect hybrid FGM plates with temperature-dependent material properties subjected to thermo-electro-mechanical loading conditions. Composite Structures. 2009;88(2):240-52.

255. Shen HS, Leung AY. Postbuckling of pressure-loaded functionally graded cylindrical panels in thermal environments. Journal of engineering mechanics. 2003;129(4):414-25.
256. Shen HS. Functionally graded materials: nonlinear analysis of plates and shells. CRC press; 2016.
257. Shen HS. Postbuckling analysis of axially loaded functionally graded cylindrical panels in thermal environments. International Journal of Solids and Structures. 2002;39(24):5991-6010.
258. Shen HS. Postbuckling analysis of pressure-loaded functionally graded cylindrical shells in thermal environments. Engineering Structures. 2003;25(4):487-97.
259. Shen HS. Postbuckling of axially loaded FGM hybrid cylindrical shells in thermal environments. Compos Sci Technol 2005;65(11–12):1675–90.
260. Shen HS. Postbuckling of shear deformable FGM cylindrical shells surrounded by an elastic medium. Int J Mech Sci 2009;51(5):372–83.
261. Shen M, Bever MB. Gradients in polymeric materials. J Mater Sci 1972; 7:741–6.
262. Sheng GG, Wang X. Non-linear response of functionally graded cylindrical shells under mechanical and thermal loads. Journal of Thermal Stresses. 2011;34(11):1105-18.
263. Sheng GG, Wang X. Studies on dynamic behavior of functionally graded cylindrical shells with PZT layers under moving loads. Journal of Sound and Vibration. 2009;323(3):772-89.
264. Sheng GG, Wang X. The dynamic stability and nonlinear vibration analysis of stiffened functionally graded cylindrical shells. Applied Mathematical Modelling. 2018;56:389-403.
265. Sheng GG, Wang X. The non-linear vibrations of rotating functionally graded cylindrical shells. Nonlinear Dynamics. 2017;87(2):1095-109.
266. Sheng GG, Wang X. Thermal vibration, buckling and dynamic stability of functionally graded cylindrical shells embedded in an elastic medium. Journal of Reinforced Plastics and Composites. 2008;27(2):117-34.
267. Shimpi RP, Patel HG. A two variable refined plate theory for orthotropic plate analysis. International Journal of Solids and Structures. 2006;43(22):6783-99.
268. Shimpi RP, Patel HG. Free vibrations of plate using two variable refined plate theory. Journal of Sound and Vibration. 2006a;296(4):979-99.
269. Shimpi RP. Refined plate theory and its variants. AIAA journal. 2002 Jan;40(1).

270. Sobhy M. An accurate shear deformation theory for vibration and buckling of FGM sandwich plates in hygrothermal environment. International Journal of Mechanical Sciences. 2016;110:62-77.
271. Soedel W, Qatu MS. Vibrations of shells and plates. The Journal of the Acoustical Society of America. 2005;117(4):1683-.
272. Sofiyev AH, Kuruoglu N. Domains of dynamic instability of FGM conical shells under time dependent periodic loads. Composite Structures. 2016;136:139-48.
273. Sofiyev AH, Osmancelebioglu E. The free vibration of sandwich truncated conical shells containing functionally graded layers within the shear deformation theory. Composites Part B: Engineering. 2017;120:197-211.
274. Sofiyev AH, Schnack E. The stability of functionally graded cylindrical shells under linearly increasing dynamic torsional loading. Engineering structures. 2004;26(10):1321-31.
275. Sofiyev AH, Zerin Z, Kuruoglu N. Thermoelastic buckling of FGM conical shells under non-linear temperature rise in the framework of the shear deformation theory. Composites Part B: Engineering. 2017;108:279-90.
276. Sofiyev AH. On the vibration and stability of shear deformable FGM truncated conical shells subjected to an axial load. Composites Part B: Engineering. 2015;80:53-62.
277. Sofiyev AH. Parametric vibration of FGM conical shells under periodic lateral pressure within the shear deformation theory. Composites Part B: Engineering. 2016;89:282-94.
278. Sofiyev AH. The buckling of FGM truncated conical shells subjected to axial compressive load and resting on Winkler–Pasternak foundations. International Journal of Pressure Vessels and Piping. 2010;87(12):753-61.
279. Sofiyev AH. The vibration and stability behavior of freely supported FGM conical shells subjected to external pressure. Composite Structures. 2009;89(3):356-66.
280. Song C, Xu Z, Li J. Structure of in situ Al/Si functionally graded materials by electromagnetic separation method. Materials & design. 2007;28(3):1012-5.
281. Sreenivasamurthy S, Ramamurti V. Coriolis effect on the vibration of flat rotating low aspect ratio cantilever plates. The Journal of Strain Analysis for Engineering Design. 1981;16(2):97-106.
282. Stein M. Nonlinear theory for plates and shells including the effects of transverse shearing. AIAA journal. 1986;24(9):1537-44.

283. Su Z, Jin G, Shi S, Ye T, Jia X. A unified solution for vibration analysis of functionally graded cylindrical, conical shells and annular plates with general boundary conditions. International Journal of Mechanical Sciences. 2014;80:62-80.
284. Sundararajan N, Prakash T, Ganapathi M. Nonlinear free flexural vibrations of functionally graded rectangular and skew plates under thermal environments. Finite Elements in Analysis and Design. 2005;42(2):152-68.
285. Sutradhar A, Paulino GH. The simple boundary element method for transient heat conduction in functionally graded materials. Computer Methods in Applied Mechanics and Engineering. 2004;193(42):4511-39.
286. Swaminathan K, Naveenkumar DT, Zenkour AM, Carrera E. Stress, vibration and buckling analyses of FGM plates—a state-of-the-art review. Composite Structures. 2015;120:10-31.
287. Swaminathan K, Sangeetha DM. Thermal analysis of FGM plates–A critical review of various modeling techniques and solution methods. Composite Structures. 2017;160:43-60.
288. Talebitooti M. Thermal effect on free vibration of ring-stiffened rotating functionally graded conical shell with clamped ends. Mechanics of Advanced Materials and Structures. 2018;25(2):155-65.
289. Talha M, Singh BN. Large amplitude free flexural vibration analysis of shear deformable FGM plates using nonlinear finite element method. Finite Elements in Analysis and Design. 2011;47(4):394-401.
290. Talha M, Singh BN. Static response and free vibration analysis of FGM plates using higher order shear deformation theory. Applied Mathematical Modelling. 2010;34(12):3991-4011.
291. Tan P, Nguyen-Thanh N, Rabczuk T, Zhou K. Static, dynamic and buckling analyses of 3D FGM plates and shells via an isogeometric-meshfree coupling approach. Composite Structures. 2018;198:35-50.
292. Tanigawa YO. Three-dimensional transient thermal stresses of functionally graded rectangular plate due to partial heating. Journal of Thermal Stresses. 1999;22(1):35-55.
293. Thai HT, Choi DH. A refined plate theory for functionally graded plates resting on elastic foundation. Composites Science and Technology. 2011;71(16):1850-8.
294. Thai HT, Choi DH. A refined shear deformation theory for free vibration of functionally graded plates on elastic foundation. Composites Part B: Engineering. 2012b;43(5):2335-47.

295. Thai HT, Choi DH. An efficient and simple refined theory for buckling analysis of functionally graded plates. Applied Mathematical Modelling. 2012;36(3):1008-22.
296. Thai HT, Choi DH. Levy solution for free vibration analysis of functionally graded plates based on a refined plate theory. KSCE Journal of Civil Engineering. 2014;18(6):1813-24.
297. Thai HT, Kim SE. A review of theories for the modeling and analysis of functionally graded plates and shells. Composite Structures. 2015;128:70-86.
298. Thai HT, Kim SE. A simple higher-order shear deformation theory for bending and free vibration analysis of functionally graded plates. Composite Structures. 2013;96:165-73.
299. Thai HT, Kim SE. A simple quasi-3D sinusoidal shear deformation theory for functionally graded plates. Composite Structures. 2013a;99:172-80.
300. Thai HT, Kim SE. Analytical solution of a two variable refined plate theory for bending analysis of orthotropic Levy-type plates. International Journal of Mechanical Sciences. 2012;54(1):269-76.
301. Thai HT, Kim SE. Levy-type solution for buckling analysis of orthotropic plates based on two variable refined plate theory. Composite Structures. 2011;93(7):1738-46.
302. Thai HT, Kim SE. Levy-type solution for free vibration analysis of orthotropic plates based on two variable refined plate theory. Applied Mathematical Modelling. 2012a;36(8):3870-82.
303. Thai HT, Park M, Choi DH. A simple refined theory for bending, buckling, and vibration of thick plates resting on elastic foundation. International Journal of Mechanical Sciences. 2013;73:40-52.
304. Thai HT, Park T, Choi DH. An efficient shear deformation theory for vibration of functionally graded plates. Archive of Applied Mechanics. 2013a;83(1):137-49.
305. Thai HT, Vo T, Bui T, Nguyen TK. A quasi-3D hyperbolic shear deformation theory for functionally graded plates. Acta Mechanica. 2014;225(3):951-64.
306. Torabi J, Kiani Y, Eslami MR. Linear thermal buckling analysis of truncated hybrid FGM conical shells. Composites Part B: Engineering. 2013;50:265-72.
307. Torki ME, Kazemi MT, Haddadpour H, Mahmoudkhani S. Dynamic stability of cantilevered functionally graded cylindrical shells under axial follower forces. Thin-Walled Structures. 2014;79:138-46.
308. Tornabene F, Ceruti A. Mixed static and dynamic optimization of four-parameter functionally graded completely doubly curved and degenerate shells and panels using GDQ method. Mathematical Problems in Engineering. 2013.

309. Tornabene F, Fantuzzi N, Bacciocchi M. Free vibrations of free-form doubly-curved shells made of functionally graded materials using higher-order equivalent single layer theories. Composites Part B: Engineering. 2014;67:490-509.
310. Tornabene F, Viola E, Inman DJ. 2-D differential quadrature solution for vibration analysis of functionally graded conical, cylindrical shell and annular plate structures. Journal of Sound and Vibration. 2009;328(3):259-90.
311. Tornabene F, Viola E. Free vibration analysis of functionally graded panels and shells of revolution. Meccanica. 2009;44(3):255-81.
312. Tornabene F, Viola E. Free vibrations of four-parameter functionally graded parabolic panels and shells of revolution. European Journal of Mechanics-A/Solids. 2009a;28(5):991-1013.
313. Tornabene F, Viola E. Static analysis of functionally graded doubly-curved shells and panels of revolution. Meccanica. 2013;48(4):901-30.
314. Tornabene F. 2-D GDQ solution for free vibrations of anisotropic doubly-curved shells and panels of revolution. Composite Structures. 2011;93(7):1854-76.
315. Tornabene F. Free vibration analysis of functionally graded conical, cylindrical shell and annular plate structures with a four-parameter power-law distribution. Computer Methods in Applied Mechanics and Engineering. 2009;198(37):2911-35.
316. Touratier M. An efficient standard plate theory. International journal of engineering science. 1991;29(8):901-16.
317. Trabelsi S, Zghal S, Frikha A. Post-buckling of FSDT of Functionally Graded Material Shell Structures. InInternational Conference Design and Modeling of Mechanical Systems 2017,pp. 217-225, Springer, Cham.
318. Van Dung D, Chan DQ. Analytical investigation on mechanical buckling of FGM truncated conical shells reinforced by orthogonal stiffeners based on FSDT. Composite Structures. 2017;159:827-41.
319. Van Tung H, Duc ND. Nonlinear response of shear deformable FGM curved panels resting on elastic foundations and subjected to mechanical and thermal loading conditions. Applied Mathematical Modelling. 2014;38(11):2848-66.
320. Van Tung H. Nonlinear axisymmetric response of FGM shallow spherical shells with tangential edge constraints and resting on elastic foundations. Composite Structures. 2016;149:231-8.
321. Vel SS, Batra RC. Exact solution for thermoelastic deformations of functionally graded thick rectangular plates. AIAA journal. 2002;40(7):1421-33.

322. Vel SS, Batra RC. Three-dimensional exact solution for the vibration of functionally graded rectangular plates. Journal of Sound and Vibration. 2004;272(3):703-30.
323. Vel SS. Exact elasticity solution for the vibration of functionally graded anisotropic cylindrical shells. Composite Structures. 2010;92(11):2712-27.
324. Viola E, Rossetti L, Fantuzzi N, Tornabene F. Static analysis of functionally graded conical shells and panels using the generalized unconstrained third order theory coupled with the stress recovery. Composite Structures. 2014;112:44-65.
325. Wang CM, Lim GT, Reddy JN, Lee KH. Relationships between bending solutions of Reissner and Mindlin plate theories. Eng Struct 2001;23(7):838–49.
326. Wang Q, Cui X, Qin B, Liang Q, Tang J. A semi-analytical method for vibration analysis of functionally graded (FG) sandwich doubly-curved panels and shells of revolution. International Journal of Mechanical Sciences. 2017;134:479-99.
327. Wang YQ, Zu JW. Large-amplitude vibration of sigmoid functionally graded thin plates with porosities. Thin-Walled Structures. 2017a;119:911-24.
328. Wang YQ, Zu JW. Vibration behaviors of functionally graded rectangular plates with porosities and moving in thermal environment. Aerospace Science and Technology. 2017;69:550-62.
329. Wang Z, Han Q, Nash DH, Liu P, Hu D. Investigation of imperfect effect on thermal buckling of cylindrical shell with FGM coating. European Journal of Mechanics-A/Solids. 2018;69:221-30.
330. Watanabe Y, Eryu H, Matsuura K. Evaluation of three-dimensional orientation of Al3Ti platelet in Al-based functionally graded materials fabricated by a centrifugal casting technique. Acta Materialia. 2001;49(5):775-83.
331. Watanabe Y, Yamanaka N, Fukui Y. Control of composition gradient in a metal-ceramic functionally graded material manufactured by the centrifugal method. Composites Part A: Applied Science and Manufacturing. 1998;29(5-6):595-601.
332. Watari F, Yokoyama A, Saso F, Uo M, Kawasaki T. Fabrication and properties of functionally graded dental implant. Compos Part B Eng 1997; 28:5–11.
333. Wattanasakulpong N, Chaikittiratana A. Flexural vibration of imperfect functionally graded beams based on Timoshenko beam theory: Chebyshev collocation method. Meccanica. 2015;50(5):1331-42.
334. Wattanasakulpong N, Prusty BG, Kelly DW, Hoffman M. Free vibration analysis of layered functionally graded beams with experimental validation. Materials & Design (1980-2015). 2012;36:182-90.

335. Wattanasakulpong N, Ungbhakorn V. Linear and nonlinear vibration analysis of elastically restrained ends FGM beams with porosities. Aerospace Science and Technology. 2014;32(1):111-20.
336. Wen PH, Sladek J, Sladek V. Three dimensional analysis of functionally graded plates. International Journal for Numerical Methods in Engineering. 2011;87(10):923-42.
337. Woo J, Meguid SA, Stranart JC, Liew KM. Thermomechanical postbuckling analysis of moderately thick functionally graded plates and shallow shells. International Journal of Mechanical Sciences. 2005;47(8):1147-71.
338. Woo J, Meguid SA. Nonlinear analysis of functionally graded plates and shallow shells. International Journal of Solids and structures. 2001;38(42):7409-21.
339. Woodward B, Kashtalyan M. 3D elasticity analysis of sandwich panels with graded core under distributed and concentrated loadings. International Journal of Mechanical Sciences. 2011;53(10):872-85.
340. Woodward B, Kashtalyan M. Three-dimensional elasticity solution for bending of transversely isotropic functionally graded plates. European Journal of Mechanics-A/Solids. 2011a;30(5):705-18.
341. Wu CP, Chiu KH, Wang YM. RMVT-based meshless collocation and elementfree Galerkin methods for the quasi-3D analysis of multilayered composite and FGM plates. Compos Struct 2011;93(2):923–43.
342. Wu CP, Chiu KH. RMVT-based meshless collocation and element-free Galerkin methods for the quasi-3D free vibration analysis of multilayered composite and FGM plates. Compos Struct 2011;93(5):1433–48.
343. Wu CP, Lo JY. An asymptotic theory for dynamic response of laminated piezoelectric shells. Acta mechanica. 2006;183(3-4):177.
344. Wu CP, Yang SW. A semi-analytical element-free Galerkin method for the 3D free vibration analysis of multilayered FGM circular hollow cylinders. J Intell Mater Syst Struct 2011a;22(17):1993–2007.
345. Wu CP, Yang SW. RMVT-based meshless collocation and element-free Galerkin methods for the approximate 3D analysis of multilayered composite and FGM circular hollow cylinders. Compos B Eng 2011;42(6):1683–700.
346. Xiang S, Chen YT, Kang GW. Local collocation method for prediction of natural frequency of functionally graded cylindrical shells. Mechanics of Advanced Materials and Structures. 2015 2;22(12):969-77.

347. Xie X, Zheng H, Jin G. Free vibration of four-parameter functionally graded spherical and parabolic shells of revolution with arbitrary boundary conditions. Composites Part B: Engineering. 2015;77:59-73.
348. Xu Y, Zhou D. Three-dimensional elasticity solution of functionally graded rectangular plates with variable thickness. Composite Structures. 2009;91(1):56-65.
349. Yahia SA, Atmane HA, Houari MS, Tounsi A. Wave propagation in functionally graded plates with porosities using various higher-order shear deformation plate theories. Structural Engineering and Mechanics. 2015;53(6):1143-65.
350. Yalamanchili VK, Sankar BV. Indentation of functionally graded beams and its application to low-velocity impact response. Composites Science and Technology. 2012;72(16):1989-94.
351. Yang J, Liew KM, Wu YF, Kitipornchai S. Thermo-mechanical post-buckling of FGM cylindrical panels with temperature-dependent properties. International Journal of Solids and Structures. 2006;43(2):307-24.
352. Yang J, Shen HS. Non-linear analysis of functionally graded plates under transverse and in-plane loads. International Journal of Non-Linear Mechanics. 2003;38(4):467-82.
353. Yang SH, Sun CT. Indentation law for composite laminates. InComposite Materials: Testing and Design (6th Conference) 1982. ASTM International.
354. Yun W, Rongqiao X, Haojiang D. Three-dimensional solution of axisymmetric bending of functionally graded circular plates. Composite Structures. 2010;92(7):1683-93.
355. Zare Jouneghani F, Dimitri R, Bacciocchi M, Tornabene F. Free Vibration Analysis of Functionally Graded Porous Doubly-Curved Shells Based on the First-Order Shear Deformation Theory. Applied Sciences. 2017;7(12):1252.
356. Zenkour AM, Sobhy M. Thermal buckling of functionally graded plates resting on elastic foundations using the trigonometric theory. Journal of Thermal Stresses. 2011;34(11):1119-38.
357. Zenkour AM. Benchmark trigonometric and 3-D elasticity solutions for an exponentially graded thick rectangular plate. Archive of Applied Mechanics. 2007;77(4):197-214.
358. Zenkour AM. Exact relationships between classical and sinusoidal theories for FGM plates. Mechanics of Advanced Materials and Structures. 2012;19(7):551-67.
359. Zenkour AM. Generalized shear deformation theory for bending analysis of functionally graded plates. Applied Mathematical Modelling. 2006;30(1):67-84.

360. Zenkour AM. Hygro-thermo-mechanical effects on FGM plates resting on elastic foundations. Composite Structures. 2010;93(1):234-8.
361. Zenkour AM. On vibration of functionally graded plates according to a refined trigonometric plate theory. International Journal of Structural Stability and Dynamics. 2005;5(02):279-97.
362. Zghal S, Frikha A, Dammak F. Free vibration analysis of carbon nanotube-reinforced functionally graded composite shell structures. Applied Mathematical Modelling. 2018;53:132-55.
363. Zhang DG, Zhou YH. A theoretical analysis of FGM thin plates based on physical neutral surface. Computational Materials Science. 2008;44(2):716-20.
364. Zhang H, Jiang JQ, Zhang ZC. Three-dimensional elasticity solutions for bending of generally supported thick functionally graded plates. Applied Mathematics and Mechanics. 2014;35(11):1467-78.
365. Zhang W, Hao YX. Nonlinear dynamic of functionally graded cylindrical shells under the thermal mechanical loads. Int Mech Eng Congr Exp 2009:331–6.
366. Zhang ZJ, Paulino GH. Wave propagation and dynamic analysis of smoothly graded heterogeneous continua using graded finite elements. International Journal of Solids and Structures. 2007;44(11):3601-26.
367. Zhao X, Lee YY, Liew KM. Free vibration analysis of functionally graded plates using the element-free kp-Ritz method. Journal of sound and Vibration. 2009;319(3):918-39.
368. Zhao X, Lee YY, Liew KM. Mechanical and thermal buckling analysis of functionally graded plates. Composite Structures. 2009a;90(2):161-71.
369. Zhao X, Liew KM. An element-free analysis of mechanical and thermal buckling of functionally graded conical shell panels. International Journal for Numerical Methods in Engineering. 2011;86(3):269-85.
370. Zhao X, Liew KM. Free vibration analysis of functionally graded conical shell panels by a meshless method. Composite Structures. 2011a;93(2):649-64.
371. Zhao X, Liew KM. Geometrically nonlinear analysis of functionally graded plates using the element-free kp-Ritz method. Computer Methods in Applied Mechanics and Engineering. 2009;198(33):2796-811.
372. Zhong Z, Shang E. Closed-form solutions of three-dimensional functionally graded plates. Mechanics of Advanced Materials and Structures. 2008;15(5):355-63.
373. Zhu J, Lai Z, Yin Z, Jeon J, Lee S. Fabrication of ZrO_2–NiCr functionally graded material by powder metallurgy. Materials chemistry and physics. 2001;68(1-3):130-5.

374. Zienkiewicz O. C., The finite element method, third edition, Tata McGraw Hill Publishing Company Limited, New Delhi, 1979.